(NASA-CR-135231) LINEAR AEROSPIKE ENGINE STUDY Final Report, Jun. 1976 - Apr. 1977 (Rocketdyne) 236 p HC A11/MF A01 CSCL 21A

N78-11082

Unclas
G3/07 52831

NASA CR-135231
RI/RD77-170

NASA

FINAL REPORT

LINEAR AEROSPIKE ENGINE STUDY

by

H. G. Diem and F. M. Kirby

Rockwell International
Rocketdyne Division

prepared for
NATIONAL AERONAUTICS AND SPACE ADMINISTRATION

NASA-Lewis Research Center
Contract NAS3-20114

1. Report No. NASA CR-135231	2. Government Accession No.	3. Recipient's Catalog No.
4. Title and Subtitle LINEAR AEROSPIKE ENGINE STUDY Final Report		5. Report Date November 1977 6. Performing Organization Code
7. Author(s) H. G. Diem and F. M. Kirby		8. Performing Organization Report No. RI/RD77-170 10. Work Unit No.
9. Performing Organization Name and Address Rockwell International, Rocketdyne Division 6633 Canoga Avenue Canoga Park, CA 91304		11. Contract or Grant No. NAS3-20114
12. Sponsoring Agency Name and Address National Aeronautics and Space Administration Lewis Research Center Cleveland, Ohio 44315		13. Type of Report and Period Covered Final (June 1976-April 1977) 14. Sponsoring Agency Code

15. Supplementary Notes

Project Manager, D. D. Scheer, NASA-Lewis Research Center, Cleveland, OH 44315

16. Abstract

This program is a study of the split combustor linear aerospike engine concept. Parametric data on split-combustor linear engine propulsion systems are presented for use in mixed-mode single-stage-to-orbit (SSTO) vehicle studies. Also provided are preliminary design data for two selected engine systems.

The split combustor is investigated for mixed-mode operations with oxygen/hydrogen propellants used in the inner combustor in Mode 2, and in conjunction with either oxygen/RP-1, oxygen/RJ-5, O_2/CH_4, or O_2/H_2 propellants in the outer combustor for Mode 1. Both gas generator and staged combustion power cycles are analyzed for providing power to the turbopumps of the inner and outer combustors.

Numerous cooling circuits and cooling fluids (propellants) are analyzed and hydrogen is selected as the preferred coolant for both combustors and the linear aerospike nozzle. The maximum operating chamber pressure is determined to be limited by the availability of hydrogen coolant pressure drop in the coolant circuit.

Parametric performance, weight, and envelope data are presented for thrust levels between 1.78×10^7 N (4×10^6 lbf) and 2.67×10^7 N (6×10^6 lbf); Mode 1 area ratios (ε_1) from 20:1 to 80:1; engine thrust splits from 0.5 to 0.8; and geometric variations in engine width-to-nozzle height ratios from 3 to 5.

Thrust vector control is provided by differential throttling.

17. Key Words (Suggested by Author(s))	18. Distribution Statement		
Split Combustor, Dual Mode, Linear Aerospike, SSTO Propulsion			
19. Security Classif. (of this report) UNCLASSIFIED	20. Security Classif. (of this page) UNCLASSIFIED	21. No. of Pages 225	22. Price*

*For sale by the National Technical Information Service, Springfield, Virginia 22151

FOREWORD

The Split Combustor Linear Aerospike Engine study was conducted at the Rocketdyne Division of Rockwell International under NASA Contract NAS3-20114. Mr. Dean D. Scheer, NASA-Lewis Research Center, was the study Project Manager. At Rocketdyne, Mr. Hal G. Diem was the study Program Manager and Mr. Frank M. Kirby was the Project Engineer.

The 10-month technical period of performance began in June 1976 and ended in April 1977.

The study effort at Rocketdyne was performed by the following team of technical specialists:

A. Martinez
W. R. Bissell
J. M. Shoji
D. F. Carson
K. H. Acton
J. Q. Weber
M. C. Wood
J. K. Hunting

CONTENTS

PRECEDING PAGE BLANK NOT FILMED

ILLUSTRATIONS

ORIGINAL PAGE IS
OF POOR QUALITY

ORIGINAL PAGE IS
OF POOR QUALITY

ORIGINAL PAGE IS
OF POOR QUALITY

TABLES

SUMMARY

This program was a study of the split combustor linear aerospike engine concept (Fig. 1). The results provide NASA and vehicle study contractors with parametric data on split-combustor linear engine propulsion systems for several propellant combinations, for use in mixed-mode single-stage-to-orbit (SSTO) vehicle studies. The program also provides preliminary design data for engine systems and propulsion system technology needs.

The split combustor is investigated for mixed-mode operations with oxygen/hydrogen propellants used in the inner combustor in Mode 2, and in conjunction with either oxygen/RP-1, oxygen/RJ-5, O_2/CH_4, or O_2/H_2 propellants in the outer combustor for Mode 1. Both gas generator and staged combustion power cycles are analyzed for providing power to the turbopumps of the inner and outer combustors.

A baseline engine thrust at sea level of 20×10^6 N (4.5×10^6 lbf) and thrust split (ratio of the outer combustor thrust to the total thrust of outer and inner combustors) of 0.65 is a ground rule design point in the analyses conducted for engine modularization, thrust chamber cooling, engine performance, weight, and envelope. Study results led to selection of a four-module design approach primarily because it has lighter weight and higher performance compared to designs with greater number of modules. Numerous cooling circuits and cooling fluids (propellants) are analyzed and hydrogen is selected as the preferred coolant for both combustors and the linear aerospike nozzle. Within the range of chamber pressures (689 N/cm^2, 1000 psia, to 3450 N/cm^2, 5000 psia) investigated, the maximum operating chamber pressure is determined to be limited by the availability of coolant (H_2) pressure drop (ΔP) in the coolant circuit. For the study, the ΔP available is expressed in terms of a ratio between coolant circuit inlet pressure (P_{inlet}) and chamber pressure (P_c) The maximum chamber pressure for a staged combustion power cycle with P_{inlet}/P_c of 2.25, is determined to be 1723 N/cm^2 (2500 psia). Both the inner and outer combustors operate at this level. For the gas generator cycle with P_{inlet}/P_c = 1.8, the maximum P_c is 1380 N/cm^2 (2000 psia).

Parametric data are presented for thrust levels between 1.78×10^7 N (4×10^6 lbf) and 2.67×10^7N (6×10^6 lbf); Mode 1 area ratios (ε_1) from 20:1 to 80:1; engine thrust splits from 0.5 to 0.8; and geometric variations in engine width-to-nozzle height (W/H) ratios from 3 to 5. The maximum operating chamber pressure presented above is defined for selected values of Mode 1 expansion area ratio and engine width-to-nozzle height ratio: ε_1 = 40:1 and W/H = 3. Any increase in these causes a reduction in operation pressure.

Based on results of the parametric analyses, an engine sea level thrust of 17.8 $\times 10^6$ N (4×10^6 lbf) is selected for preliminary design of two engine concepts: (1) a hybrid power cycle where the outer combustor uses a gas generator power cycle with oxygen/RP-1 propellants and the inner combustor uses a staged combustion power cycle with oxygen/hydrogen propellants, and(2) an all staged combustion power cycle with oxygen/hydrogen propellants. The engine designs are described in Table 1. Thrust vector control is provided by differential

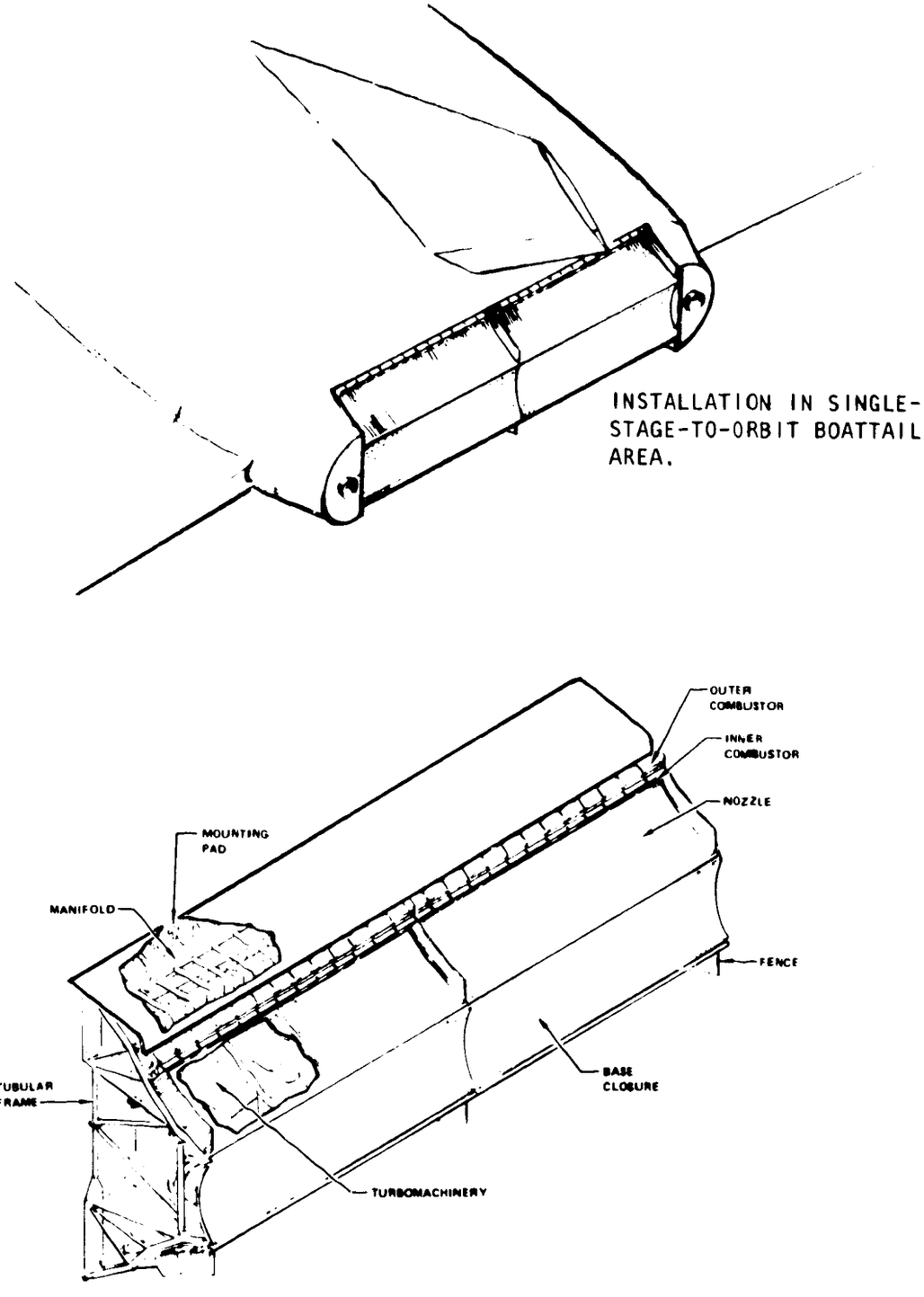

Figure 1. Four-Module, Split-Combustor, Dual-Fuel Linear Aerospike Engine

ORIGINAL PAGE IS
OF POOR QUALITY

TABLE 1. LINEAR ENGINE PRELIMINARY DESIGN DESCRIPTION

	Concept 1	Concept 2
Engine Thrust, Newtons (pounds)		
Mode 1		
Sea Level	$17.8 \times 10^6 (4 \times 10^6)$	$17.8 \times 10^6 (4 \times 10^6)$
Vacuum	$20.0 \times 10^6 (4.5 \times 10^6)$	$20.0 \times 10^6 (4.5 \times 10^6)$
Mode 2		
Vacuum	$7.36 \times 10^6 (1.65 \times 10^6)$	$7.36 \times 10^6 (1.65 \times 10^6)$
Thrust Split at Sea Level	0.65	0.65
Chamber Pressure, N/cm^2 (psia)		
Outer Combustor	1380 (2000)	1724 (2500)
Inner Combustor	1724 (2500)	1724 (2500)
Propellant Combination		
Outer Combustor	O_2/RP-1	O_2/H_2
Inner Combustor	O_2/H_2	O_2/H_2
Engine Mixture Ratio		
Outer Combustor	2.8	7.0
Inner Combustor	7.0	7.0
Expansion Area Ratio		
Mode 1	40:1	40:1
Mode 2	114:1	114:1
Specific Impulse, N-s/kg (seconds)		
Mode 1		
Sea Level	3151 (321.3)	3820 (389.5)
Vacuum	3601 (367.2)	4302 (438.7)
Mode 2		
Vacumm	4466 (455.4)	4466 (455.4)
Power Cycle		
Outer Combustor	Gas Generator	Staged Combustion
Inner Combustor	Staged Combustion	Staged Combustion
Nozzle Percent Length, % of 15-Degree Cone	20	20
Engine Width-to-Nozzle Height Ratio	3.0:1	3.0:1
P_{inlet}/P_c		
Outer Combustor	2.8	2.8
Inner Combustor	2.8	2.8
Engine Envelope, meters (inches)		
Width	8.8 (346)	8.8 (346)
Height	4.4 (172)	4.4 (175)
Length	2.1 (84.5)	2.1 (84.5)
Engine Weight, kg (pounds)	20070 (44250)	22850 (50380)

ORIGINAL PAGE IS
OF POOR QUALITY

throttling; with 25 percent throttling, 2 degrees in yaw and 0.8 degree in pitch are projected based on the dimensions between the engine and center of gravity of the vehicle assumed to be representative of SSTO vehicles. Engine weights for the two preliminary designs are 20070 kg (44250 lbm) and 22850 kg (50380 lbm) for concepts 1 and 2, respectively.

Recommended supporting research and technology programs for the split combustor linear aerospike engine concept are:

- Preliminary design and analysis - Phase II
- Split-combustor thrust chamber feasibility demonstration
- High-pressure O_2/RP-1 combustion investigation
- High-pressure O_2/RP-1 gas generator operation
- Investigation of composite materials for engine parts

INTRODUCTION

The dual-fuel, modular, split-combustor linear aerospike engine concept discussed in this report is an integrated engine for a reusable (SSTO) vehicle (Fig. 1). It is an engine that can burn either two fuels (hydrogen and a hydrocarbon) with oxygen in separate combustors or all-hydrogen fuel. Combustion gases expand on a linear aerospike nozzle. The fuels are burned in parallel in Mode 1 phase of the mission with individually optimized injectors at desired mixture ratios. A step decrease in thrust and simultaneous increase in expansion area ratios are achieved in Mode 2 operation by shutdown of one feed system. Mode change does not require moving parts other than shutoff valves. In addition to the step increase in area ratio, there is the inherent automatic and continuous altitude compensation feature which is characteristic for aerospike nozzles.

The overall objective of the program was to define a baseline engine concept, provide parametric data, and complete the preliminary designs for a split-combustor chamber linear engine for NASA, for use in vehicle studies, and to identify propulsion system technology needs.

The program was divided into six technical tasks. Tasks I through V comprised analytical efforts that were mutually supporting. The results of these tasks supported Task VI, "Engine Preliminary Design" of two selected engine concepts. Together, the six technical tasks provide the required parametric data, engine description, and technology identification in support of NASA-supported vehicle studies.

Task I was devoted to accumulation of data describing the properties of the propellants, and the generation of theoretical performance of the products of combustion. Data needed for the performance program were available at Rocketdyne or (in the case of RJ-5) were obtained from NASA. The theoretical performance of oxygen/hydrogen in one combustor and oxygen with either methane, kerosene (RP-1), Shelldyne (RJ-5), or hydrogen burning in the other combustor of the split-combustor linear engine, was generated, summarized, tabulated, and graphed for use in subsequent tasks.

During Task II, the module size was selected for the baseline configurations of the linear engine. In Task III, cooling methodologies were investigated for the four propellant combinations, the module size selected, and the relative cooling capability as a function of chamber pressure determined. Baseline engine performance data for the four concepts under study were established in Task IV, and assessment of the effects on maximum chamber pressure attainable of alternate power cycles was made. For this effort, staged combustion and gas generator cycles were studied. Other major parameters generated included engine delivered specific impulse, weight, and envelope.

Task V was devoted to the generation of engine performance, weight, and envelope parametrics for the power cycle selected, and suitable for use in vehicle design studies. Principal variables included: thrust level, thrust split ratio, expansion area ratio, and cross-sectional engine dimensions (weight to height).

ORIGINAL PAGE IS
OF POOR QUALITY

Following selection, with NASA approval, of an oxygen/hydrocarbon-oxygen/hydrogen concept, Task VI addressed the preliminary design of an engine embodying this concept. Preliminary design was also conducted for an all-hydrogen-fueled, split-combustor linear engine.

The technical program effort is discussed by tasks in subsequent sections.

TASK I: PROPELLANT PROPERTIES AND PERFORMANCE

SPLIT COMBUSTOR LINEAR ENGINE THEORETICAL PERFORMANCE

The split-combustor thrust chamber concept studied in the contract (Fig. 2) operated with either O_2/H_2 propellants in the inner combustor and O_2/hydrocarbon propellants in the outer combustor or with O_2/H_2 propellants in both combustors. Combustion gases expand without mixing to an intermediate area ratio (where the inner and outer combustor walls meet) and continue to expand with some mixing to the overall expansion area ratio of the nozzle. The overall expansion area ratio is determined by the outer combustor exit area (defined by the product of nozzle height (Fig. 2) times engine width) divided by the sum of the throat areas of the inner and outer combustors. The inner combustor area ratio is determined by the inner combustor exit area divided by the inner combustor throat area.

Theoretical Vacuum Specific Impulse

The maximum vacuum theoretical specific impulse performance of the split-combustor nozzle is determined by the overall expansion area ratio, the individual mixture ratios of the combustors, the relative amounts of the propellants combusted, and the combustor chamber pressure. Individual combustor chamber pressures are assumed equal. The theoretical specific impulse for the split combustor, defined in the following equation, is equal to the weight-flow-averaged sum of the individual stream specific impulses (I_{sI}, I_{sO}) with a mixing parameter ($\Delta I_{s_{mix}}$) term added to account for the difference in performance due to mixing

$$I_s = I_s \text{ (unmixed streams)} + \Delta I_{s_{mix}}$$

$$I_s = \frac{\dot{w}_I}{\dot{w}_T} I_{s_I} + \frac{\dot{w}_o}{\dot{w}_T} I_{s_O} + \Delta I_{s_{mix}}$$

The maximum value for $\Delta I_{s_{mix}}$ occurs when the streams are mixed at the injector. Calculations performed with Rocketdyne's Free Energy Program have shown that the performance of the mixed stream is of the order of 0.5 percent (Fig. 3) greater than the performance of the unmixed stream. Since, in the actual case, mixing begins at an expansion area ratio of approximately 10, and proceeds down the contour at rates governed by the physical properties of the fluids, it is not likely that complete mixing will occur within the confines of the nozzle. Therefore, it was decided to ignore the mixing contribution to overall specific impulse. This procedure greatly simplifies establishing overall performance, as it is then only a function of the independently determined individual stream specific impulse and the fraction of the total flow contained in each stream.

ORIGINAL PAGE IS
OF POOR QUALITY

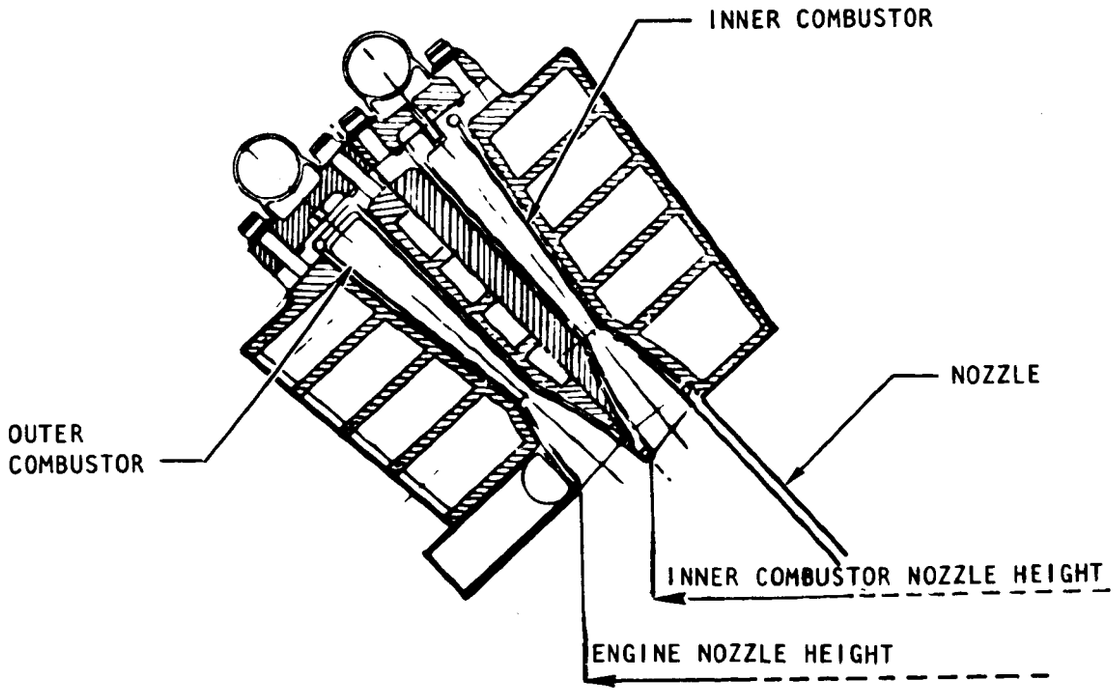

Figure 1. Split-Combustor Linear Engine

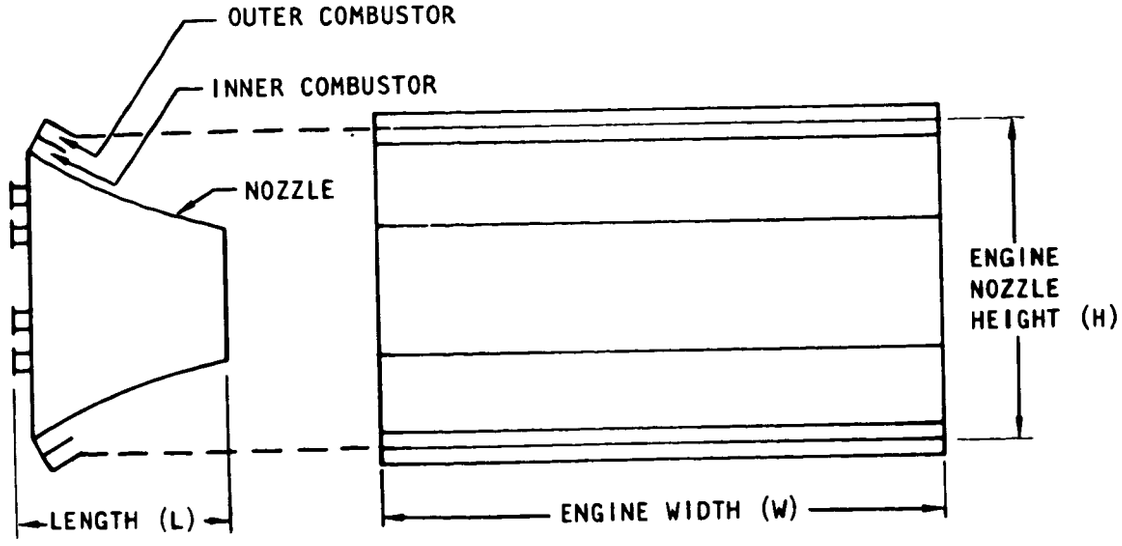

Figure 2. Split-Combustor Linear Engine

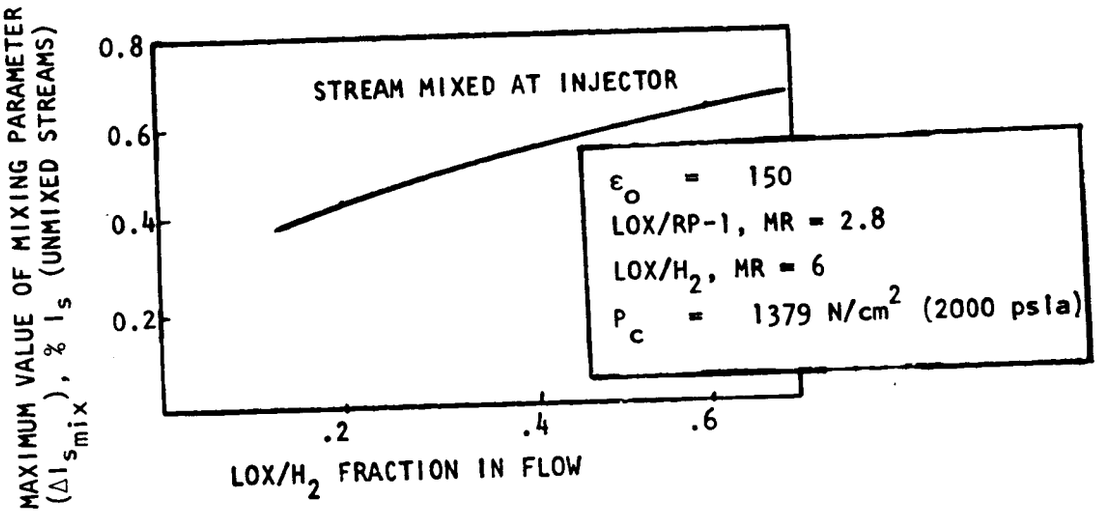

Figure 3. Split-Combustor Linear Engine

Other assumptions made in generating theoretical split-combustor linear engine performance are indicated in Table 2. The thrust split at seal level (a known parameter) is assumed equal to the combustor thrust split in vacuum at the throat plane. This assumption enables calculations of the flowrate split between combustors without iteration and with an error between 0.1 and 0.5 percent. Calculation of the flowrate split allows calculation of the specific impulse.

The characteristic velocity for the composite flow is calculated as the weight-flow average of the individual stream characteristic velocities. This is possible because at the throat of the combustors the individual stream thrust coefficients differ by approximately 0-0.1 percent and can be assumed equal.

Theoretical split-combustor linear engine performance was calculated for the propellant combinations and conditions indicated in Table 3, and are presented in Fig. 4 through 8. Since performance is a function of thrust split, data for thrust splits of 0.5 and 0.8 are presented also. Performance data are presented for Mode 1 operation and Mode 2 operation. Data are plotted for every 6.89 x 10^6 N/m^2 (1000 psia). Mode 1 expansion area ratio range is 20 to 100 and Mode 2 expansion area ratio range is 100 to 300.

Theoretical Sea-Level Specific Impulse

The theoretical split-combustor linear engine performance at sea level was calculated using assumptions presented in the previous section for the four propellant combinations of Table 3. The maximum theoretical sea level performance is presented in Fig. 9 through 12 as a function of chamber pressure.

ORIGINAL PAGE IS OF POOR QUALITY

TABLE 2. SPLIT COMBUSTOR ENGINE PERFORMANCE ASSUMPTIONS

Thrust split $\left(F_O/F_T\right)_{\text{Sea Level}}$	$= \left(\frac{F_O}{F_T}\right)_{\substack{\text{VAC} \\ \varepsilon=1}}$
Flow split $\left(\dot{w}_O/\dot{w}_I\right)$	$= \left(\frac{F_O}{F_I} \times \frac{I_{s_I}}{I_{s_O}}\right)_{\substack{\text{VAC} \\ \varepsilon=1}}$
Specific Impulse, I_s	$= \frac{\dot{W}_I}{\dot{W}_I+\dot{W}_O} I_{s_I} + \frac{\dot{W}_O}{\dot{W}_I+\dot{W}_O} I_{s_O}$
Characteristic Velocity, c*	$= \frac{\dot{W}_I}{\dot{W}_I+\dot{W}_O} c^*_I + \frac{\dot{W}_O}{\dot{W}_I+\dot{W}_O} c^*_O$
Thrust Coefficient, C_F	$= \left[\frac{I_s\, g}{c^*}\right]$

TABLE 3. SPLIT COMBUSTOR LINEAR AEROSPIKE CONCEPTS

Engine Concept No.	Sea Level Thrust, Newtons (pounds)	F_o/F_T Thrust Split $\left(\frac{\text{Outer Chamber}}{\text{Total}}\right)$	Outer Chamber		Inner Chamber	
			Propellant Combination	Mixture Ratio (o/f)	Propellant Combination	Mixture Ratio (o/f)
1	20×10^6 (4.5×10^6)	0.65	O_2/RP-1	2.8	O_2/H_2	7.0
2	20×10^6 (4.5×10^6)	0.65	O_2/RJ-5	2.7	O_2/H_2	7.0
3	20×10^6 (4.5×10^6)	0.65.	O_2/CH_4	3.5	O_2/H_2	7.0
4	20×10^6 (4.5×10^6)	0.65	O_2/H_2	7.0	O_2/H_2	7.0

Engine Operations Conditions:

Mode 1: Outer Thrust Chamber On
Inner Thrust Chamber On

Mode 2: Outer Thrust Chamber Off
Inner Thrust Chamber On

Propellants enter engine at NBP

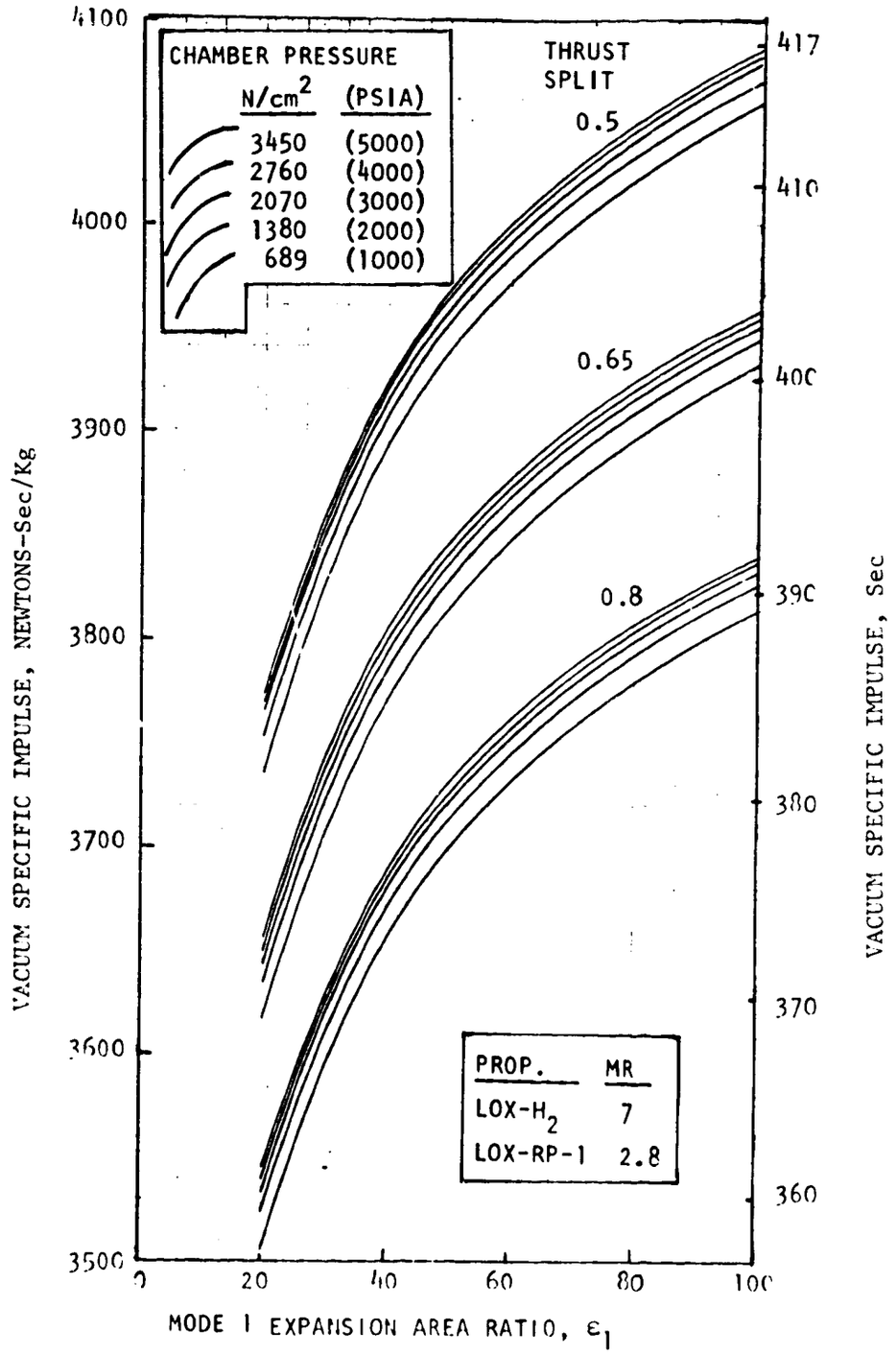

Figure 4. Linear Engine Theoretical Vacuum Specific Impulse, LOX-RP-1/LOX-H_2

ORIGINAL PAGE IS
OF POOR QUALITY

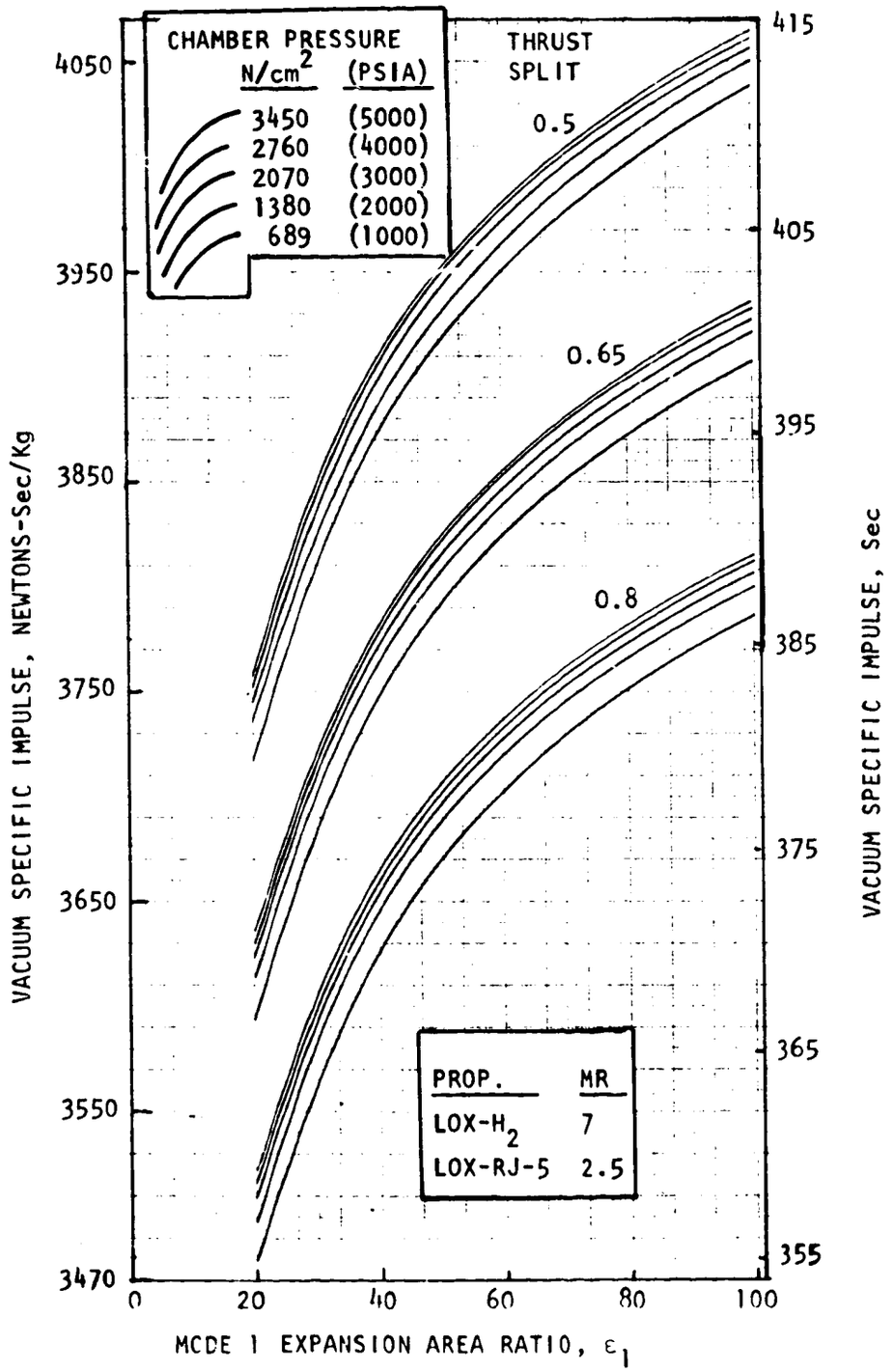

Figure 5. Linear Engine Theoretical Vacuum Specific Impulse, LOX/RJ-5/LOX-H_2

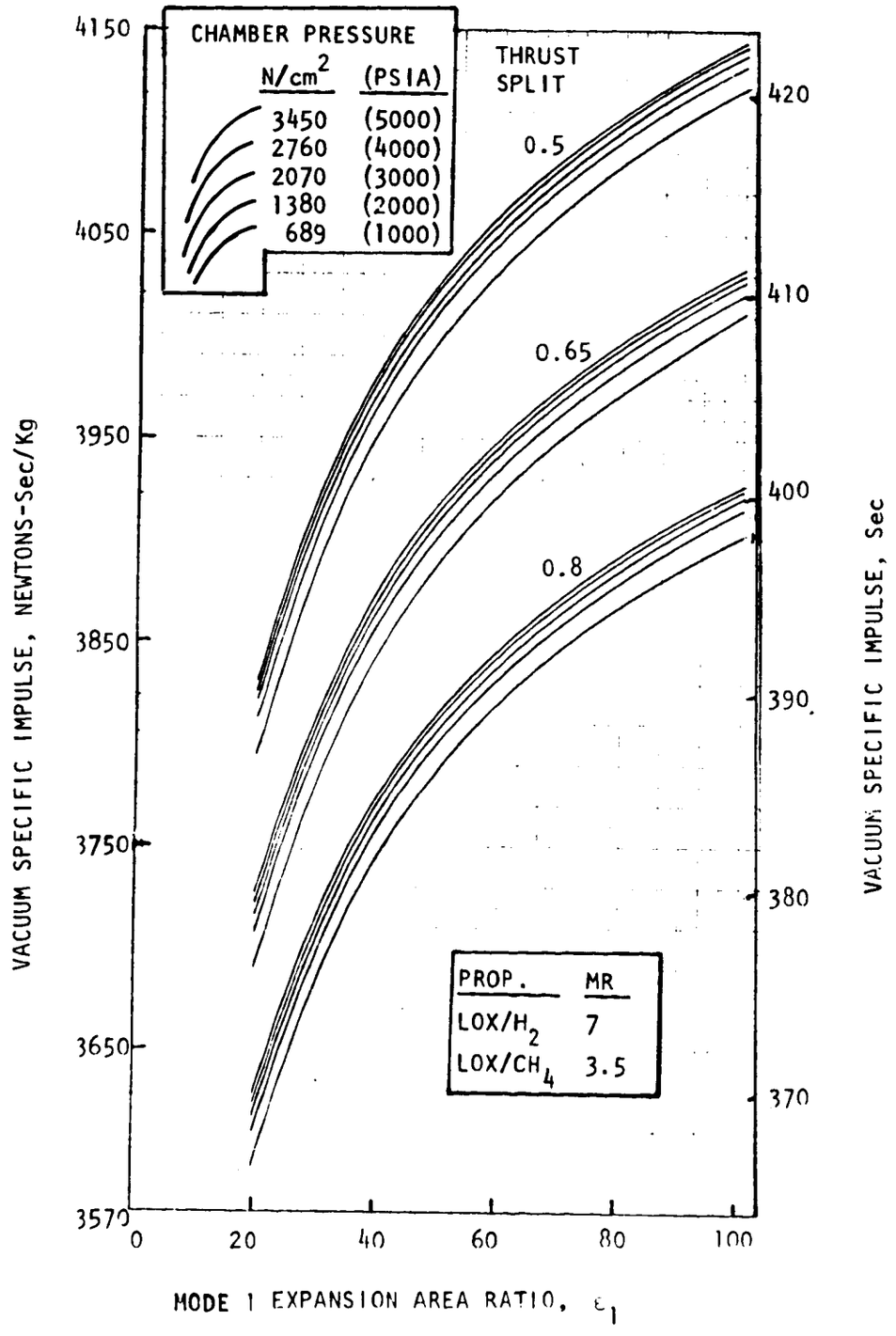

Figure 6. Linear Engine Theoretical Vacuum Specific Impulse, $LOX-CH_4/LOX-H_2$

ORIGINAL PAGE IS
OF POOR QUALITY

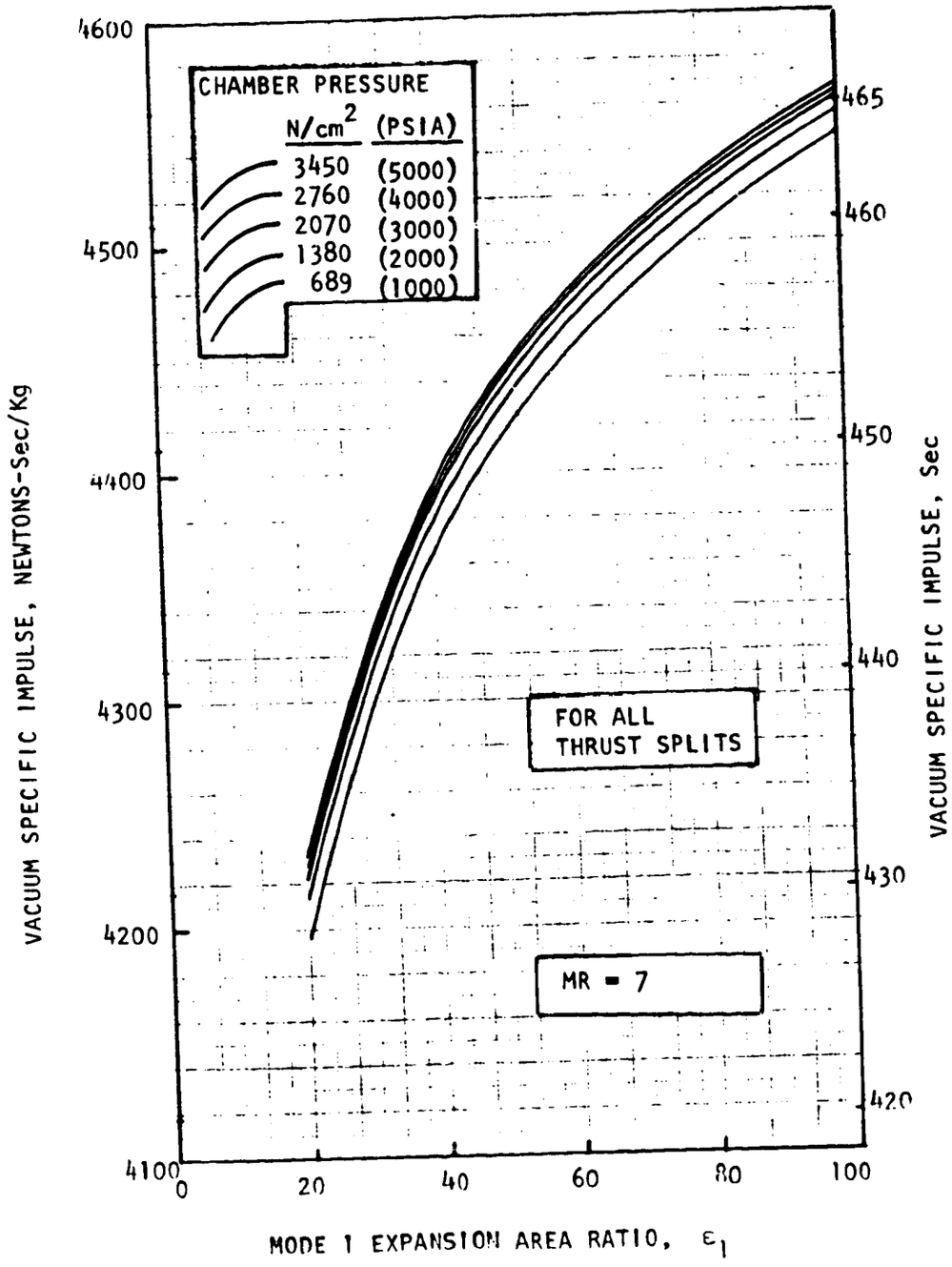

Figure 7. Linear Engine Theoretical Vacuum Specific Impulse, $LOX-H_2/LOX-H_2$

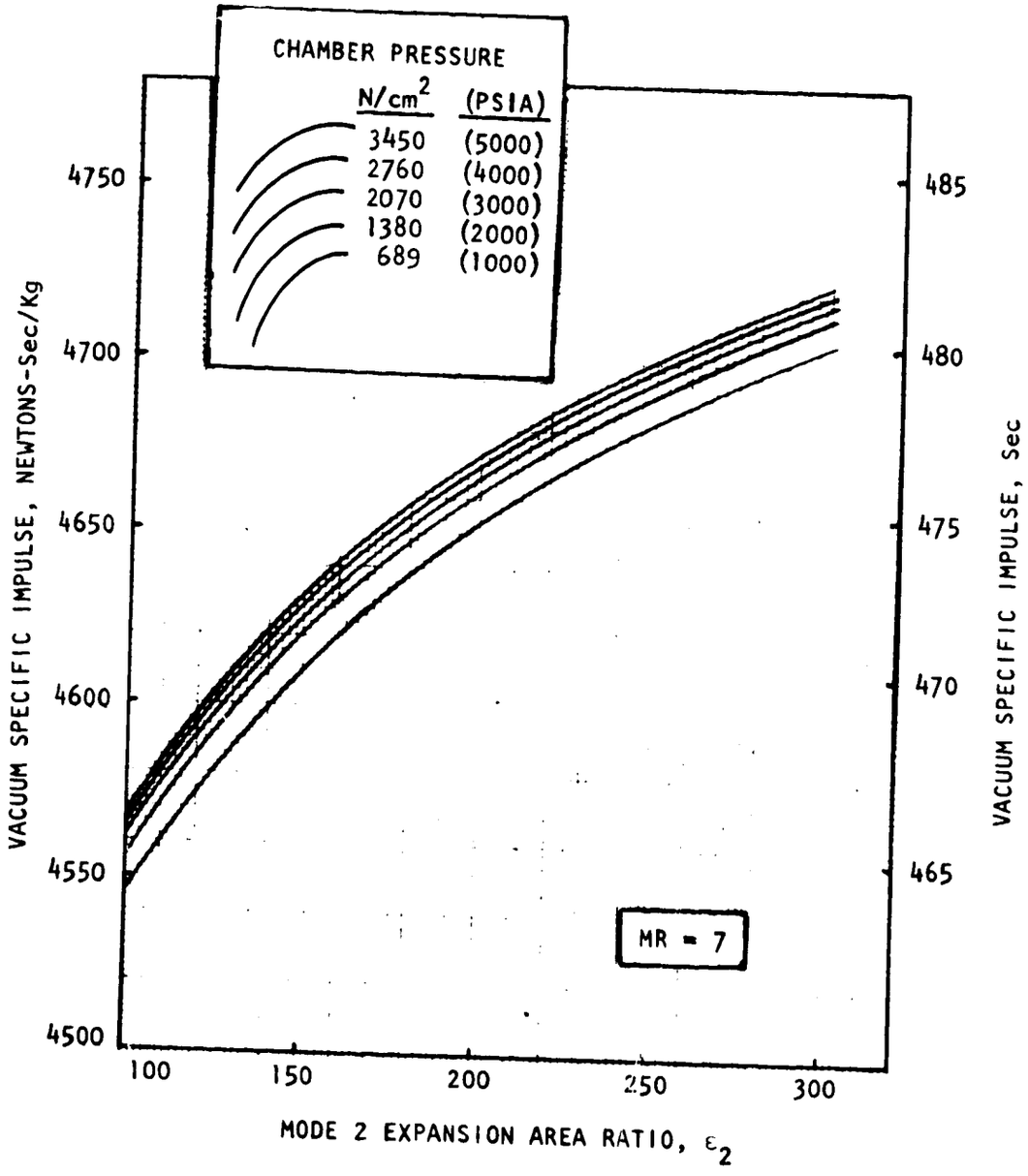

Figure 8. LOX/H_2 Inner Combustor Theoretical Vacuum Specific Impulse

ORIGINAL PAGE IS
OF POOR QUALITY

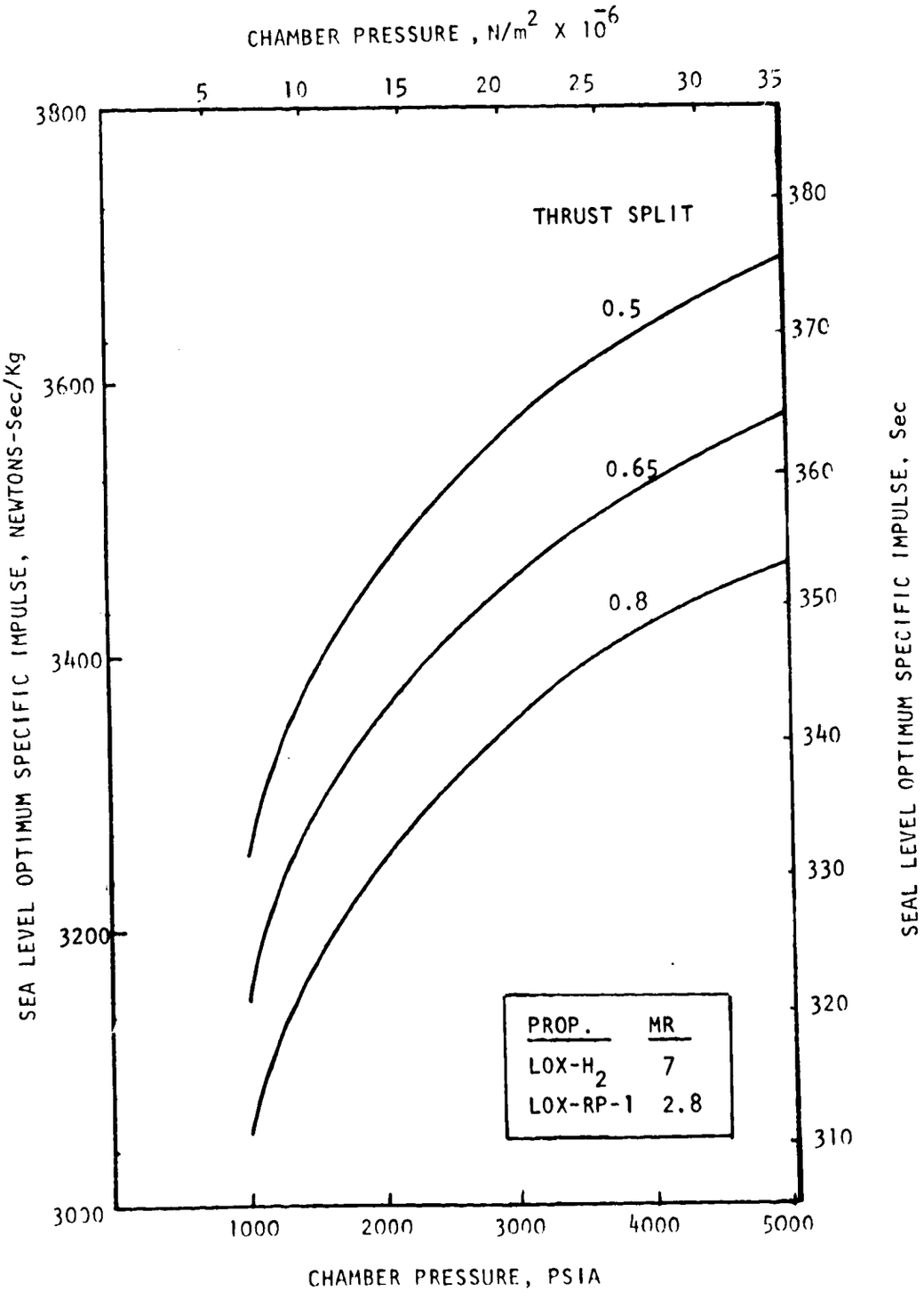

Figure 9. Linear Engine Sea-Level Optimum Theoretical Specific Impulse, LOX-RP-1/LOX-H_2

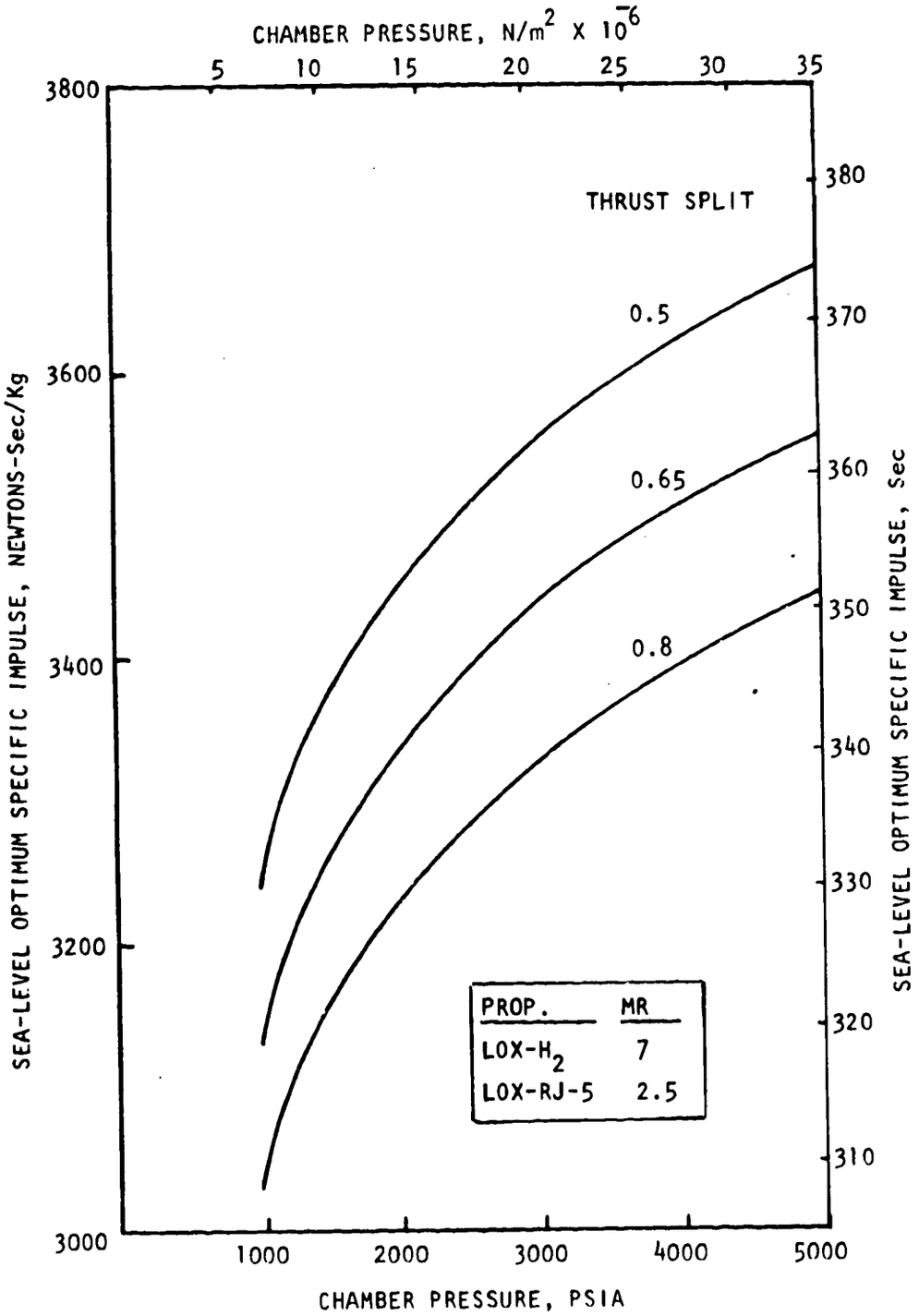

Figure 10. Linear Engine Sea-Level Optimum Theoretical Specific Impulse, LOX-RJ-5/LOX-H_2

ORIGINAL PAGE IS OF POOR QUALITY

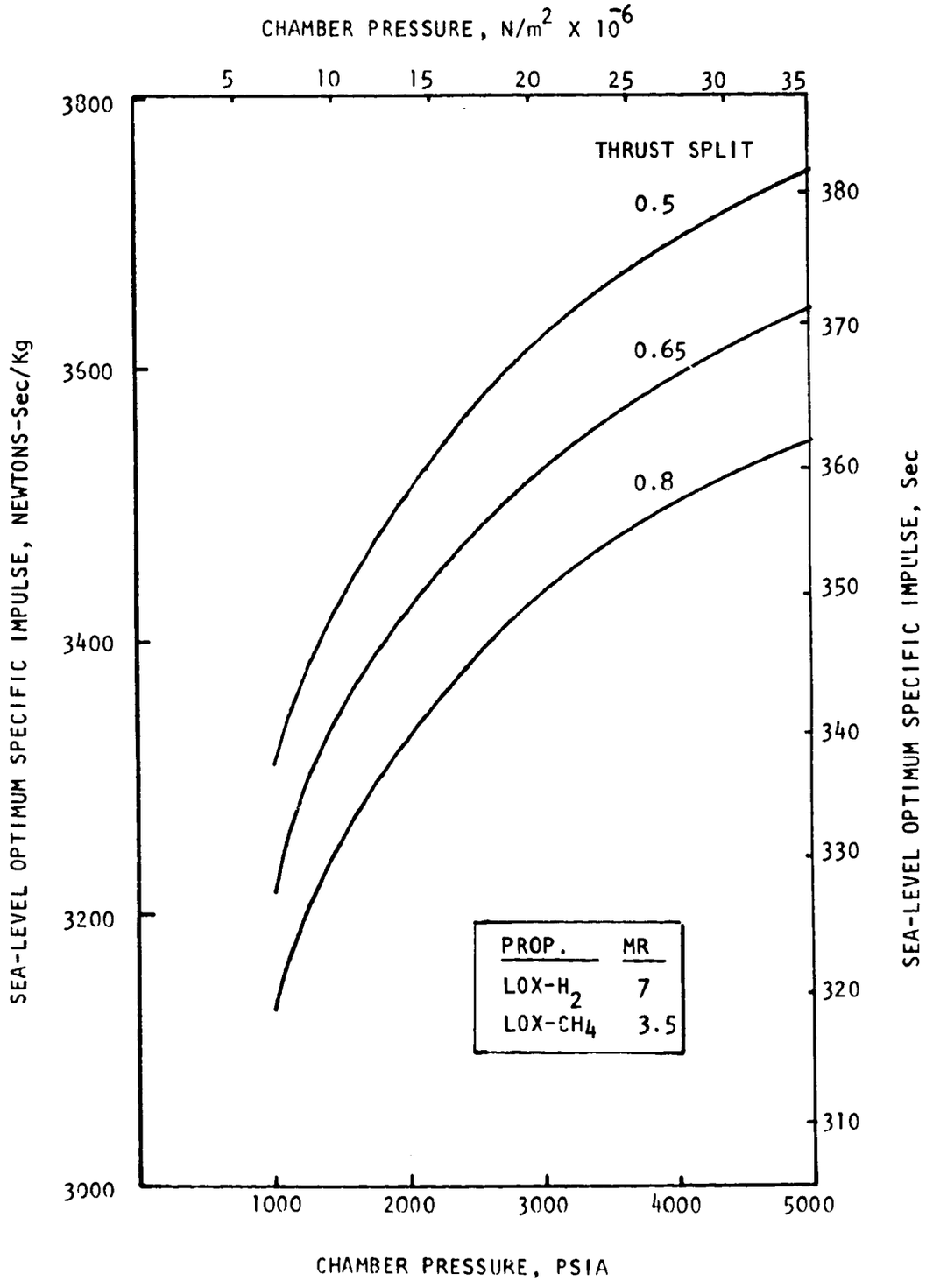

Figure 11. Linear Engine Sea-Level Optimum Theoretical Specific Impulse, LOX-CH_4/LOX-H_2

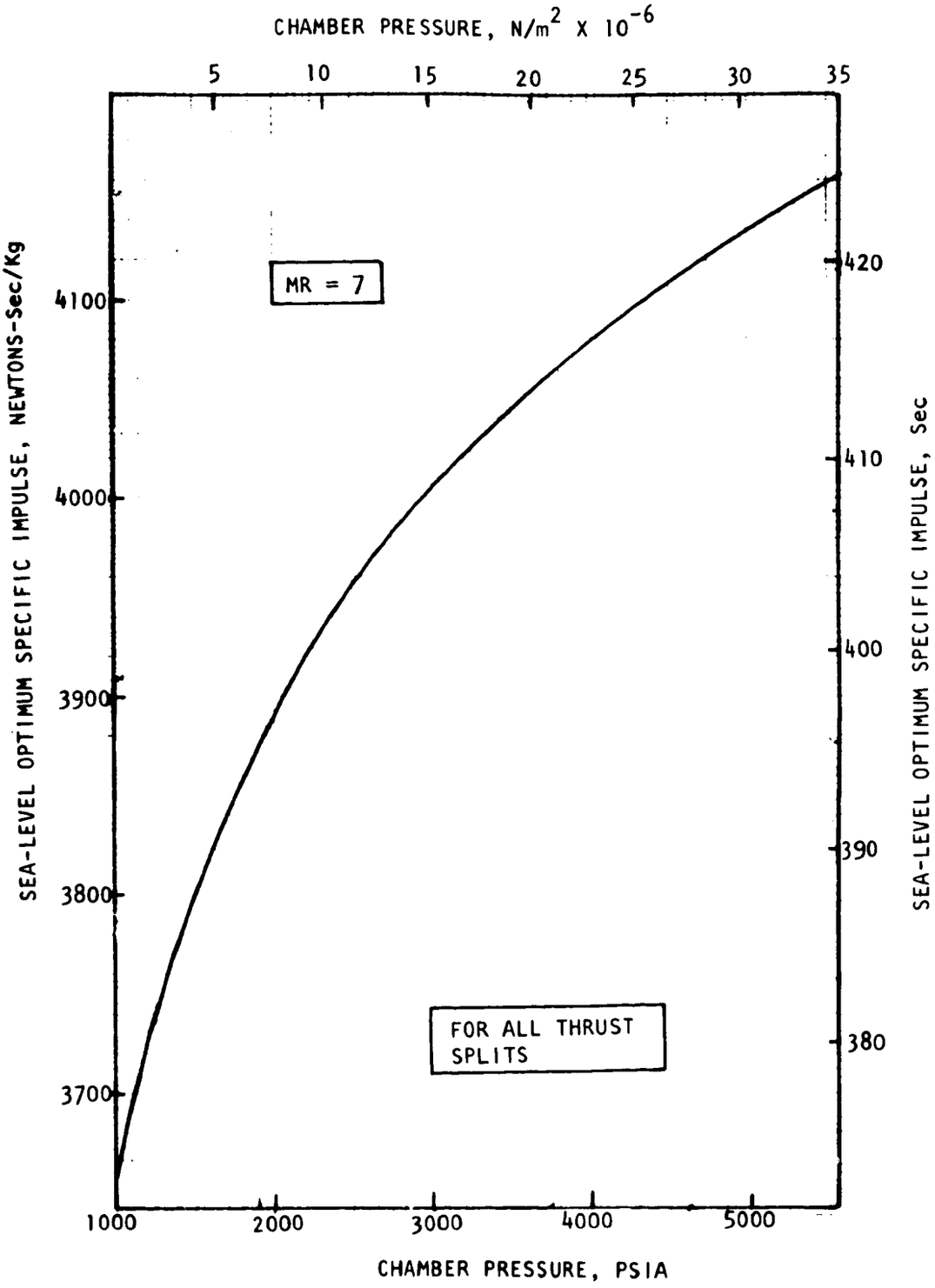

Figure 12. Linear Engine Sea-Level Optimum Theoretical Specific Impulse, $LOX-H_2/LOX-H_2$

ORIGINAL PAGE IS OF POOR QUALITY

TASK II: ENGINE MODULE SELECTION

The Task II effort was to conduct parametric analyses to establish the number of engine modules to be utilized in the linear aerospike engine concepts. An engine module is defined as a split combustor thrust chamber assembly, a turbomachinery set, a controller, and one expansion surface of the truncated two-dimensional spike nozzle. An opposite module is required to complete the nozzle; the base closure is shared by two modules. As a result of the design approach, the complete engine consists of an even number of modules.

The propellant combination, engine power cycle, and engine cooling method did not have an apparent effect on the trends in engine performance, weight, or other factors considered in selecting the number of modules. Operating chamber pressure also did not affect the selection of the number of modules.

To aid in the module selection process, two basic engine schematics were defined. The gas generator power cycle schematic (Fig. 13) and the staged combustion power cycle schematic (Fig. 14) indicate the pump, turbine, turbine power source, combustors, valves, and propellant flow paths. Each module in the engine has four main pumps, four boost pumps, four preburners or gas generators (GG), a controller, and all necessary valves and lines. The number of pumps and preburners (or GG's) was selected to meet a requirement of 50 percent thrust throttling per combustor to provide differential throttling for TVC. There did not appear to be any difference between cycles in their effect on selecting the optimum number of modules. As a result, the gas generator cycle was used as the basis of evaluation in this task.

The Task II effort concluded with a recommendation to NASA that four modules be selected for the baseline design. The recommendation was based on the trends in engine performance, relative turbomachinery weight, relative engine weight, and vehicle acceleration control as a function of the number of engine modules. Four modules minimize the engine weight and maintain a higher engine performance level. For the thrust splits of the study, four modules do not require an excessive degree of throttling to achieve required acceleration control.

Mode 1 expansion area ratio was selected at a value of 40:1 for the Task II baseline engine. Mode 2 expansion area ratio is presented in Table 4 as a function of Mode 1 area ratio and engine thrust split. For the baseline thrust split of 0.65, the Mode 2 area ratio is 114:1 for the baseline Mode 1 area ratio. The impact of the selected baseline area ratio is investigated in the parametric studies of Task V, described in a following section of this report.

Key dimensions for a linear engine at the baseline thrust level of 20×10^6 N (4.5×10^6 lbf) at sea level, baseline engine width-to-nozzle height ratio of 4 and a mid-range value of chamber pressure 1720 N/cm^2 (2500 psia) are: width of 9.2 meters (362.2 in.), length of 1.63 m (64.2 in.), and height of 2.96 m (116.6 in.). The throat gaps (Table 5) for the inner and outer combustors for the 0.65 thrust split are sufficiently large to avoid any fabrication problems.

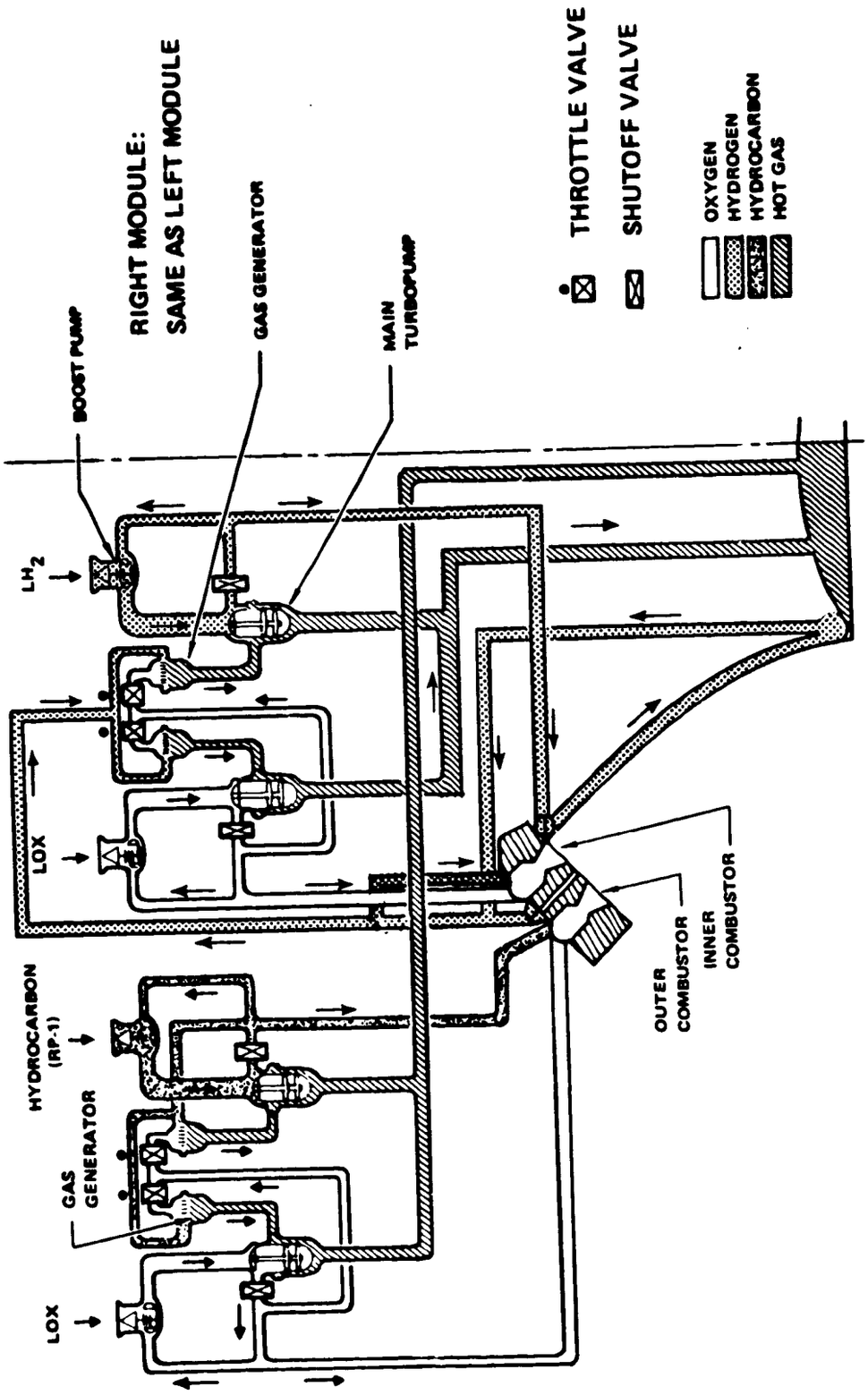

Figure 13. Gas Generator Power Cycle

ORIGINAL PAGE IS
OF POOR QUALITY

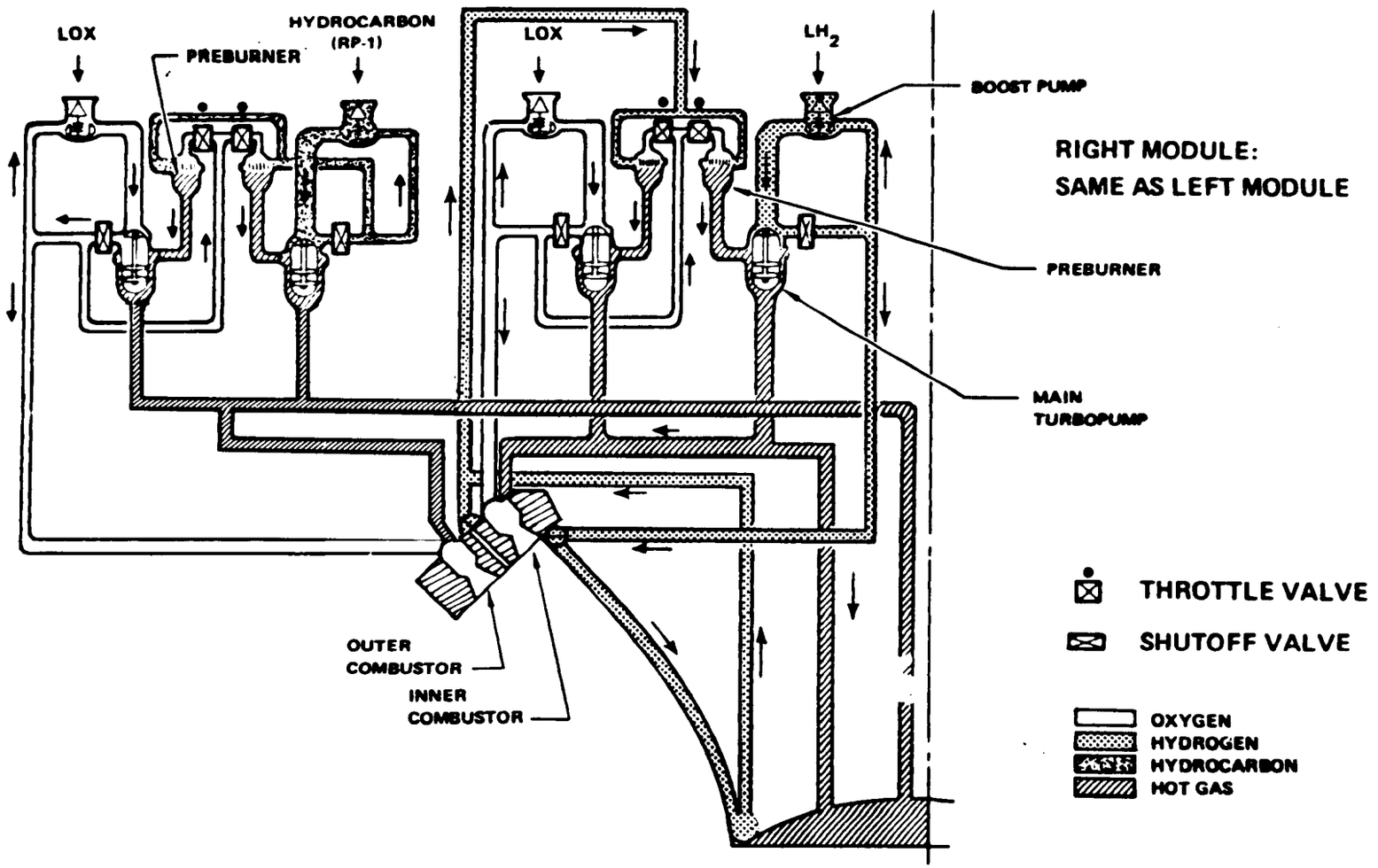

Figure 14. Staged Combustion Power Cycle

TABLE 4. AREA RATIO RELATIONSHIP

ε_1 Mode 1 Area Ratio	F_o/F_T Thrust Split	ε_2 Mode 2 Area Ratio
40	0.5	80
	0.65	114
	0.8	200
60	0.5	120
	0.65	171
	0.8	300

TABLE 5. COMBUSTOR THROAT GEOMETRY

Aerodynamic Throat Area

Outer Combustor = 0.439 m^2 (680 $in.^2$)

Inner Combustor = 0.236 m^2 (366 $in.^2$)

Throat Gap

Outer Combustor = 2.11 cm (0.83 in.)

Inner Combustor = 1.14 cm (0.45 in.)

ORIGINAL PAGE IS OF POOR QUALITY

MODULE THRUST

As a part of the evaluation leading to selection of the baseline number of modules, the module thrust level was calculated (Table 6). At the minimum number of modules, the outer combustor thrust level is about 6.5×10^6 N (1.46×10^6 lbf) compared to the inner combustor thrust level of 3.5×10^6 N (0.787×10^6 lbf). Combustor thrust levels are low for a total number of modules equal to 10. The thrust level of the inner combustor for four modules is approximately equal to the thrust level of the oxygen/hydrogen Space Shuttle Main Engine (SSME) being developed for NASA. Components from the SSME may be directly applicable to the inner combustor for the staged combustion power cycle.

Module propellant flowrates for the O_2/RP-1-O_2/H_2 and O_2/H_2-O_2/H_2 propellant combinations, Fig. 15 and 16, respectively, were calculated to aid in defining the turbomachinery. Flowrates for RJ-5 and CH_4 systems are presented in Fig. 17 and 18 to indicate the relatively small influence of hydrocarbon fuel on module selection.

PERFORMANCE

The effect of the number of modules on engine performance is shown in Fig. 19 for a gas generator cycle. Engine performance decreases approximately 9 N-sec/kg (1 sec) when the number of modules is increased from 2 to 10. This is the result of the turbomachinery efficiencies which decrease as the size of the pumps decrease. For fixed thrust, the number of pumps increases as number of modules increases, thus decreasing pump size, and increasing pump boundary layer inefficiency effects.

WEIGHTS

Preliminary turbomachinery weights were calculated as a function of the number of modules. The reference for the turbomachinery weight calculations was the SSME turbomachinery weight. The variations with chamber pressure and engine coolant fluids are indicated in the graphical display of Fig. 20 and 21. The coolant affects the turbopump discharge pressure which, in turn, affects turbopump weight. The heaviest weight is associated with all-oxygen cooling of the combustors.

The preliminary turbomachinery and engine weights presented in this section of the report were later finalized in Task IV parametrics. The weight data generated for this task were used to establish trends in weight as a function of number of modules rather than to determine absolute values.

Installed engine weights, presented in Fig. 22 and 23, increase with increasing number of modules due primarily to the "fixed" increment of weight for each module that is independent of module size. The controller and small fluid lines for such uses as purges, pressurization, etc., are contained in this "fixed" increment of weight. The curves indicate there is a chamber pressure between the limits included in the study that minimizes engine weight. A cross-plot (Fig. 24) of the weight data at six modules shows the minimum to occur at a pressure of about 18×10^6 N/m^2 (2610 psia).

TABLE 6. MODULE THRUST LEVEL

ENGINE THRUST LEVEL = 20×10^6N (4.5×10^6 lbf) @ Sea Level

THRUST SPLIT = 0.65 (Outer/Total)

	NUMBER OF MODULES				
MODULE THRUST	2	4	6	8	10
OUTER COMBUSTOR (O_2/HC or O_2/H_2)	$6.5X10^6$N (1462K lbf)	$3.25X10^6$N (731K lbf)	$2.17X10^6$N (488K lbf)	$1.62X10^6$N (365K lbf)	$1.3X10^6$N (292K lbf)
INNER COMBUSTOR (O_2/H_2)	$3.5X10^6$N (787K lbf)	$1.75X10^6$N (394K lbf)	$1.17X10^6$N (262K lbf)	$0.87X10^6$N (197K lbf)	$0.7X10^6$N (158K lbf)

Weight data for the other propellant combinations showed similar trends with the number of modules.

MODULE THROTTLING

To aid in the selection of number of modules, the module throttling required to achieve a prescribed thrust level was investigated. Prescribed thrust levels were obtained from a vehicle acceleration profile (Fig. 25) obtained by assuming a liftoff thrust-to-weight ratio of 1.3 and a vehicle acceleration limit of 3 g. Other assumptions are shown in Fig. 25.

Throttling is performed by two processes, depending on the engine operational mode. At the completion of Mode 1, all outer combustors are shut down. During Mode 2 operation, the vehicle acceleration is controlled by shutting down some of the LOX/hydrogen combustors and throttling the remaining combustors. The number of combustors that can be shut down depends on the lateral symmetry of module cluster, i.e., two and four modules allow no throttling through shutdown of combustors. Throttling depth for the remaining combustors depends on the number that can be shut down, and on the number of modules used (Fig. 25). The extent of throttling is also a function of thrust split. The least amount of throttling occurs with eight modules for thrust splits of 0.5, 0.65, and 0.75. Up-thrusting is required for a thrust split of 0.8.

ORIGINAL PAGE IS OF POOR QUALITY

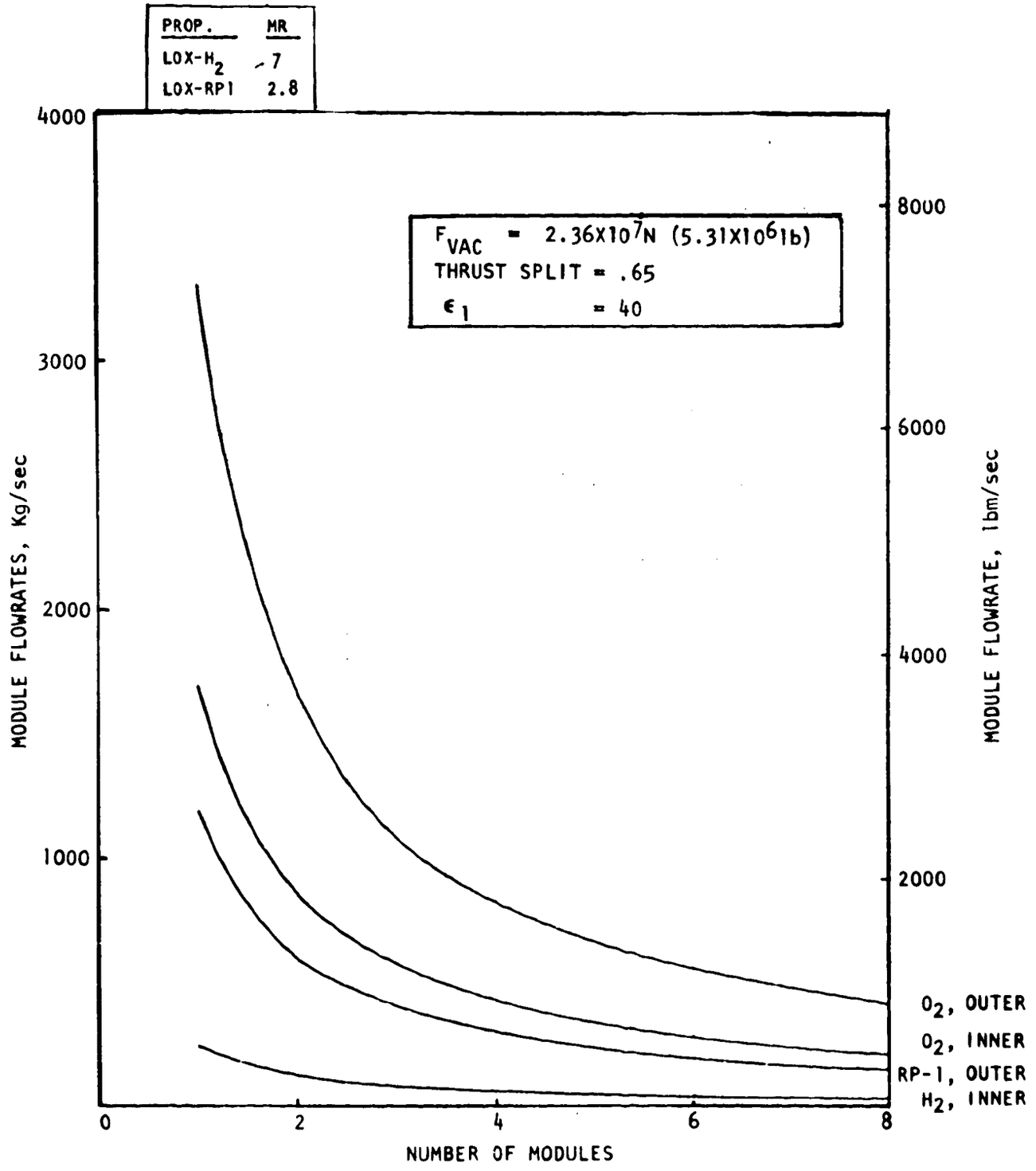

Figure 15. Linear Engine Split-Combustor Module Flowrates, LOX-RP-1/LOX-H_2

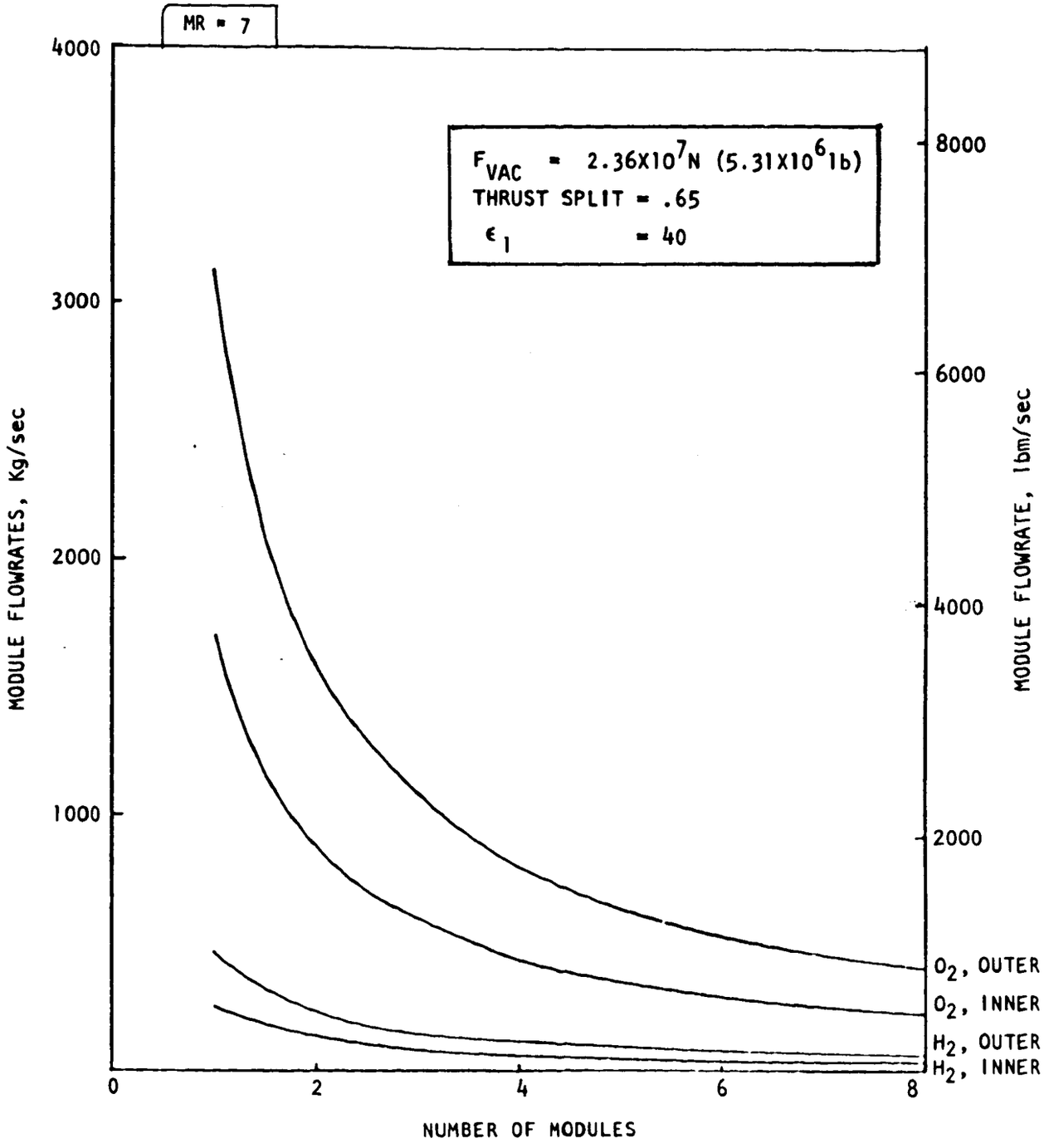

Figure 16. Linear Engine Split-Combustor Module Flowrates, LOX-H_2/LOX-H_2

ORIGINAL PAGE IS OF POOR QUALITY

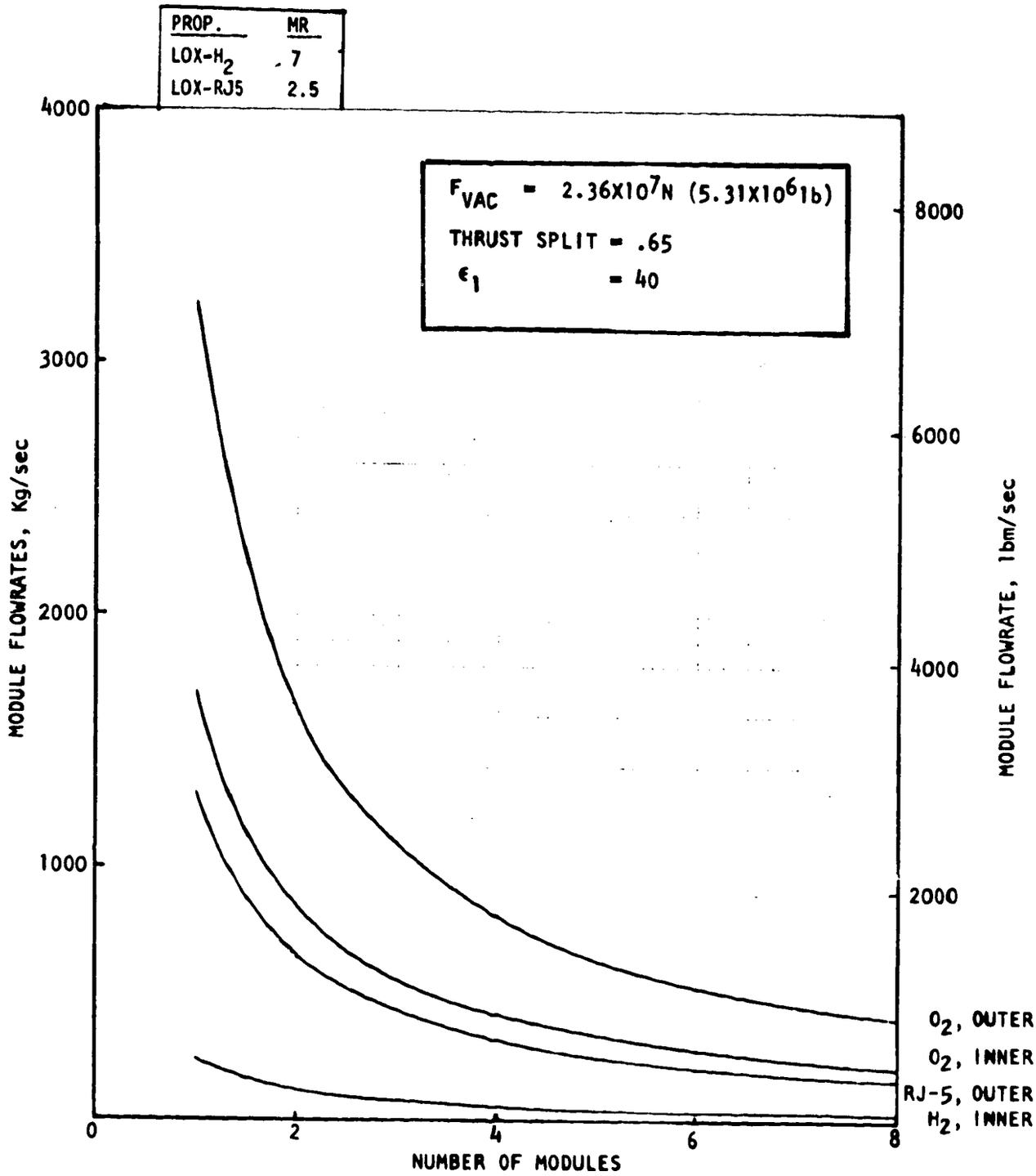

Figure 17. Linear Engine Split-Combustor Module Flowrates, LOX-RJ-5/LOX-H_2

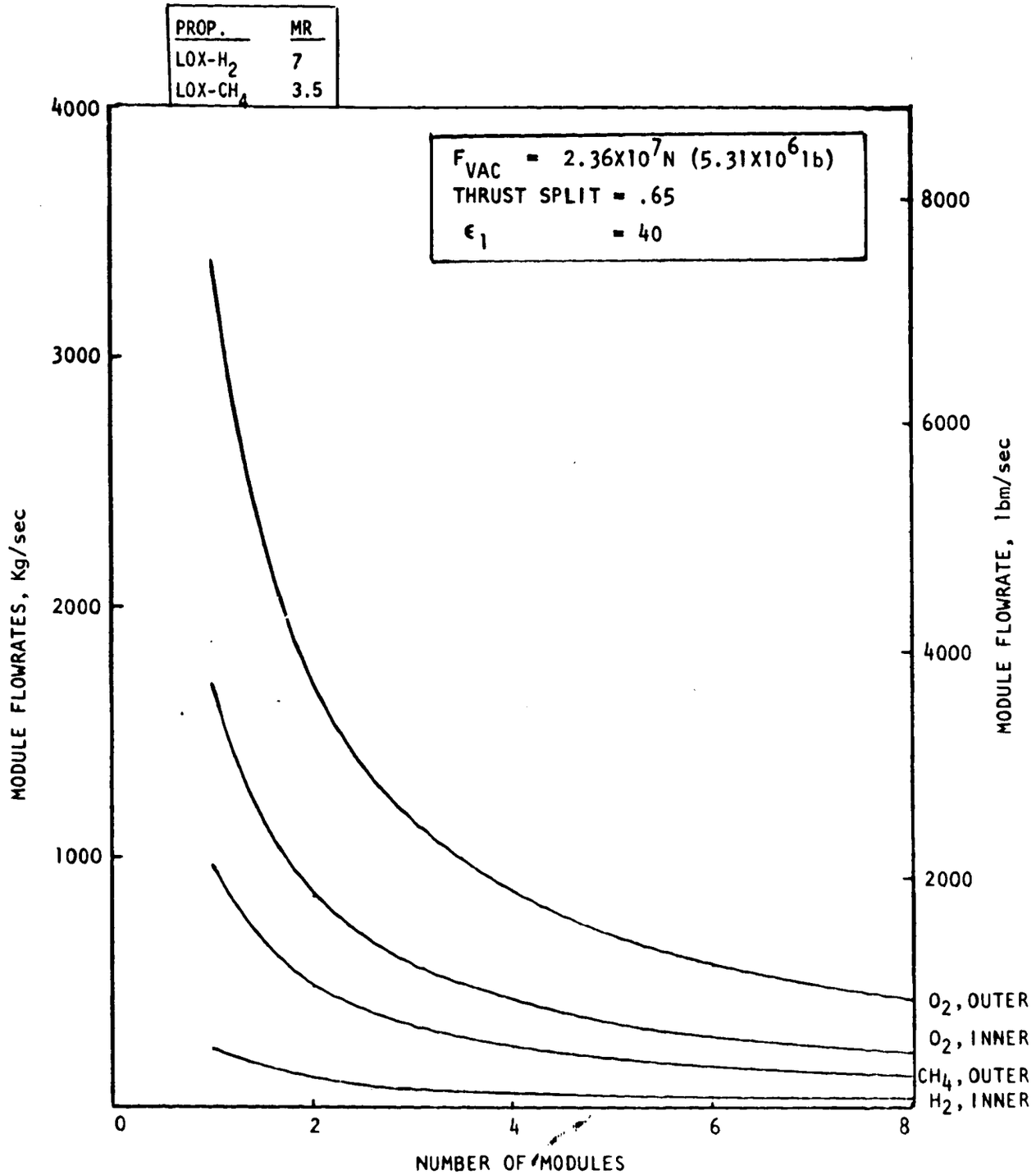

Figure 18. Linear Engine Split-Combustor Module Flowrates, LOX/CH_4/LOX-H_2

ORIGINAL PAGE IS OF POOR QUALITY

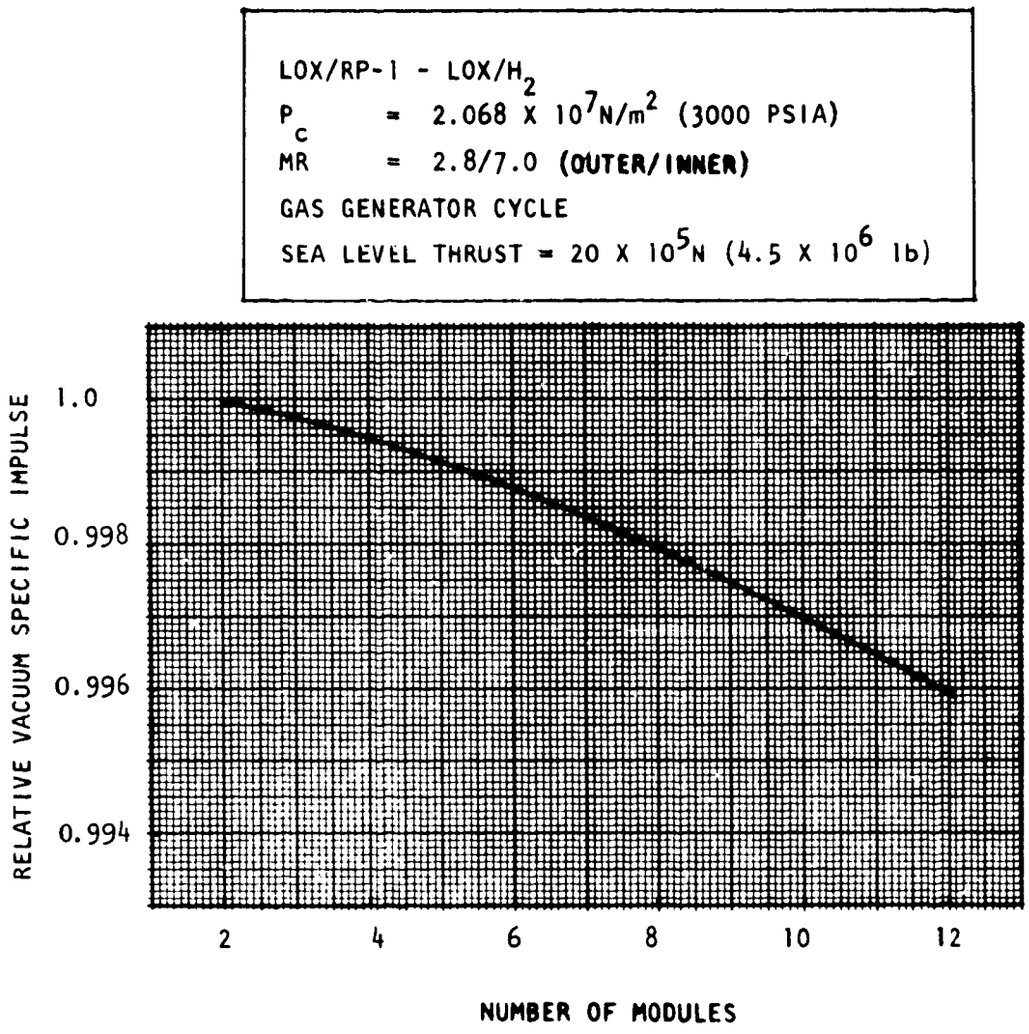

Figure 19. Linear Engine Performance as a Function of Number of Modules

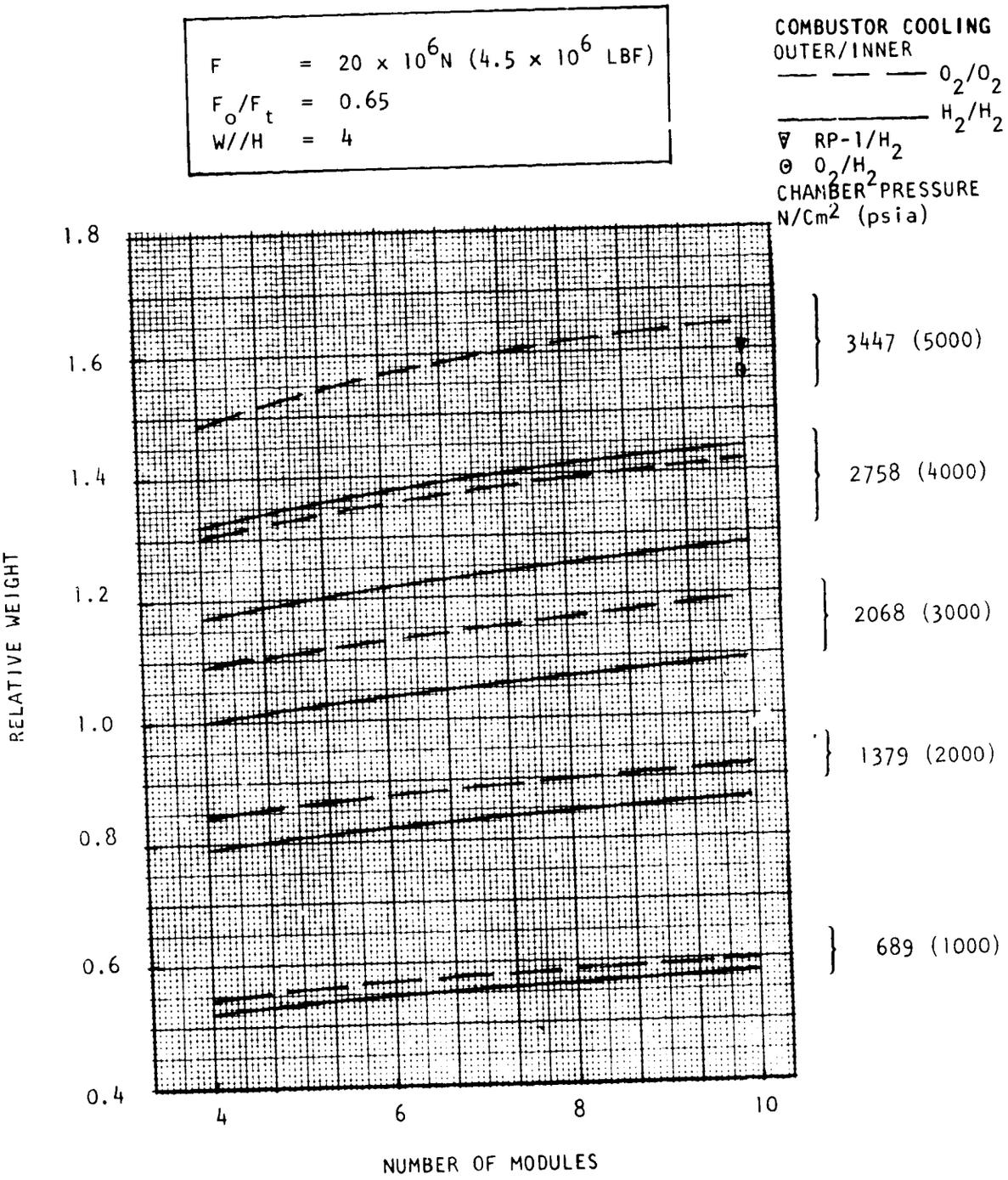

Figure 20. Relative Preliminary Turbomachinery Weight, Inner: LO_2/LH_2, **Outer: LO_2/RP-1, (RJ-5) Linear Aerospike**

ORIGINAL PAGE IS
OF POOR QUALITY

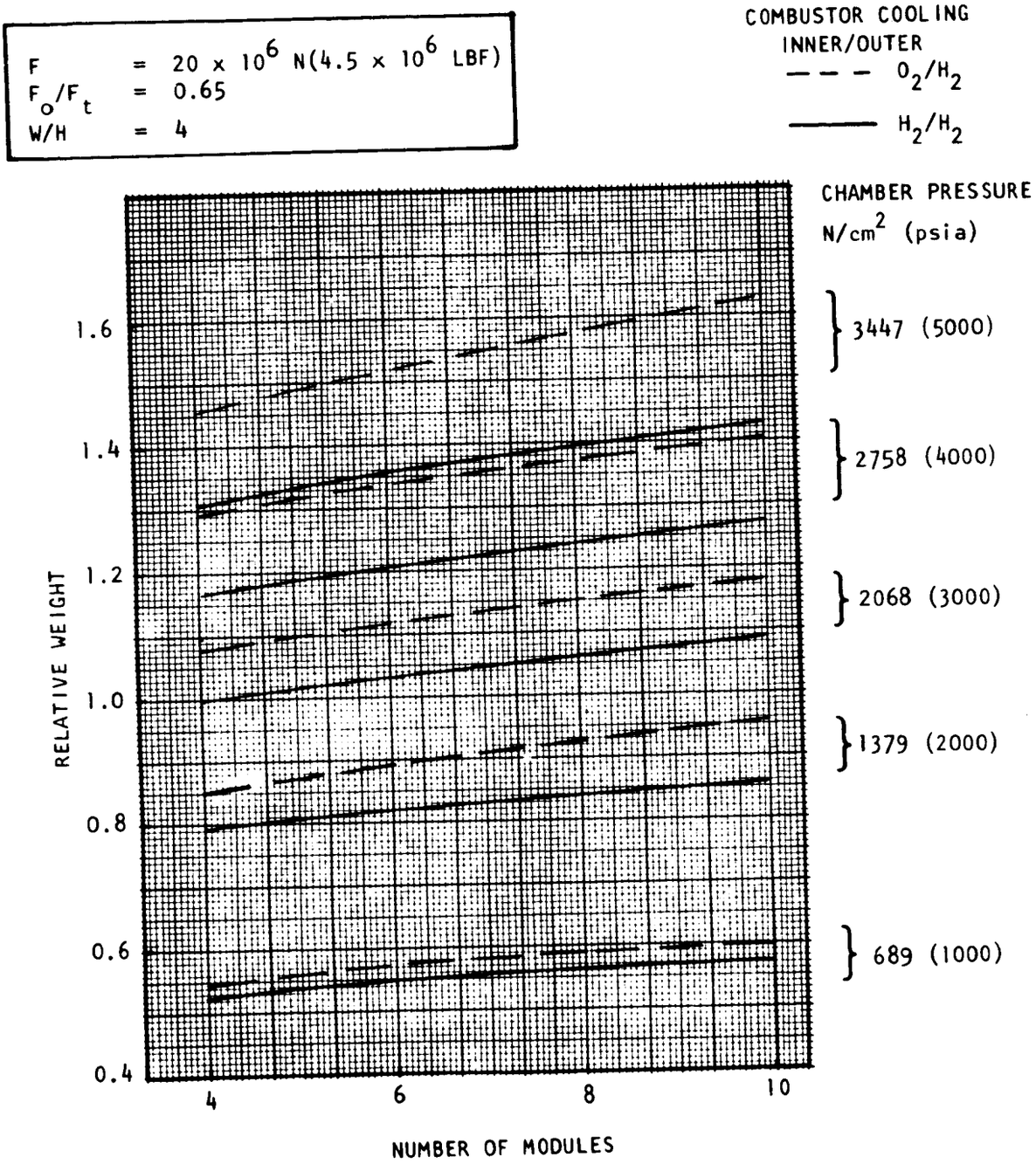

Figure 21. Relative Turbomachinery Weight, Inner: LO_2/LH_2, Outer: LO_2/LH_2, Linear Aerospike

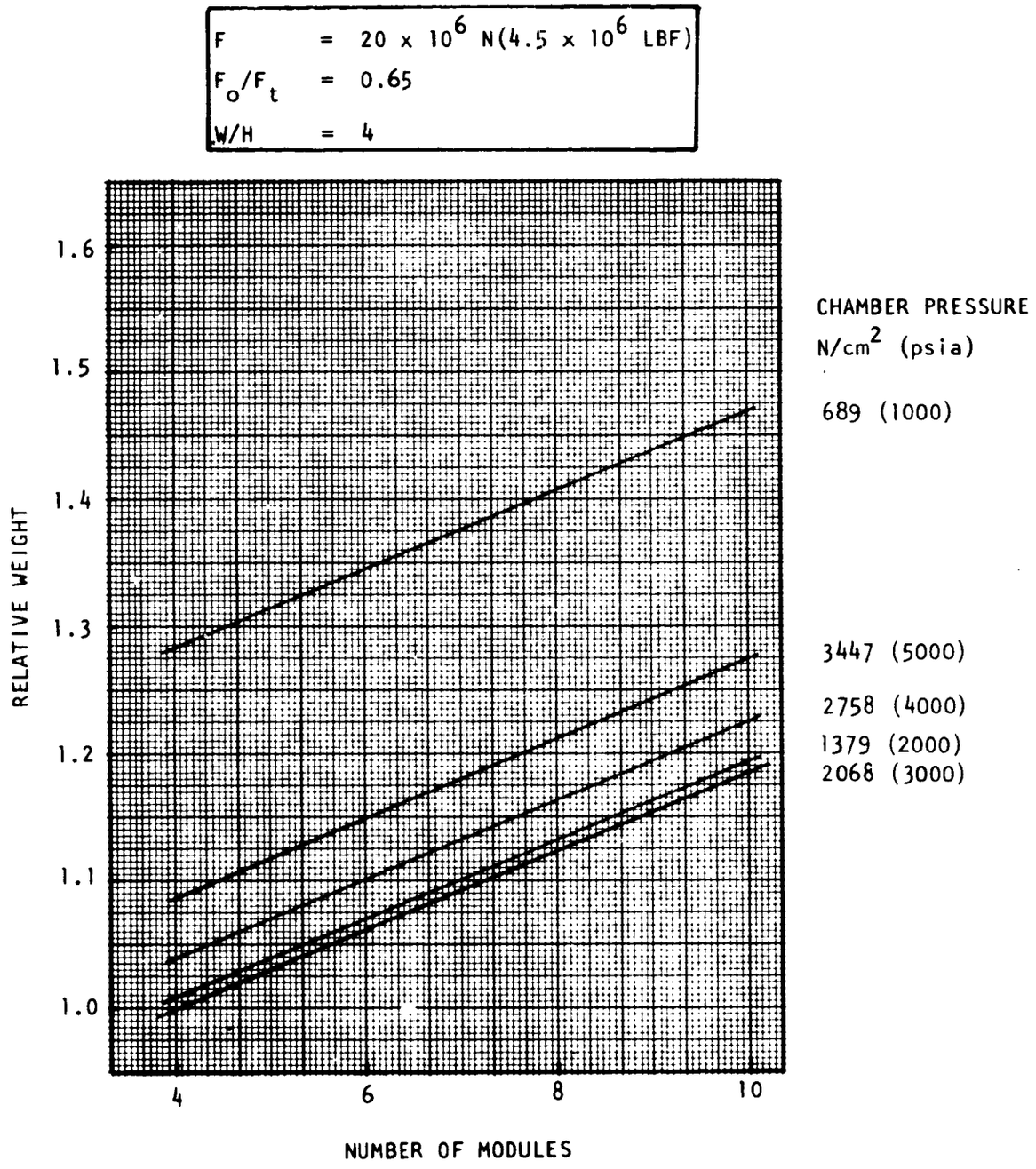

Figure 22. Relative Installed Engine Weight, Inner: LO_2/LH_2, Outer: LO_2/RP, RJ Linear Aerospike

ORIGINAL PAGE IS
OF POOR QUALITY

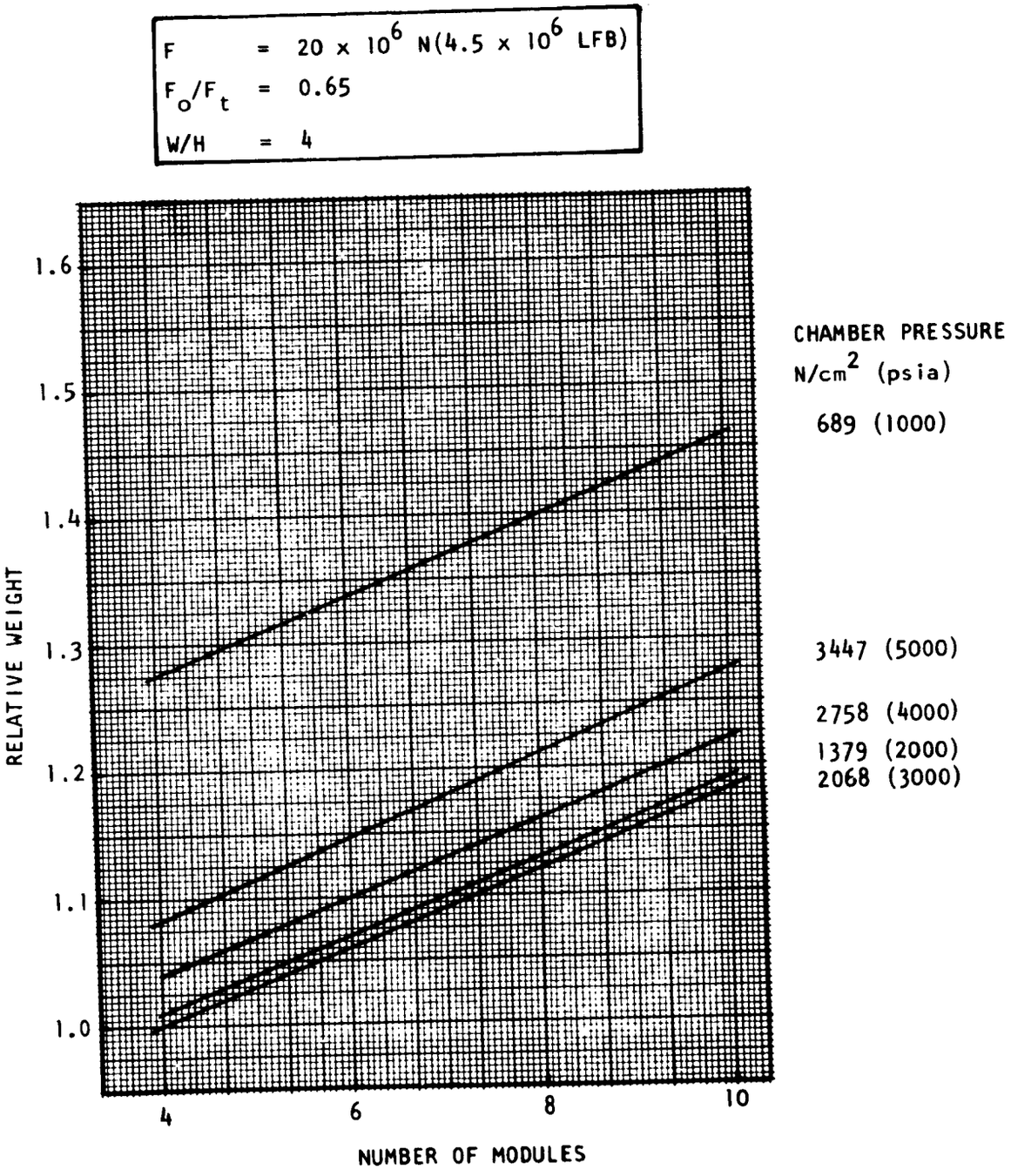

Figure 23. Relative Installed Engine Weight, Inner: LO_2/LH_2, Outer: LO_2/LH_2, Linear Aerospike

F	=	20×10^6 N (4.5×10^6 LBF)
F_o/F_t	=	0.65
W/H	=	4

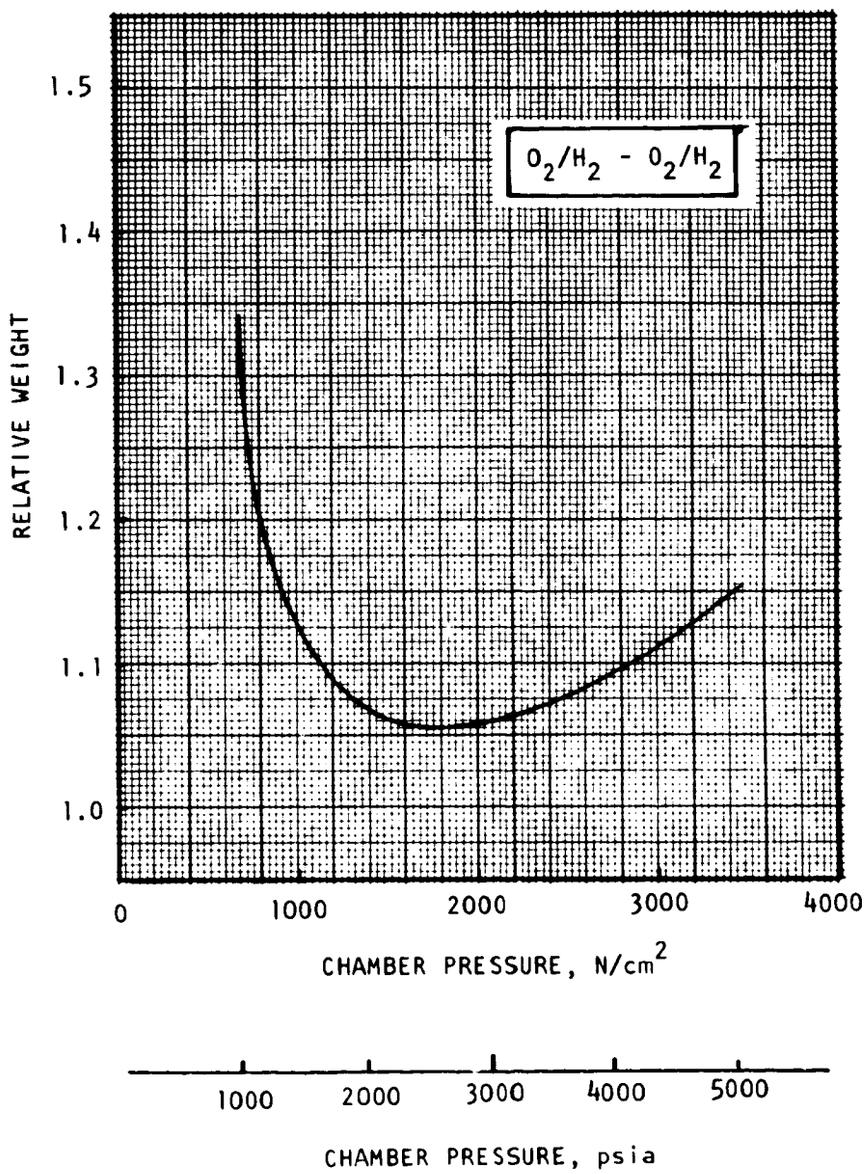

Figure 24. Relative Installed Engine Weight
Number of Modules 6 - Linear Aerospike

ORIGINAL PAGE IS
OF POOR QUALITY

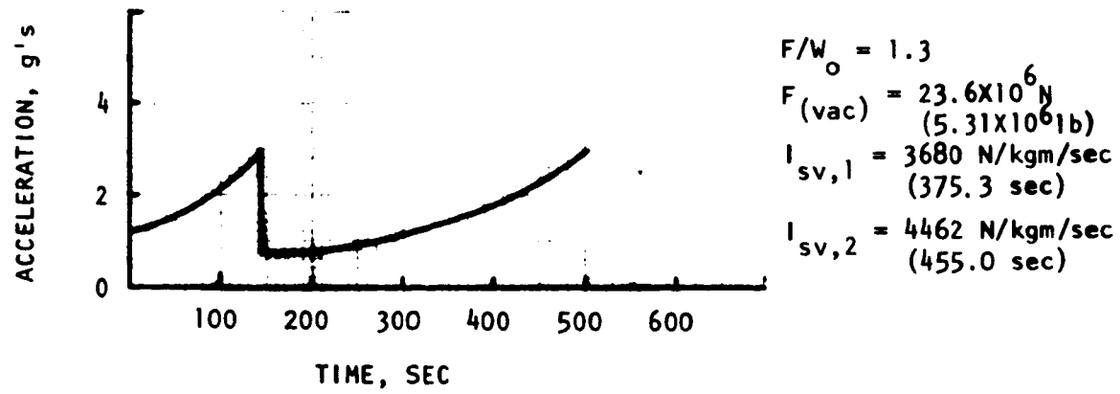

Fig. Acceleration Profile, Linear Split-Combustor Engine

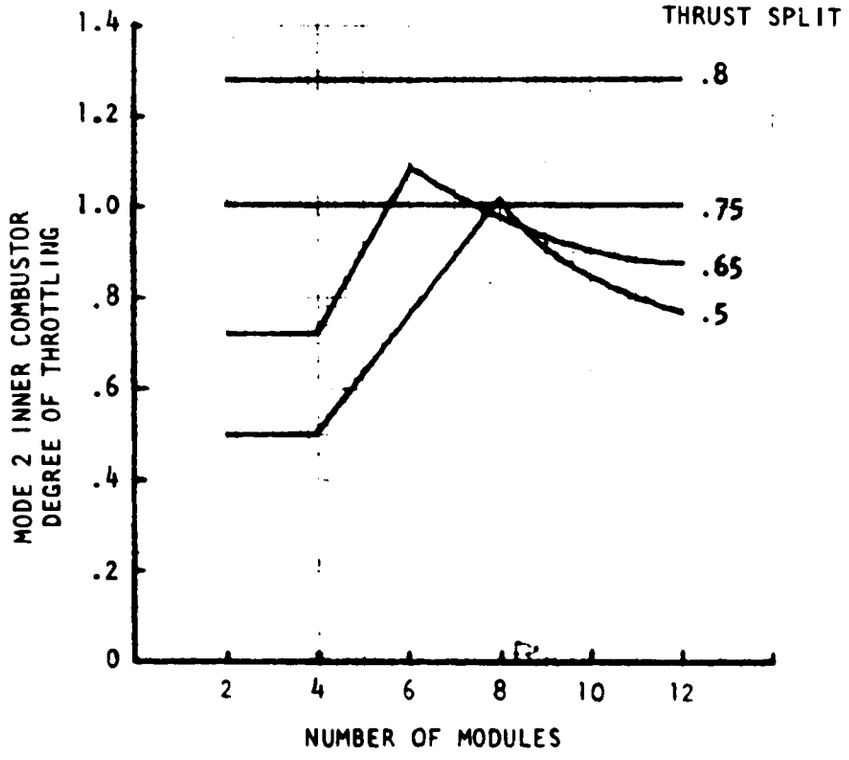

Figure 25. Throttling Requirements, Linear Split-Combustor Engine

TASK III: THRUST CHAMBER COOLING EVALUATION

This task conducted parametric analyses to determine the relative cooling capability of the propellants. Potential cooling methods and study guidelines defined by NASA used in the study are presented in Tables 3 and 7. To conduct the analysis, thrust chamber geometry and various potential cooling circuits were defined. Heat transfer analysis provided coolant flowrates, pressure loss, bulk temperature rise, hot-gas side-wall temperature and wall maximum temperature differential for a range in chamber pressures from 6.89×10^6 N/m^2 (1000 psia) to 34.5×10^6 N/m^2 (5000 psia). Low-cycle fatigue analysis determined allowable thrust chamber wall temperature corresponding to a service life of 250 cycles. Based on the results of the analyses, chamber pressure limits, thrust chamber cooling circuits, and fluids for use in the remainder of the split-combustor linear aerospike study were recommended by Rocketdyne and approved by the NASA program manager.

COOLING EVALUATION SUMMARY

The coolant circuit to provide the minimum coolant pressure drop is a parallel combustor and nozzle coolant circuit as shown in Fig. 26. The four sides of each combustor segment are cooled in a parallel uppass circuit. The nozzle is cooled with a single downpass circuit.

An outer combustor utilizing O_2/RP-1 or O_2/RJ-5 can be cooled with either fuel, oxygen from the outer combustor, or hydrogen from the inner combustor. An outer combustor using O_2/CH_4 can be cooled with either methane or hydrogen, and an O_2/H_2 combustor (inner or outer) is cooled with hydrogen.

A summary of the chamber pressure limits for the various coolant-propellant combinations is presented in Fig. 27 and 28, for coolant inlet pressures of 1.8 and 2.25 times chamber pressure, respectively. The maximum chamber pressures for cooling of the O_2/RP-1 or O_2/RJ-5 outer combustor with RP-1 or RJ-5 are 0.372×10^7 N/m^2 (540 psia) and 0.483×10^7 N/M^2 (700 psia) due to a maximum coolant-side wall temperature of 315.5 C (600 F). As indicated, the maximum chamber pressure that can be attained and still satisfy the maximum coolant-side wall temperature increases as the coolant inlet pressure to chamber pressure ratio increases. The higher coolant inlet pressure permits the use of higher coolant velocities to meet the coolant wall temperature limit. However, there is a maximum chamber pressure, 689 N/cm^2 (1000 psia), and corresponding coolant inlet pressure ($P_{inlet}/P_c = 3.5$) beyond which increases in coolant inlet pressure cannot maintain coolant side wall temperature at 315.5 C (600 F) or below. This limit on chamber pressure is defined for this study as the coking limit.

For the other coolants (O_2, CH_4, and H_2), the high cycle life (250 x 4 cycles) limits wall temperatures to approximately 468 C (890 F). This wall temperature level is not achievable at higher chamber pressures (higher heat fluxes) since the coolant flow chokes with the available coolant inlet pressure. Assuming both combustors operate at the same chamber pressure, the maximum operable chamber pressure is 1.722×10^7 N/m^2 (2500 psia) for a coolant inlet pressure of 2.25 times chamber pressure. The maximum chamber pressure decreases to 1.38×10^7 N/m^2 (2000 psia) for a coolant inlet pressure of 1.8 times chamber pressure.

ORIGINAL PAGE IS
OF POOR QUALITY

TABLE 7. COOLANT EVALUATION STUDY GUIDELINES

PROPELLANT COMBINATION	COOLANT	AVAILABLE COOLANT	COOLANT INLET TEMPERATURE, R
RJ-5/Oxygen	Oxygen	Total Flow	200
RJ-5/Oxygen	RJ-5	Total Flow	560
RP-1/Oxygen	Hydrogen	(Minimize)	110
RP-1/Oxygen	Oxygen		200
RP-1/Oxygen	RP-1	Total Flow	560
CH_4/Oxygen	Oxygen	Total Flow	200
CH_4/Oxygen	CH_4	Total Flow	200

Thrust Chamber Configuration

- Regeneratively cooled
- Inlet pressure - 2.25 times chamber pressure (staged combustion)
  1.8 times chamber pressure (gas generator)
- High heat flux portion of chamber will be of nontubular construction with the following dimensional limits:

  Minimum Slot Width = 0.03 inch
  Maximum Slot Depth/Width = 4 to 1
  Minimum Web Thickness = 0.03 inch
  Minimum Wall Thickness = 0.025 inch

- Material (nontubular portion): copper alloy (zirconium copper)
- Service free life: 250 cycles times a safety factor of 4
- Maximum Coolant Velocity

  Gas - Mach Number ≤ 0.5

- Possible benefit of carbon deposition of hot-gas side wall shall be neglected
- Coking Limit

  RP-1 and RJ-5 - Coolant $T_{wc} \leq 600F$

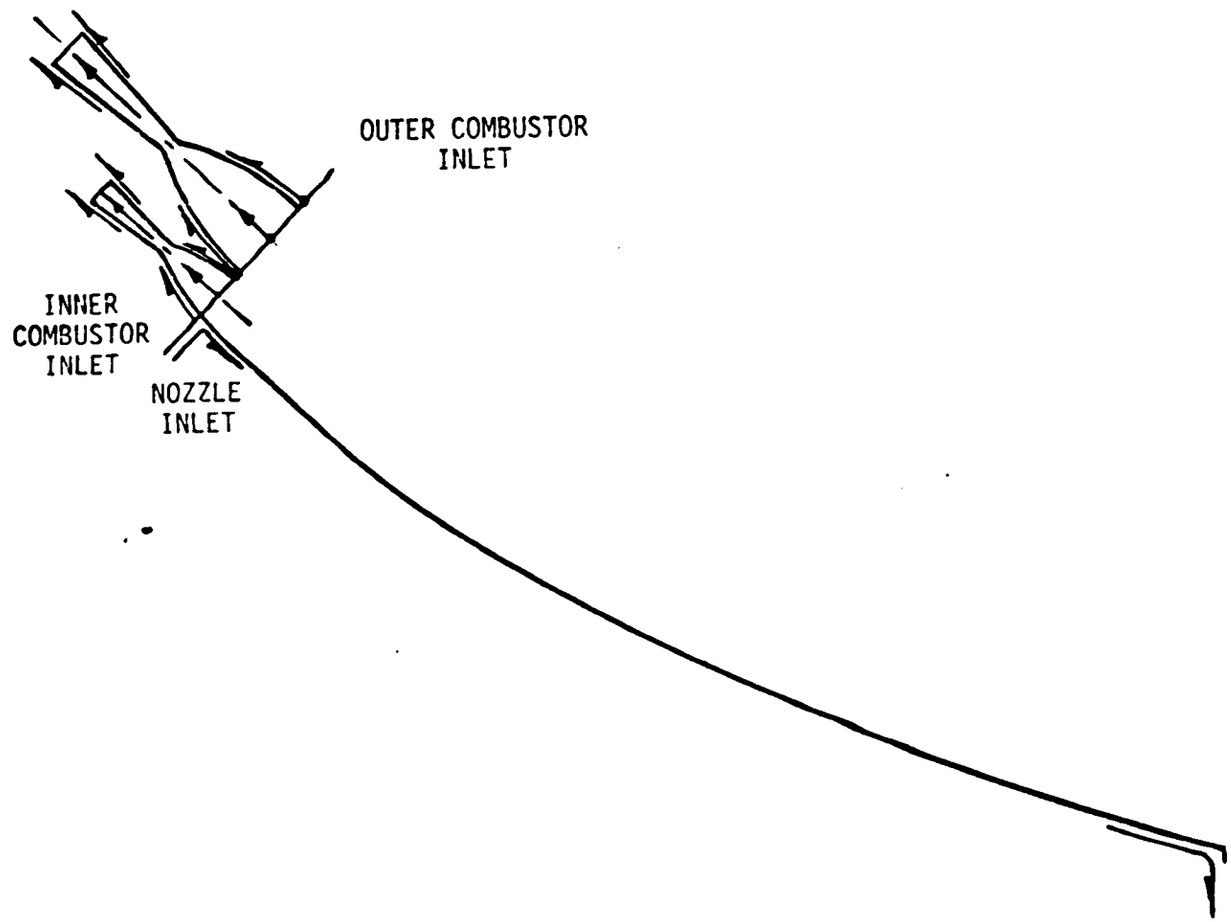

Figure 26. Parallel Combustor and Nozzle Cooling Circuit

ORIGINAL PAGE IS
OF POOR QUALITY

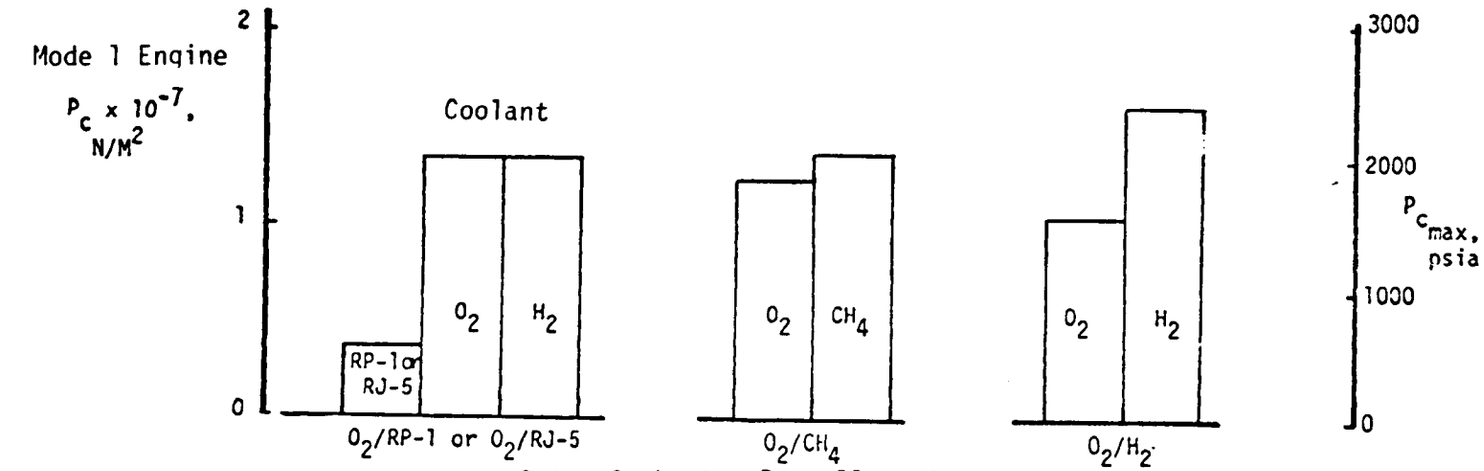

Outer Combustor Propellant Combination

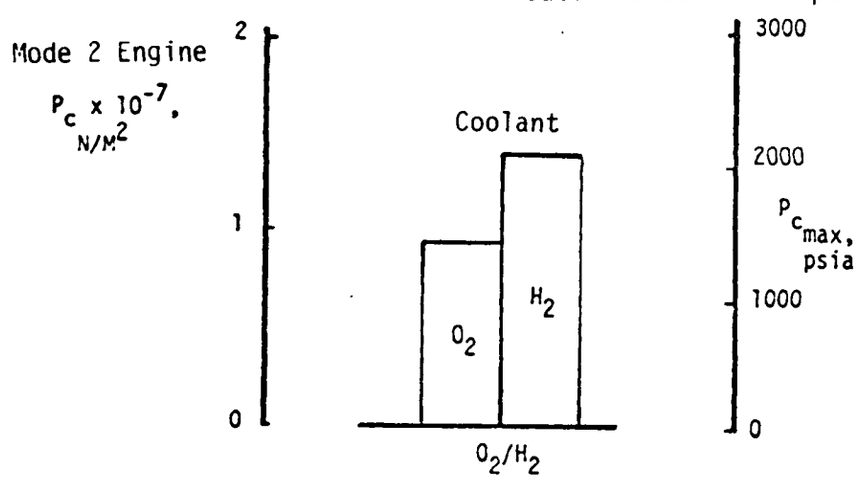

Inner Combustor Propellant Combination

Figure 27. Chamber Pressure Limits

($P_{inlet} = 1.8 \times P_c$)

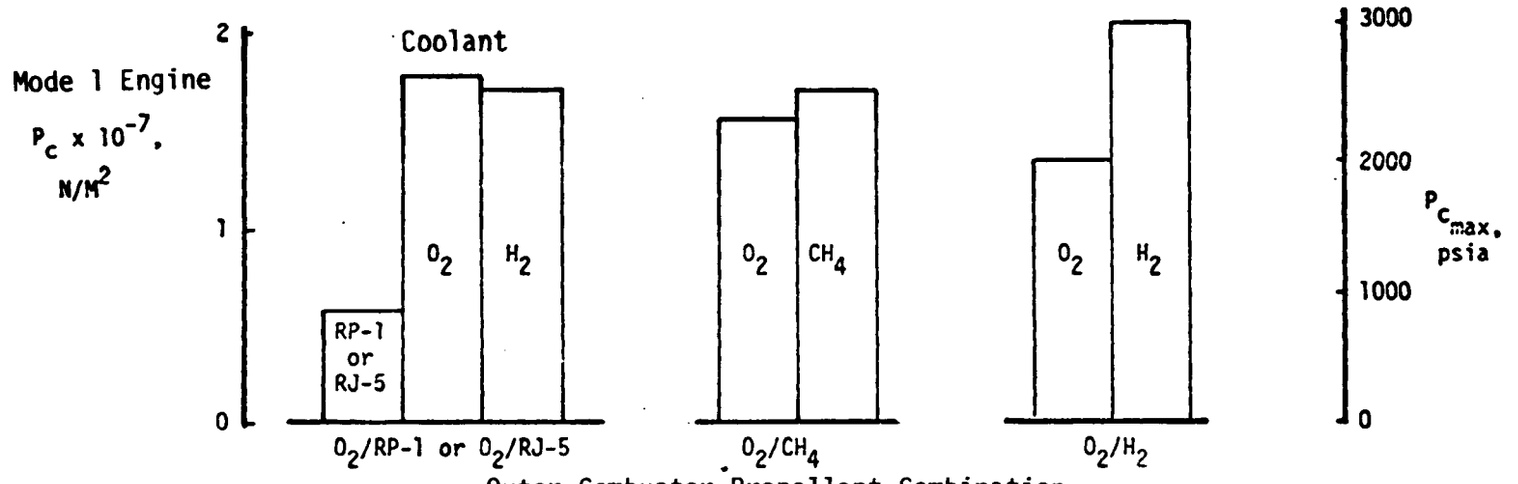

Outer Combustor Propellant Combination

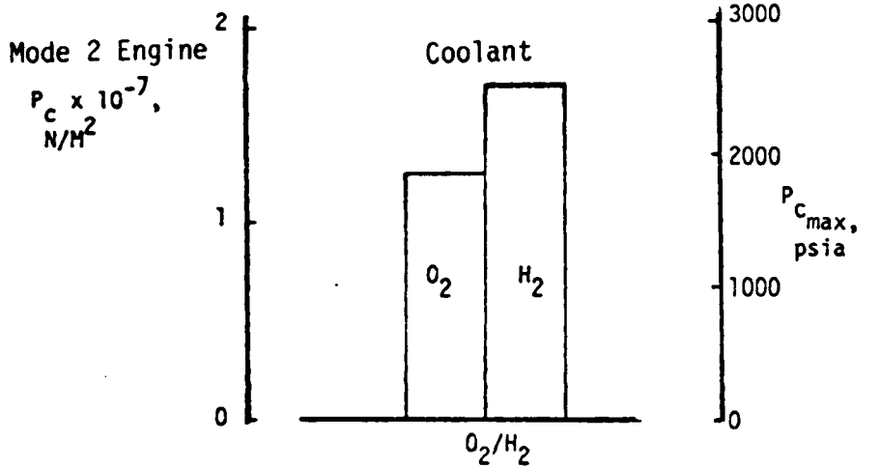

Inner Combustor Propellant Combination

Figure 28. Chamber Pressure Limits

($P_{inlet} = 2.25 \times P_c$)

ORIGINAL PAGE IS OF POOR QUALITY

COMBUSTION CHAMBER/NOZZLE GEOMETRY

The design of the split-combustor linear aerospike nozzle contour was generated using an available Rocketdyne computer program employing the method of characteristics solution. As illustrated in Fig. 29 , the first step was the design of a plane-flow ideal spike with an area ratio equal to that of the Mode 2 operation. To determine the required shroud area ratio of the inner combustor, the Prandtl-Meyer angle and the orientation of the inner combustor shroud (angle β) must be known. For simplicity, a β of 45 degrees was chosen. The Mode 2 area ratio and the combustion gas properties of the inner combustor determine the shroud Prandtl-Meyer angle (μ). The angle (μ shroud) minus the angle β determines the shroud area ratio. This procedure was followed for both combustors and a parametric set of ideal plane-flow bells is generated for each shroud.

For the inner combustor, the outer wall of the contour is truncated at a wall angle of approximately 6 degrees. The contour is then translated along the ordinate $Y/G_2 = \varepsilon_2$ (Fig. 30) until the inner wall of one of the contours matches the ideal spike contour. This results in the desired inner combustor shroud contour.

The outer combustor shroud contour is developed by truncating the generated shroud contours at a wall angle of 6 degrees. The selected contour is the contour that results in the same shroud exit pressure as that of the inner shroud. Therefore, the nozzle contour is completed by orienting the outer shroud at β and aligning the exit with the inner shroud.

The completed nozzle contour having a 114:1 Mode 2 area ratio and a 42.8:1 Mode 1 area ratio is presented in Fig. 30.

THRUST CHAMBER COOLING CIRCUITS

The high heat fluxes encountered in high chamber pressure engines necessitate high thermal conductivity materials such as zirconium-copper (Zr-Cu). In addition, the high strength of this type of copper alloy and the "fin conduction" created by the channel wall construction provide a superior cooling concept to steel tubes in high heat flux regions. In low heat flux regions such as in the nozzle, tubular construction provides adequate cooling and light weight. This configuration of combining channel wall and tubular construction results in a thrust chamber with high performance, light weight, and high cyclic life and is currently the concept being employed in the Space Shuttle Main Engine (SSME).

As specified by the work statement, the coolant and propellant combinations which were evaluated are illustrated in Table 8. The open blocks indicate the combinations analyzed.

Typical candidate thrust chamber cooling circuits are schematically illustrated in Fig. 31. The first cooling circuit is a parallel uppass cooling circuit in

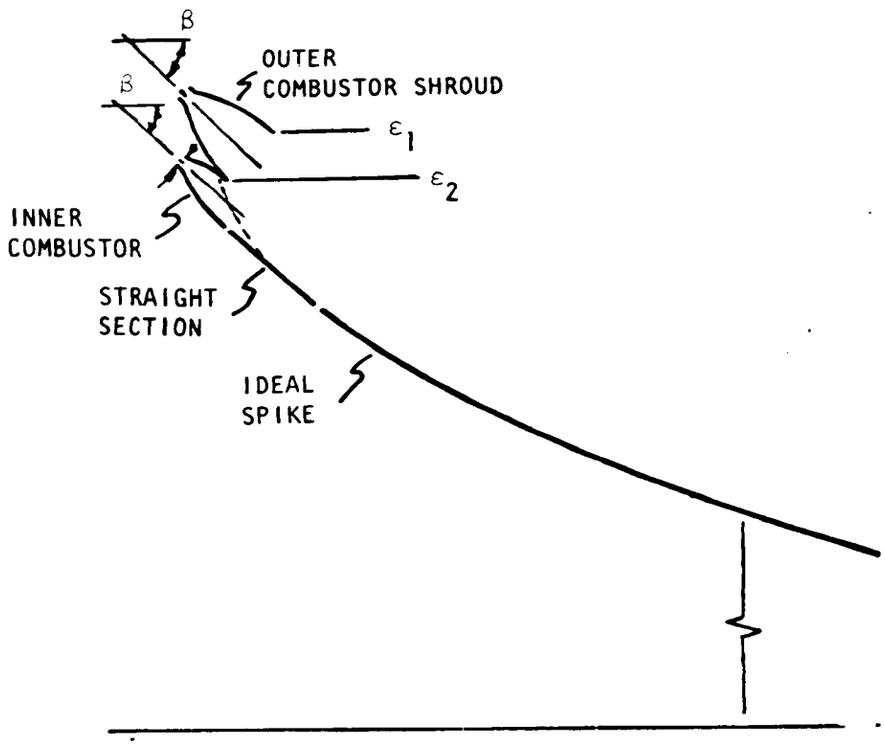

- DEVELOP IDEAL SPIKE CONTOUR (PLANE FLOW)
  - $\epsilon = \epsilon_2$ (MODE 2 AREA RATIO)
- GENERATE PARAMETRIC IDEAL BELLS (PLANE FLOW) FOR INNER AND OUTER SHROUDS
  - SELECT β
  - CHOSE ϵ_{IDEAL} ARRAY

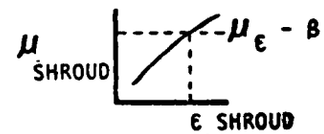

- INNER COMBUSTOR SHROUD
  - TRUNCATE OUTER WALL (θ≅6 degree) AND MAINTAIN IDEAL CONTOUR ON INNER WALL
  - ORIENT SHROUD AT β AND TRANSLATE ALONG $Y/G_2 = \epsilon_2$ UNTIL INNER WALL LINES UP
- OUTER COMBUSTOR SHROUD
  - TRUNCATE IDEAL BELL CONTOUR (θ≅6 degree)
  - SELECT CONTOUR WHICH HAS THE SAME SHROUD EXIT PRESSURE
  - ORIENT OUTER SHROUD AT β AND ALIGN WITH INNER SHROUD

Figure 29. Linear Split-Combustor Aerospike Contour Design

ORIGINAL PAGE IS
OF POOR QUALITY

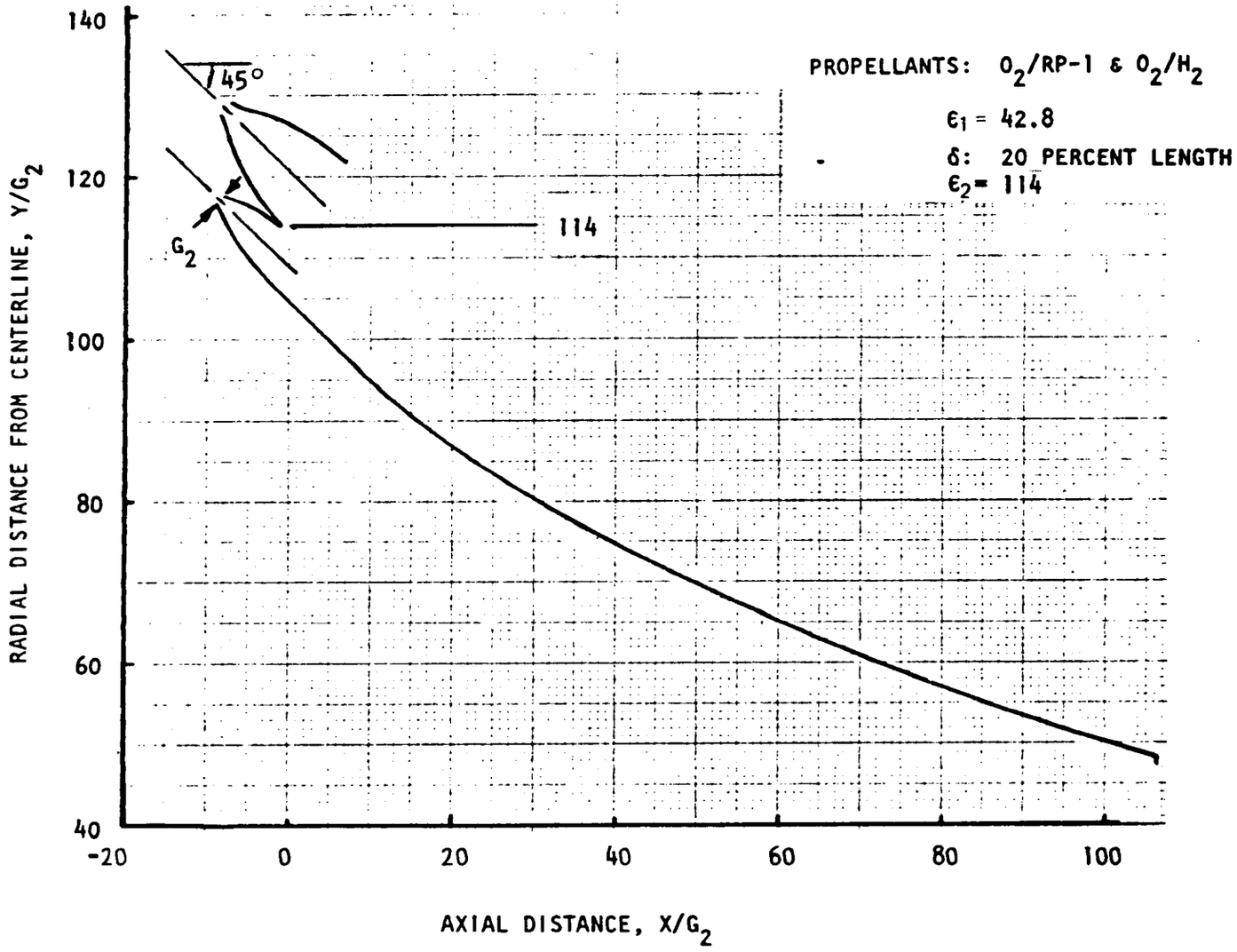

Figure 30. Split-Combustor Linear Aerospike Nozzle Contour

TABLE 8. COOLANT/PROPELLANT COMBINATION MATRIX

	Outer Combustor $\varepsilon_1 = 40$				Inner Combustor $\varepsilon_2 = 114$	
Coolant / Propellant	H_2	O_2	RP-1 or RJ-5	CH_4	H_2	O_2
O_2/RP-1						
O_2/RJ-5						
O_2/CH_4						
O_2/H_2						

ORIGINAL PAGE IS
OF POOR QUALITY

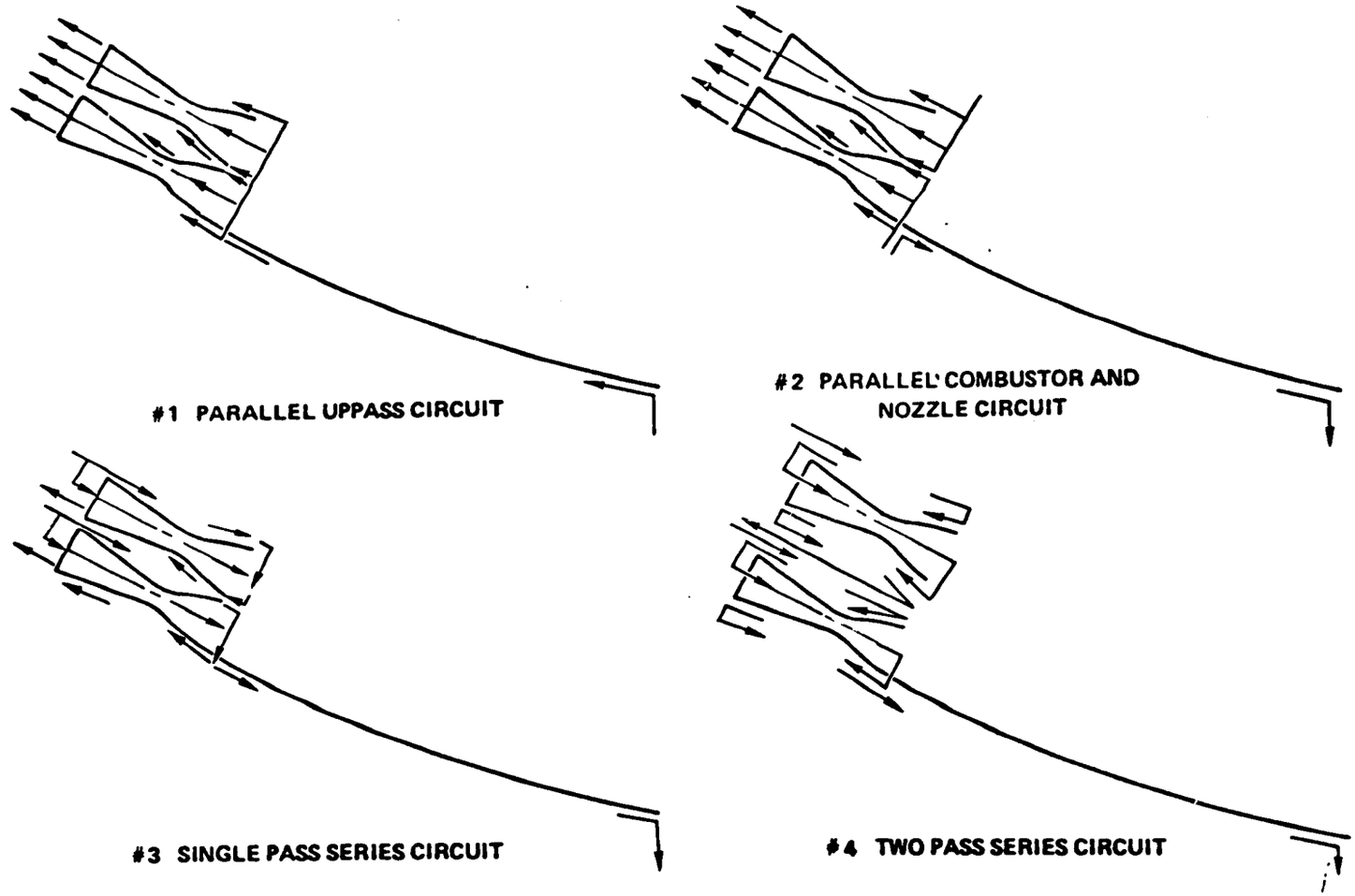

Figure 31. Candidate Cooling Circuits

which the coolant enters the nozzle exit and flows up the nozzle to the combustor exits. The coolant splits at two combustor exits to cool the combustors in a parallel uppass circuit. The second cooling circuit has the combustor and nozzle in parallel. The combustors are cooled with their respective coolant in a parallel uppass circuit which cools the inner and outer contour walls and the two panels of each combustor. The nozzle, in the second circuit, is cooled using a single downpass circuit. Since this circuit cools the combustor and nozzle in parallel, it will tend to minimize the required coolant pressure drop. The third cooling circuit is a single-pass series circuit. For the outer combustor, the coolant enters the injector end of the outer contoured wall and side panels and flows down to the combustor exits and returns up the inner contour wall. The circuit for the inner combustor is similar to that of the outer combustor except that the flow exiting the outer contour wall and side panels splits to cool the inner contour wall and nozzle. The fourth cooling circuit is a two-pass combustor circuit version of the third cooling circuit.

In view of the requirement to limit the thrust chamber coolant inlet pressure, the parallel combustor and nozzle circuit (Circuit No. 2) was selected as the cooling circuit to be used in the generation of the parametric data. This circuit offers the lowest coolant pressure drop and also provides the added flexibility that the nozzle may be cooled with a different coolant than used for the inner or outer combustor.

HEAT TRANSFER COEFFICIENTS

Combustion chamber lengths (injector-to-throat) selected for the respective propellants were representative of that required to achieve a high characteristic velocity efficiency. The O_2/H_2 J-2 linear aerospike (Ref. 1) had a 12.7-cm (5-inch) length and this value was used in this study. The O_2/CH_4 propellant would require a longer length than O_2/H_2 and a combustor length of 17.78 cm (7 inches) was chosen for this propellant combination. A longer length would be required for O_2/RP-1, and O_2/RJ-5 and a 22.86-cm (9-inch) length was selected.

Hot-Gas Side

The gas-side heat transfer coefficient distributions for the different combustor configurations were extrapolated from the J-2 linear test data (Fig. 32) using the general relationship:

$$h_g \propto \frac{P_c^{0.8}}{D_H^{0.2}} \phi_p$$

ORIGINAL PAGE IS
OF POOR QUALITY

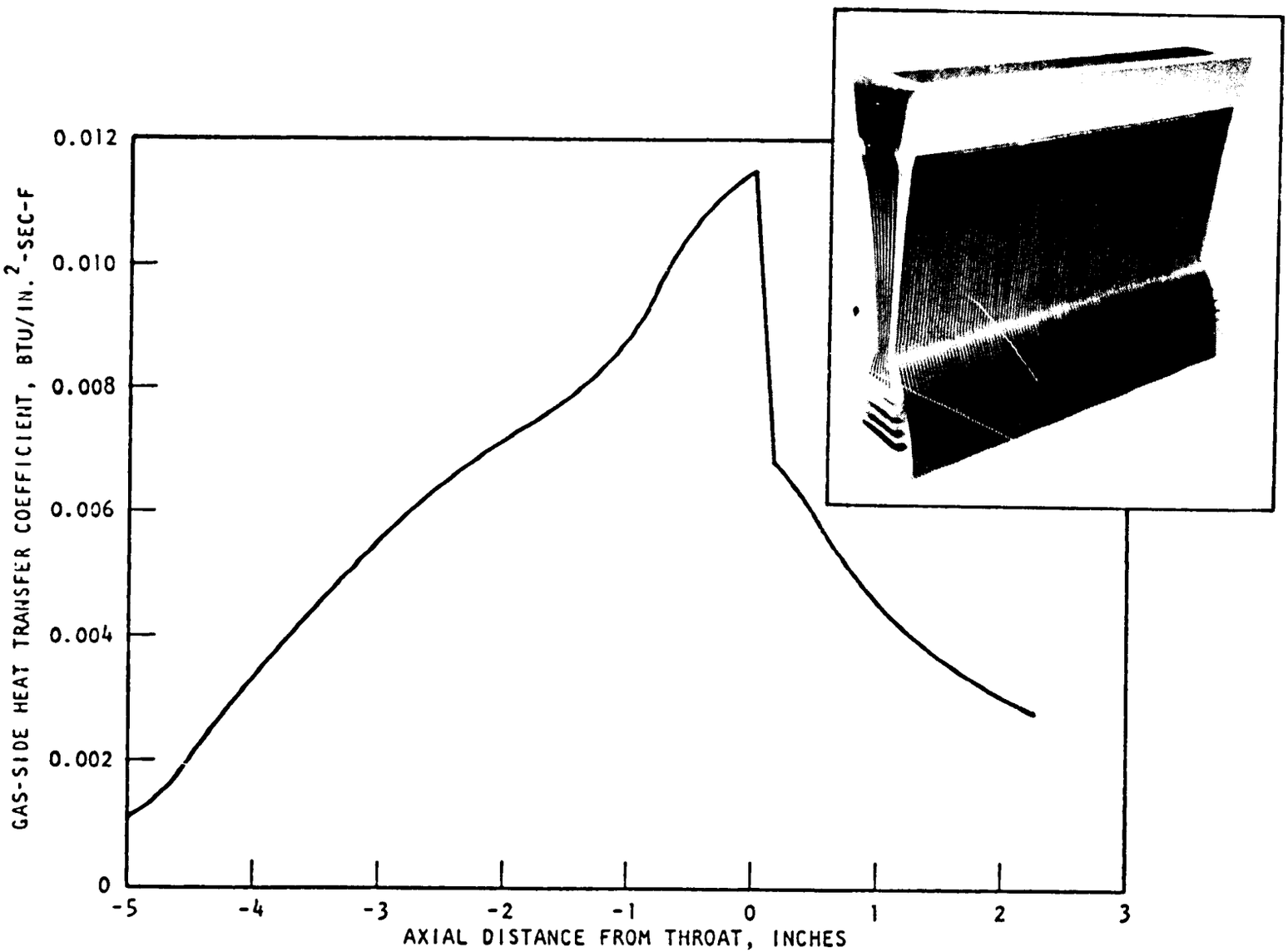

Figure 32. Gas Side Heat Transfer Coefficient Distribution, Cast Segment, J-2 Linear

where

h_g = Gas-side heat transfer coefficient

P_c = Chamber pressure

D_H = Hydraulic diameter (two times the throat gap)

ϕ_p = Propellant property correction term which includes the influence of combustion gas specific heat, viscosity, and Prandtl number.

The influence of the carbon layer which may be deposited on the chamber wall by the O_2/hydrocarbon fuel propellants was neglected as specified in the study guidelines.

An analytical prediction of the nozzle gas-side heat transfer coefficient distribution during Mode 1 operation for a 1.378×10^7 N/m^2 (2000 psia) chamber pressure engine using O_2/RP-1 and O_2/H_2 is shown in Fig. 33.

Coolant Side

Coolants evaluated were RP-1, oxygen, methane, and hydrogen. The RJ-5 was not evaluated in detail due to the very limited transport property data available at the time of the study.

RP-1. The Rocketdyne-developed (Ref. 2) coolant correlation for RP-1:

$$h_{C_{RP-1}} = 0.0054 \frac{k}{D_H} (R_e)^{0.95} (P_R)^{0.4} \phi_c \phi_E$$

was used in this study. Due to the shallow curvature of the linear aerospike contour in the throat region, a coolant curvature enhancement, ϕ_c, of 1.0 was assumed. The entrance enhancement, ϕ_E, was determined using the relation:

$$\phi_E = 1 + 0.06 \frac{(R_e)^{0.25}}{(\ell/D_H)}$$

Carbon-containing fuels such as RP-1 and RJ-5 at high coolant-side wall temperature becomes thermally unstable and may undergo either polymerization or cracking to form coke. Excessive formation of coke on the inside coolant passage walls increases the resistance to heat transfer and causes the walls to overheat. RP-1 coking starts at approximately 263 C (500 F) wall temperature and proceeds at progressively faster rates with increasing wall temperatures. References 2 and 3 indicate that coking at temperatures below 368 C (700 F) is much less severe at the high coolant velocities required in high chamber pressure engines. As specified by the study guidelines, a coking limit temperature (maximum coolant-side wall temperature) of 316 C (600 F) was used

ORIGINAL PAGE IS
OF POOR QUALITY

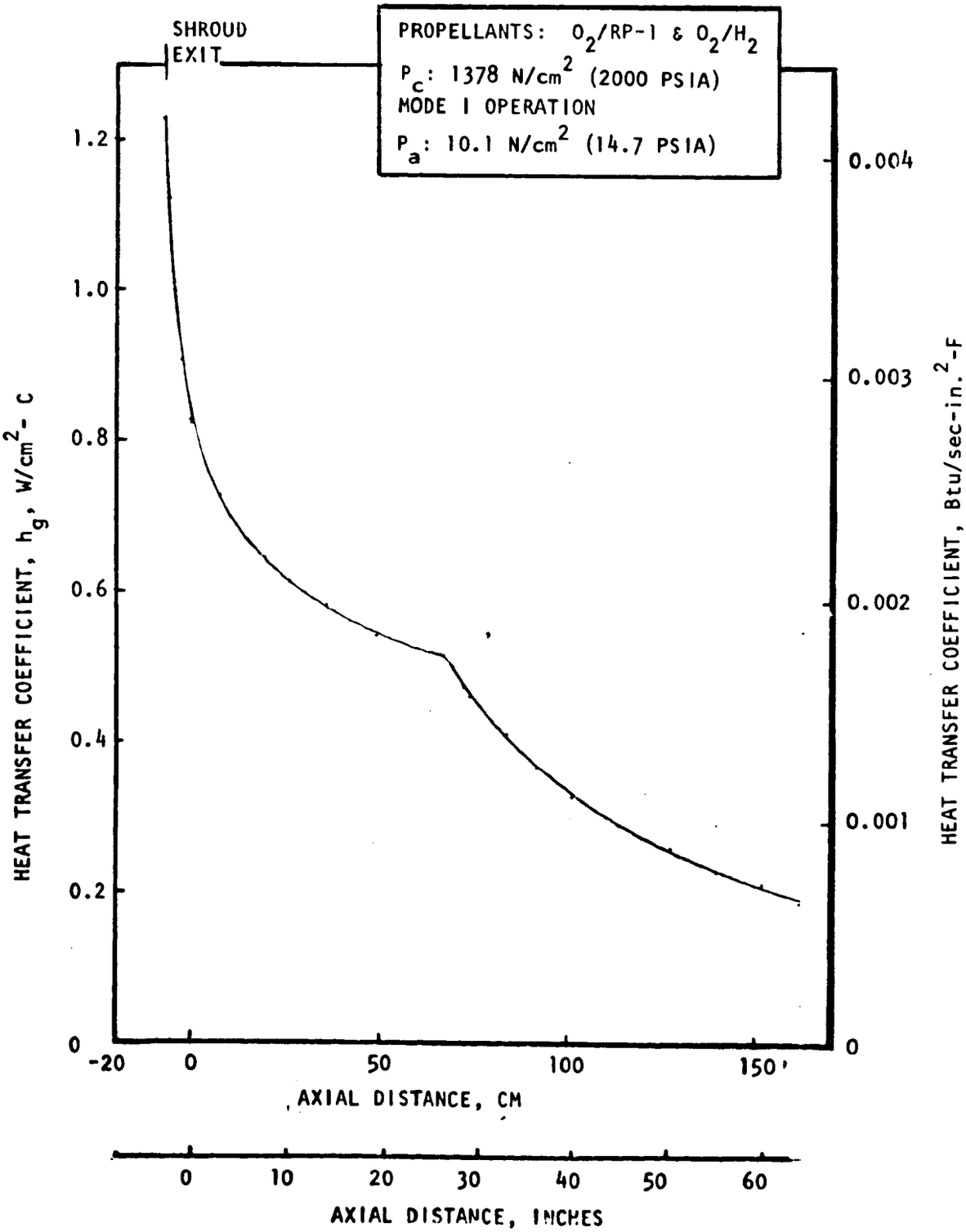

Figure 33. O_2/RP-1 and O_2/H_2 Mode 1 Nozzle Heat Transfer Coefficient Distribution (Sea Level Operation)

Oxygen. For oxygen cooling, a standard gaseous coolant correlation with a wall temperature influence was employed:

$$h_{CO_2} = 0.0265 \frac{k}{D_H} (R_e)^{0.8} (P_R)^{0.4} \left(\frac{T_B}{T_{WC}}\right)^{0.55} \phi_c \phi_E$$

A coolant curvature enhancement, ϕ_c, of 1.0 was assumed.

Limited oxygen coolant correlation data exists (Ref. 4) for the supercritical conditions experienced in these high chamber pressure engines. Therefore, further analytical and experimental evaluation of oxygen cooling is recommended to establish cooling at supercritical pressures.

There are some potential problems which may be encountered in using oxygen cooling. When a gas-side-wall oxygen leak occurs, the gas temperature adjacent to the wall varies from that of pure oxygen to the stoichiometric value and then to the mainstream valve. If the mixing of the oxygen and mainstream gases causes a stoichiometric condition to exit adjacent to the wall, then local wall heating will occur. Mixing would be dependent on the oxygen leak flowrate, velocity, and orientation to the mainstream gas.

Hydrogen. Hydrogen is the most evaluated coolant. Investigations have studied the effects of curvature, roughness, and entrance enhancements. For the linear engine study, the Rocketdyne hydrogen coolant correlation (Ref. 2) was used:

$$h_c = C_H \, G \, C_p \left(\frac{T_B}{T_{WC}}\right)^{0.55} \phi_c \, \phi_E$$

where

$$C_H = \frac{f/8}{0.92 + \sqrt{f/8}\left[g\,(\varepsilon^*) - 8.48\right]}$$

and

$$g\,(\varepsilon^*) = 4.7\,\varepsilon^{*0.2} \qquad \text{for } \varepsilon^* \geq 7.0$$

$$g\,(\varepsilon^*) = 4.5 + 0.57\,\varepsilon^{*0.75} \text{ for } \varepsilon^* < 7.0$$

A coolant curvature of 1.0 was assumed and the following entrance enhancement equation was used:

$$\phi_E = 1.53 \left(\frac{\ell}{D_H}\right)^{-0.015} \qquad \infty \geq \phi_C \geq 1.0$$

Methane. The Rocketdyne-developed methane coolant correlation (Ref. 5) shown below (the standard coolant correlation) was used in this study:

$$h_c = 0.023 \frac{k}{D_H} (R_e)^{0.8} (P_R)^{0.4} \phi_c \phi_E$$

ORIGINAL PAGE IS
OF POOR QUALITY

OUTER COMBUSTOR COOLING ANALYSES

In this evaluation, only the contoured panel of the combustor was analyzed. An assumption used in the study was that 94 percent of the combustor coolant flow cools the contoured panels and 6 percent the side panels.

The coolant passage design constraints and their interrelation are illustrated pictorially in Fig. 34 for a typical chamber and coolant flowrate. As the thrust chamber coolant inlet pressure is decreased, choked flow is approached, and higher wall temperatures are obtained. Higher gas-side wall temperatures result in a decreased cycle life and less coking margin for RP-1 and RJ-5. Therefore, the coking limit, the life cycle requirement, and the coolant velocity requirements must all be satisfied. In addition, the coolant flowrate can be varied. For hydrogen, the coolant flowrate was reduced to a minimum in evaluating the combustor design.

O_2/RP-1 or O_2/RJ-5 Propellants

RP-1 or RJ-5 Cooling. In addition to the restrictions of the thrust chamber coolant inlet pressure and the cycle lifes, RP-1 and RJ-5 cooling requires an added restriction since these fuels tend to coke at elevated temperatures. To achieve a 316 C (600 F) or less coolant-side wall temperature, low gas-side wall temperatures are required and the predicted cycle life (Fig. 35) is well in excess of that required. However, due to the low gas-side wall temperature requirement, high coolant velocities result which, in turn, require high coolant inlet pressures. For RP-1 and RJ-5 cooling, the maximum chamber pressure limit is approximately 0.372×10^7 N/m^2 (540 psia) and 0.483×10^7 N/m^2 (700 psia) for the coolant inlet-to-chamber pressure ratios (P_{inlet}/P_c) of 1.8 and 2.25, respectively.

As the P_{inlet}/P_c ratio increases, the maximum chamber pressure increases; but, as shown in Fig. 35, increasing P_{inlet}/P_c beyond 3.5 results in coolant-side wall temperatures (T_{wc}) exceeding 316 C (600 F). This coking limit occurs at a 1000-psia chamber pressure.

The combustor heat input and coolant temperature rise variations with chamber pressure are presented in Fig. 36. Also, note in Fig. 36 that 100 percent of the fuel was utilized for cooling. The minimum channel dimensions are shown in Fig. 37.

The cooling limits using RJ-5 cooling are assumed the same as those with RP-1 cooling. The RJ-5 coolant pressure drop and coolant heat input are determined using the following relationships:

$$\Delta P_{RJ-5} = 1.021\ \Delta P_{RP-1}$$

$$Q_{RP-5} = 0.952\ Q_{RP-1}$$

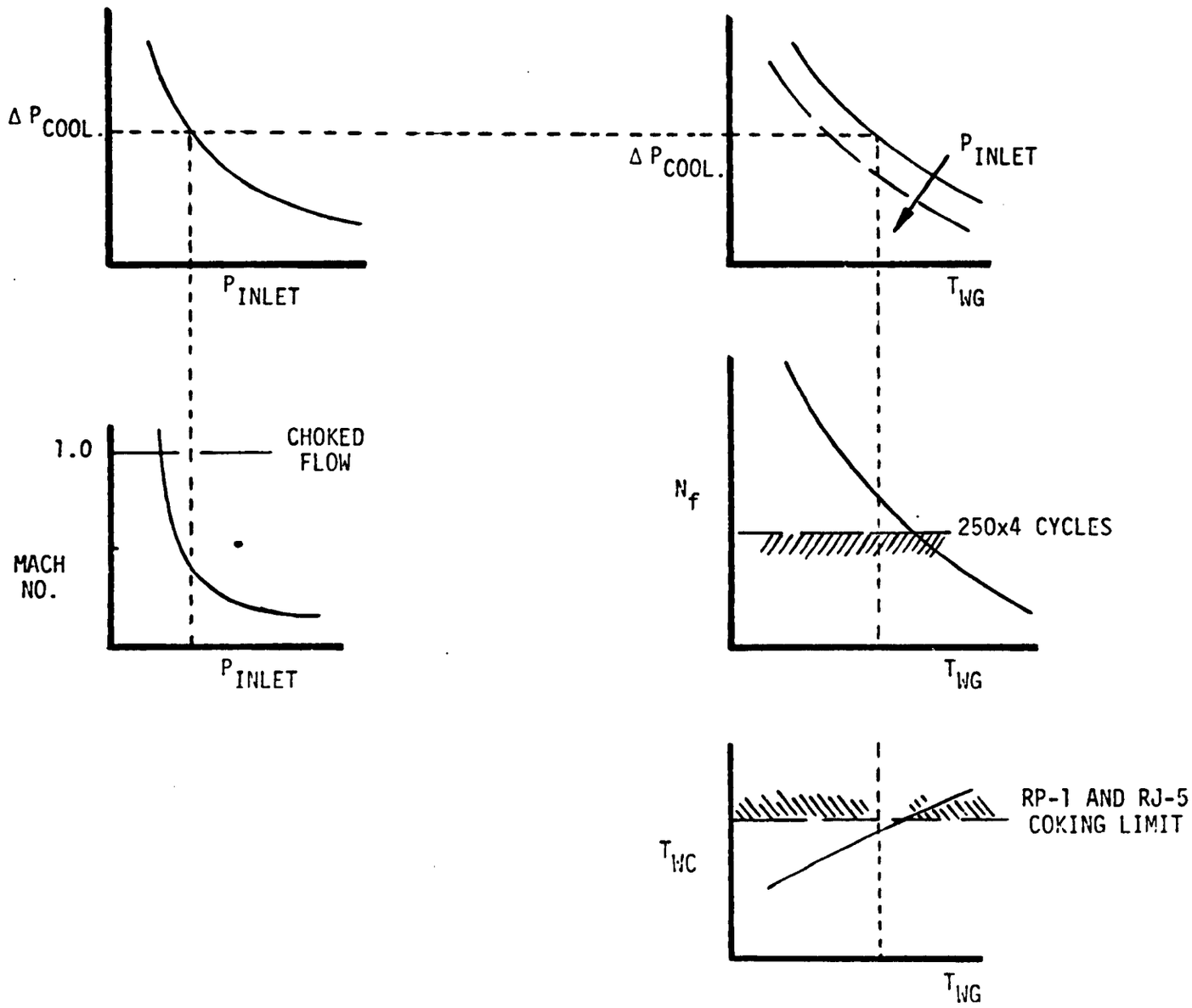

Figure 34. Coolant Passage Design Constraints

ORIGINAL PAGE IS OF POOR QUALITY

F_{SL} : 20 X 10^6N (4.5 X 10^6 lbf)

OUTER COMBUSTOR

PROPELLANT: O_2/RP-1

MR: 2.8

ϵ_1: 40

F_O/F_t = 0.65

W/H: 3.0

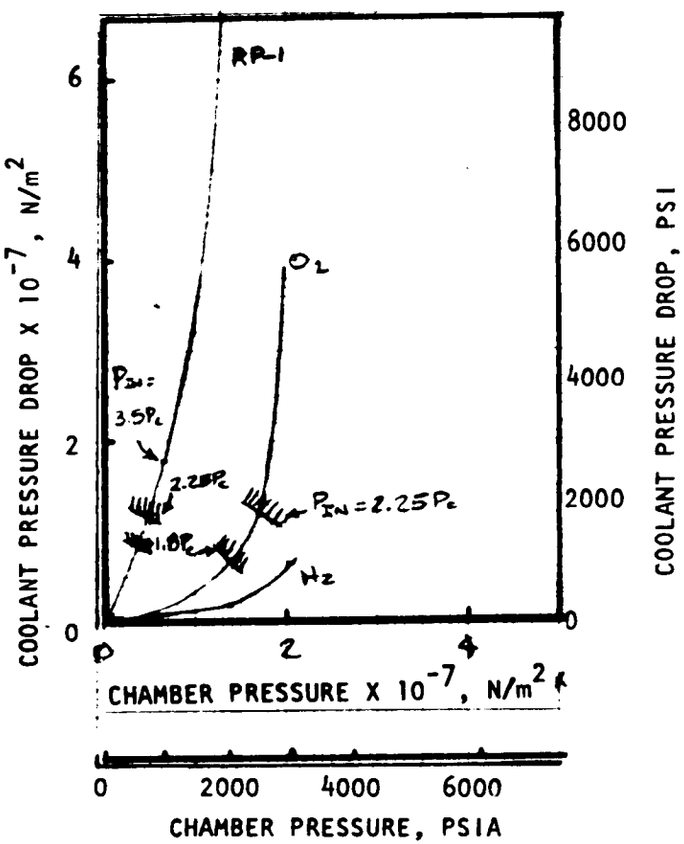

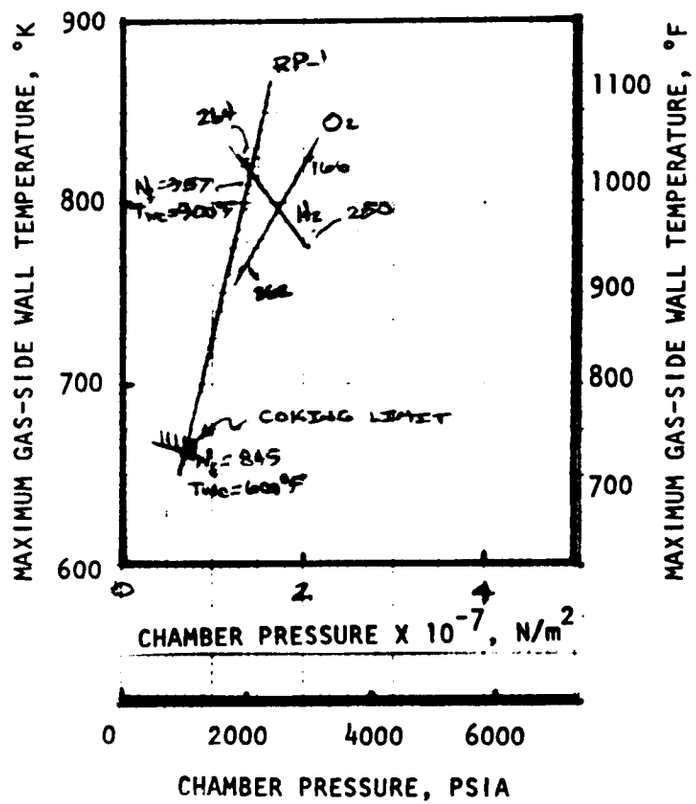

Figure 35. O_2/RP-1 Combustor Coolant Pressure Drop and Maximum Gas-Side Wall Temperature Variation With Chamber Pressure

F_{SL}: 20 X 10^6N (4.5 X 10^6 LBF)

OUTER COMBUSTOR PROPELLANT: O_2/RP-1

MR: 2.8 ε_1: 40

F_o/F_t: 0.65 W/H: 3

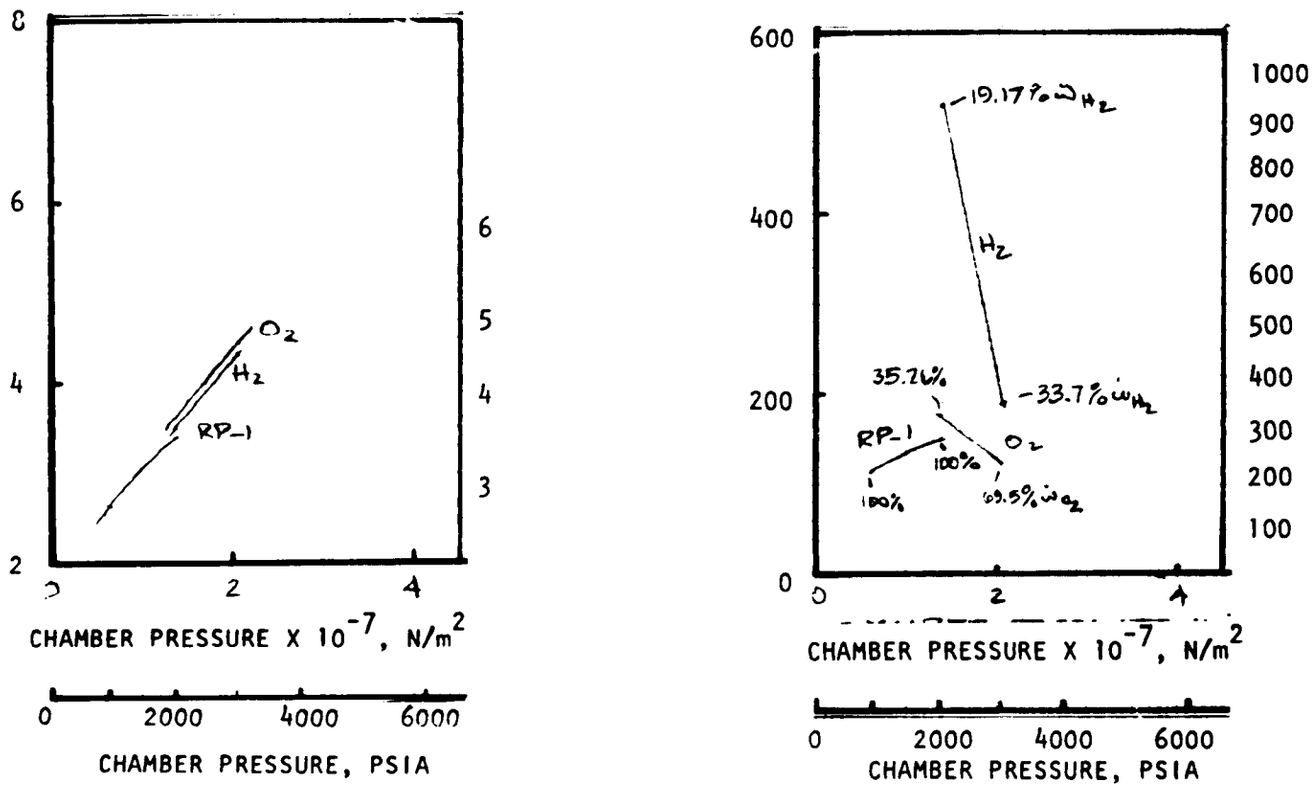

Figure 36. O_2/RP-1 Combustor Heat Input and Coolant Temperature Rise Variation With Chamber Pressure

ORIGINAL PAGE IS OF POOR QUALITY

F_{SL}: $20X10^6$N (4.5 X 10^6 LBF)

OUTER COMBUSTOR PROPELLANT: O_2/RP-1

F_o/F_t: 0.65

W/H: 3.0

MR: 2.8

ε_1: 40

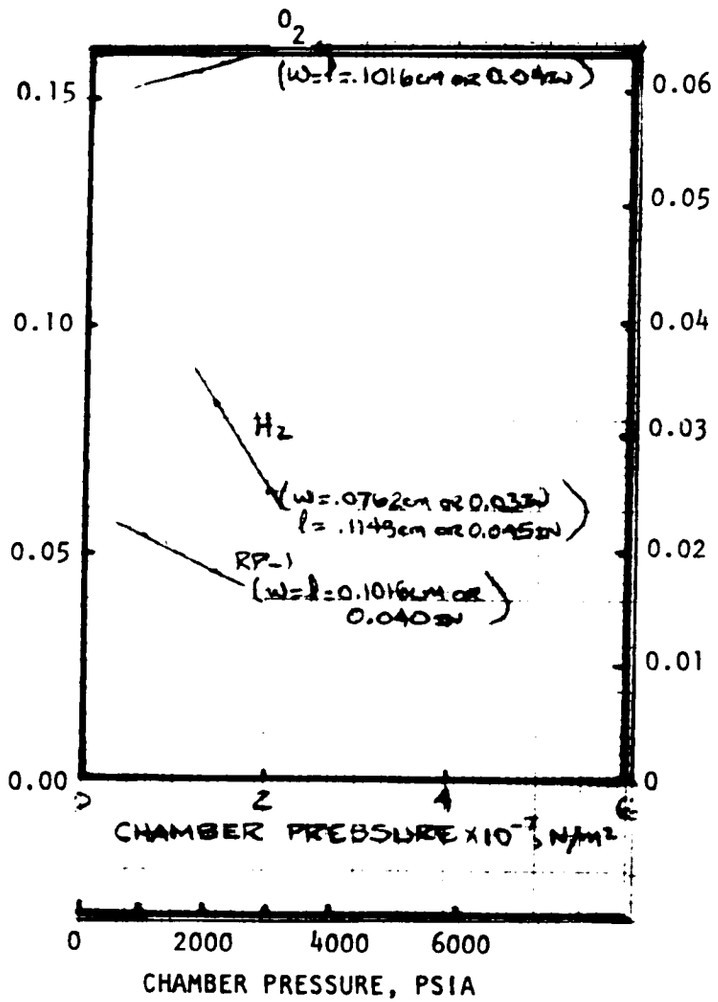

Figure 37. O_2/RP-1 Combustor Minimum Channel Depth Variation With Chamber Pressure

Oxygen Cooling. Cooling with oxygen increases the maximum coolable chamber pressure to 1.378×10^7 N/m^2 (2000 psia) and 1.7222×10^7 N/m^2 (2500 psia) for coolant inlet-to-chamber pressure ratios of 1.8 and 2.25, respectively (Fig. 35). Combustor gas-side wall temperatures of 492 C (918 F) to 551 C (1024 F) are obtained. At and below a chamber pressure of 1.7222×10^7 N/m^2 (2500 psia), the required cycle life is met. The coolant heat input, coolant temperature rise, and the minimum coolant channel dimensions are presented in Fig. 36 and 37.

Hydrogen Cooling. Hydrogen for cooling an O_2/RP-1 or O_2/RJ-5 is obtained from the inner combustor. This, of course, reduces the hydrogen cooling flow available for the inner combustor and nozzle. Therefore, for this case, the cooling limits of the nozzle are also defined. For the coolant flowrates selected, the combustor design met the cycle life and coolant inlet pressure requirements (Fig. 35 through 37). Due to the nozzle coolant flow reduction, the nozzle cooling is limited to 1.722×10^7 N/m^2 (2500 psia) chamber pressure.

Of the three coolants evaluated for O_2/RP-1, hydrogen cooling provides the highest chamber pressure. In addition, this cooling scheme allows cooling of the outer combustor (probably at a reduced flow) during Mode 2, in which hot gas from the inner combustor may be recirculating into the outer combustor.

O_2/CH_4 Propellant

Oxygen Cooling. Slightly higher heat fluxes are encountered with O_2/CH_4 than with O_2/RP-1 and cooling a thrust chamber is slightly more difficult. For the P_{inlet}/P_c ratios of 1.8 and 2.25, the chamber pressure limits (as shown in Fig. 38) are 1.24×10^7 N/m^2 (1800 psia) and 1.586×10^7 N/m^2 (2300 psia), respectively. Maximum combustor gas-side wall temperatures obtained, presented in Fig. 38, varied from 428 C (802 F) to 527 C (980 F). The required cycle life is achieved (Fig. 38) with 10 to 30 percent of the total oxygen flow. The combustor heat input and the coolant temperature rise are presented in Fig. 39. The variation of the minimum channel size with chamber pressure is shown in Fig. 40.

Methane Cooling. As shown in Fig. 38, cooling with methane increased the maximum chamber pressure limits to 1.44×10^7 N/m^2 (2080 psia) and 1.77×10^7 N/m^2 (2600 psia) for the P_{inlet}/P_c ratios of 1.8 and 2.25, respectively. All methane is used as coolant for the outer combustor. The other pertinent parametric data are presented in Fig. 39 and 40.

O_2/H_2 Propellant

Oxygen Cooling. Of the four candidate propellant combinations, O_2/H_2 will have the highest heat flux. The high heat flux reduces the maximum chamber pressure for oxygen cooling (Fig. 41) to 1.06×10^7 N/m^2 (1540 psia) and 1.388×10^7 N/m^2 (2000 psia), for the P_{inlet}/P_c ratios of 1.8 and 2.25, respectively. As shown in Fig. 41, the total outer combustor oxygen flow varies between 22 to 73 percent. The variation of coolant heat input, coolant temperature rise, minimum channel size with chamber pressures are presented in Fig. 42 and 43.

ORIGINAL PAGE IS OF POOR QUALITY

F_{SL}: 20 X 10^6N (4.5 X 10^6 LBF)

OUTER COMBUSTOR PROPELLANT: O_2/CH_4

MR: 3.5

ε_1: 40

F_o/F_t: 0.65

W/H: 3.0

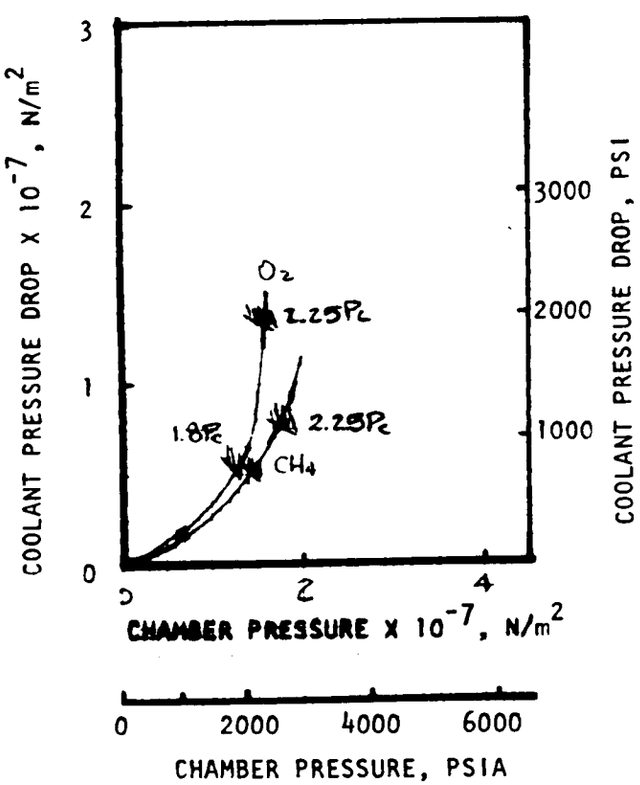

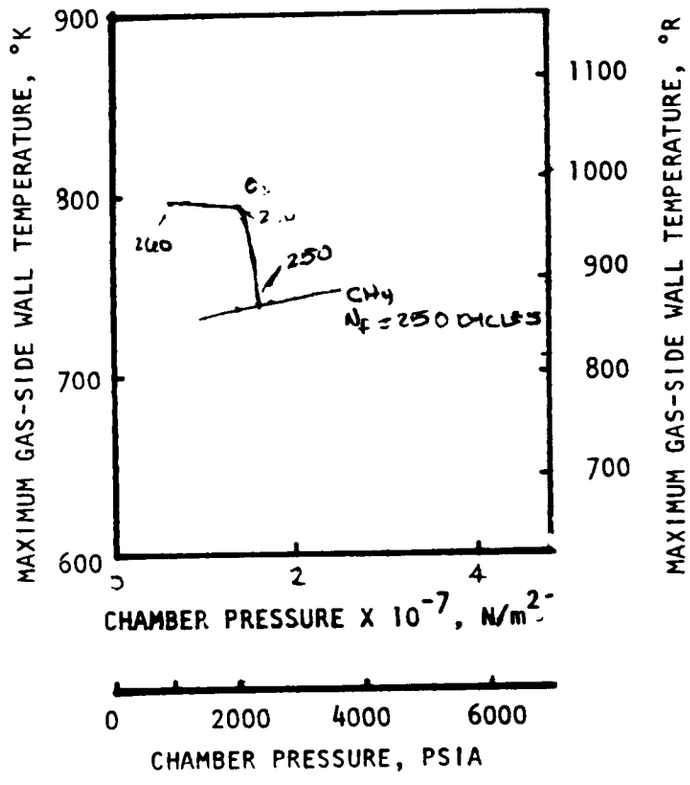

Figure 38. O_2/CH_4 Combustor Pressure Drop and Maximum Gas-Side Wall Temperature Variation With Chamber Pressure

F_{SL}: 20 X 10^6N (4.5 X 10^6 LBF)

OUTER COMBUSTOR PROPELLANT: O_2/CH_4

MR: 3.5

ε_1: 40

F_o/F_t: 0.65

W/H: 3.0

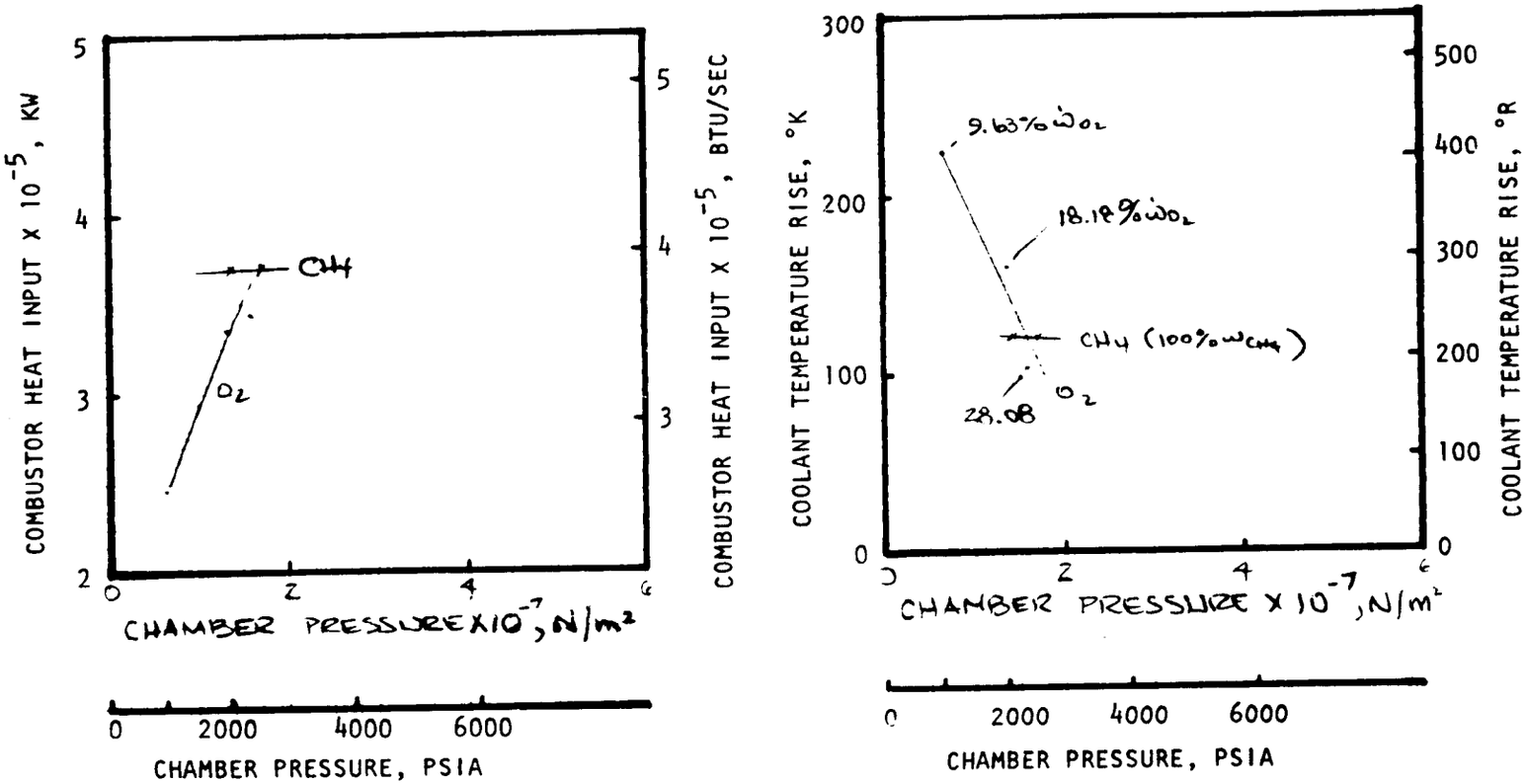

Figure 39. O_2/CH_4 Combustor Heat Input and Coolant Temperature Rise Variation With Chamber Pressure

ORIGINAL PAGE IS OF POOR QUALITY

F_{SL}: 20 X 10^6N (4.5 X 10^6 LBF)

OUTER COMBUSTOR PROPELLANT: O_2/CH_4

MR: 3.5

ϵ_1: 40

F_o/F_t: 0.65

W/H: 3.0

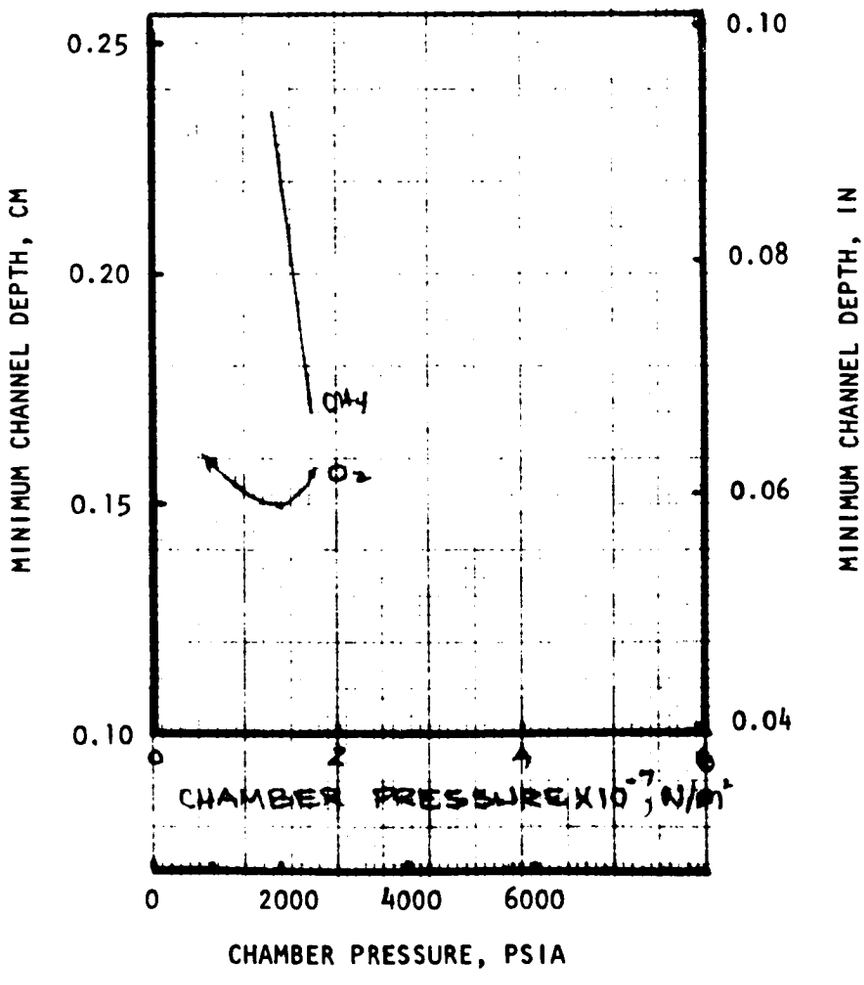

Figure 40. O_2/CH_4 Combustor Minimum Channel Depth Variation With Chamber Pressure

F_{SL}: 20 X 10^6N (4.5 X 10^6 LBF)

OUTER COMBUSTOR PROPELLANT: O_2/H_2

MR: 7

ε_1: 40

F_o/F_t: 0.65

W/H: 3.0

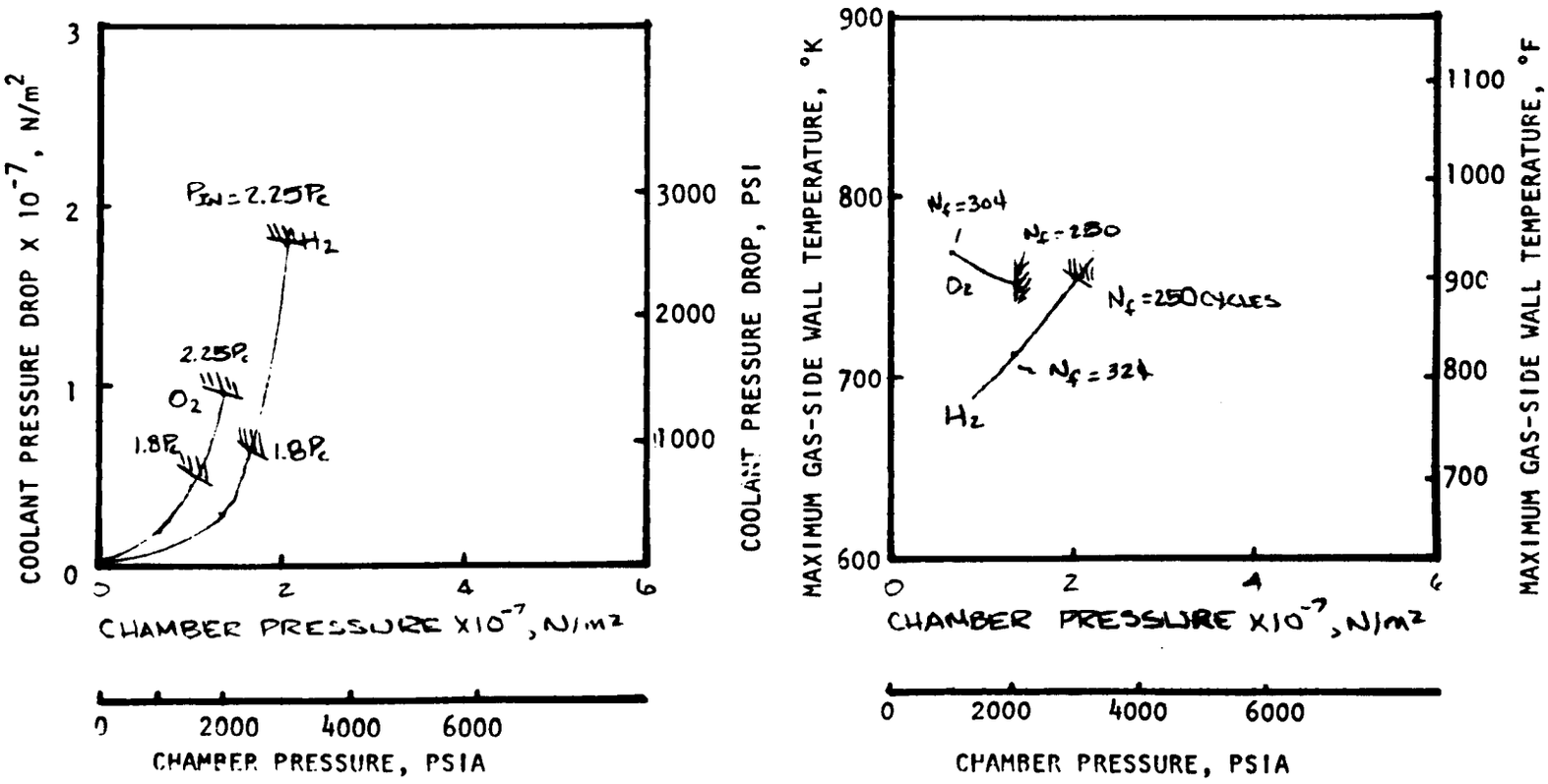

Figure 41. O_2/H_2 (Mode 1) Combustor Coolant Pressure Drop and Maximum Gas-Side Wall Temperature Variation With Chamber Pressure

ORIGINAL PAGE IS
OF POOR QUALITY

F_{SL}: 20 X 10^6N (4.5 X 10^6 LBF)

OUTER COMBUSTOR PROPELLANT: O_2/H_2

MR: 7

ε_1: 40

F_o/F_t: 0.65

W/H: 3.0

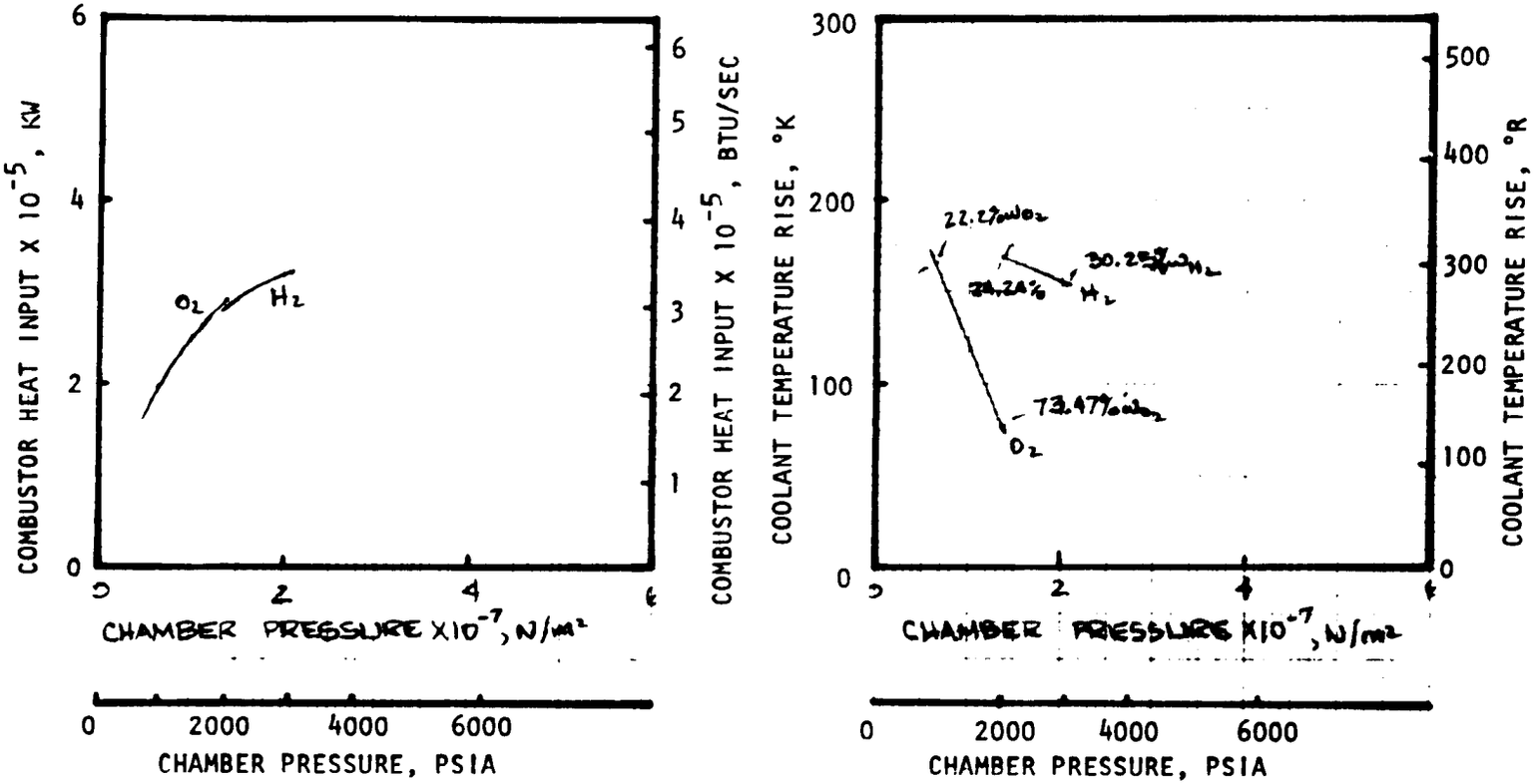

Figure 42. O_2/H_2 (Mode 1) Combustor Heat Input and Coolant Temperature Rise Variation With Chamber Pressure

F_{SL}: 20 X 10^6N (4.5 X 10^6 LBF)

OUTER COMBUSTOR PROPELLANT: O_2/H_2 F_o/F_t: 0.65

MR: 7

ε_1: 40 W/H: 3.0

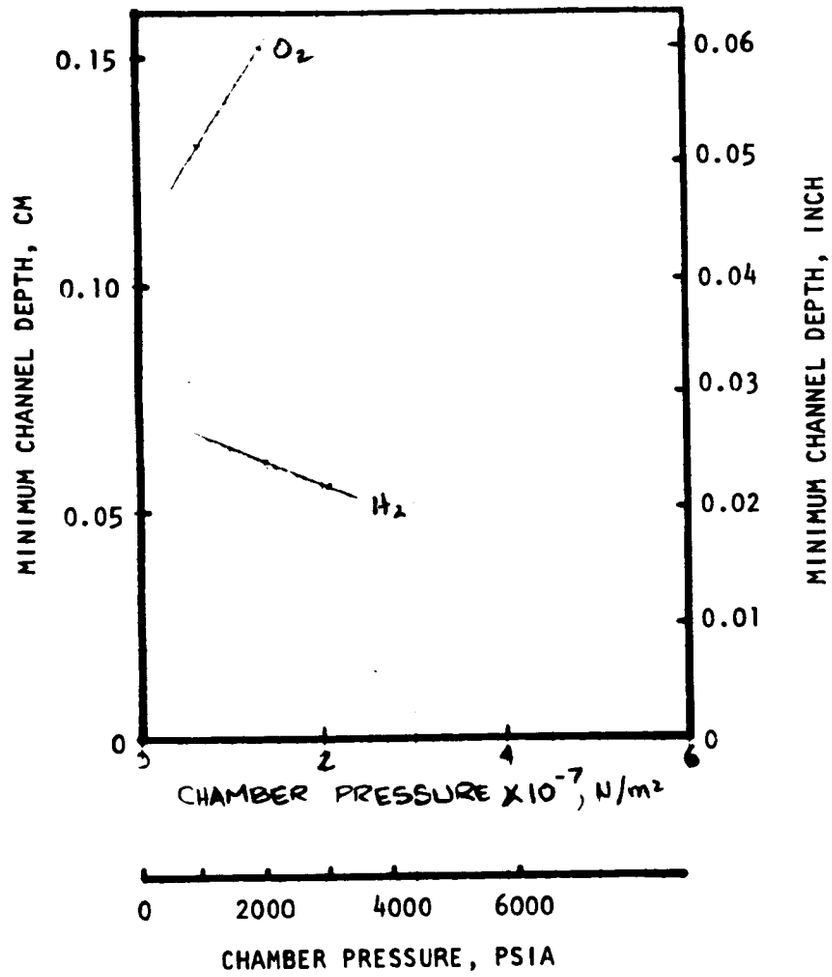

Figure 43. O_2/H_2 (Mode 1) Combustor Minimum Channel Depth Variation With Chamber Pressure

ORIGINAL PAGE IS
OF POOR QUALITY

Hydrogen Cooling. Hydrogen cooling results in maximum chamber pressures of 1.64×10^7 N/m^2 (2380 psia) and 2.07×10^7 N/m^2 (3000 psia) for the 1.8 and 2.25 P_{inlet}/P_c ratios, respectively, as shown in Fig. 41. As shown in Fig. 42 and 43, the required cycle life is achieved using 24 to 30 percent of the total outer combustor hydrogen flow.

INNER COMBUSTOR COOLING ANALYSES

O_2/H_2 Propellant

Since the inner O_2/H_2 combustor fires during both Modes 1 and 2, the cooling is accomplished using either the oxidizer and/or the fuel of the inner combustor.

Oxygen Cooling. The cooling limits with oxygen cooling are shown in Fig. 44. The chamber pressure limits are 0.92×10^7 N/m^2 (1335 psia), 1.24×10^7 N/m^2 (1800 psia), and 1.38×10^7 N/m^2 (2000 psia) for the P_{inlet}/P_c ratios of 1.8, 2.25, and 3.0, respectively. The maximum gas-side wall temperatures varies from 427 C to 554 C (800 F to 1030 F) as shown in Fig. 44, meeting the required cycle life with 40 to 91 percent of the total oxygen flow (Fig. 45). The combustor heat input and the coolant temperature rise are presented in Fig. 45. The variation of the minimum channel size with chamber pressure is shown in Fig. 46.

Hydrogen Cooling. As one would expect, hydrogen cooling increases the cooling limits above those attainable with oxygen cooling. The chamber limits (shown in Fig. 44) are 1.38×10^7 N/m^2 (2000 psia), 1.72×10^7 N/m^2 (2500 psia) and 2.07×10^7 N/m^2 (3000 psia) for the P_{inlet}/P_c ratios of 1.8, 2.25, and 3.0, respectively. Also, as shown in Fig. 44, the maximum gas-side wall temperatures are an acceptable 449 C to 482 C (840 F to 900 F). As shown in Fig. 45, the percent of the total hydrogen flowrate for combustor cooling increases from 41 to 67 percent as the chamber pressure increases from 1.38×10^7 N/m^2 (2000 psia) to 2.07×10^7 N/m^2 (3000 psia).

COMBUSTOR COOLING TRENDS

The two trends illustrated in Fig. 47 and 48 show the influence of coolant flowrate and coolant passage configuration on coolant passage design. A minimum coolant pressure drop (Fig. 47) can be achieved for hydrogen cooling when the optimum coolant bulk temperature range, approximately -162 C to -134 C (-260 F to -210 F), is reached in the high-heat-flux region. As the coolant flow decreases, the coolant bulk temperature increases. When the optimum coolant temperature range is reached, the coolant pressure drop attains a minimum. At high coolant flows, the back-side temperature is low and, to achieve the desired cycle life, a lower gas-side wall temperature is required. Decreasing the coolant flow below the optimum results in a reduced cooling capability. The coolant pressure increases substantially due to the reduced density and the smaller hydraulic diameters required to maintain the gas-side wall temperature at a level to achieve the required cycle life.

F_{SL}: 20 X 10^6N (4.5 X 10^6 LBF)

INNER COMBUSTOR PROPELLANT: O_2/H_2

MR: 7

ε_2: 114

F_o/F_t: 0.65

W/H: 3.0

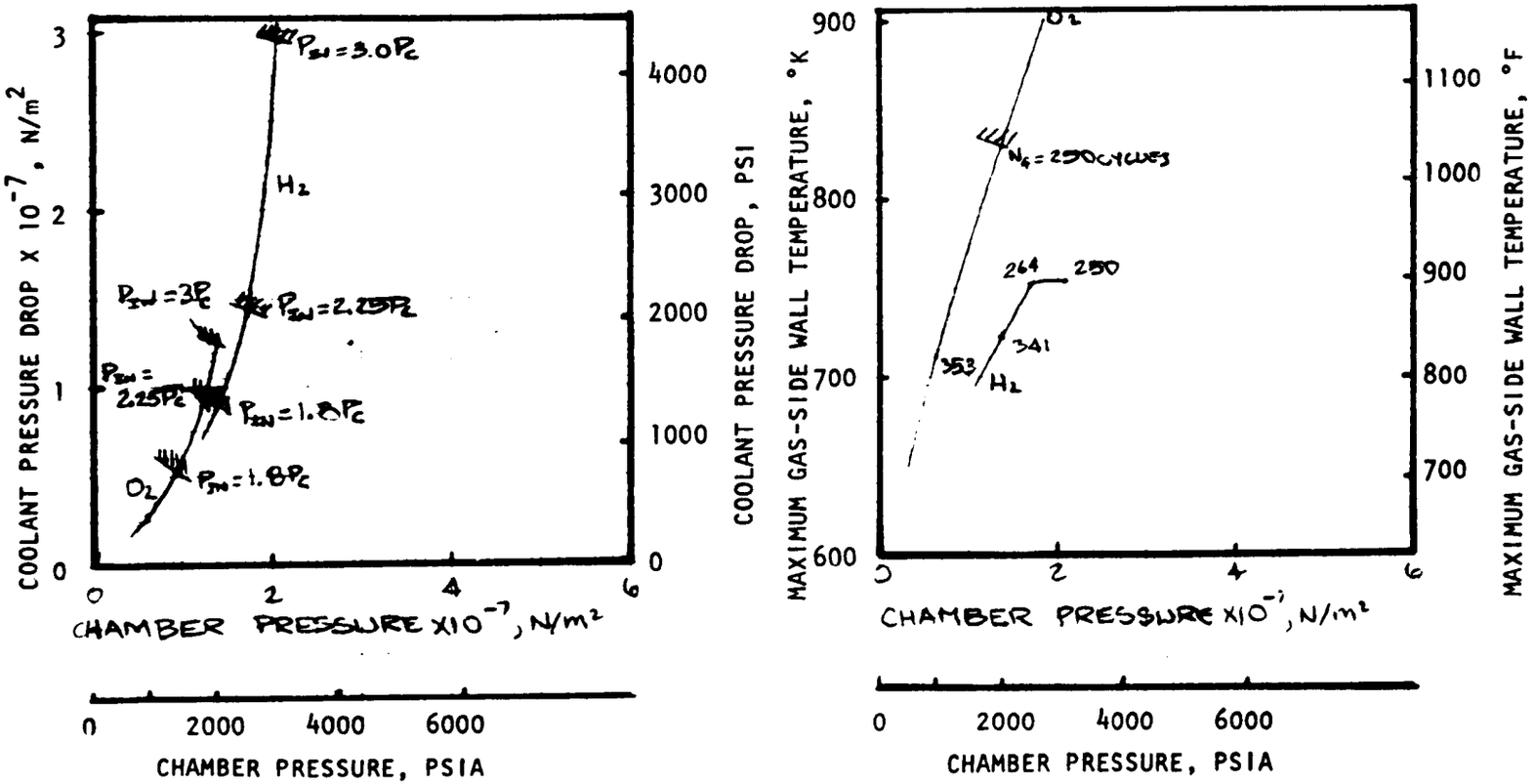

Figure 44. Mode 2 O_2/H_2 Combustor Coolant Pressure Drop and Maximum Gas-Side Wall Temperature Variation With Chamber Pressure

ORIGINAL PAGE IS OF POOR QUALITY

F_{SL}: 20 X 10^6N (4.5 X 10^6 LBF)

INNER COMBUSTOR PROPELLANT: O_2/H_2

MR: 7

ε_2: 114

F_o/F_t: 0.65

W/H: 3.0

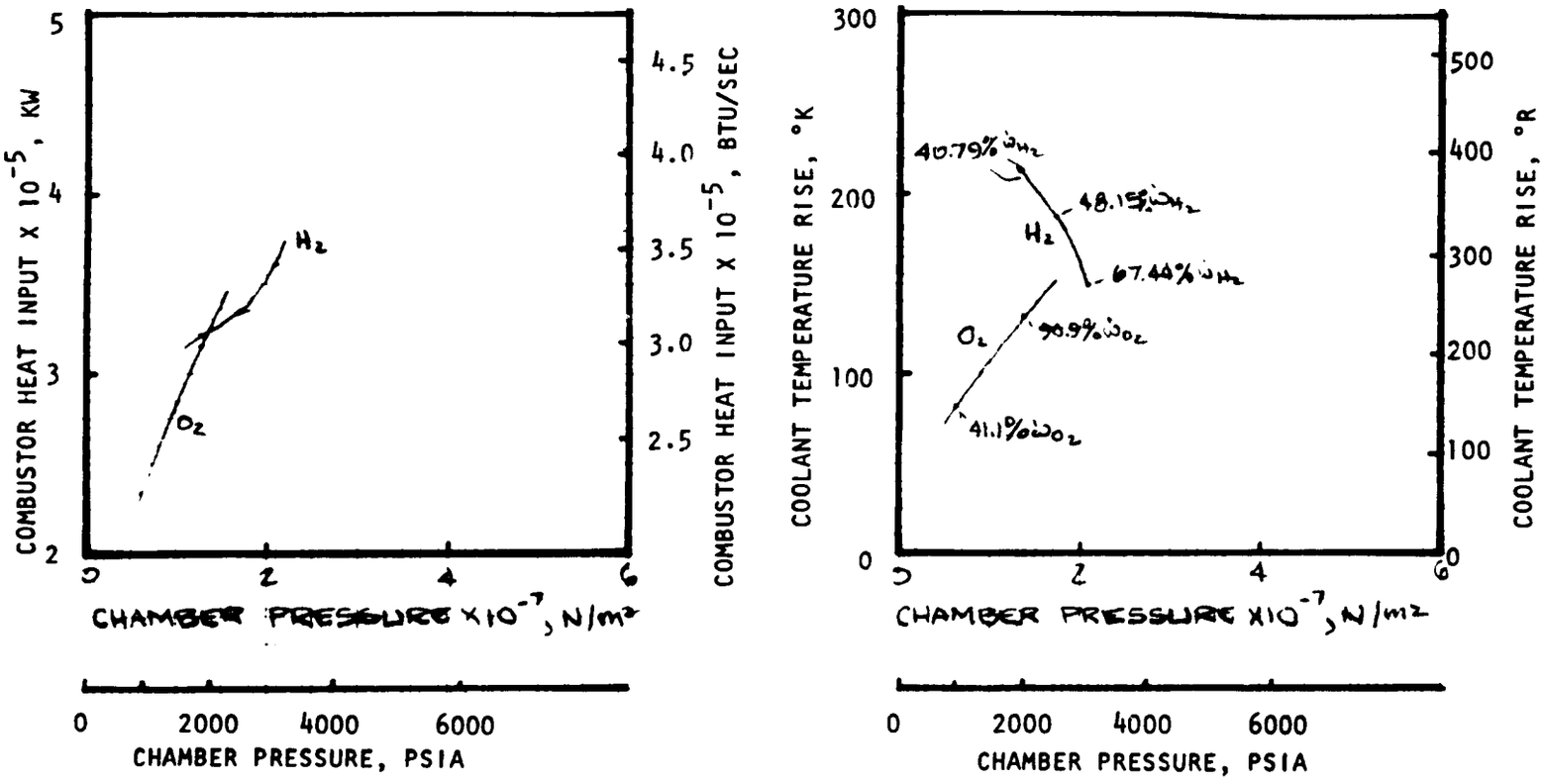

Figure 45. Mode 2 O_2/H_2 Combustor Heat Input and Coolant Temperature Rise Variation With Chamber Pressure

F_{SL}: 20 X 10^6N (4.5 X 10^6 LBF)

INNER COMBUSTOR

PROPELLANT: O_2/H_2 F_o/F_t: 0.65

MR: 7

ε_2: 114

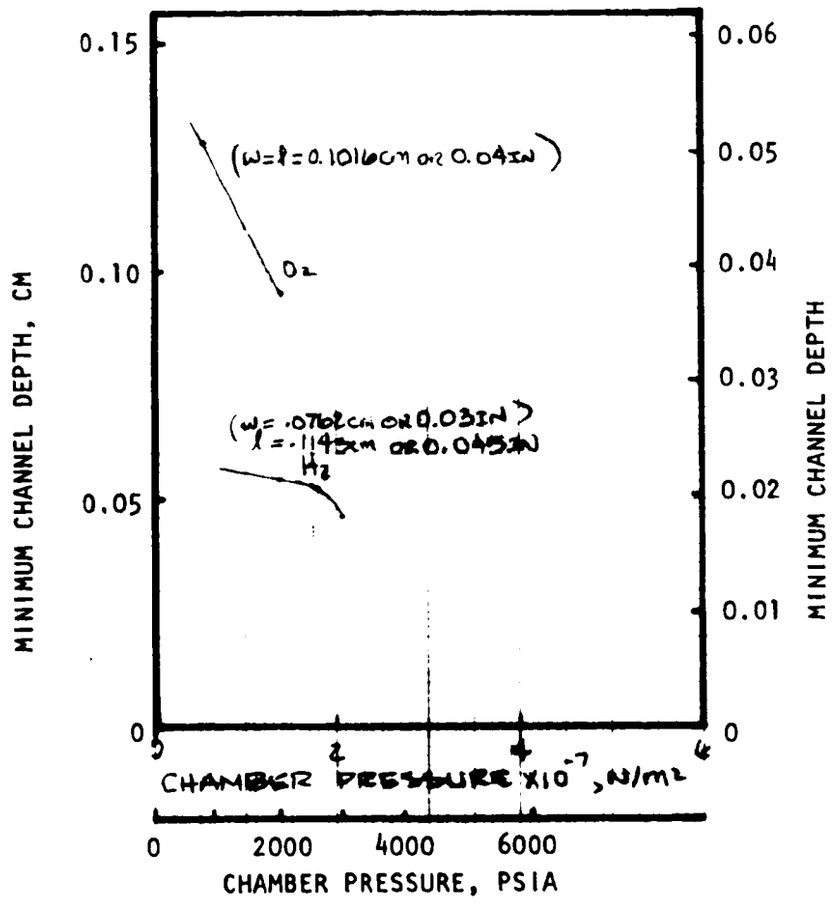

Figure 46. Mode 2 O_2/H_2 Combustor Minimum Channel Depth Variation With Chamber Pressure

ORIGINAL PAGE IS
OF POOR QUALITY

F_{SL}: 20 X 10^6N (4.5 X 10^6 LBF)

OUTER COMBUSTOR

PROPELLANT: O_2/RP-1

P_c: 2068 N/cm^2 (3000 PSIA)

MR: 2.8

COOLANT: HYDROGEN

N_f: ~250 X 4 CYCLES

F_o/F_t: 0.65

W/H: 3.0

ε_1: 40

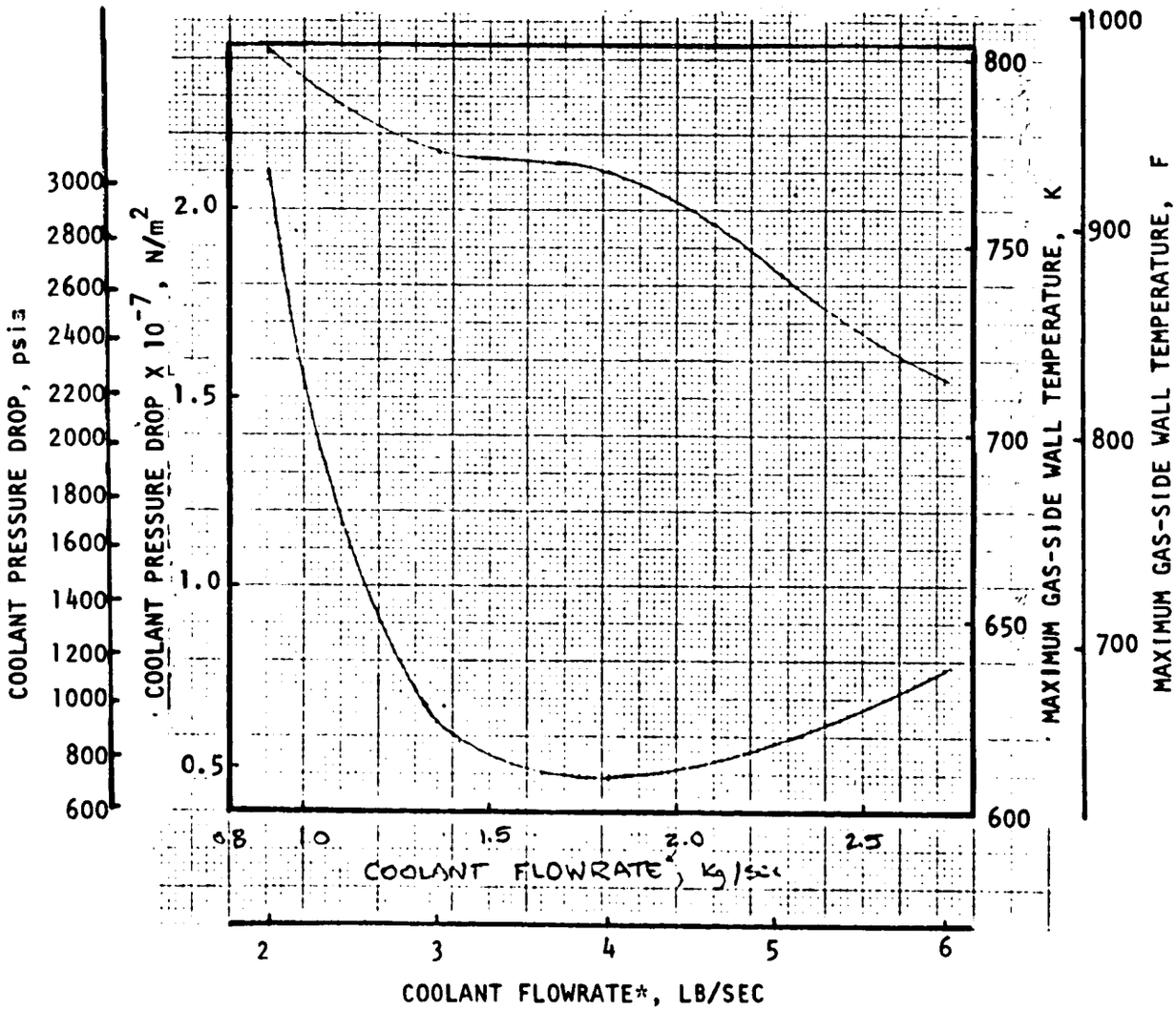

Figure 47. Influence of Hydrogen Coolant Flow on Combustor Coolant Passage Design

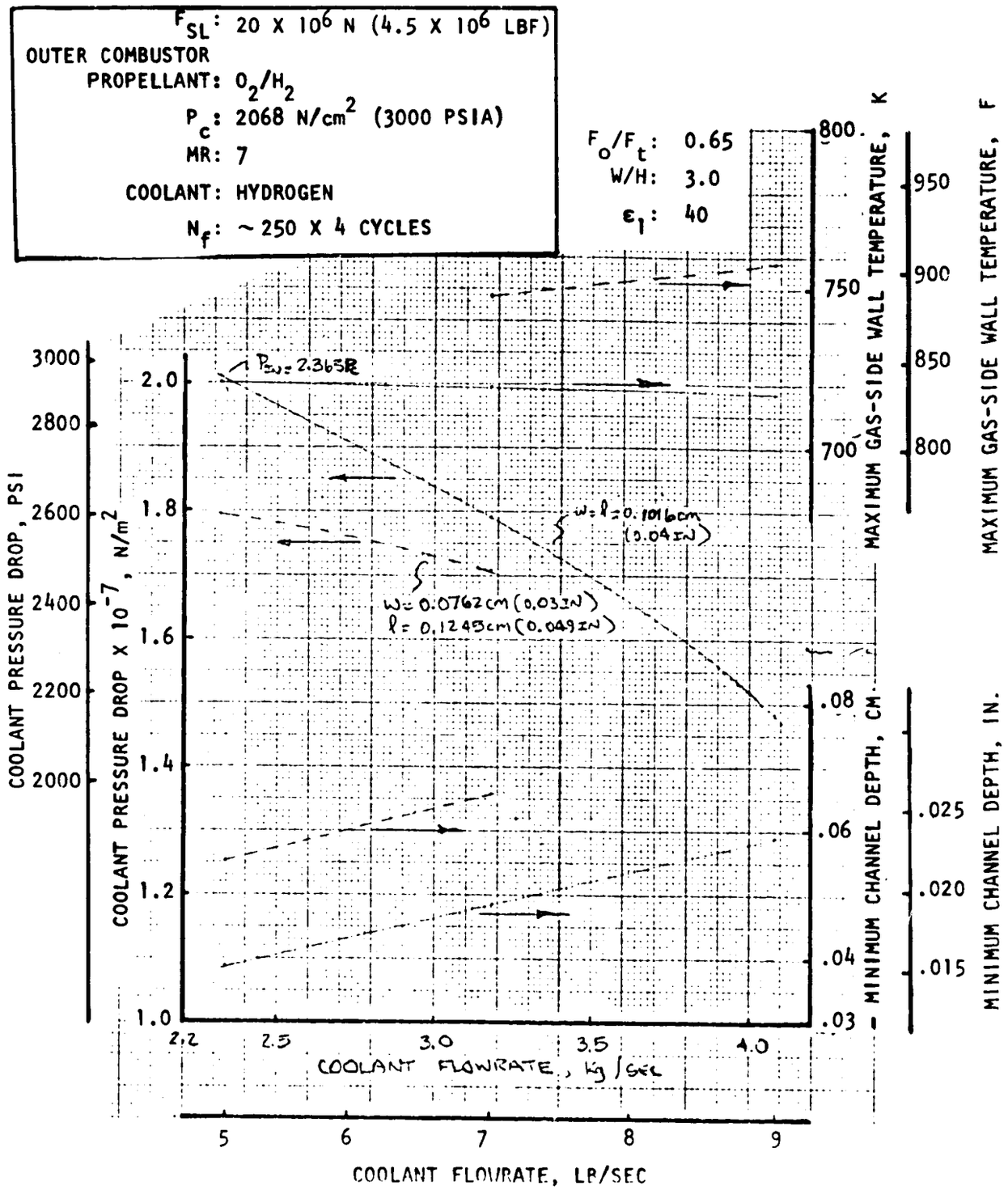

Figure 48. Influence of Coolant Channel Width on Combustor Coolant Passage Design

ORIGINAL PAGE IS
OF POOR QUALITY

The influence of coolant passage width is illustrated in Fig. 48. The cycle life for a channel wall chamber is dependent on the temperature differential between the gas-side and the back wall. For this specific application, the narrower channel width 0.0762 cm (0.03 inch), which is the minimum acceptable value based on the study guidelines, results in a high back-wall temperature. This is due to the combination of wider channel lands and the narrower width. The result is a high allowable gas-side wall temperature and substantially lower coolant pressure drop.

NOZZLE COOLANT PASSAGE DESIGN/ANALYSIS

As indicated in the coolant circuit schematic (Fig. 26), the nozzle is cooled using a single downpass cooling circuit. Stainless-steel tubes provide satisfactory cooling and a lightweight nozzle. In the Mode 2 operation, only the inner combustor fires and the nozzle must be cooled using propellants of the inner combustor. Mode 1 operation is the most difficult nozzle cooling condition (higher heat fluxes) since the overall nozzle area ratio results in lower Mach numbers and high heat fluxes than those during Mode 2 operation.

O_2/RP-1 and O_2/H_2 Propellants

Hydrogen Cooling. If a portion of the hydrogen flow of the inner combustor is used to cool the outer combustor, the amount of hydrogen flow available for the nozzle decreases as the chamber pressure increases (Fig. 49). The maximum chamber pressure that can be cooled depends upon dividing the hydrogen flow to satisfy both cooling requirements.

The maximum chamber pressure which can be cooled is approximately 1.722×10^7 N/m^2 (2500 psia) based on using round tubes in the nozzle (Fig. 50). Cooling is limited by the near choking coolant conditions. The maximum gas-side wall temperature, heat input, and coolant temperature rise are shown in Fig. 50 and 51.

If hydrogen is not used to cool the outer combustor, the nozzle can be cooled well beyond the 1.722×10^7 N/m^2 (2500 psia) chamber pressure limit set by the inner combustion chamber cooling. Since the inner combustor is limited to this chamber pressure, these nozzle cooling data above 1722 N/m^2 (2500 psia) were not generated.

Oxygen Cooling. Using all the oxygen flow of the inner combustor to cool the nozzle, the nozzle can be cooled beyond a chamber pressure of 1.722×10^7 N/m^2 (2500 psia) which, as discussed previously, is the chamber limit for the hydrogen-cooled inner combustor for P_{inlet}/P_c ratio of 2.25. Since there is so much oxygen for cooling based on the assumptions of the analysis, the coolant pressure drop, and maximum gas-side wall temperature obtained for oxygen are less than those for hydrogen cooling, as shown in Fig. 50.

O_2/H_2 and O_2/H_2 Propellants

Hydrogen Cooling. For the configuration where both combustors operate on O_2/H_2, the inner combustor hydrogen flow can be used to cool the inner combustor and

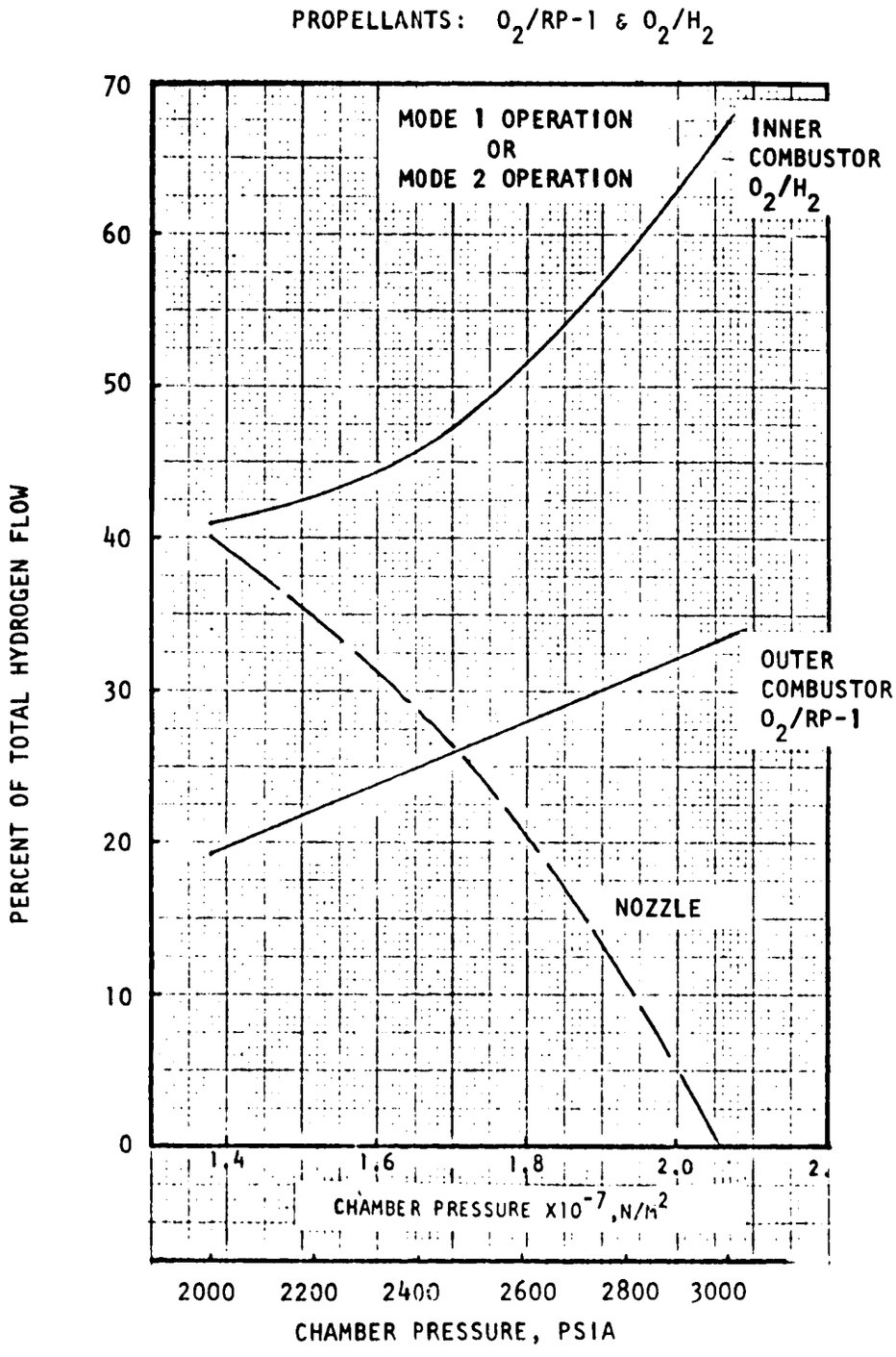

Figure 49. Combustor and Nozzle Coolant Flow (Hydrogen) Variation With Chamber Pressure (O_2/RP-1 and O_2/H_2 Configuration)

ORIGINAL PAGE IS
OF POOR QUALITY

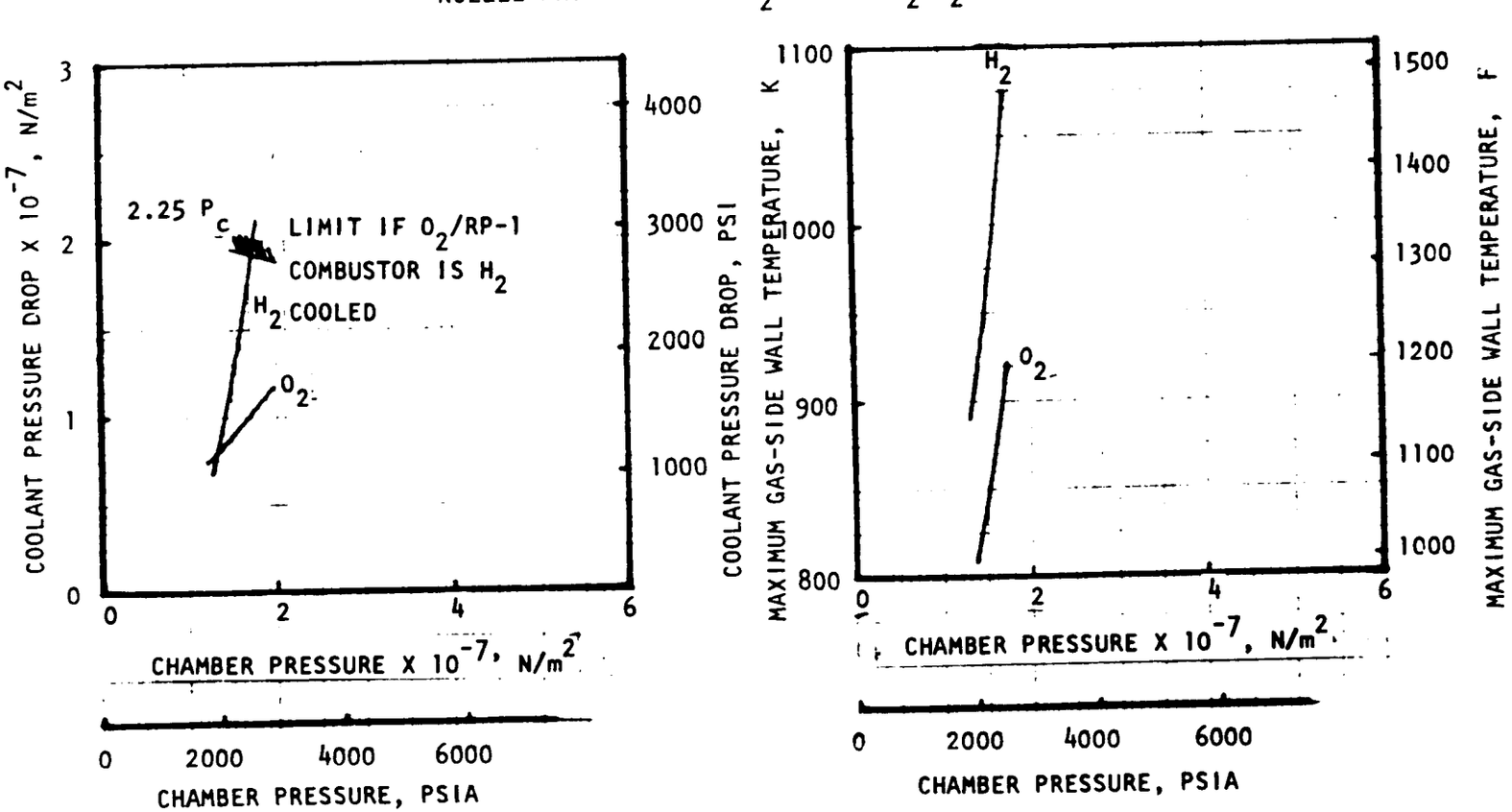

Figure 50. O_2/RP-1 and O_2/H_2 Nozzle Coolant Pressure Drop and Maximum Gas-Side Wall Temperature Variation With Chamber Pressure

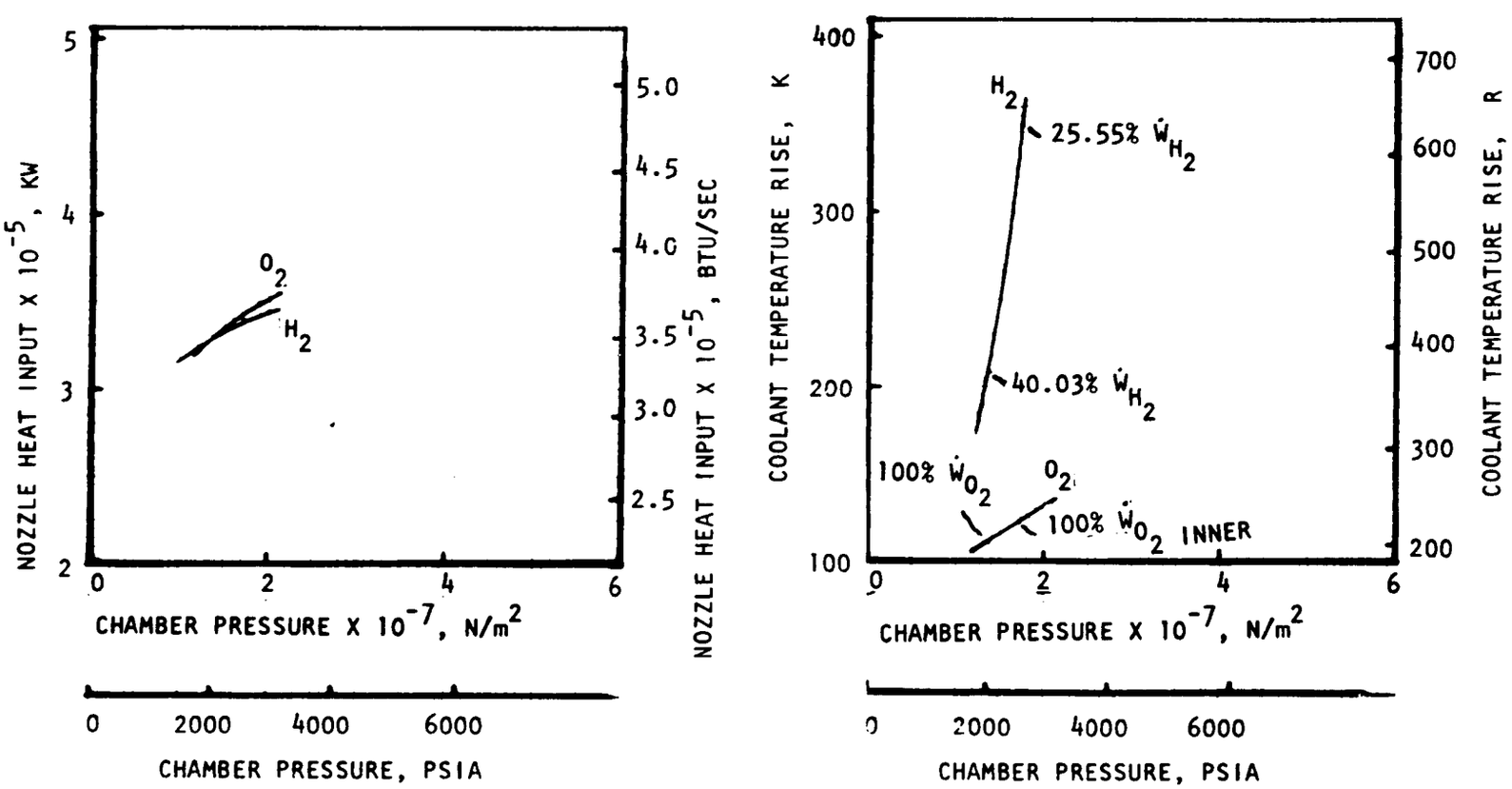

Figure 51. O_2/RP-1 and O_2/H_2 Nozzle Heat Input and Coolant Temperature Rise Variation With Chamber Pressure

ORIGINAL PAGE IS
OF POOR QUALITY

nozzle. As shcwn in Fig. 52, the available hydrogen flow decreases with chamber pressure. Comparing Fig. 50 and 53, the influence of non-hydrogen cooling of the outer combustor is illustrated. The nozzle can be easily cooled at 1.722×10^7 N/m^2 (2500 psia) with a lower coolant pressure drop and lower wall temperatures. The variation of heat input and coolant temperature rise with chamber pressure are presented in Fig. 54.

Oxygen Cooling. Comparing Fig. 50 and 53, the influence of the outer combustor propellant combination is shown. The coolant pressure drop and maximum wall temperatures are approximately the same.

WIDTH-TO-HEIGHT RATIO INFLUENCE

All cooling analysis was performed for an engine with a nozzle width-to-height (W/H) ratio of 3.0. As the width-to-height (W/H) ratio increases, the surface area exposed to the hot gas increases. For a fixed thrust and chamber pressure, the available coolant flow remains constant and thrust chamber cooling becomes more difficult as W/H increases. An analysis to evaluate the W/H was performed (Table 9) for an inner combustor using hydrogen as a coolant. Designs which resulted in the same cyclic life were selected. As shown in Table 9, the amount of coolant flow required and the coolant pressure drop increased substantially for the higher width-to-height ratio, which indicates a more difficult cooling condition.

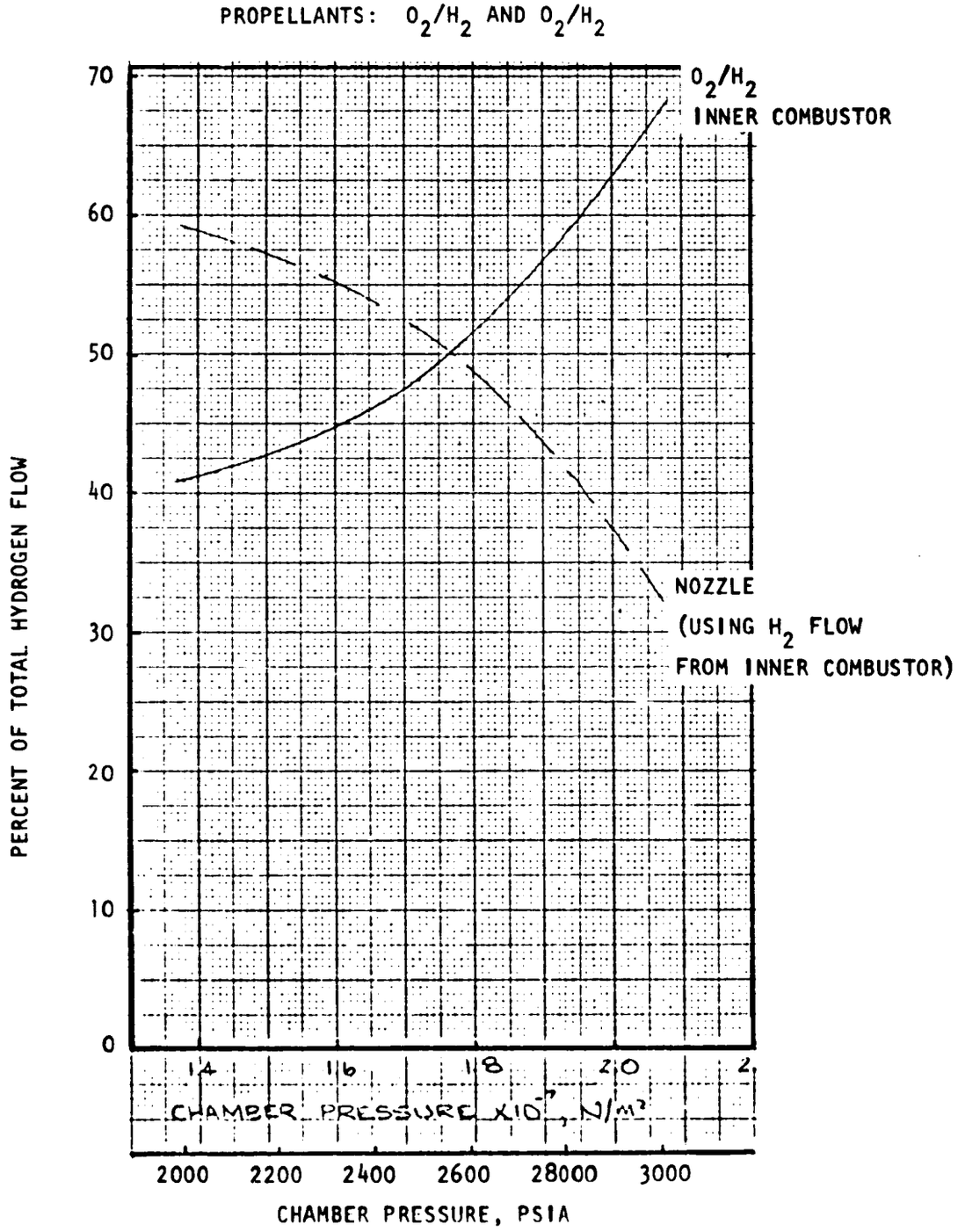

Figure 52. Combustor and Nozzle Coolant Flow (Hydrogen) Variation With Chamber Pressure (All O_2/H_2 Configuration)

ORIGINAL PAGE IS
OF POOR QUALITY

PROPELLANTS: O_2/H_2 AND O_2/H_2 (INNER AND OUTER COMBUSTORS)

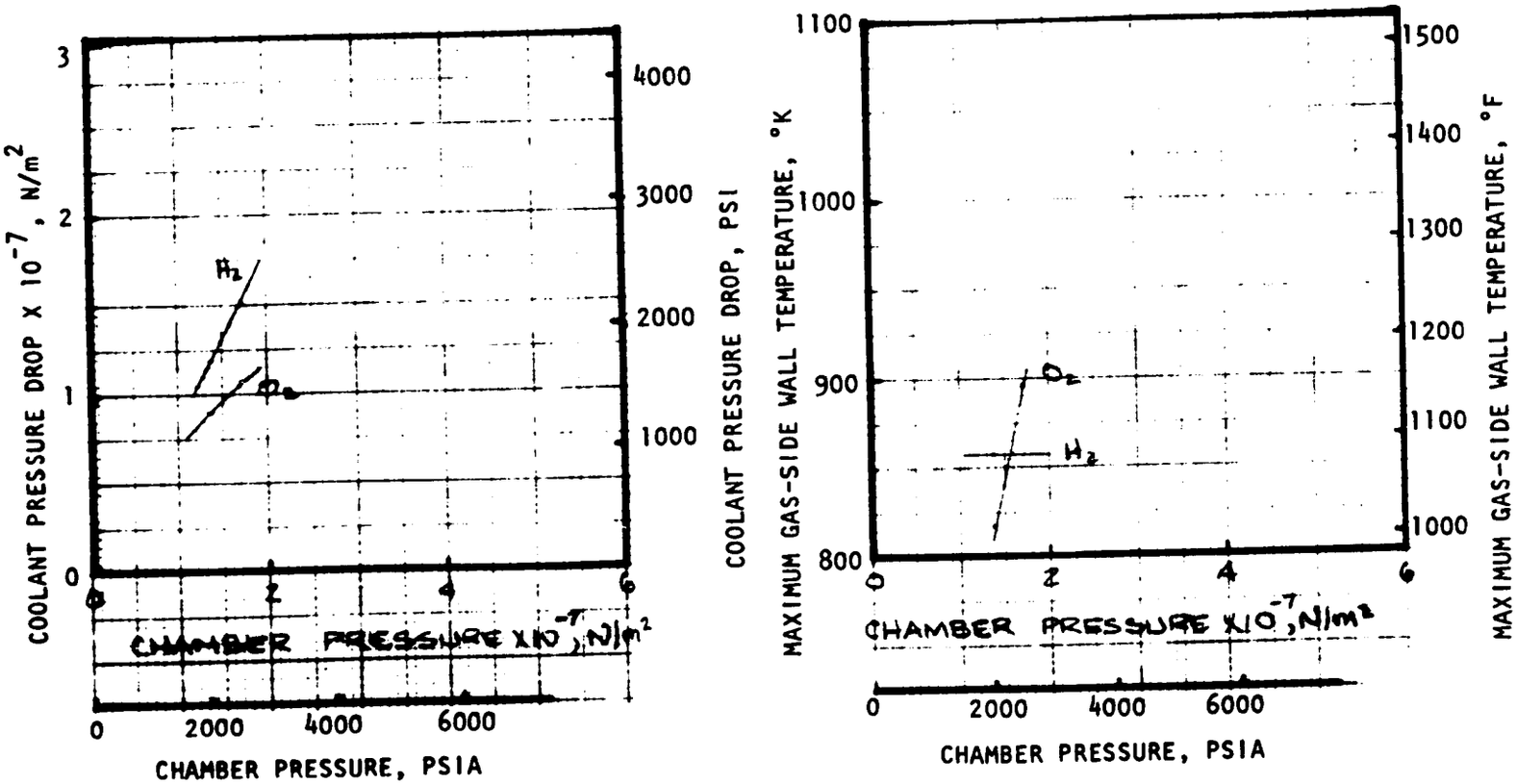

Figure 53. Nozzle Coolant Pressure Drop and Maximum Gas-Side Wall Temperature Variation With Chamber Pressure

PROPELLANTS: O_2/H_2 AND O_2/H_2 (INNER AND OUTER COMBUSTORS)

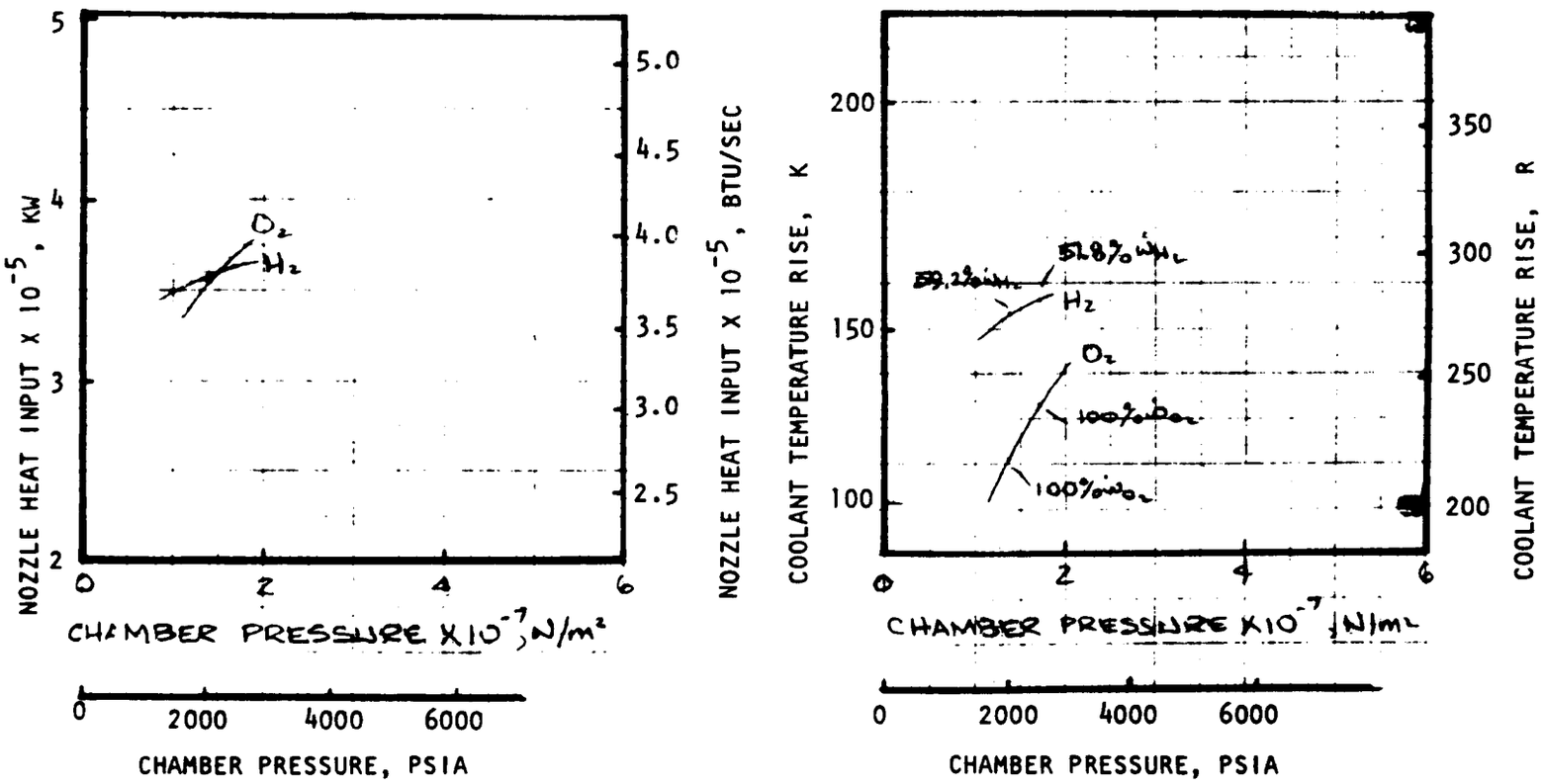

Figure 54. Nozzle Heat Input and Coolant Temperature Rise Variation With Chamber Pressure

ORIGINAL PAGE IS
OF POOR QUALITY

TABLE 9. INFLUENCE OF WIDTH-TO-HEIGHT RATIO ON COMBUSTOR HEAT TRANSFER

PROPELLANT: O_2/H_2

P_c: $1.379 \times 10^7 N/m^2$ (2000 PSIA)

MR: 7

MODE 2 OPERATION: $\epsilon_2 = 114$

COOLANT: HYDROGEN

COMBUSTOR MATERIAL: Zr - CU

NOZZLE W/H	3	4
CYCLIC LIFE (N_F), CYCLES	313	314
MAXIMUM GAS-SIDE WALL TEMP., K	720	722
(R)	(836)	(840)
COOLANT PRESSURE DROP, N/m^2	7.088×10^6	11.182×10^6
(PSI)	(1028)	(1622)
PERCENTAGE OF TOTAL COOLANT	47.59	54.59
MAXIMUM COOLANT MACH NUMBER	0.4465	0.584
MAXIMUM CHANNEL DEPTH, CM	0.0627	0.0579
(IN.)	(0.0247)	(0.0228)

TASK IV: BASELINE ENGINE PERFORMANCE, WEIGHT, AND ENVELOPE

The primary objective of this task was to generate engine delivered performance, weight, and envelope for the four linear engine concepts indicated in Table 3 and to determine engine power cycle requirements. In the process, power-cycle data such as flows, temperatures, pressures, and turbomachinery performance were obtained. The guidelines for this task are presented in Table 10.

Each concept of Table 3 was analyzed over a chamber pressure range of 6.89 x 10^6 N/m^2 to 34.5 x 10^6 N/m^2 (1000 psia to 5000 psia) to determine the maximum attainable chamber pressure corresponding to the power-cycle limits.

POWER CYCLE ANALYSIS

The power-cycle analysis was performed with chamber pressure as a variable parameter holding expansion area ratio, thrust, and thrust split constant at values shown in Table 3. Data were generated for both the gas generator cycle and the staged combustion cycles.

Results of Task I, II, and III were utilized. Injector, valve, and line pressure drops were held at the minimum values specified in Table 10. Combustion efficiency for the LOX/hydrogen propellants were based on both the test results for the linear test bed No. 1 (Ref. 1) and on the performance of the SSME. Specific impulse efficiencies of 0.9667 and 0.9552, respectively, for the LOX/hydrogen and LOX/hydrocarbon propellant combinations were calculated based on these combustion efficiencies. The I_s efficiencies apply to the main combustors (exclusive of base thrust contribution). They are based on tank inlet conditions, and nozzle efficiencies representative of experimentally realizable values.

Gas Generator Cycle

The engine schematic for the gas generator cycle is shown in Fig. 13. Two individual sets of pumps are used for each module. For ease in engine control, each pump is provided with its own gas generator. Gas generator sets are operated with the propellants of their respective combustor at the minimum flowrate required to provide pump power. The fuel-rich exhaust flows from each turbine set are mixed and introduced in the nozzle base where additional thrust is generated from the base pressure. Thrust chamber pressure is assumed equal in both combustors and turbine pressure ratio of 20 is used.

Performance. Vacuum and sea level performances for the gas generator cycle are shown in Fig. 55 through 58 as a function of chamber pressure for the four propellant combinations of interest. The performance reflects the specific impulse of the split-combustor engine while both combustors are in operation. Pump and turbine efficiencies are discussed in the Turbomachinery section. The inner combustors of each propellant combination are cooled with hydrogen. The outer combustor of the LOX/RP-1 case is also cooled with hydrogen. As shown in Task III, best cooling (lower pressure drops, longer cycle-life, and higher chamber pressures) is obtained with hydrogen. In the LOX/RJ-5 case, the outer combustor is cooled with hydrogen. The outer combustor of the LOX/CH_4 system is cooled with methane.

TABLE 10. BASELINE ENGINE POWER-CYCLE AND PERFORMANCE, GROUNDRULES

EXPANSION AREA RATIO (MODE 1/MODE 2)	40:1/114:1
ENGINE MIXTURE RATIO (OXYGEN/FUEL)	
LOX/H_2	7.1:1
LOX/RP-1	2.8:1
LOX/RJ-5	2.7:1
LOX/CH_4	3.5:1
PREBURNER MIXTURE RATIO (OXYGEN/FUEL)	
LOX/H_2	1.12:1
LOX/RP-1	0.40:1
LOX/RJ-5	0.40:1
LOX/CH_4	0.43:1
TURBINE PRESSURE RATIO	
GAS GENERATOR	20
STAGED COMBUSTION	~1.5
NOZZLE WIDTH-TO-HEIGHT RATIO	4
NUMBER OF MODULES	4
COMBUSTION EFFICIENCIES	
LOX/H_2	0.995
LOX/HYDROCARBON	0.98
INJECTOR PRESSURE DROPS(1)	
LIQUID (MINIMUM), %	15
GASEOUS (MINIMUM), %	8
VALVE PRESSURE DROPS(1)	
SHUTOFF, %	1
CONTROL (LIQUID, MINIMUM), %	5
CONTROL (GAS, MINIMUM),%	10

(1) PERCENT OF UPSTREAM PRESSURE

ORIGINAL PAGE IS
OF POOR QUALITY

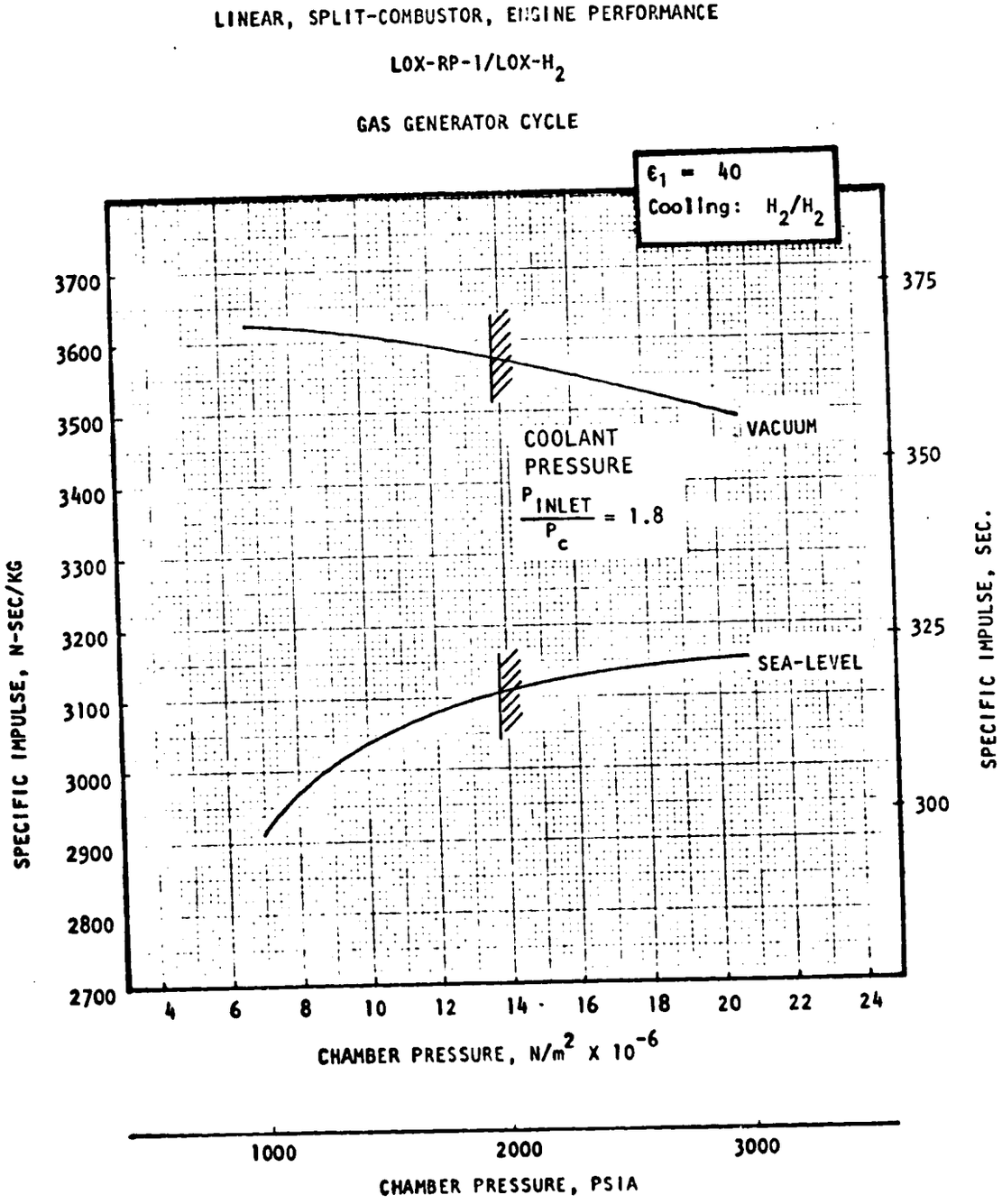

Figure 55. Linear, Split-Combustor, Mode 1 Engine Performance LOX-RP-1/LOX-H_2 Gas Generator Cycle

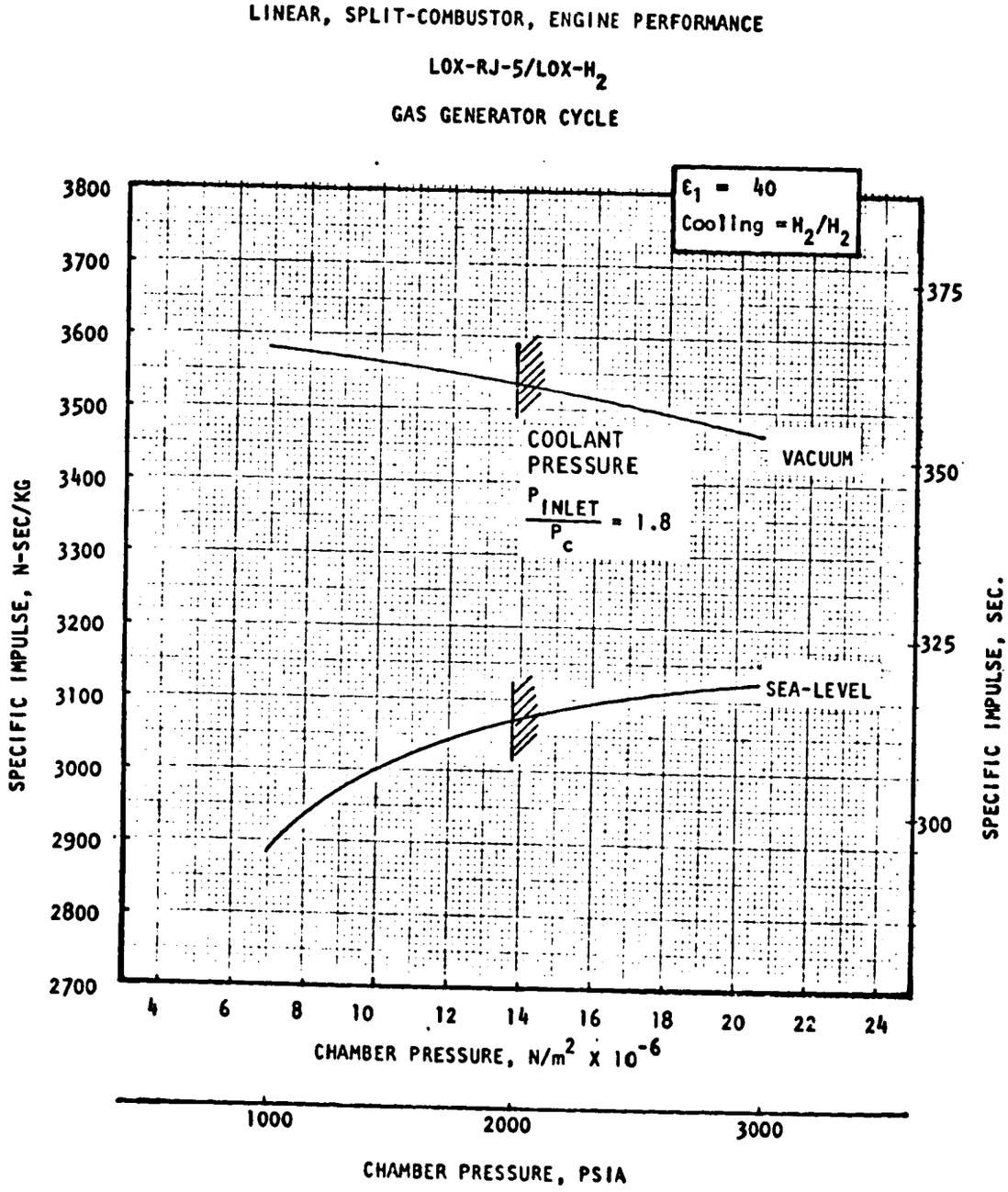

Figure 56. Linear, Split-Combustor, Mode 1 Engine Performance LOX-RJ-5/LOX-H_2, Gas Generator Cycle

ORIGINAL PAGE IS
OF POOR QUALITY

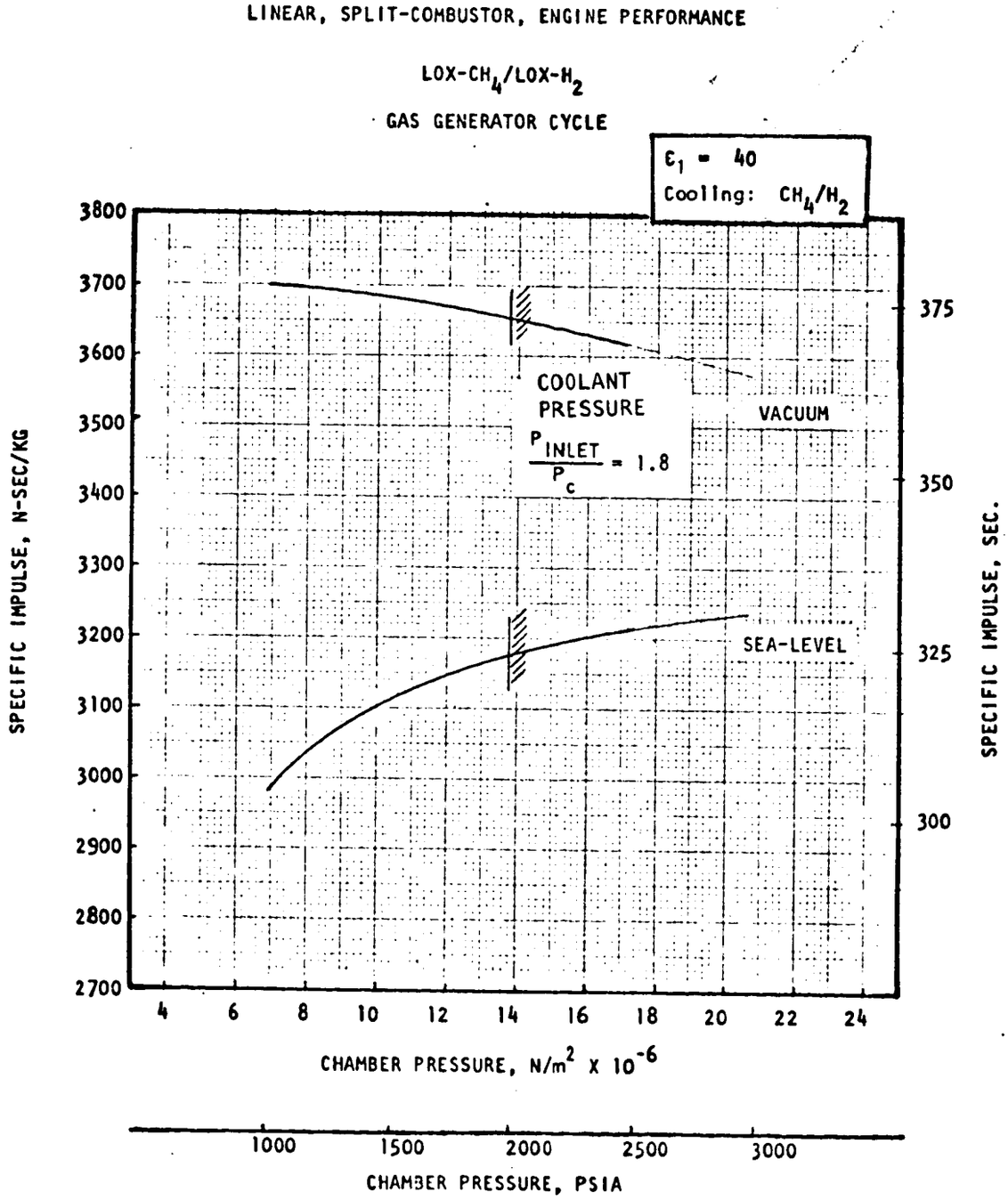

Figure 57. Linear, Split-Combustor, Mode 1 Engine Performance $LOX-CH_4/LOX-H_2$, Gas Generator Cycle

ORIGINAL PAGE IS
OF POOR QUALITY

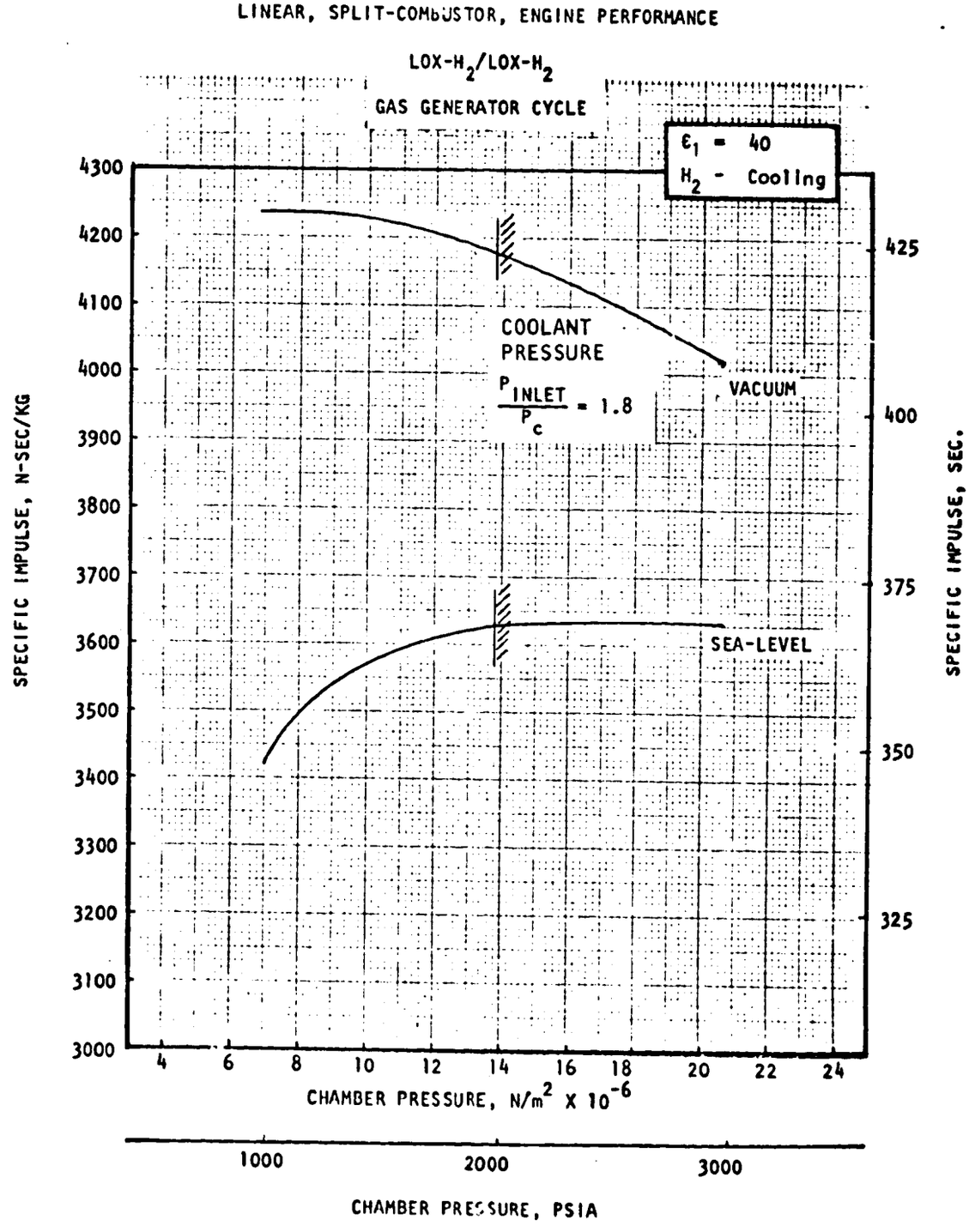

Figure 58. Linear, Split-Combustor, Mode 1 Engine Performance $LOX-H_2/LOX-H_2$, Gas Generator Cycle

In all four cases, the gas generator cycle vacuum performance decreases with chamber pressure. This is the result of the increased pump power requirements as chamber pressure is increased. Increased pump power at constant turbine pressure ratio is met by increasing the turbine flow. For fixed engine and gas generator mixture ratio, the increased turbine flow shifts the main thrust chamber mixture ratio above the optimum value, decreasing performance. Also, an increasing fraction of the flow is combusted at the fuel-rich gas generator mixture ratio, also decreasing performance.

At sea level, increasing chamber pressure at constant thrust and area ratio reduces the ambient pressure drag ($-\varepsilon P_a/P_c$), therefore increasing performance. However, part of this performance increase is cancelled by the increased turbine power demands with increasing chamber pressure (as in the vacuum case).

Of the hydrocarbons considered, methane yields the highest performance (Fig.57) followed by RP-1 (Fig. 55) and RJ-5 (Fig. 56). Methane provides approximately 80 N-sec/kg (8.2 sec) improvement over RP-1; and RP-1 provides approximately 40 N-sec/kg (4.1 sec) improvement over RJ-5. These differences result from the respective theoretical performances of the three hydrocarbons and the differences in cycle power (jacket pressure drop) resulting from the coolant selected in each case: methane, hydrogen, and hydrogen, respectively.

Inner combustor-only performance for the gas generator cycle is shown in Fig.59 as a function of chamber pressure. All four propellant concepts display similar inner combustor performance.

Chamber Pressure Limits. No chamber pressure limit attributable to cycle power limits exists for the gas generator cycle. The penalty of the increased power demand, however, is performance which decreases with chamber pressure.

As illustrated in Table 11, the chamber pressure limits of the gas generator cycles are set by the P_{inlet}/P_c ratios used as ground rules for Task III studies. For the cycles using RJ-5 or RP-1 cooling, this limit results in a chamber pressure of 0.372×10^7 N/m^2 (540 psia), taking precedence over the coking limits of 689 N/Cm^2 (1000 psia). The same ground rule results in a chamber pressure limit of 1.1×10^7 N/m^2 (1600 psia) for oxygen cooling and 1.38×10^7 N/m^2 (2000 psia) for hydrogen cooling.

Staged Combustion Cycle

The engine schematic for the staged combustion cycle is shown in Fig. 14. As in the gas generator cycle, two individual sets of turbopumps are used for each module. Each turbopump is equipped with its own preburner.

Performance. Performance for the staged combustion cycle cases is shown in Fig. 60 through 63 for both vacuum and sea level. Thrust chamber coolant used in each case is indicated in the figures and is the same as used in the gas generator cycle thrust chamber. Optimum amount of secondary flow (base flow) is extracted from the inner and outer combustor turbine discharge and

ORIGINAL PAGE IS
OF POOR QUALITY

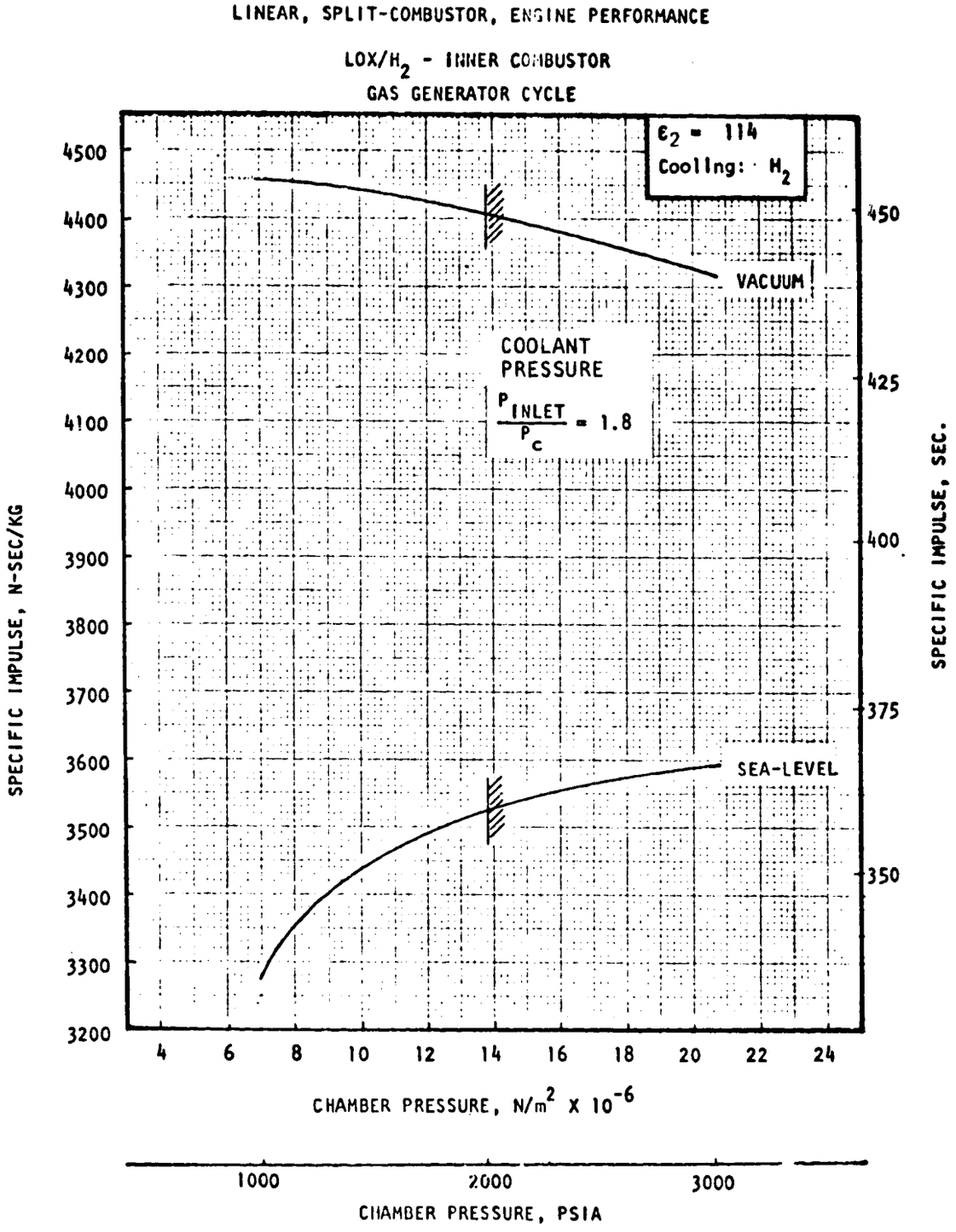

Figure 59. Linear, Split-Combustor, Mode 2 Engine Performance LOX/H_2-Inner Combustor, Gas Generator Cycle

TABLE 11. GAS GENERATOR ENGINE CHAMBER PRESSURE LIMITS

PROPELLANTS	COOLANT	CHAMBER PRESSURE LIMITS, N/cm^2 (PSIA)		
		COKING LIMIT	$\frac{P_{INLET}}{P_c}$ (1) LIMIT	TURBINE POWER LIMIT
OUTER COMBUSTOR:				
LOX/RP-1	H_2	-	1380 (2000)	No Limit
	RP-1	690 (1000)	320 (540)	No Limit
	O_2	-	1380 (2000)	No Limit
LOX/RJ-5	H_2	-	1380 (2000)	No Limit
	RJ-5	690 (1000)	320 (540)	No Limit
	O_2	-	1380 (2000)	No Limit
LOX/CH_4	H_2	-	1380 (2000)	No Limit
	CH_4	-	1380 (2000)	No Limit
	O_2	-	1240 (1800)	No Limit
LOX/H_2	H_2	-	1380 (2000)	No Limit
	O_2	-	1100 (1600)	No Limit
INNER COMBUSTOR:				
LOX/H_2	H_2	-	1380 (2000)	No Limit
	O_2	-	940 (1360)	No Limit

(1) BASED ON TASK III GROUND RULES OF: P_{INLET}/P_C EQUALS 1.8 FOR GAS GENERATOR CYCLE, AND 250 x 4 CYCLIC LIFE

ORIGINAL PAGE IS OF POOR QUALITY

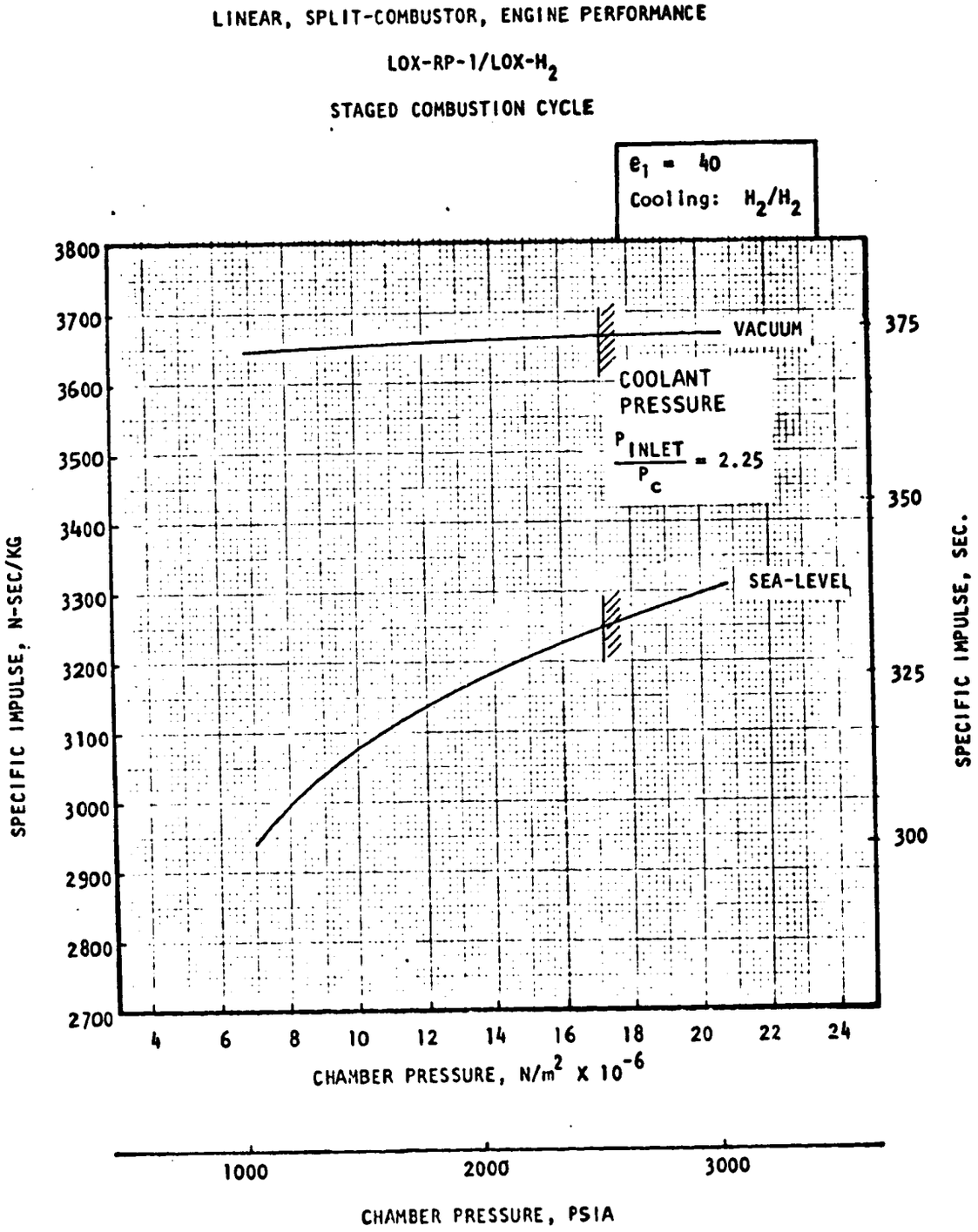

Figure 60. Linear, Split-Combustor, Mode 1 Engine Performance LOX-RP-1/LOX-H_2, Staged Combustion Cycle

C-2

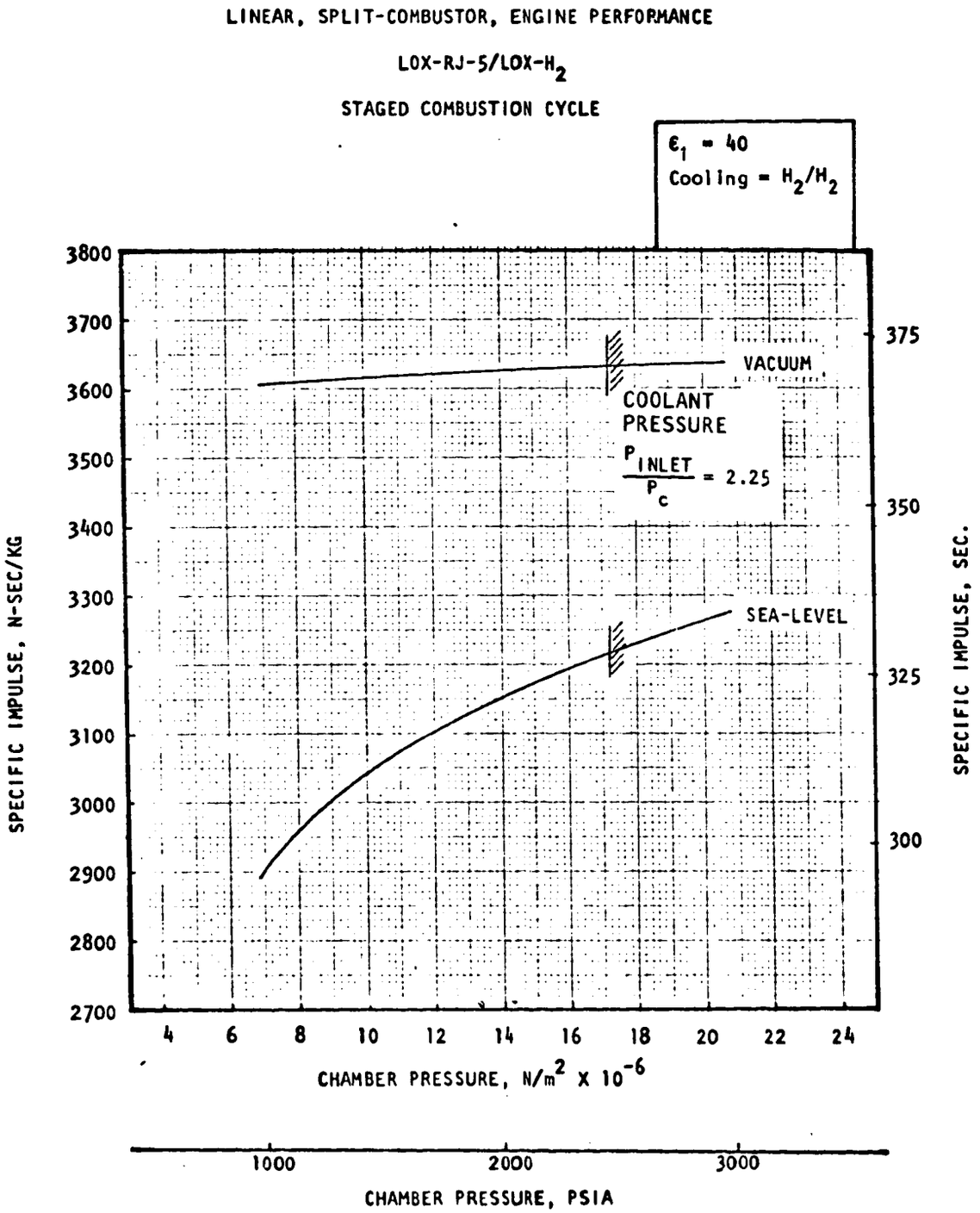

Figure 61. Linear, Split-Combustor, Mode 1 Engine Performance LOX-RJ-5/LOX-H_2, Staged Combustion Cycle

ORIGINAL PAGE IS OF POOR QUALITY

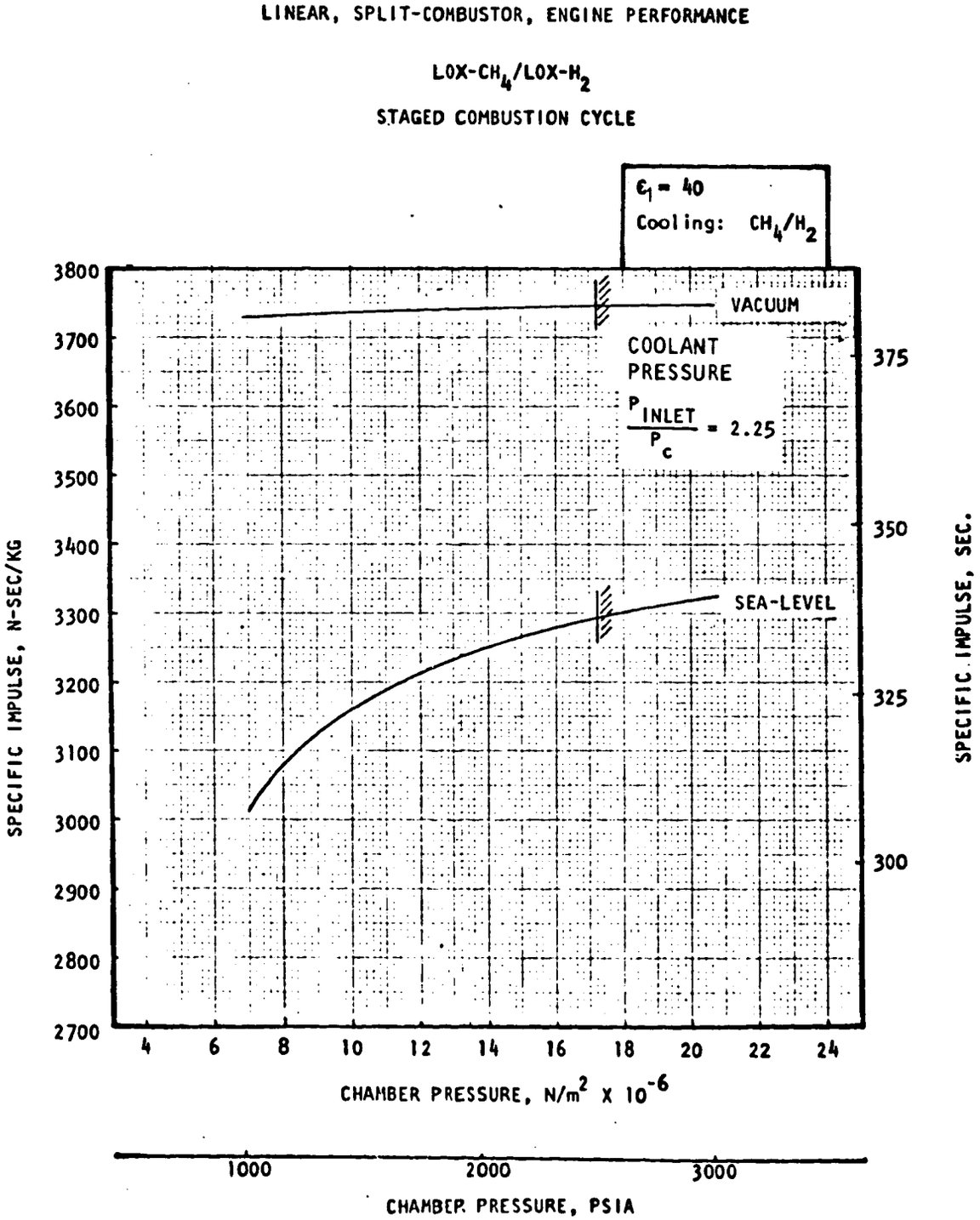

Figure 62. Linear, Split-Combustor, Mode 1 Engine Performance $LOX-CH_4/LOX-H_2$, Staged Combustion Cycle

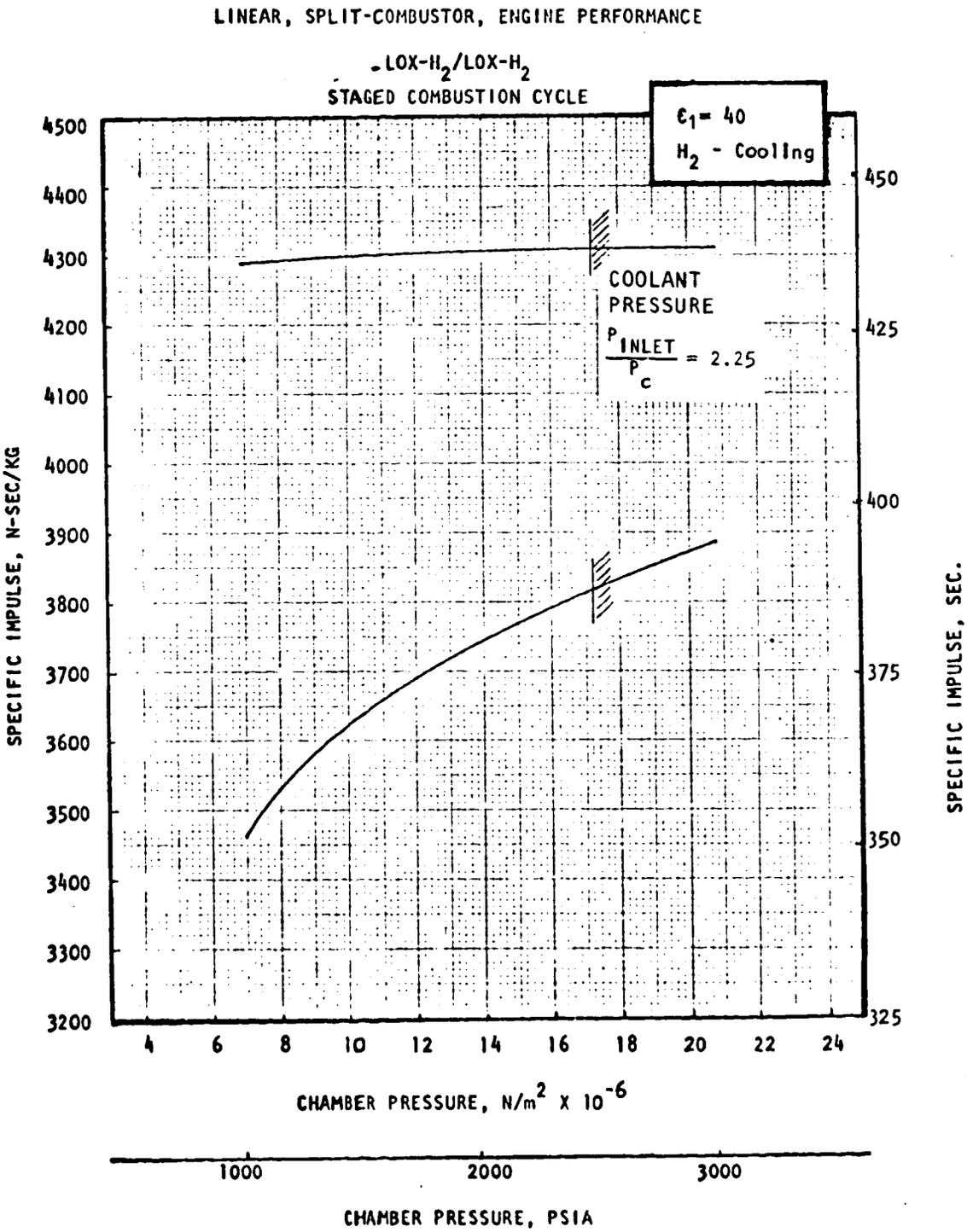

Figure 63. Linear, Split-Combustor, Mode 1 Engine Performance $LOX-H_2/LOX-H_2$, Staged Combustion Cycle

ORIGINAL PAGE IS
OF POOR QUALITY

introduced in the engine base to develop optimum thrust. Because of this secondary flow, a mixture ratio shift away from optimum value occurs in the primary stream (combustor) resulting in a loss in delivered primary specific impulse. The same effect is present at sea level. However, at sea level, ambient pressure drag ($-\varepsilon P_a/P_c$) reduction with chamber pressure is predominant and a faster (than the GG cycle) increase of specific impulse with chamber pressure is obtained.

Inner combustor-only performance for the staged combustion cycle is presented in Fig. 64 as a function of chamber pressure. All four propellant concepts display similar inner combustor performance.

A comparison of the gas generator and staged combustion cycle sea level performance for the LOX/RP-1 hydrogen-coolant case is shown in Fig. 65. At the low chamber pressures where the required turbine power is lower and the secondary (base) flows for the staged combustion and gas generator cycles are similar, performance for both cycles is also similar. At the higher chamber pressures where the turbine power requires large flows for the gas generator cycle, the difference in performance between the two cycles is approximately 160 N-sec/kg (16 sec.), with the staged combustion cycle providing the higher performance.

Chamber Pressure Limits. The various limits on operating chamber pressure are presented in Table 12. The limits due to coolant circuit inlet pressure (P_{inlet}/P_c) are from the cooling analysis of Task III and presented in Fig. 28. The turbine power cycle limits (Table 13) were calculated by matching the power available from the turbines with the power required by pumps at the discharge pressure needed to meet system pressure drop requirements. Of the hydrocarbon fuels, the lowest turbine power limit (2.41×10^7 N/m^2, 3500 psia) is with LOX/RP-1 propellants. This propellant combination has the lowest horsepower per pound of turbine gas (lowest C_p). The LOX/RJ-5 system with turbine-gas properties similar to LOX/RP-1 has the highest turbine power limit (2.69×10^7 N/m^2, 3900 psia) because of its high fuel density (lower fuel pump power), and high available turbine flow-ratio (a function of overall mixture ratio and preburner mixture ratio). The LOX/CH_4 system has higher fuel pump horsepower requirements (low fuel density and higher coolant jacket pressure drop) than both the LOX/RP-1 and LOX/RJ-5 systems, but enough horsepower per pound of turbine flow (higher C_p) and enough available turbine flow to be able to attain a higher turbine power limit (2.55×10^7 N/m^2, psia) than LOX/RP-1, but lower than LOX/RJ-5.

All preburners are operated fuel-rich. Therefore, a limit exists on the amount of turbine flow when all of the fuel is used to generate turbine power. As the engine mixture ratio increases, the available turbine flow ratio (turbine to total flow) decreases. The ratio is lowest for the LOX/H_2 system with an engine mixture ratio of 7. The system is penalized also by the lowest fuel density. Although it has the highest horsepower per pound of turbine flow (highest C_p), the low turbine flow available and low fuel density lead to a turbine power limit of 2.41×10^7 N/m^2 (3500 psia).

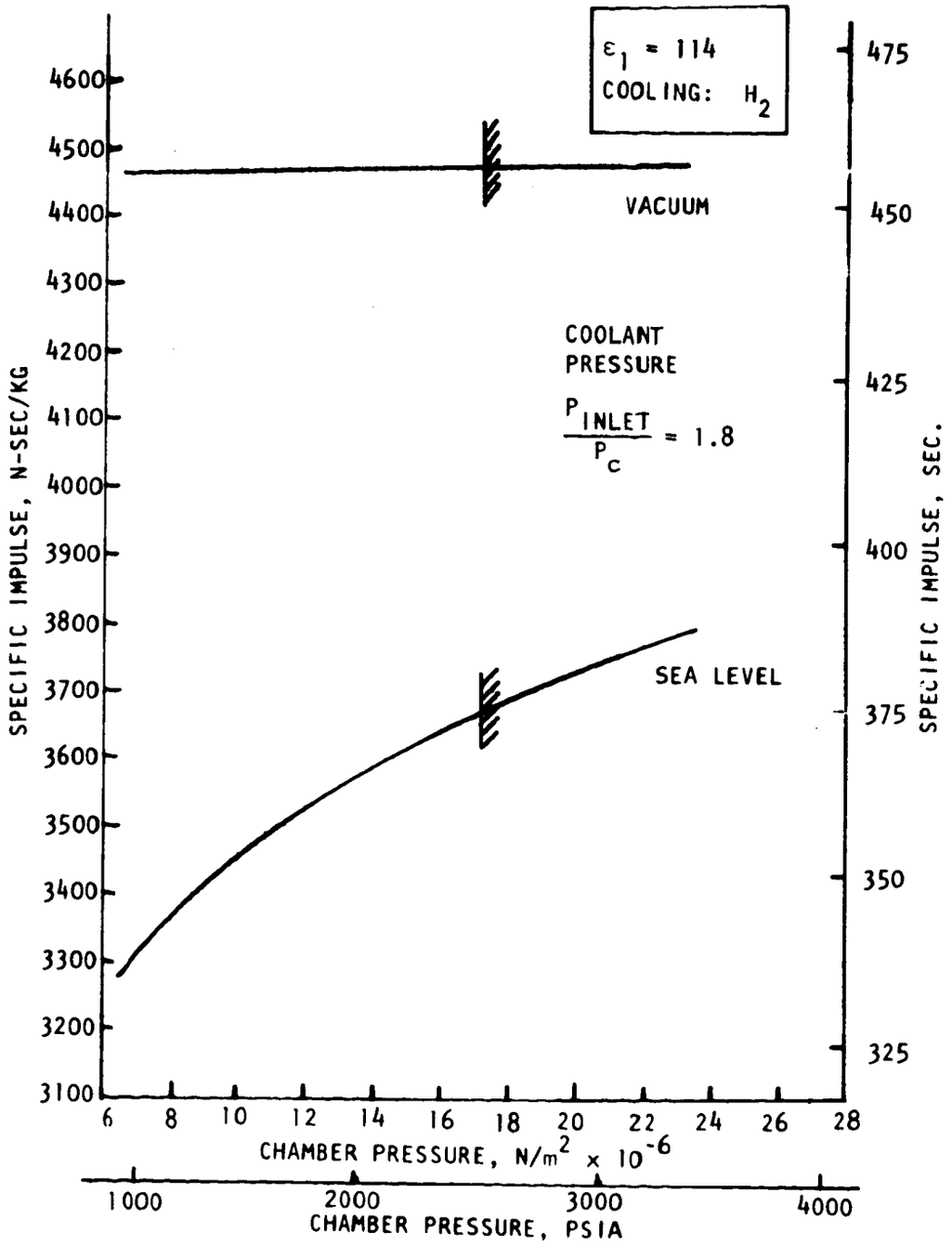

Figure 64. Linear, Split-Combustor, Mode 2 Engine Performance LOX/H_2-LOX/H_2 Inner Combustor, Staged Combustion Cycle

ORIGINAL PAGE IS
OF POOR QUALITY

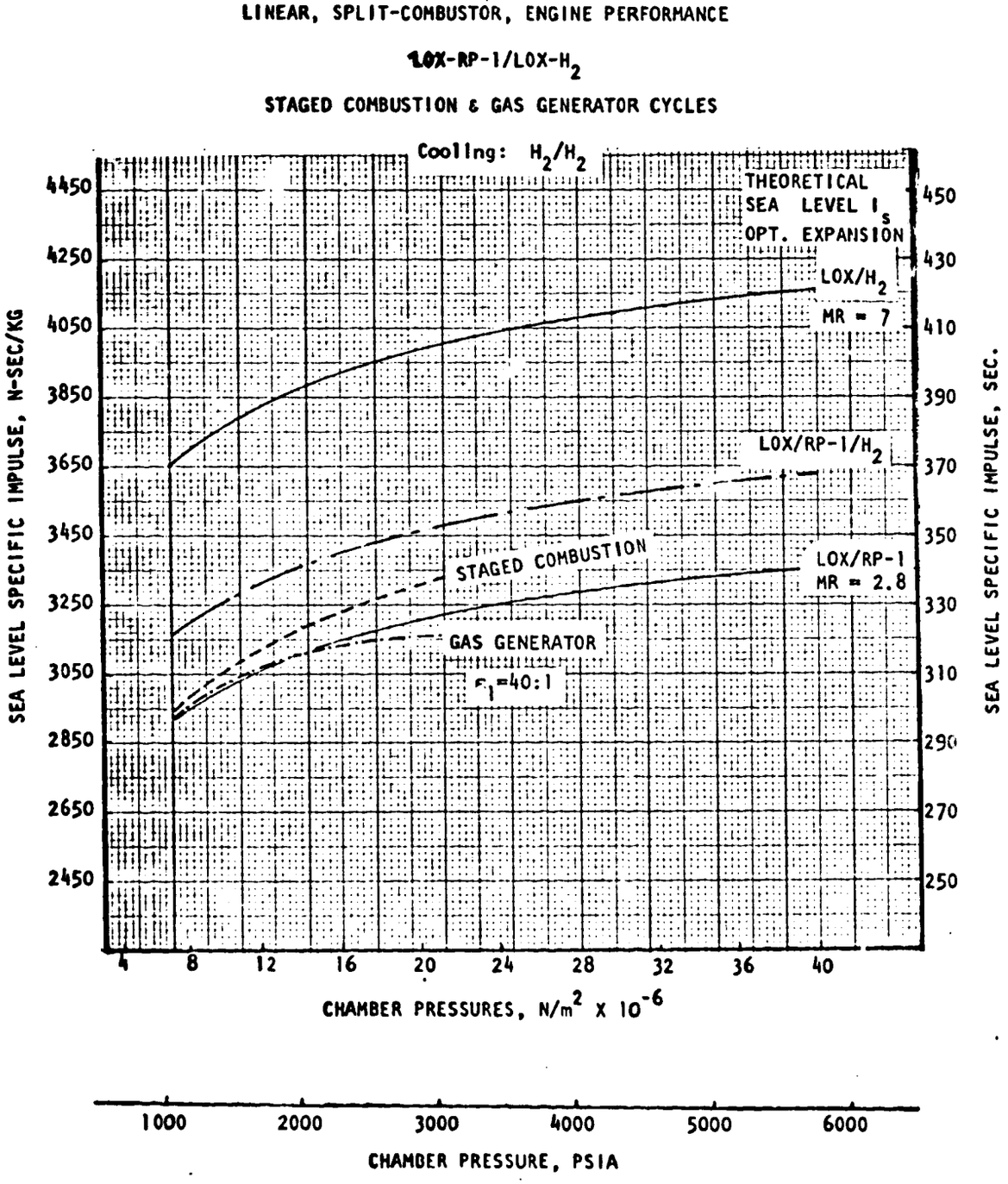

Figure 65. Linear, Split-Combustor, Mode, Engine Performance LOX-RP-1/ $LOX-H_2$, Staged Combustion and Gas Generator Cycles

TABLE 12. STAGED COMBUSTION ENGINE CHAMBER PRESSURE LIMITS

Propellants	Coolant	Chamber Pressure Limits, N/cm^2 (psia)		
		Coking Limit	P_{inlet}/P_c* Limit	Turbine Power Limit
Outer Combustor:				
LOX/RP-1	H_2	-	1720 (2500)	2410 (3500)
	PR-1	690 (1000)	480 (700)	-
	O_2	-	1790 (2600)	-
LOX/RJ-5	H_2	-	1720 (2500)	2690 (3900)
	RJ-5	690 (1000)	480 (700)	-
	O_2	-	1790 (2600)	-
LOX/CH_4	H_2	-	>1720 >(2500)	-
	CH_4	-	1720 (2500)	2760 (3700)
	O_2	-	1590 (2300)	-
LOX/H_2	H_2	-	2070 (3000)	2410 (3500)
	O_2	-	1380 (2000)	-
Inner Combustor:				
LOX/H_2	H_2	-	1720 (2500)	2340 (3400)
	O_2	-	1350 (1960)	-

*Based on Task III ground rules of P_{inlet}/P_c equals 2.25 for staged combustion, and 250 x 4 cyclic life

ORIGINAL PAGE IS
OF POOR QUALITY

TABLE 13. STAGED COMBUSTION POWER CYCLE LIMITS OUTER COMBUSTOR, SPLIT COMBUSTOR LINEAR AEROSPIKE

Propellants	Engine Mixture Ratio MR_E	Fuel Density Kg/M^3, (Lb/Ft^3) ρ_f	TURBINE GAS				Chamber Pressure Limit, N/cm^2 (PSIA) $P_{c_{limit}}$	Coolant Jacket ΔP, N/cm^2 (PSIA)
			Joule/Kg K (Btu/LB F) C_p	γ	Mixture Ratio MR_s	Flow Ratio W_t/W_p		
LOX/RP-1	2.8	808.9(50.5)	2742(.655)	1.132	.4	.372	2410 (3500)	0
LOX/RJ-5	2.7	1065.2(66.5)	2742(.655)	1.132	.425	.389	2690 (3900)	0
LOX/CH_4	3.5	414.9(25.9)	3886(.928)	1.185	.43	.320	2760 (3700)	1010 (1460)
LOX/H_2	7.0	75.4(4.5)	7545(1.802)	1.348	1.12	.267	2410 (3500)	0

The turbine power limits are set by the inner combustor (Table 12) since both combustors operate at the same chamber pressure. The inner combustor, however, operates at a lower thrust (lower H_2 flows) and its hydrogen cools the high expansion area ratio (high surface area) nozzle. Higher coolant fluid velocities are required which result in higher jacket pressure drops and higher required pump power per pound of available turbine flow than in the outer combustor. The turbine power limit on the inner combustor is, therefore, lower than the outer combustor. Each propellant concept is turbine power limited to 2.34×10^7 N/m^2 (3400 psia), the limit of the inner combustor.

Pump discharge pressures for each propellant concept are shown in Fig. 66 through 70. The highest fuel pump discharge pressure (1.03×10^8 N/m^2, 14,900 psia) occurs with methane which is used as a coolant in the O_2/CH_4 system. Methane also has a low density compared to the other hydrocarbon fuels. The lowest oxygen pump discharge pressure, 5.08×10^7 N/m^2 (7370 psia), occurs in the LOX/H_2 system.

The chamber pressure limit of the split-combustor staged combustion engines is set by the inner combustor since both combustors operate at the same chamber pressure. For each propellant concept, the chamber pressure determined by the coolant pressure ratio limit of 2.25 is 1.724×10^7 N/m^2 (2500 psia), which corresponds to 74 percent of turbine power limit as established by the LOX/H_2 inner combustor.

TURBOMACHINERY ANALYSIS

An analytical study was conducted to generate the turbomachinery data required in Tasks II and IV. The data generated included pump and turbine efficiencies for both engine cycles and turbopump weight for the gas generator cycle. Since turbopump rotational speed is the single most important parameter used in estimating both pump efficiency and turbopump weight, a significant portion of the study was devoted to rotational speed prediction. NASA ground rules for the study are presented in Appendix A.

Gas Generator Cycle

Rotational Speed. In making the turbomachinery rotational speed predictions, it was assumed that the turbopumps are designed at the maximum allowable speed to minimize weight. In other words, the turbopumps are designed at the lowest of the applicable speed limits. In addition, it is assumed that the bearing DN and the seal rubbing velocity limits on speed are relieved through (1) technology advances, (2) changing the arrangement (e.g., by using outboard bearings), or (3) the use of relatively unlimited components as nonrubbing seals and nonrolling contact bearings. Technology advances may well be sufficient because the 3 million bearing DN required to equal or exceed the other limits in this study has been achieved with rolling contact bearings (Ref. 6). Also, outboard bearings, labyrinth seals, and controlled leakage face-type seals are used in the high-pressure turbopumps for the SSME (Ref. 7 and 8). If the bearing and seal limits are not relieved, the rotational speeds at high pump pressure rises are about 40 percent of those used. This, in turn, doubles both the turbopump weight and the number of pump stages required to attain a given efficiency.

ORIGINAL PAGE IS
OF POOR QUALITY

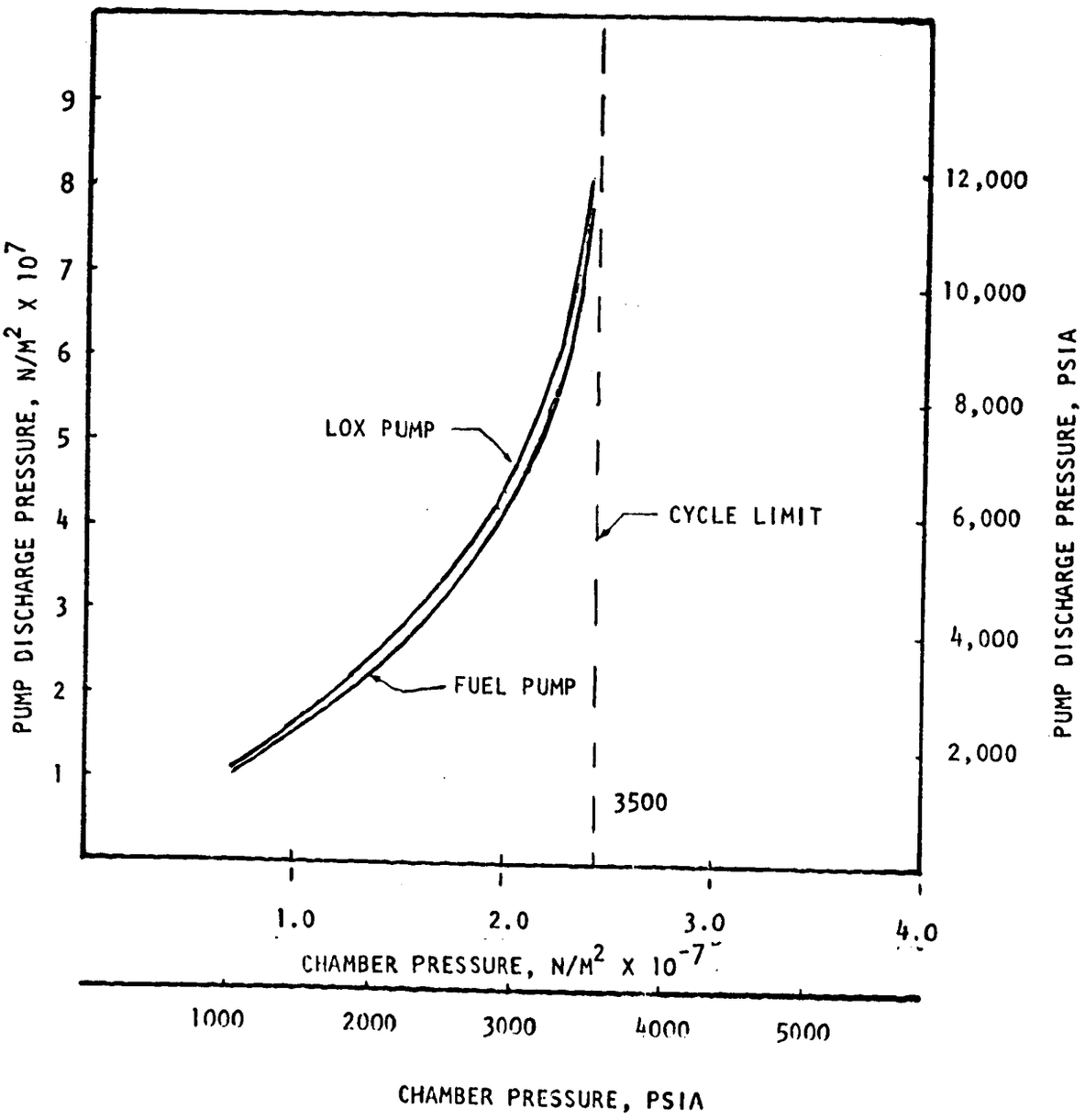

Figure 66. Staged Combustion Cycle Limits, LOX/RP-1, MR = 2.8, Outer Combustor Fuel-Rich Preburners, Hydrogen Cooled

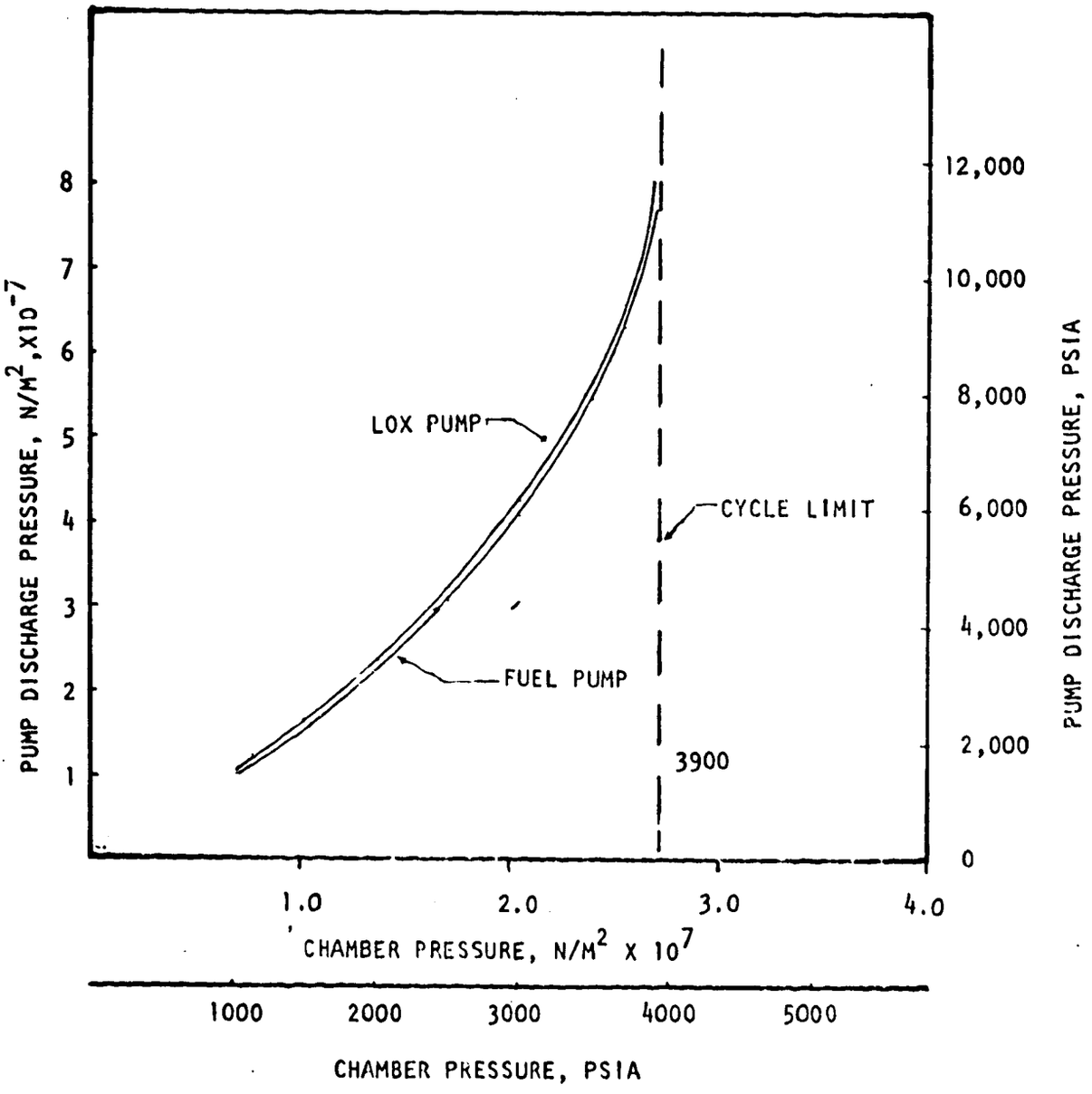

Figure 67. Staged Combustion Cycle Limits, LOX/RH-5, MR = 2.7, Outer Combustor Fuel-Rich Preburners, Hydrogen Cooled

ORIGINAL PAGE IS
OF POOR QUALITY

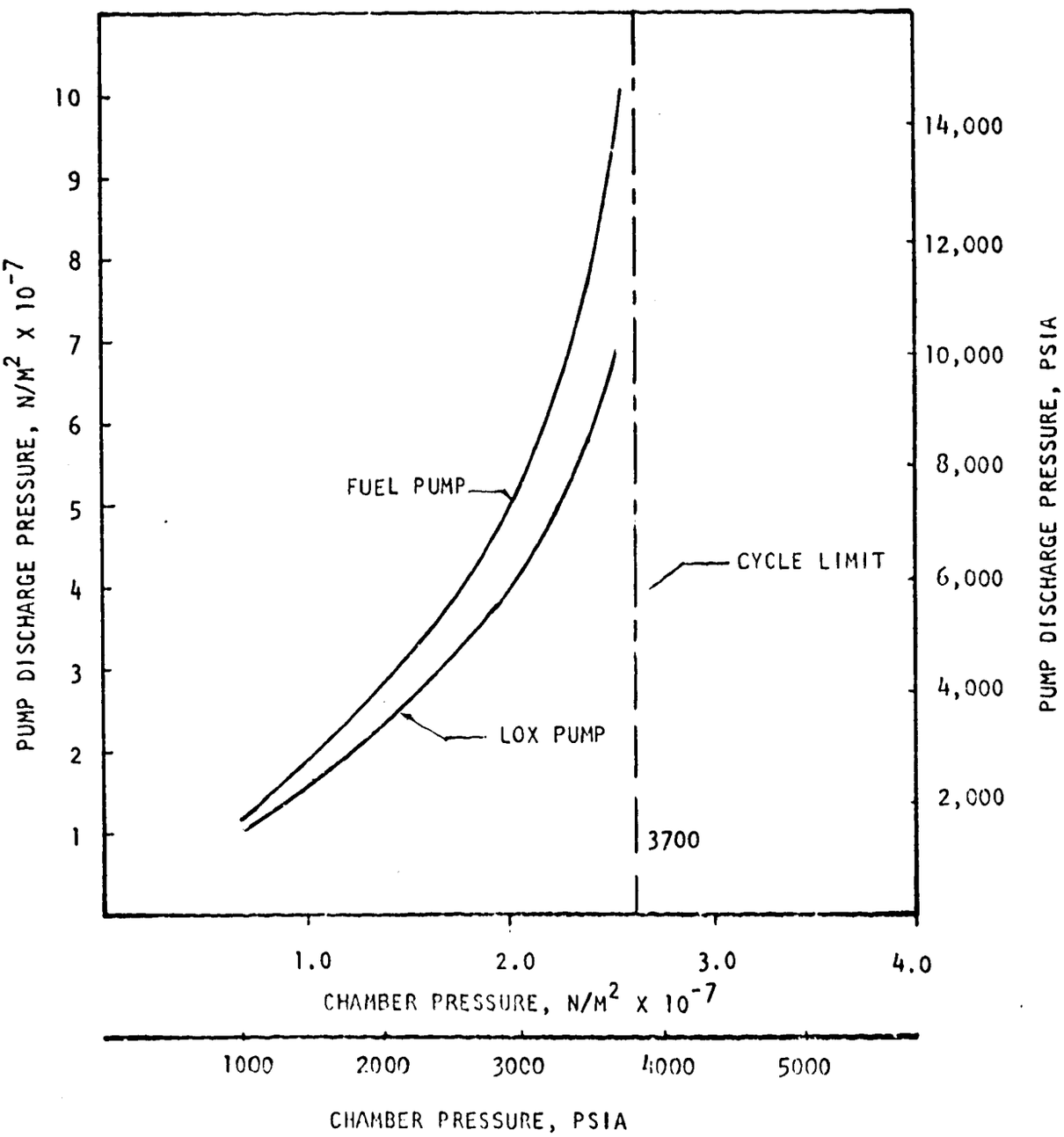

Figure 68. Staged Combustion Cycle Limits, LOX/CH_4, MR = 3.5, Outer Combustor Fuel-Rich Preburners, Methane Cooled

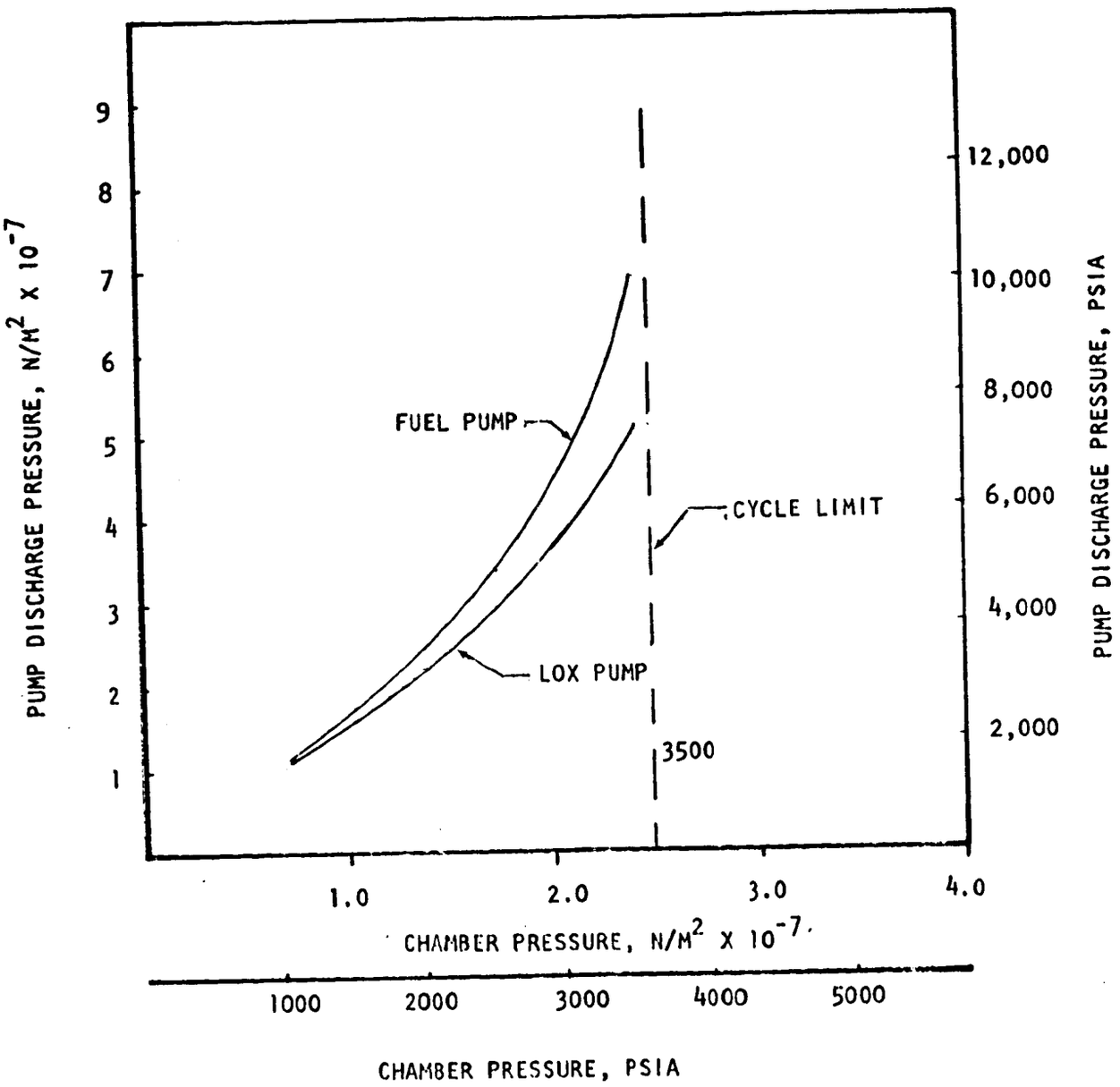

Figure 69. Staged Combustion Cycle Limits, LOX/H_2, MR = 7, Outer Combustor Fuel-Rich Preburners, Hydrogen Cooled

ORIGINAL PAGE IS
OF POOR QUALITY

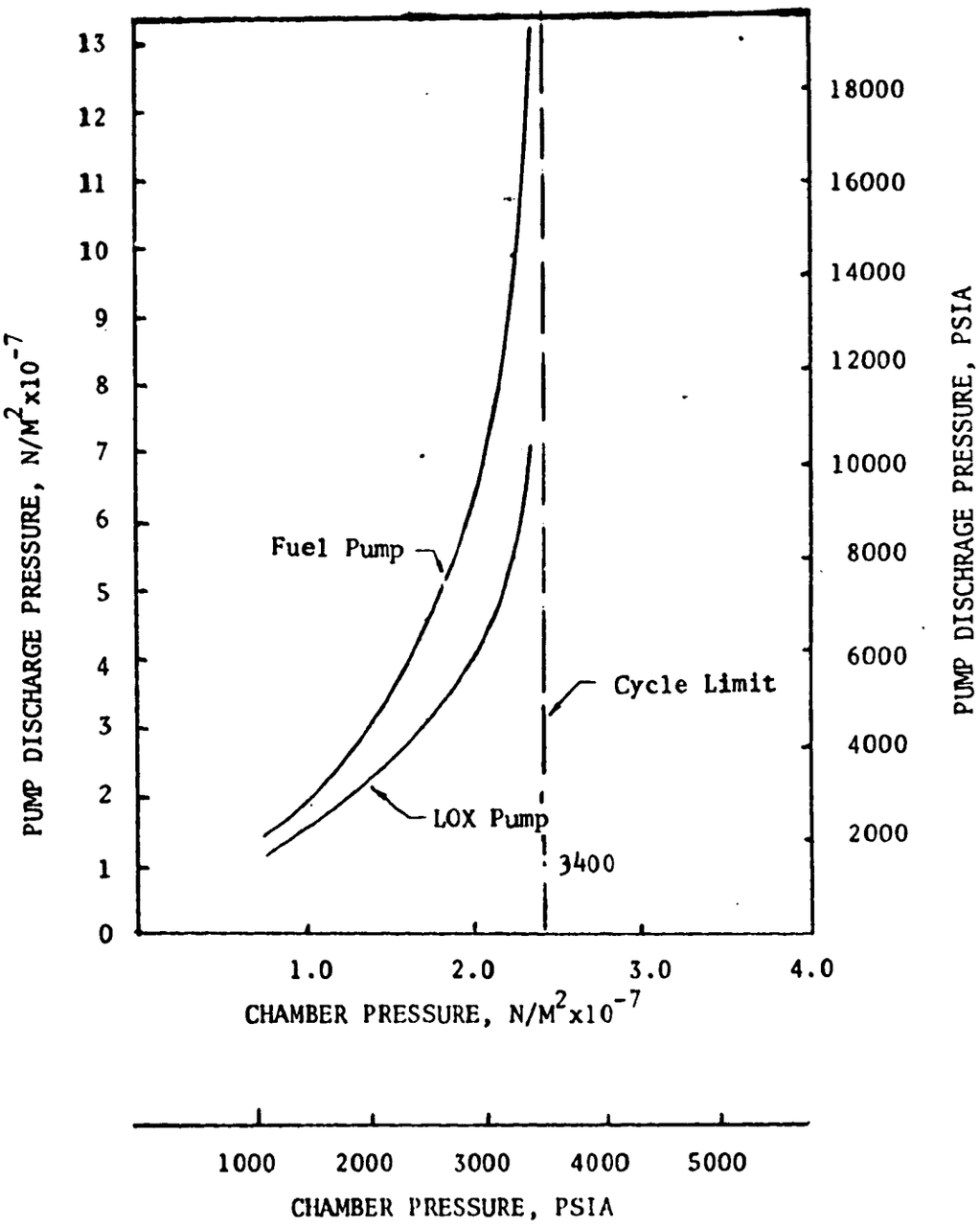

Figure 70. Staged Combustion Cycle Limits, LOX/H_2, MR = 7, Inner Combustor Fuel-Rich Preburners, Hydrogen Cooled

Another speed limit that was assumed to be relieved in the main high-pressure pumps is cavitation. This was done by assuming the use of boost pumps, as in the SSME (Ref. 7).

As shown in Ref. 8, the removal of the bearing, seal, and cavitation limits on speed leaves only the pump specific speed and the turbine stress limits. The pump specific speed limit is the specific speed at which single-stage centrifugal pumps reach their maximum efficiency. For a single entry pump, this value is:

$$37 \text{ rpm } \sqrt{m^3/sec}/m^{3/4} \quad (1900 \text{ rpm } \sqrt{gpm}/ft^{3/4})$$

By using a double-entry pump, as used for the SSME high-pressure oxygen pump (Ref. 7), this value can be increased 40 percent to:

$$52 \text{ rpm } \sqrt{m^3/sec}/m^{3/4} \quad (2700 \text{ rpm } \sqrt{gpm}/ft^{3/4})$$

The latter is used in this study.

The other applicable limit, the turbine stress, is caused by the centrifugal force. A turbine blade fails at the root if the product of the turbine annulus area and the square of the rotational speed ($A_a N^2$) exceeds a limiting value. The value is a function of the blade temperature, the material, and the geometry. A more complete discussion of the limit is presented in Ref. 9. In this study, a value of 2.58×10^7 m^2 rpm^2 (40×10^9 $in.^2$ rpm^2) is assumed for $A_a N^2$.

In making the actual calculations, pump propellant properties from Ref. 10 and 11 and turbine drive gas properties from Ref. 12 and 13 are used. The pump pressure rises are assumed to be 2.25 times the chamber pressure.

The equation used for the specific speed limits is:

$$N_{MAX} = \frac{(N_s)_{max} \Delta H^{0.75}}{Q^{0.5}} = \text{Constant} \times P_c^{0.75}/\rho^{0.25} \dot{w}^{0.5}$$

An existing computer program was used to make the speed estimates at the turbine stress limit.

The results indicate the double entry pump specific speed limit applies at low chamber pressures and the turbine stress limit applies at high chamber pressures. This occurs because the specific speed limit increases with chamber pressure whereas the turbine stress limit is essentially independent of chamber pressure, if the turbine pressure ratio and the ratio of the turbine inlet pressure to the chamber pressure are held constant. The chamber pressures at which the transition from the specific speed limit to the turbine stress limit occurs are listed in Table 14 as a function of the pump and the turbine fluids.

ORIGINAL PAGE IS
OF POOR QUALITY

TABLE 14. CHAMBER PRESSURES AT ROTATIONAL SPEED LIMIT TRANSITION

PUMP PROPELLANT	TURBINE DRIVE GAS	CHAMBER PRESSURE @ TRANSITION, P_{C_T}*, N/CM^2 (PSIA)
H_2	LOX/LH_2	145 (210)
CH_4	LOX/CH_4	627 (910)
RP-1	LOX/RP-1	752 (1090)
RJ-5	LOX/RJ-5	979 (1420)
LOX	LOX/LH_2	2140 (3100)
LOX	LOX/CH_4	1724 (2500)
LOX	LOX/RP-1	1055 (1530)
LOX	LOX/RJ-5	1034 (1500)

*P_{C_T} below which speed limit is double entry pump specific speed and above which speed limit is turbine blade centrifugal stress.

If the pump discharge pressure-to-chamber pressure ratio is dropped from 2.25 to 1.8, the pump head rise decreases 20 percent and, in turn, the speed at the specific speed limit decreases 15 percent. At the same time, the turbine flowrate decreases 20 percent, which causes the speed at the turbine stress limit to increase 12 percent. The net effect is to increase by 56 percent the chamber pressure at the rotational speed limit transition point (where the speed limit changes from pump specific speed to turbine stress).

Pump Efficiency. The Rocketdyne centrifugal pump preliminary design computer program was used to estimate the pump efficiencies at the calculated rotational speeds. The computer program uses data from Ref. 14 to predict the effect of size on pump perforamnce. In the case of pumps other than hydrogen, the number of pump stages is increased if the pump efficiency falls below 95 percent of the maximum value (i.e., at Ns_{MAX}). For hydrogen pumps, the minimum number of pump stages within the impeller tip speed limit of 640 m/sec (2100 ft/sec)) is used to minimize the turbopump shaft length. This minimizes the critical speed problems often encountered in large, high-pressure turbopumps.

The assumptions made, the resulting pump configurations, and the large size pump efficiencies are summarized in Table 15. For all propellants at all chamber pressures, pump efficiency fell off at low pump flowrates, as illustrated in Fig. 71. This is caused by two basic factors: (1) pump tip speed is a constant for a given engine chamber pressure, and (2) rotational speed increases with decreasing pump flowrate. The pump impeller decreases in size with decreasing flowrate which, in turn, decreases the efficiency (Ref. 14).

It is apparent the results are influenced to some degree by assumptions. If it were assumed that critical speed problems can be easily alleviated, doubling the number of stages could add 8 to 10 points onto the LH_2 pump efficiency without a significant increase in weight (the smaller diameter should make up for the increased length). If bearing and seal speed limits are assumed to be applicable and if the turbines are assumed to be overhung, more pump stages might be necessary to obtain high efficiency at high chamber pressures. In all cases, the maximum efficiency could be obtained by a combination of designing at a speed lower than the limit and using a stage number that would optimize efficiency. However, this would result in increased weight and complexity. The assumptions made for this study are felt to be reasonable.

Turbine Efficiency. The estimated turbine efficiencies are shown in Table 16 as a function of the type of engine fuel for both two- and three-rotor turbines. The assumptions are also listed in this table. The analyses conducted indicated no blade height limitations over the flowrate and chamber pressure ranges of interest and, therefore, within the assumptions listed, turbine efficiency is not influenced by either engine size or chamber pressure. The turbines for the LOX pumps have the same efficiencies as those for the corresponding fuel pumps. The efficiencies are obtained by deducting 5 percentage points (to account for unconsidered losses) from the parametric turbine efficiency curves in Ref. 8. Both two- and three-rotor designs are shown, the two-rotor being simpler, lighter, and less subject to critical

ORIGINAL PAGE IS
OF POOR QUALITY

TABLE 15. PUMP CONFIGURATIONS FOR GG LINEAR AEROSPIKE

PUMP $\Delta P = 2.25\ P_c$

$U_{T_{MAX}}$ = 640 m/sec (2100 FT/SEC)

STAGE NO. MINIMIZED FOR LH_2 DUE TO POSSIBLE CRITICAL SPEED LIMITATIONS

ROTATIONAL SPEED MAXIMIZED TO MINIMIZE WEIGHT

BEARING AND SEAL SPEED LIMITS ALLEVIATED BY TECHNOLOGY AND/OR TURBOPUMP ARRANGEMENT

FOR PUMPS OTHER THAN LH_2, MULTISTAGE IF η FALLS BELOW 95 PERCENT OF η MAX.

ENGINE	PUMP	FLOW DENSITY ρ_{AVG}, Kg/m^3 (LB/FT^3)	CHAMBER PRESSURE P_c, $N/m^2 X10^{-6}$ (PSIA)	NO. OF STAGES	ENTRY	SPEED LIMIT	η FOR $D_T \leq .254m$ (10")
LOX/LH_2	LH_2	75.4 (4.71)	6.9 (1000)	1	SINGLE	TURB. STRESS	73.0
			20.7 (3000)	3	"	"	73.8
			34.5 (5000)	5	"	"	73.9
	LOX	1134 (70.8)	6.9 (1000)	1	DOUBLE	D.E. NS	83.3
			20.7 (3000)	1	"	"	83.3
			34.5 (5000)	1	SINGLE	TURB. STRESS	83.3
LOX/CH_4	CH_4	415 (25.9)	6.9 (1000)	1	DOUBLE	"	83.3
			20.7 (3000)	1	SINGLE	"	79.1
			34.5 (5000)	2	"	"	82.3
	LOX	1134 (70.8)	6.9 (1000)	1	DOUBLE	D.E. NS	83.3
			20.7 (3000)	1	"	TURB. STRESS	83.1
			34.5 (5000)	1	SINGLE	"	83.0
LOX/RP-1	RP-1	809 (50.5)	6.9 (1000)	1	DOUBLE	D.E. NS	83.3
			20.7 (3000)	1	SINGLE	TURB. STRESS	81.0
			34.5 (5000)	2	"	"	83.8
	LOX	1134 (70.8)	6.9 (1000)	1	DOUBLE	D.E. NS	83.3
			20.7 (3000)	1	SINGLE	TURB. STRESS	83.0
			34.5 (5000)	1	"	"	79.1
LOX/RJ-5	RJ-5	1065 (66.5)	6.9 (1000)	1	DOUBLE	D.E. NS	83.3
			20.7 (3000)	1	"	TURB. STRESS	83.3
			34.5 (5000)	1	SINGLE	"	83.2
	LOX	1134 (70.8)	6.9 (1000)	1	DOUBLE	D.E. NS	83.3
			20.7 (3000)	1	"	TURB. STRESS	83.3
			34.5 (5000)	1	SINGLE	"	83.3

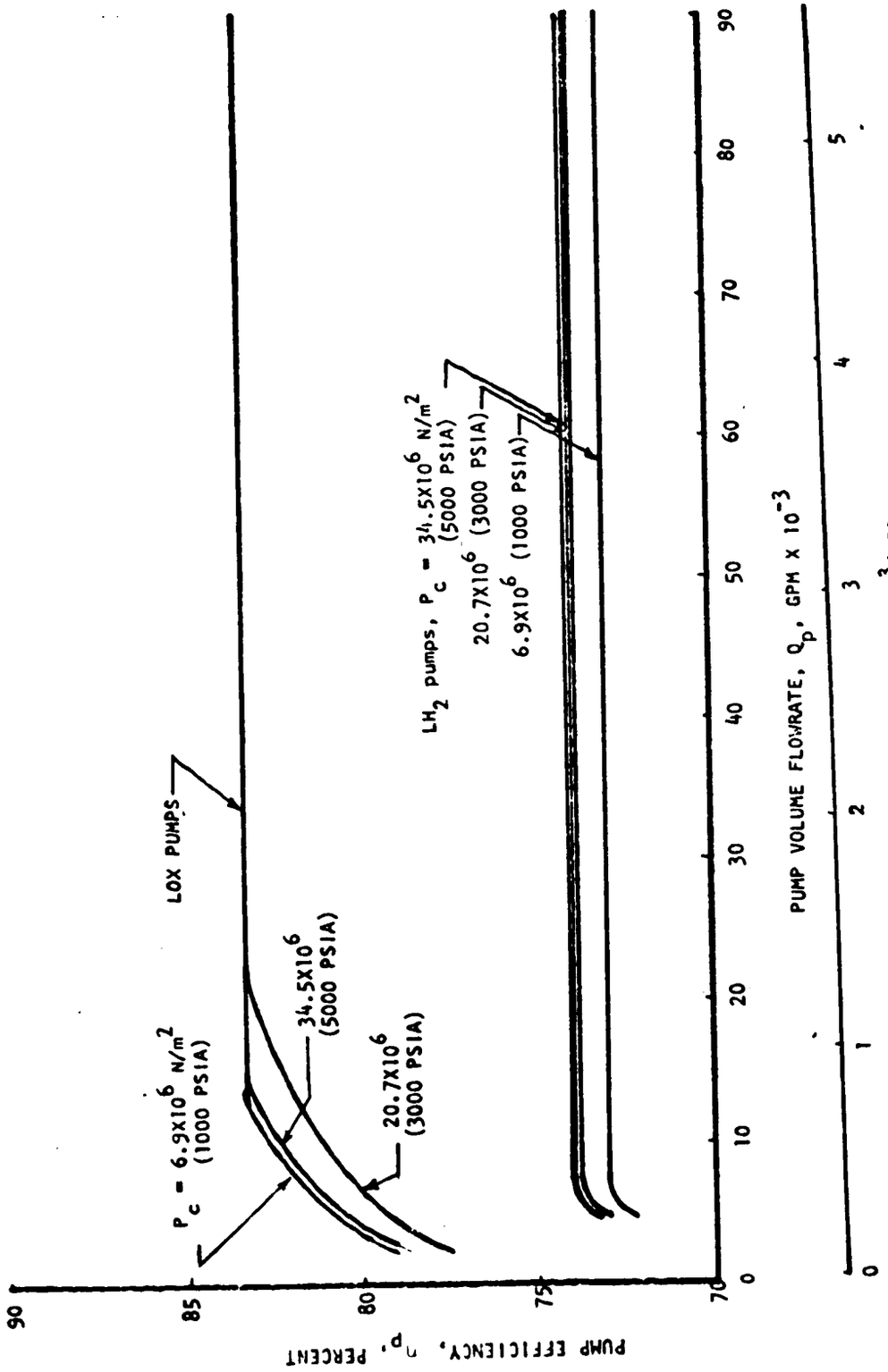

Figure 71. Pump Efficiencies for LOX/LH_2, GG, Linear Aerospike

ORIGINAL PAGE IS
OF POOR QUALITY

TABLE 16. TURBINE EFFICIENCIES FOR GG LINEAR AEROSPACE

PRESSURE RATIO = 20

U_M = 457 m/SEC (1500 FT/SEC)

TURBINE INLET TEMPERATURE = 1089° K (1960° R)

$P_{olT} = P_c$

FUEL RICH GASES

FUEL	Y	C_p, joule/Kg K (BTU/LB F)	TWO-ROTOR		THREE-ROTOR	
			TYPE	η,%	TYPE	η,%
LH_2	1.348	7545 (1.802)	2 ROW - V.C.	55	3 STG. - P.C.	65
CH_4	1.183	3886 (.928)	2 STG. - P.C.	72	3 STG. - P.C.	77
RP-1	1.132	2742 (.655)	2 STG. - REAC.	79	3 STG. - REAC.	84
RJ-5	1.132	2742 (.655)	2 STG. - REAC.	79	3 STG. - REAC.	84

speed problems and the three-rotor being more efficient. Considering the importance of turbine efficiency to the gas generator cycle, the three-rotor design is selected.

Staged Combustion Cycle

Rotational Speed. For the same reasons stated for the gas generator cycle, the turbopumps are assumed to be designed at the lowest of the two applicable rotational speed limits, the double-entry pump specific speed, and the turbine centrifugal stress. However, due to the nature of the engine cycle, an additional variable was considered, the turbine flow fraction. This variable is the fraction of the fuel that passes through the turbine. The reason for considering it is that in a staged combustion cycle, the use of lower flow, higher pressure ratio turbines decreases both the discharge annulus areas and the discharge temperatures. Therefore, they can be operated at higher speeds within the turbine blade centrifugal stress limit. This, in turn, results in less weight, as shown in the bottom graph in Fig. 72.

The disadvantage of partial fuel flow turbines is there is less pressure drop left in the turbine fluids for the other engine components, such as the combustion chamber main injector. Therefore, unless the specific speed limit is limiting, or all the fuel flowrate is used at a turbine pressure ratio greater than 1.6, the turbine pressure ratio is set at 1.6, which is considerably less than the ratio of pump discharge pressure to chamber pressure. The turbine fuel fraction is set to just meet the pump power requirements and the turbopump is assumed to operate at the turbine stress limit under these conditions. This procedure minimizes turbopump weight while leaving some pressure drop for the other engine components.

The resulting speed limits, turbine fuel flow fractions, and turbine velocity ratio (U/C_o) are summarized in Table 17 as a function of chamber pressure, pump propellant and turbine propellant combination. Gas properties are shown in Table 13. The 457 m/sec (1500 ft/sec) pitchline velocity (U) and relatively low theoretical spouting velocity (C_o) results in high values of U/C_o which, in turn, results in all turbines being of the 50 percent reaction type.

Finally, the pump discharge pressure was assumed to be 2.25 times the chamber pressure. The assumption provides sufficient information for determining the rotational speeds of all the turbopumps listed in Table 17.

Pump and Turbine Efficiency. The rotational speeds and the number of pump and turbine stages shown in Table 17 resulted in efficiencies of, on the average, 83 percent for all turbines and for pumps other than LH_2 pumps. In LH_2 pumps, minimizing the number of stages (within the 640 m/sec, 2100 ft/sec, tip speed limit) results in an efficiency of 74 percent. The number of pump and turbine stages in Table 16 is reasonable, which leads to the conclusion that the high efficiencies are attainable with reasonable turbopump configurations.

ORIGINAL PAGE IS
OF POOR QUALITY

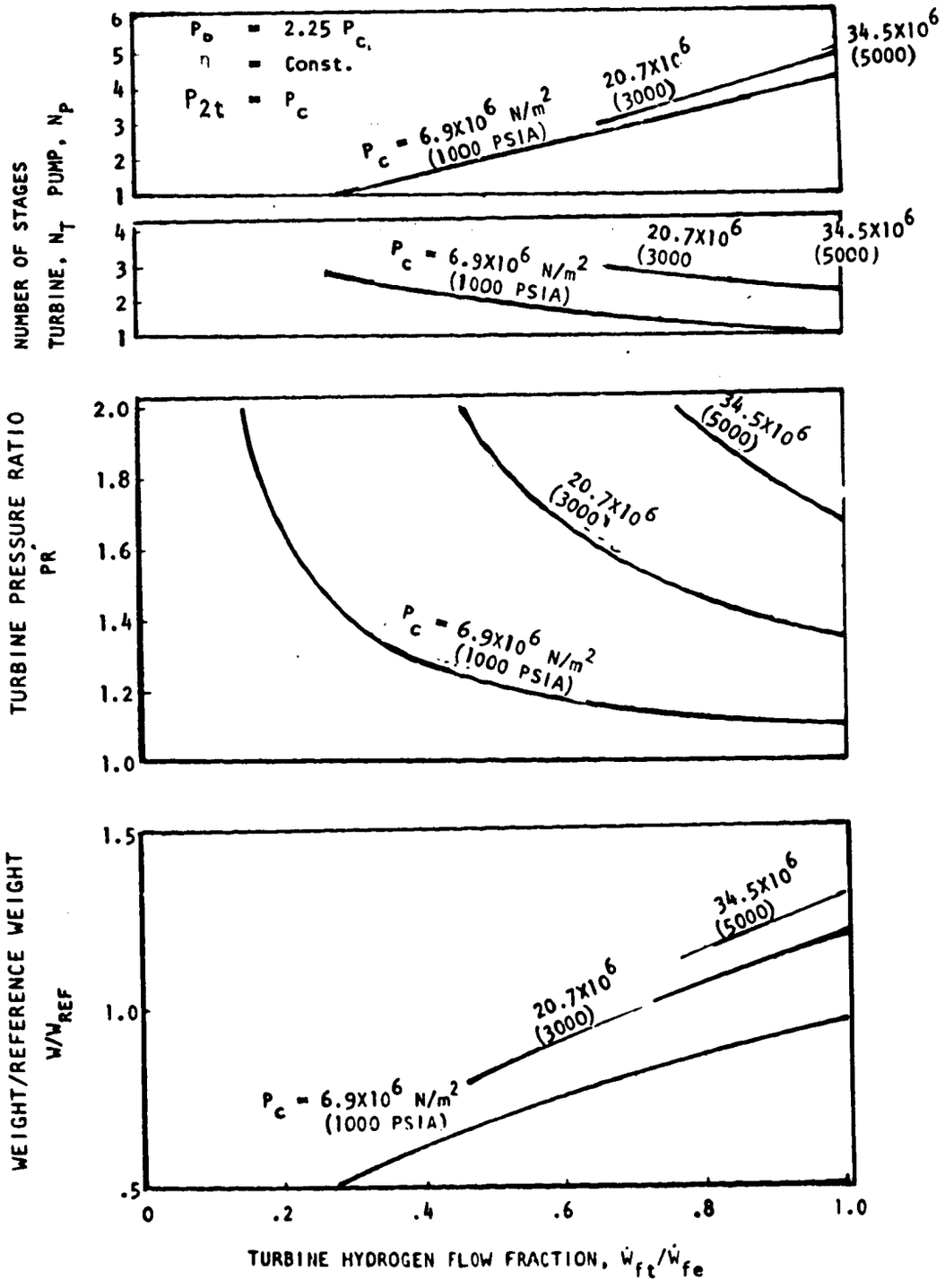

Figure 72. Effect of Turbine Hydrogen Flow Fraction and Chamber Pressure on Hydrogen Turbopump Parameters for a LO_2/LH, Staged Combustion Engine With Fuel-Rich Turbine Gas

TABLE 17. TURBOPUMP CONFIGURATIONS FOR THE STAGED COMBUSTION II EAR AEROSPIKE WITH FUEL-RICH TURBINE GAS

				TURBINE				PUMP		
ENGINE	PUMP	CHAMBER PRESSURE, $N/m^2 \times 10^6$ (PSIA)	SPEED LIMIT	FUEL FLOW FRACTION, W_{ft}/W_{fo}	VELOCITY RATIO, U/C_o	NO. OF STAGES, N_T	EFFICIENCY η_T, %	NO. OF STAGES, N_P	NO. OF ENTRIES	EFFICIENCY η_p, %
LOX/LH_2	LH_2	6.9 (1000)	TURB STRESS	.28	.37	2	81	1	1	74
		20.7 (3000)	TURB STRESS	.68	.34	3	84	3	1	74
		34.5 (5000)	TURB STRESS	1.00	.32	3	83	5	1	74
	LOX	6.9 (1000)	D.E. NS	.28	.37	2	81	1	2	83
		20.7 (3000)	D.E. NS	.68	.34	3	84	1	2	83
		34.5 (5000)	TURB STRESS	1.00	.32	3	83	1	1	83
LOX/CH_4	CH_4	6.9 (1000)	D.E. NS	.28	.58	1	81	1	2	83
		20.7 (3000)	TURB STRESS	.80	.57	1	81	1	1	83
		34.5 (5000)	TURB STRESS	1.00	.49	2	84	2	1	83
	LOX	6.9 (1000)	D.E. NS	.28	.58	1	81	1	2	83
		20.7 (3000)	TURB STRESS	.80	.57	1	81	1	2	83
		34.5 (5000)	TURB STRESS	1.00	.49	2	84	1	1	83
LOX/RP-1	RP-1	6.9 (1000)	D.E. NS	.5	.68	1	82	1	2	83
		20.7 (3000)	TURB STRESS	1.00	.68	1	82	1	1	83
		34.5 (5000)	TURB STRESS	1.00	.59	1	81	2	1	83
	LOX	6.9 (1000)	D.E. NS	.5	.68	1	82	1	2	83
		20.7 (3000)	TURB STRESS	1.00	.68	1	82	1	1	83
		34.5 (5000)	TURB STRESS	1.00	.59	1	81	1	1	83
LOX/RJ-5	RJ-5	6.9 (1000)	D.E. NS	.6	.68	1	82	1	2	83
		20.7 (3000)	TURB STRESS	1.00	.68	1	82	1	1	83
		34.5 (5000)	TURB STRESS	1.00	.62	1	82	1	1	83
	LOX	6.9 (1000)	D.E. NS	.6	.68	1	82	1	2	83
		20.7 (3000)	TURB STRESS	1.00	.68	1	82	1	1	83
		34.5 (5000)	TURB STRESS	1.00	.62	1	82	1	1	83

ORIGINAL PAGE IS
OF POOR QUALITY

Engine analysis conducted in parallel with the turbopump analysis indicates that it could be better to increase the turbine hydrogen flow fraction, decrease the turbine pressure ratio and, consequently, decrease the pump discharge pressure requirement. In turn, this increases the maximum chamber pressure attainable with a staged combustion engine. Figure 72 shows that this can be done at the expense of having heavier turbopumps. Figure 72 also shows that, to maintain the same high pump efficiencies, the number of pump stages must be increased. On the other hand, increasing the turbine flow fraction decreases the number of turbine stages required.

Weight

The scaling equations for predicting the turbopump weights are listed in Table 18 as a function of the type of speed limit. The reference value for hydrogen turbopump predictions is the SSME hydrogen turbopump. For prediction of other propellant turbopump weights, the SSME LOX turbopump is used. For the gas generator cycle, the equation at the double-entry pump specific speed limit is used if the chamber pressure is below the values shown in Table 14, and if the chamber pressure is greater than in Table 14, the equation at the turbine stress limit is used. Similar transitions were used for the staged combustion cycle.

TABLE 18. TURBOPUMP WEIGHT PREDICTION SUMMARY

SPEED LIMIT	TURBOPUMP WEIGHT =
DOUBLE ENTRY PUMP SPECIFIC SPEED	$W_{REF} \left(\frac{Q}{Q_{REF}}\right)^{.9} \left(\frac{\Delta P}{\Delta P_{REF}}\right)^{.15} \left(\frac{\rho}{\rho_{REF}}\right)^{.45}$
TURBINE STRESS	$W_{REF} \left(\frac{Q}{Q_{REF}}\right)^{.6} \left(\frac{\Delta P}{\Delta P_{REF}}\right)^{.6} \left(\frac{N_{REF}}{N}\right)^{.6}$
	where: $N = \frac{2675}{\sqrt{Q}} [144\ \Delta P/\rho]^{3/4}$

ORIGINAL PAGE IS
OF POOR QUALITY

TASK V: ENGINE PERFORMANCE, WEIGHT, AND ENVELOPE PARAMETRICS

Using Task IV results as a base, analyses were conducted for the parametric ranges presented in Table 20 to determine effect of thrust level, thrust split, Mode 1 area ratio, and width-to-height ratio on engine delivered performance and envelope. The specific values within the range of the parameters examined are indicated in Table 19.

TABLE 19. TASK V PARAMETRIC STUDIES

PARAMETERS	RANGE VALUES				
Thrust, N x 10^{-7} (lb x 10^{-6})	0.67(1.5)(1)	1.78(4)	2.0(4.5) *	2.22(5)	2.67(6)
Thrust Split		.5	.65	.8	
Mode 1 Area Ratio		20	40	60	80
Width-To-Nozzle Height Ratio		3	4	5	
(1) LOX/H_2 only					
* Nominal Values					

The parametric data were generated for the hydrogen-cooled gas generator cycle and staged combustion cycle linear engines for LOX/RP-1-LOX/H_2 and LOX/H_2 propellant combinations. Since trends were found similar with these two propellant combinations, detailed LOX/RJ-5-LOX/H_2 and LOX/CH_4-LOX/H_2 parametrics were not determined. They are readily derivable from the baseline engine performance for these propellants and from the trends found in Task IV for the two propellant combinations. Baseline engine performance was presented previously in Task IV effort.

PARAMETRIC COOLING LIMITS

In this subtask, the parametric thrust chamber cooling limits were determined using guidelines set forth in Table 7. The method employed utilizes a combination of detailed analytical cooling limit data for the inner combustor from Task III and derived analytical scaling relationships. This was accomplished by defining a cooling limit curve for each coolant inlet pressure-to-chamber pressure ratio in terms of the peak heat flux and the available coolant flow per unit length of engine width ($\dot{w}_{cool}/W$), and analytically expressing peak heat flux and $\dot{w}_{cool}/W$ as a function of the following variables which describe the thrust chamber:

1. Total thrust, F_t
2. Thrust split (outer combustor thrust-to-total thrust), F_o/F_t
3. Inner and outer combustor chamber pressure, P_c
4. Width-to-nozzle height ratio, W/H
5. Mode 1 area ratio, ϵ_1

TABLE 20. ENGINE PERFORMANCE, WEIGHT, AND ENVELOPE PARAMETRICS

Engine Concept No.	Outer Chamber Propellant Combination	Inner Chamber Propellant Combination	Thrust Level, N x 10^6 (lb x 10^6)	Thrust Split $\frac{\text{Outer}}{\text{Total}}$	Mode 1 Area Ratio	Width-to-Nozzle Height Ratio
1	$O_2/RP\text{-}1$	O_2/H_2	17.8 to 26.7 (4 to 6)	0.5 to 0.8	20 to 80	3:1 to 5:1
2	O_2/H_2	O_2/H_2	6.8 to 26.7 (1.5 to 6)	0.5 to 0.8	20 to 80	3:1 to 5:1

ORIGINAL PAGE IS
OF POOR QUALITY

The intersection of the peak heat flux versus $\dot{w}_{cool}/W$ analytical curve for a set of thrust chamber parameters and the cooling limit curve is the cooling limit for that thrust chamber. This method of determining the cooling limits was computerized for rapid and efficient determination.

Typical cooling limit results are presented in Fig. 73 through 81 for three values of pressure ratio (P_{in}/P_c): 1.8, 2.25, and 3.0. The data were plotted three different ways for each P_{in}/P_c. First, the cooling limit chamber pressure for a fixed total thrust is plotted versus thrust split for various width-to-height ratios and Mode 1 area ratios (Fig. 73, 76, and 79). In Fig. 74, 77, and 80, the chamber pressure limit for a fixed total thrust is plotted versus width-to-height ratio for various thrust split and Mode 1 area ratios. The third combination of the chamber pressure limit for a fixed total thrust is plotted versus Mode 1 area ratio for various thrust splits and width-to-height ratios in Fig. 75, 78, and 81.

The cooling limit curves indicate that the limiting chamber pressure increases with increase in total thrust and decreases with increase in thrust split and Mode 1 area ratio.

Cooling limits as a function of P_{in}/P_c are presented in Fig. 82. As shown in the figure, an increase in P_{in}/P_c at a fixed chamber pressure and total thrust results in an increase in the allowable Mode 1 area ratio, thrust split, and width-to-height ratio.

In using these cooling limits, it must be remembered that the limits are approximate and, after a design point is selected, a detailed cooling analysis should be performed to verify or alter the design point. Also, these cooling parametrics do not indicate possible limits due to cycle power balance.

PARAMETRIC ENGINE PERFORMANCE AND ENVELOPE

The parametric data were generated by taking each parameter through its prescribed range and holding the remaining parameters at the baseline (Task IV) value.

The parametric data generated are presented in Fig. 83 through 98. The graphs include plots of Mode 2 and Mode 1 engine vacuum specific impulse, Mode 1 engine sea level specific impulse, engine width, height, and nozzle length. Nozzle length is the longitudinal distance from the combustor throat to the plane containing the base closure of the nozzle. Engine length is nozzle length plus the powerhead length (the distance from the throat to the engine/vehicle attachment plane). Preliminary designs indicate that powerhead length is approximately 115 cm (45 inches) for an engine thrust level of 1.78×10^7 N (4×10^6 lbf), a chamber pressure of 1724 N/cm^2 (2500 psia) and a 3.0 width-to-nozzle height ratio. Also, noted in the figures are coolant inlet pressure-to-chamber pressure ratios within the range of interest.

Engine performance data as a function of nozzle length are presented in Fig. 99 for the gas generator and staged combustion cycle for LOX/RP-1/LOX-H_2 propellants and in Fig. 100 for LOX/H_2/LOX/H_2 propellants. Other design parameters

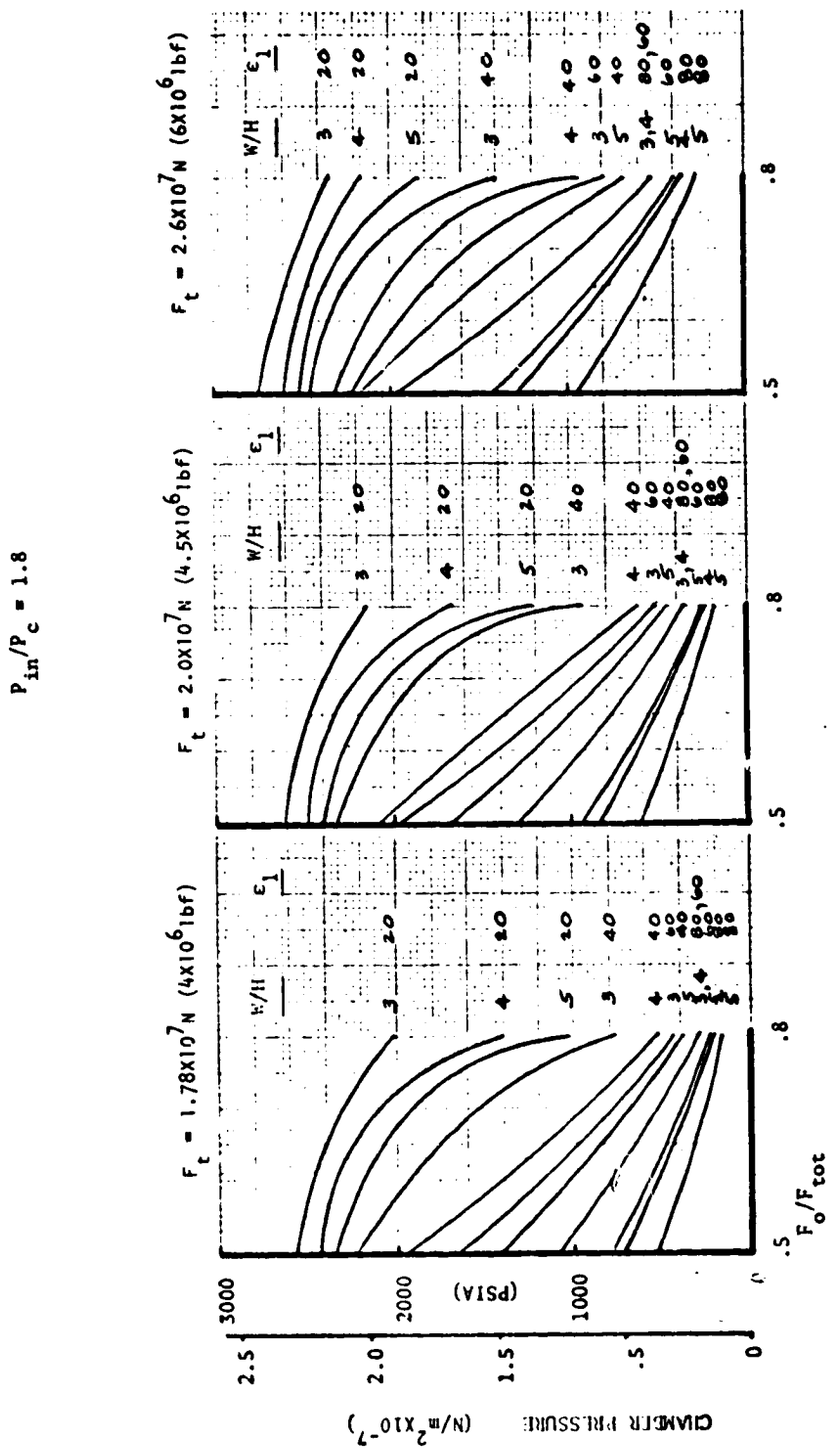

Figure 73. Chamber Pressure Cooling Limit Variation With Thrust Split (P_{in}/P_c = 1.8)

ORIGINAL PAGE IS
OF POOR QUALITY

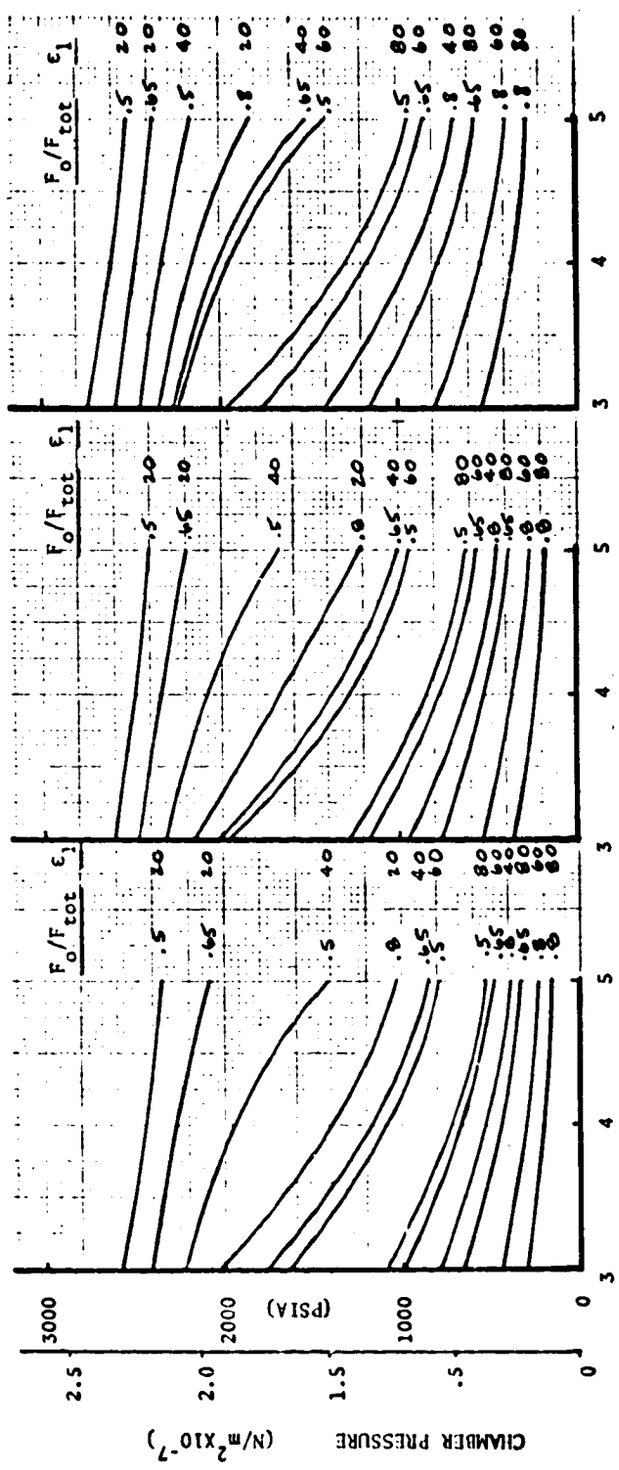

Figure 74. Chamber Pressure Cooling Limit Variation With Width-to-Height Ratio (P_{in}/P_c = 1.8)

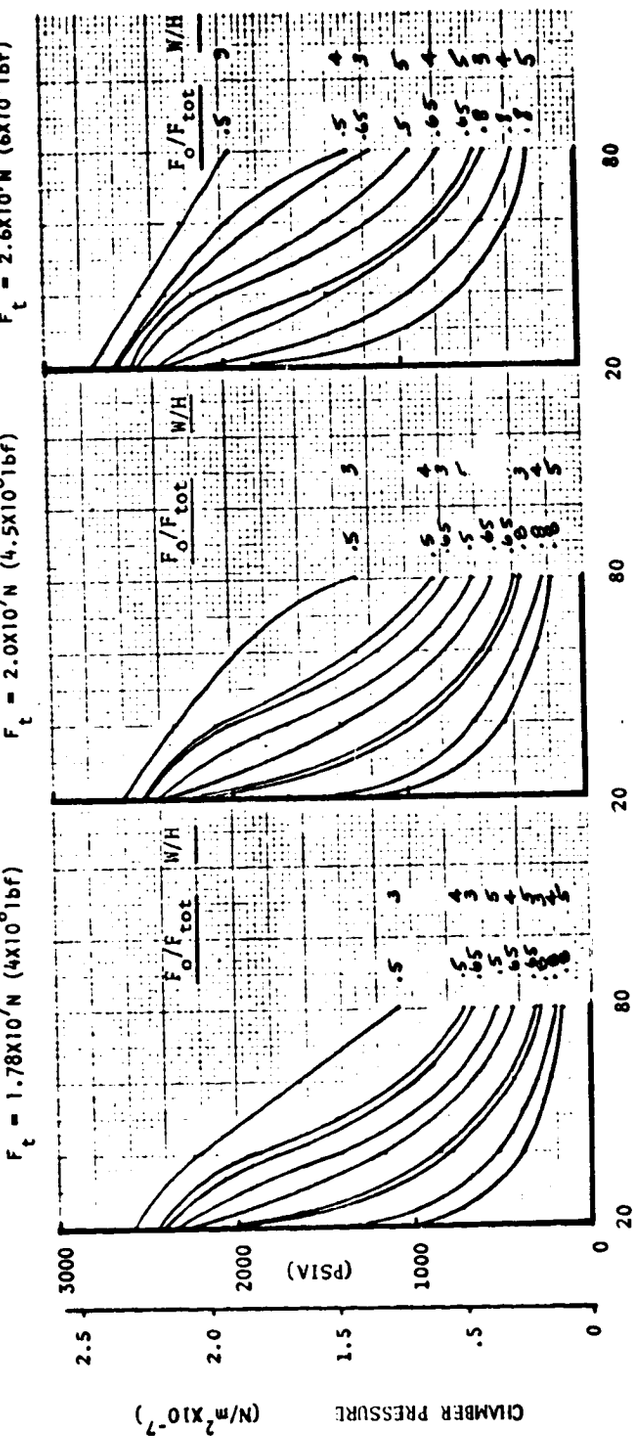

Figure 75. Chamber Pressure Cooling Limit Variation With Mode 1 Area Ratio (P_{in}/P_c = 1.8)

ORIGINAL PAGE IS
OF POOR QUALITY

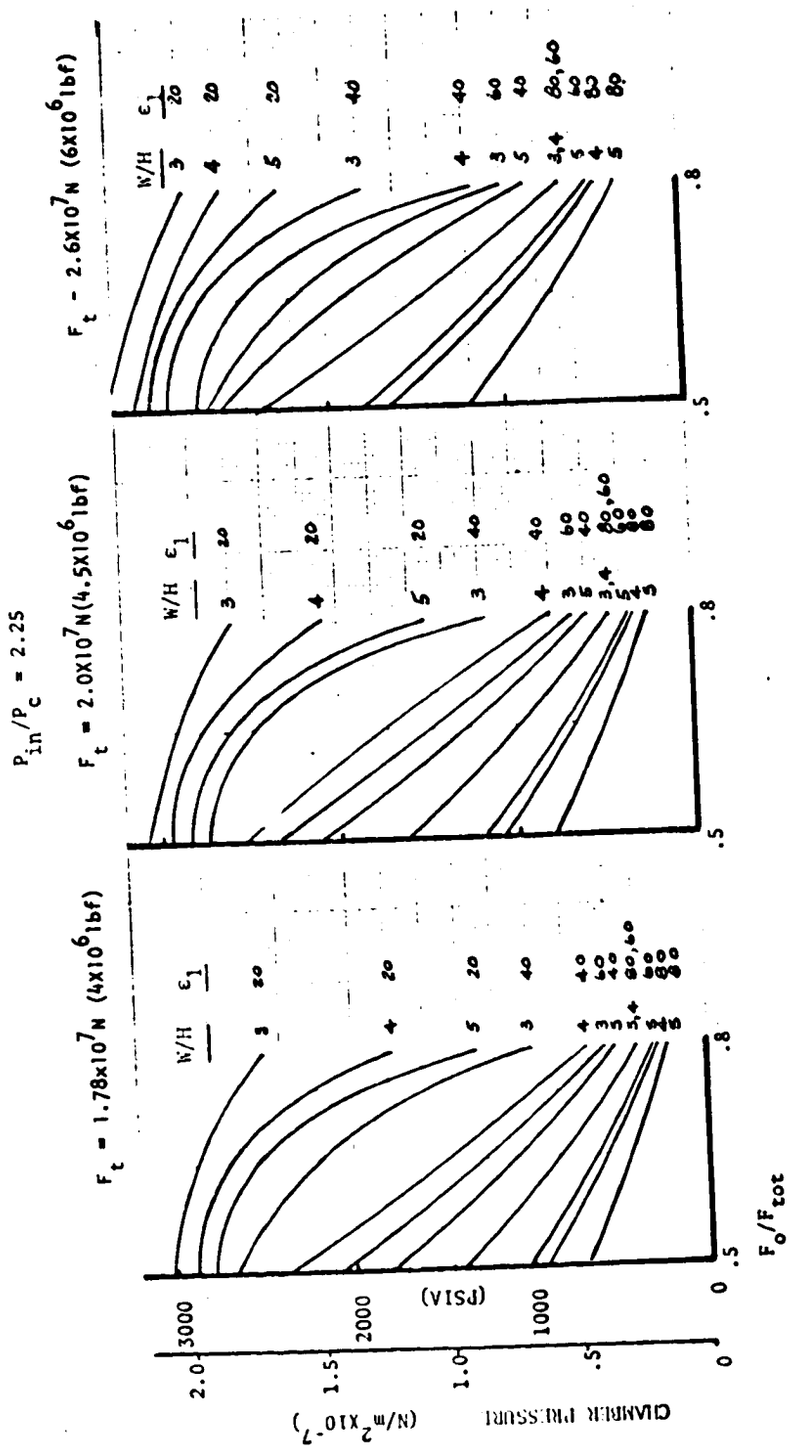

Figure 76. Chamber Pressure Cooling Limit Variation With Thrust Split (P_{in}/P_c = 2.25)

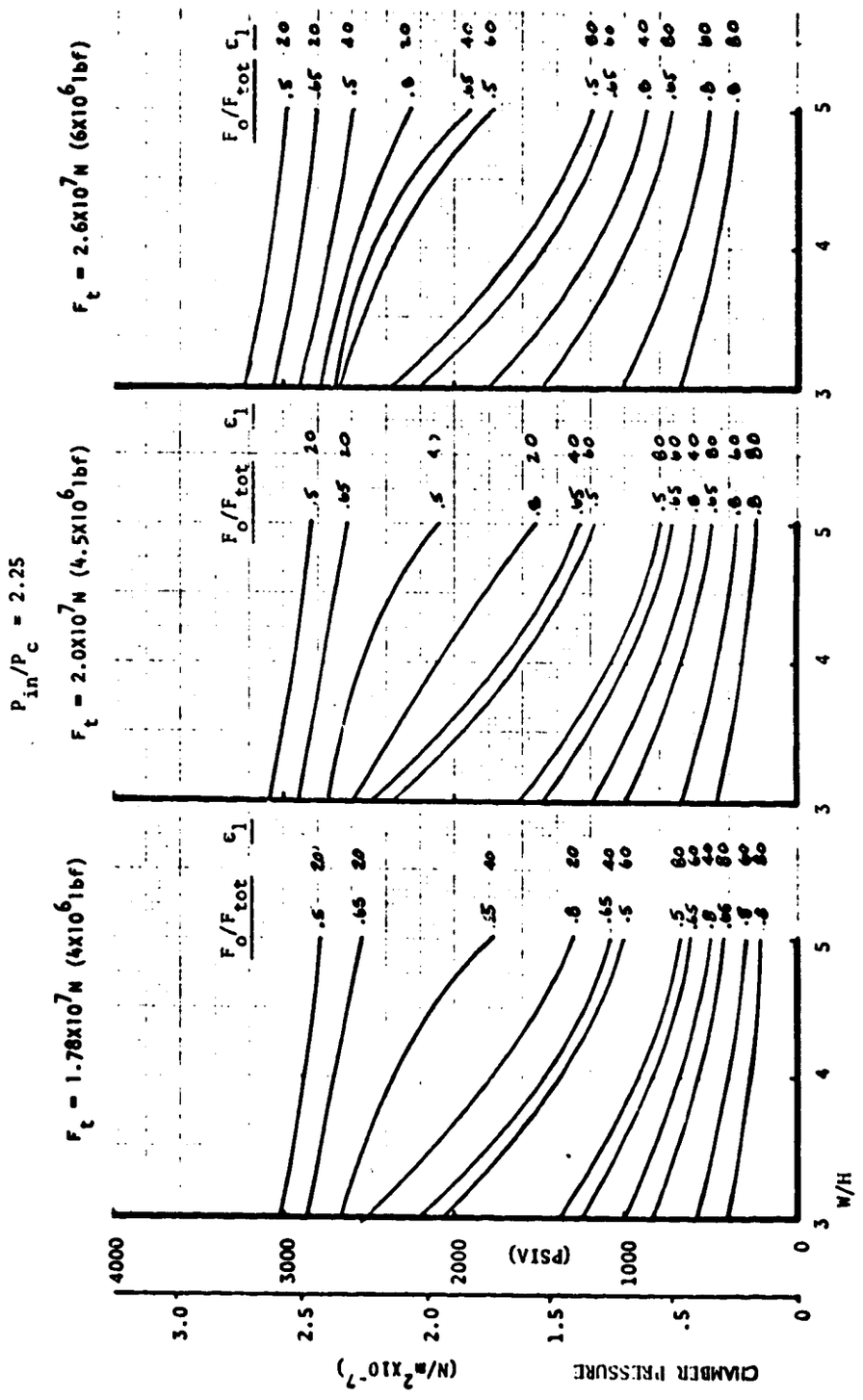

Figure 77. Chamber Pressure Cooling Limit Variation With Width-to-Height Ratio (P_{in}/P_c = 2.25)

ORIGINAL PAGE IS
OF POOR QUALITY

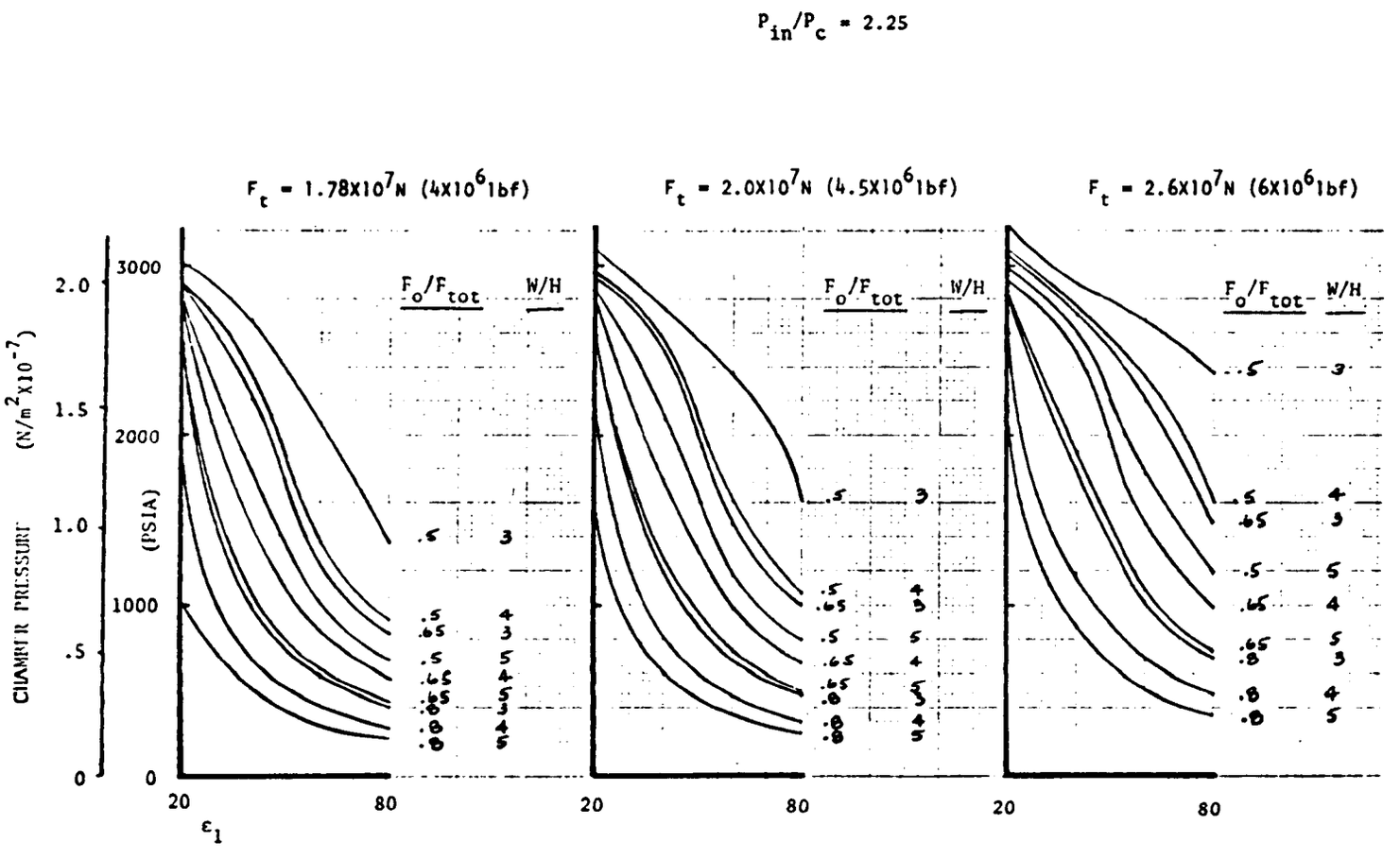

Figure 78. Chamber Pressure Cooling Limit Variation With Mode 1 Area Ratio (P_{in}/P_c = 2.25)

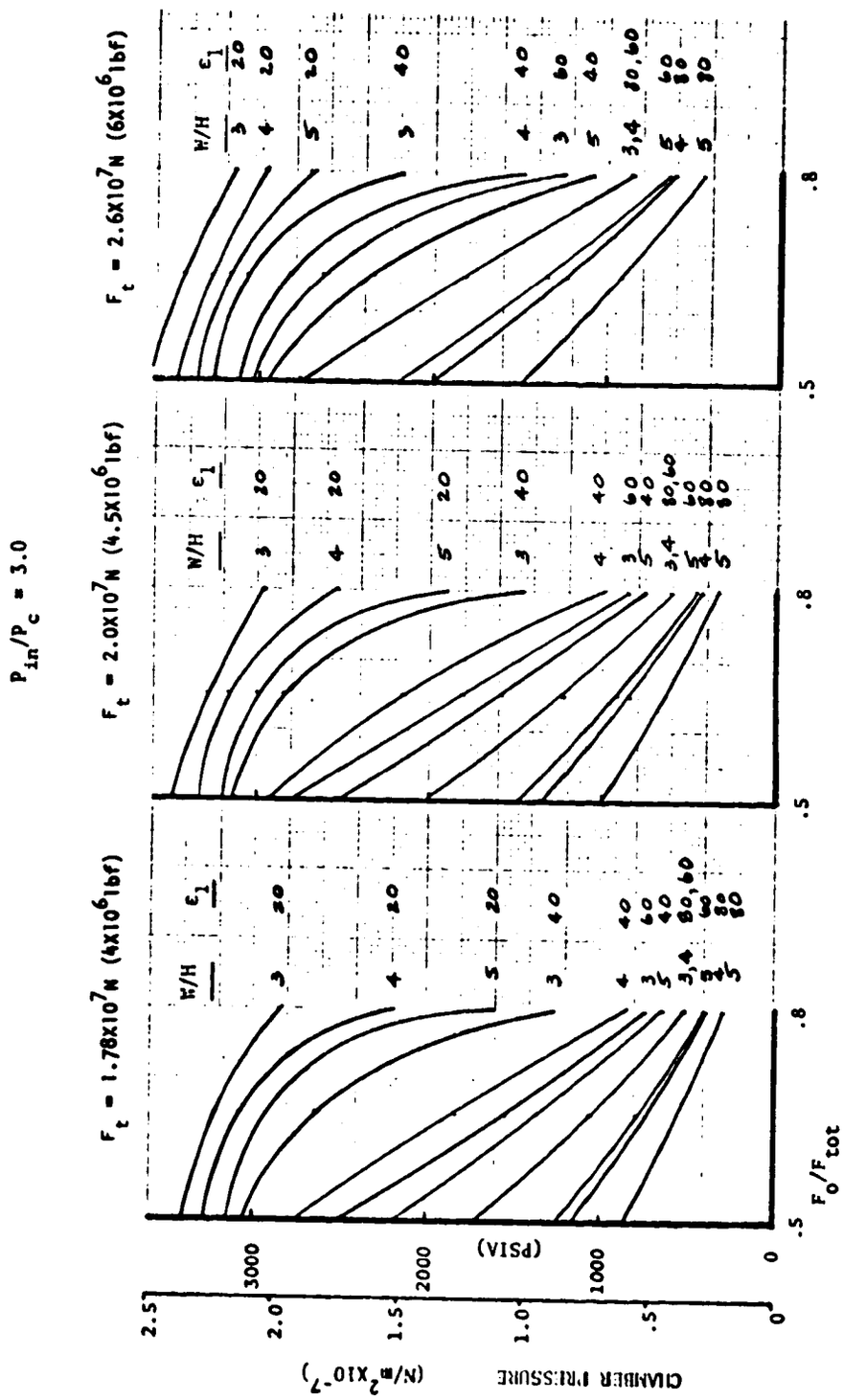

Figure 79. Chamber Pressure Cooling Limit Variation With Thrust Split (P_{in}/P_c = 3.0)

ORIGINAL PAGE IS
OF POOR QUALITY

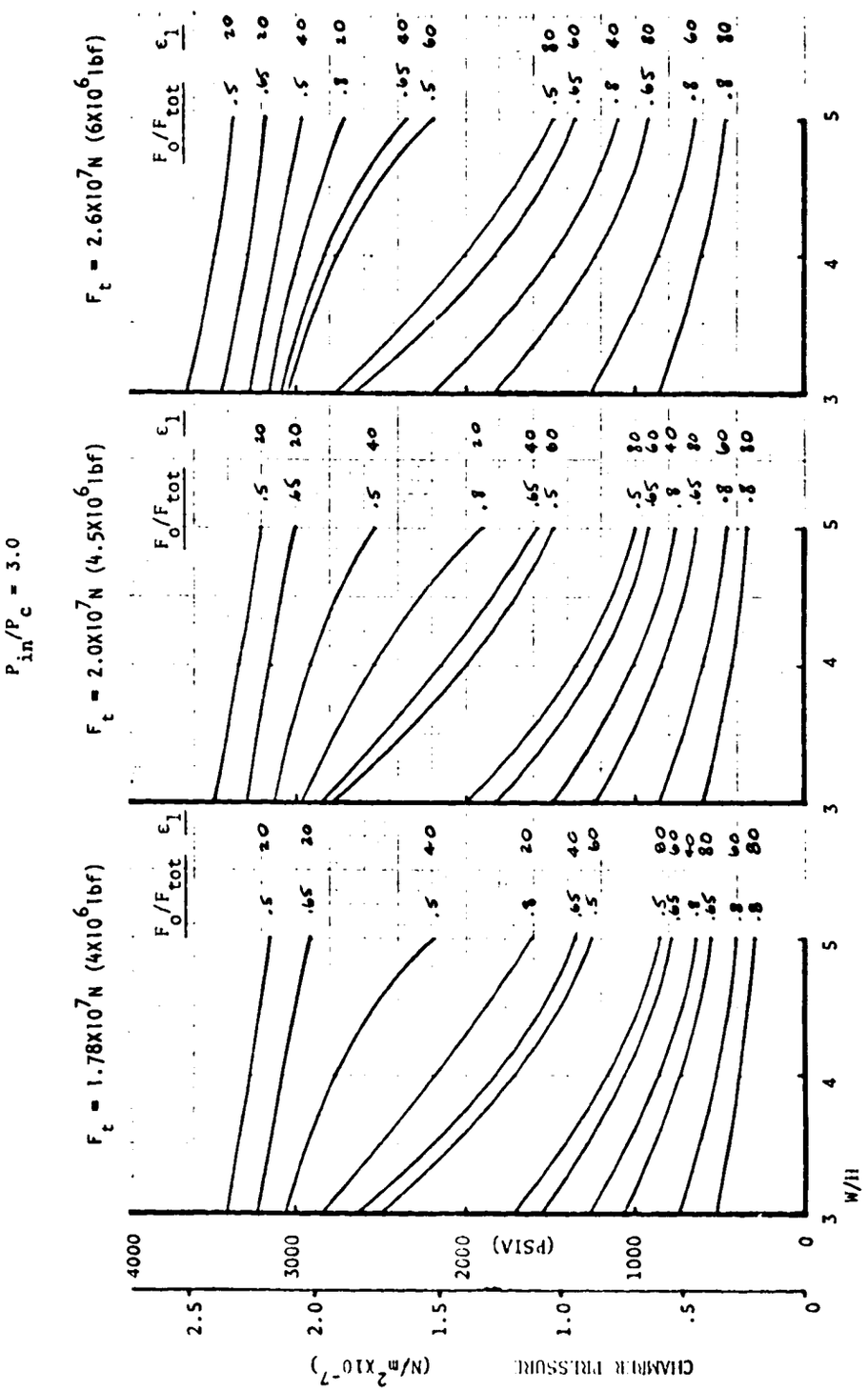

Figure 80. Chamber Pressure Cooling Limit Variation With Width-to-Height Ratio (P_{in}/P_c = 3.0)

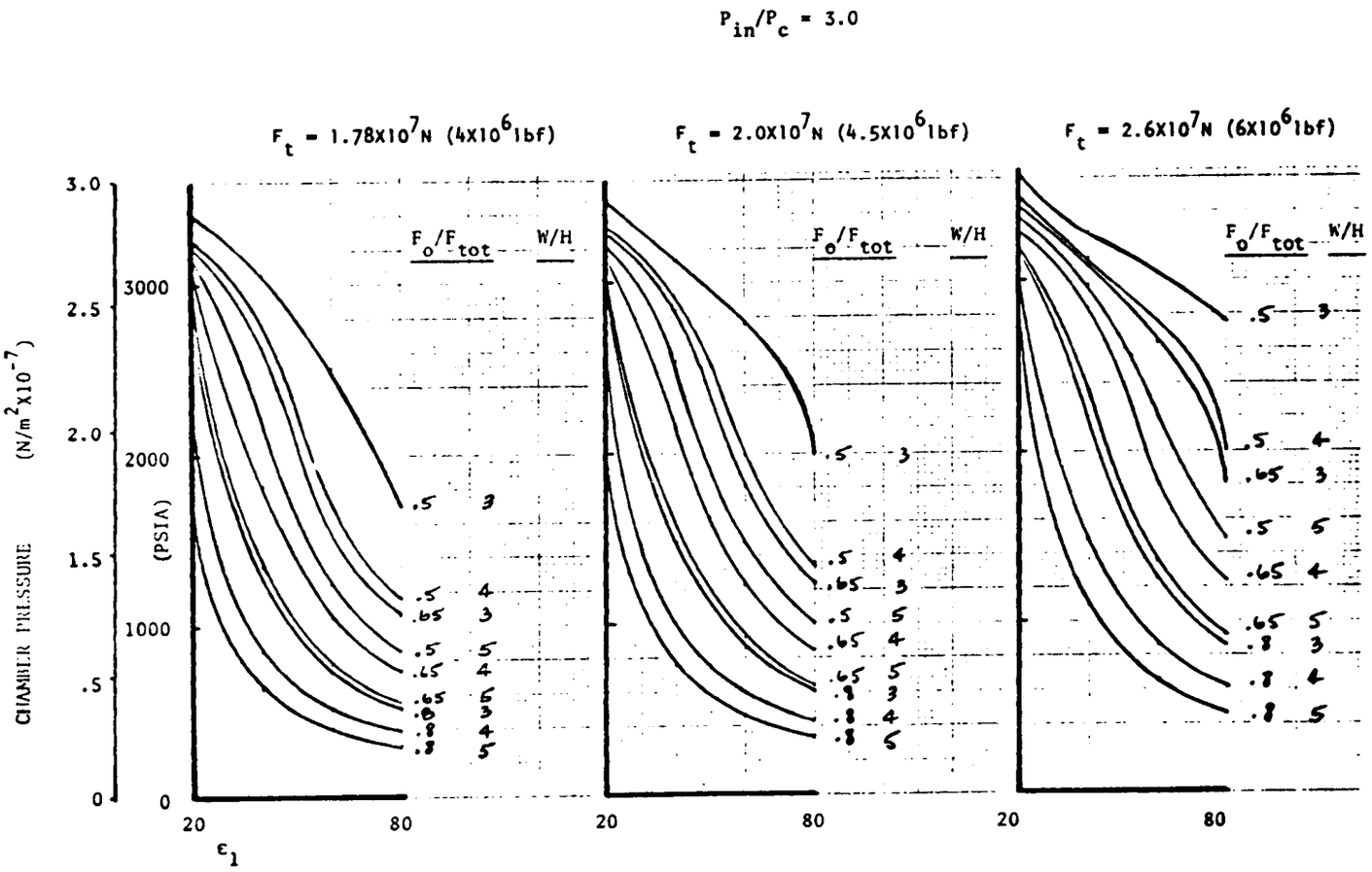

Figure 81. Chamber Pressure Cooling Limit Variation With Mode 1 Area Ratio (P_{in}/P_c = 3.0)

ORIGINAL PAGE IS
OF POOR QUALITY

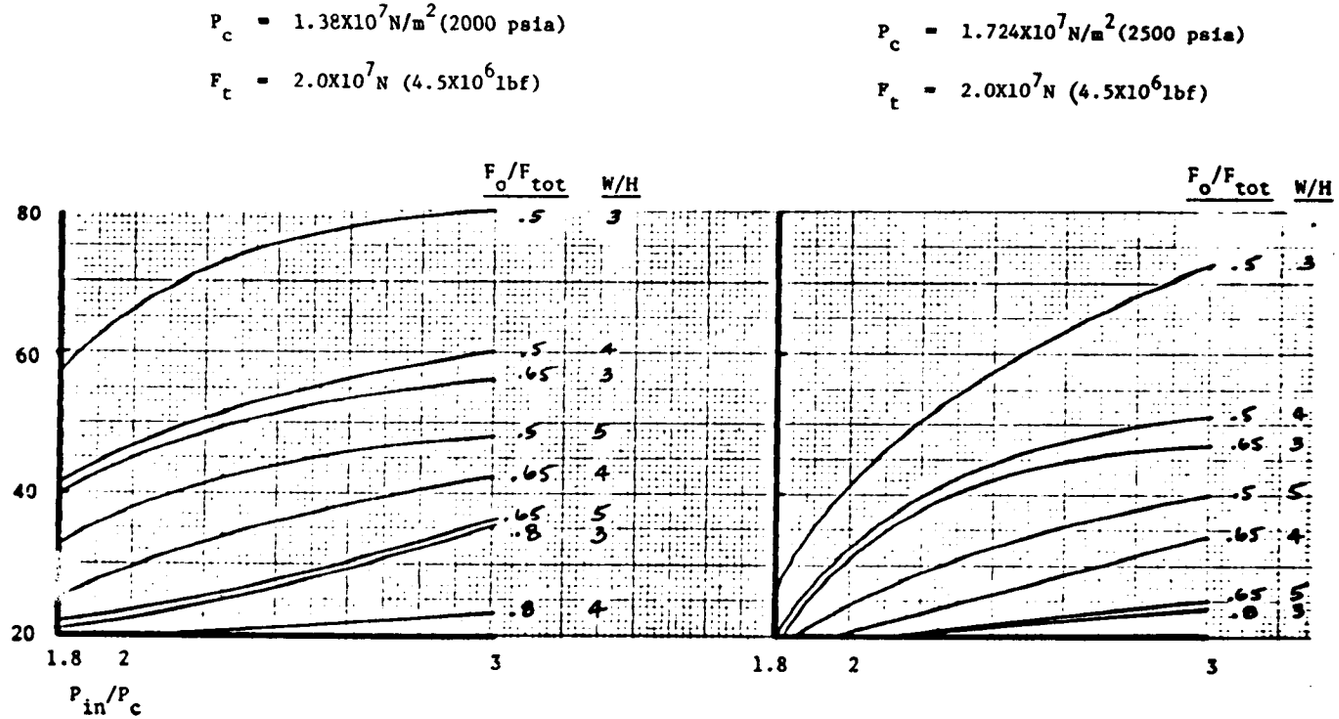

Figure 82. Chamber Pressure Cooling Limit Variation With P_{in}/P_c

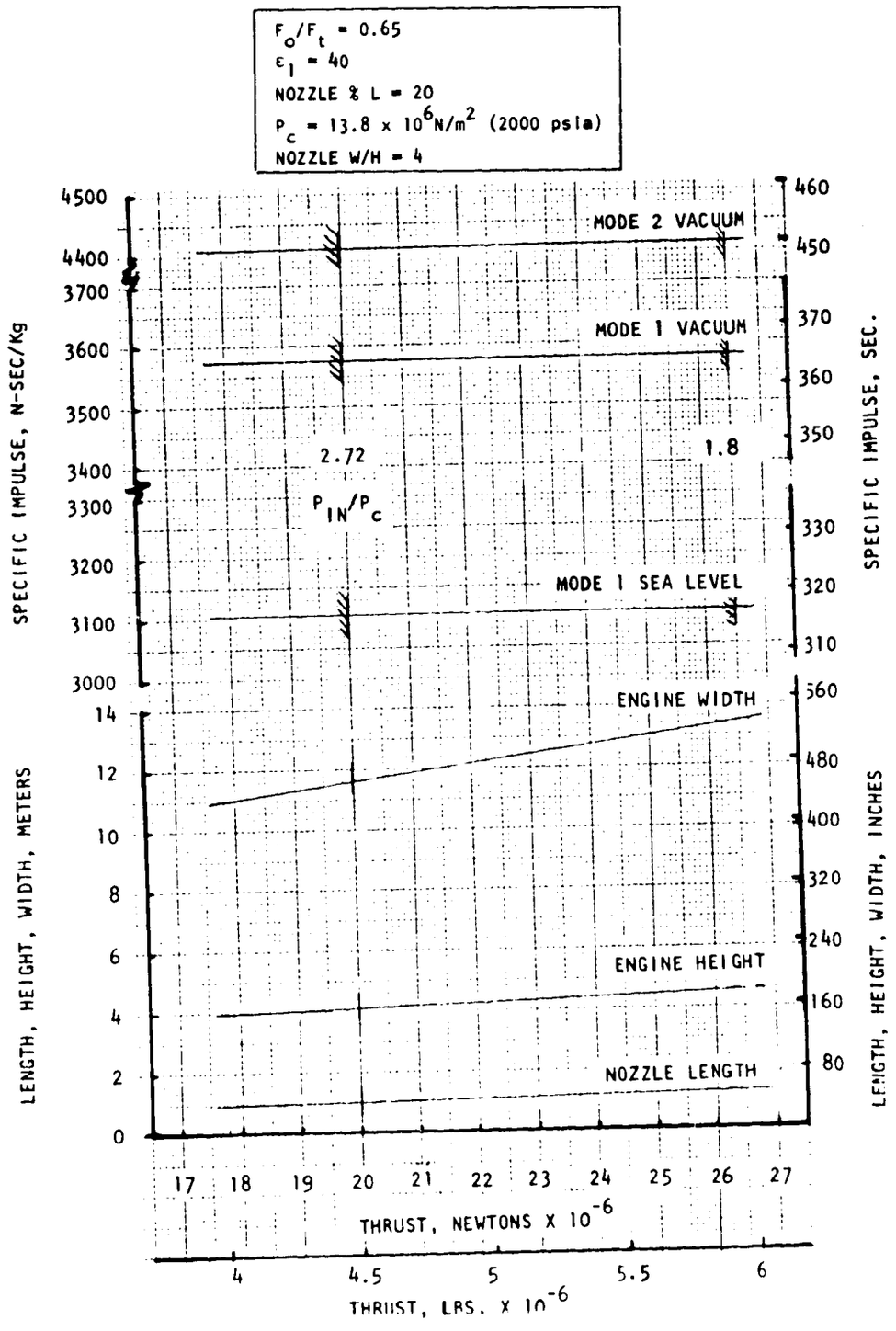

Figure 83. Split-Combustor Linear Engine Performance and Envelope vs Thrust LOX/RP-1 Gas Generator Cycle

ORIGINAL PAGE IS
OF POOR QUALITY

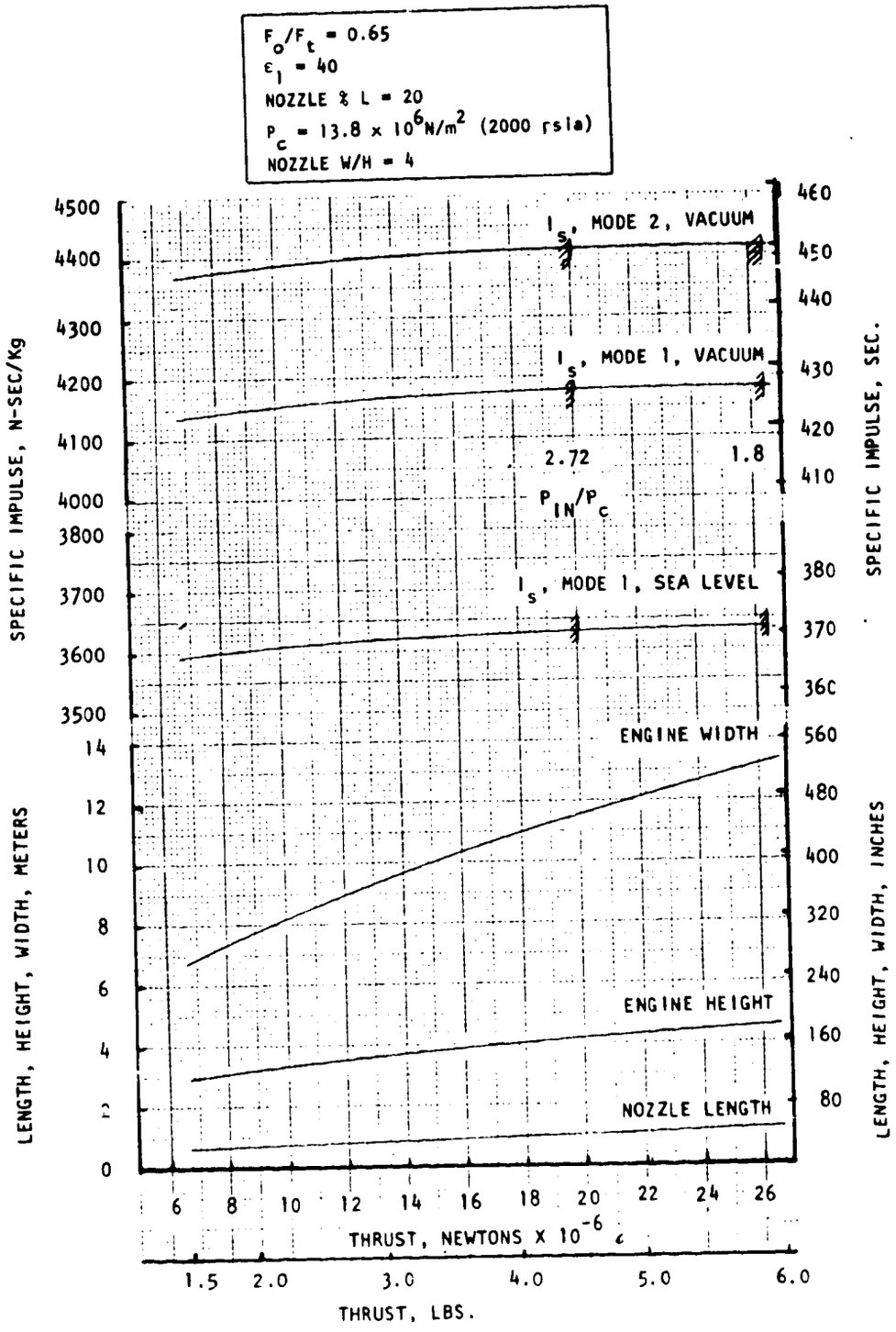

Figure 84. Split-Combustor Linear Engine Performance and Envelope vs Thrust LOX/H_2, Gas Generator Cycle

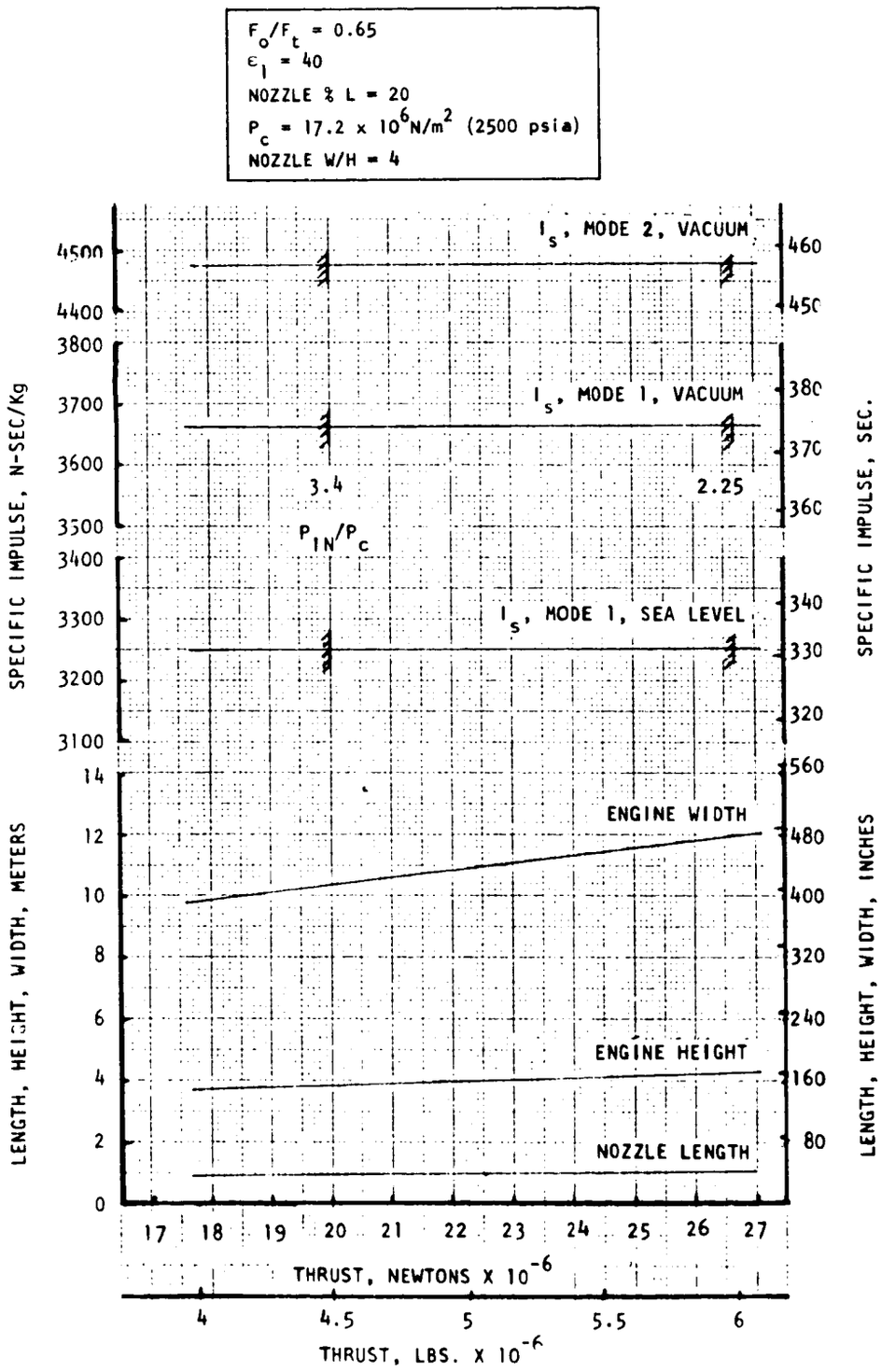

Figure 85. Split-Combustor Linear Engine Performance and Envelope vs Thrust LOX/RP-1, Staged Combustion Cycle

ORIGINAL PAGE IS
OF POOR QUALITY

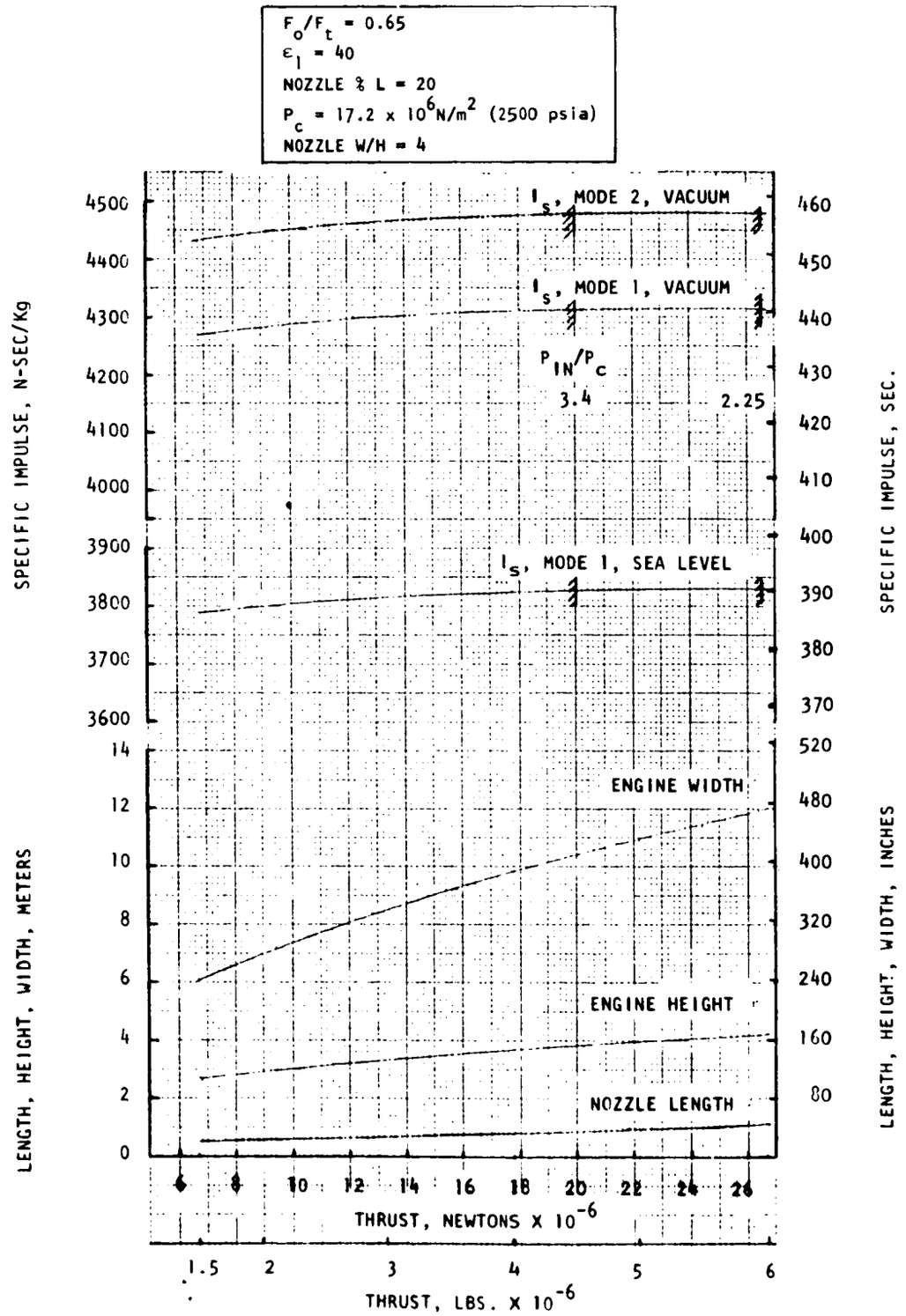

Figure 86. Split-Combustor Linear Engine Performance and Envelope vs Thrust LOX/H_2, Staged Combustion Cycle

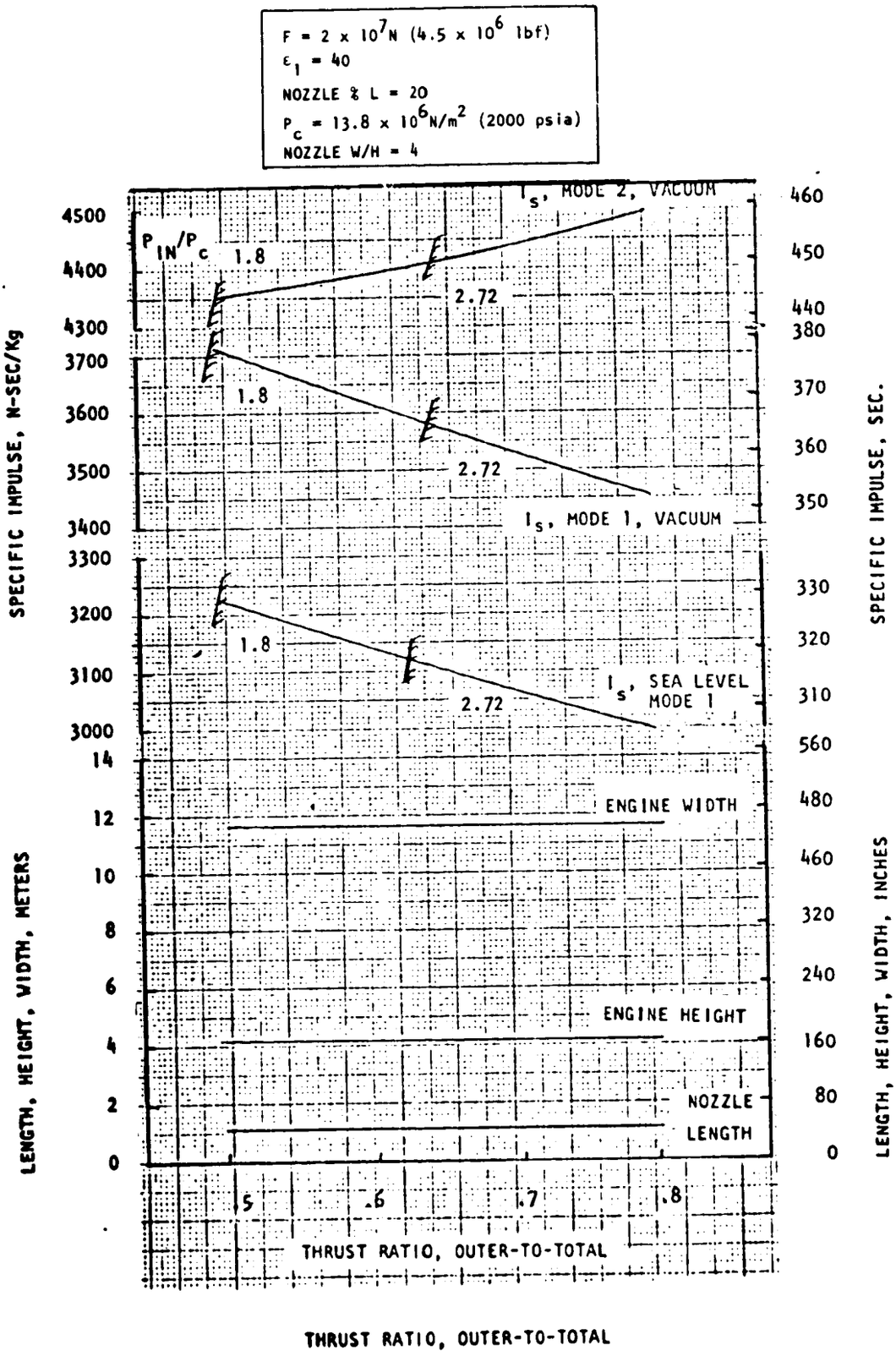

Figure 87. Split-Combustor Linear Engine Performance and Envelope vs Thrust LOX/RP-1, Gas Generator Cycle

ORIGINAL PAGE IS
OF POOR QUALITY

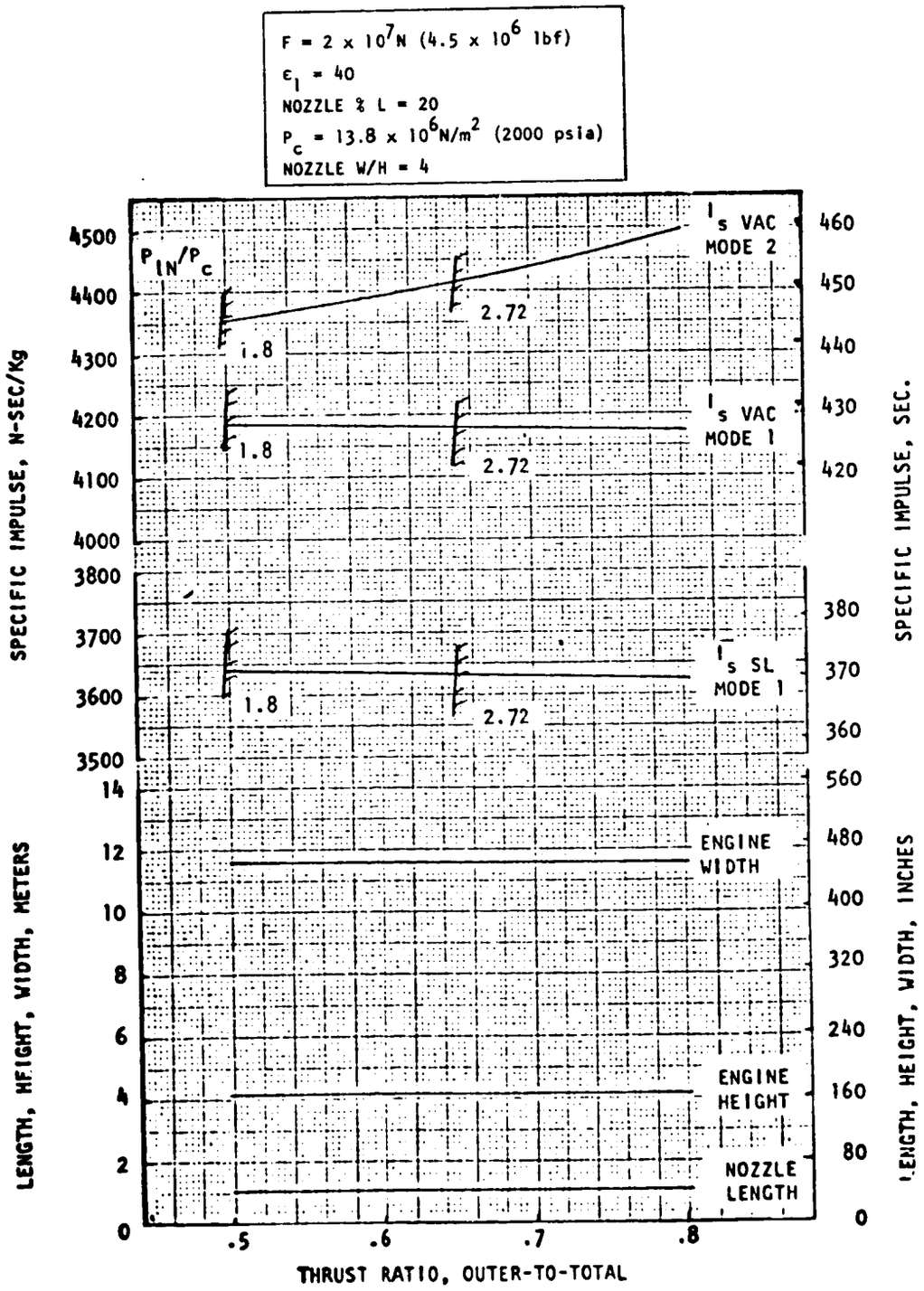

Figure 88. Split-Combustor Linear Engine Performance and Envelope vs Thrust Split LOX/H_2, Gas Generator Cycle

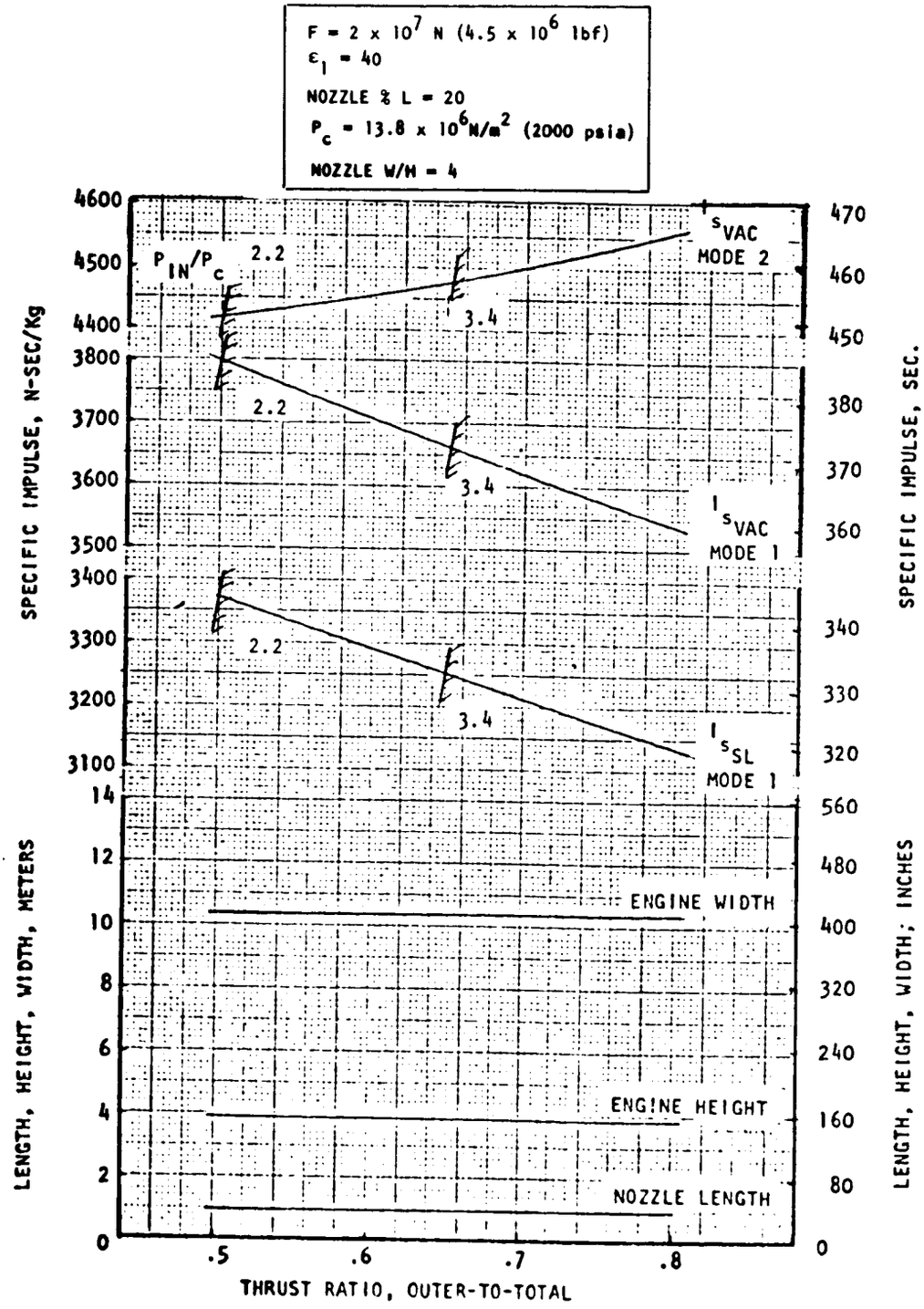

Figure 89. Split-Combustor Linear Engine Performance and Envelope vs Thrust Split LOX/RP-1, Staged Combustion Cycle

ORIGINAL PAGE IS
OF POOR QUALITY

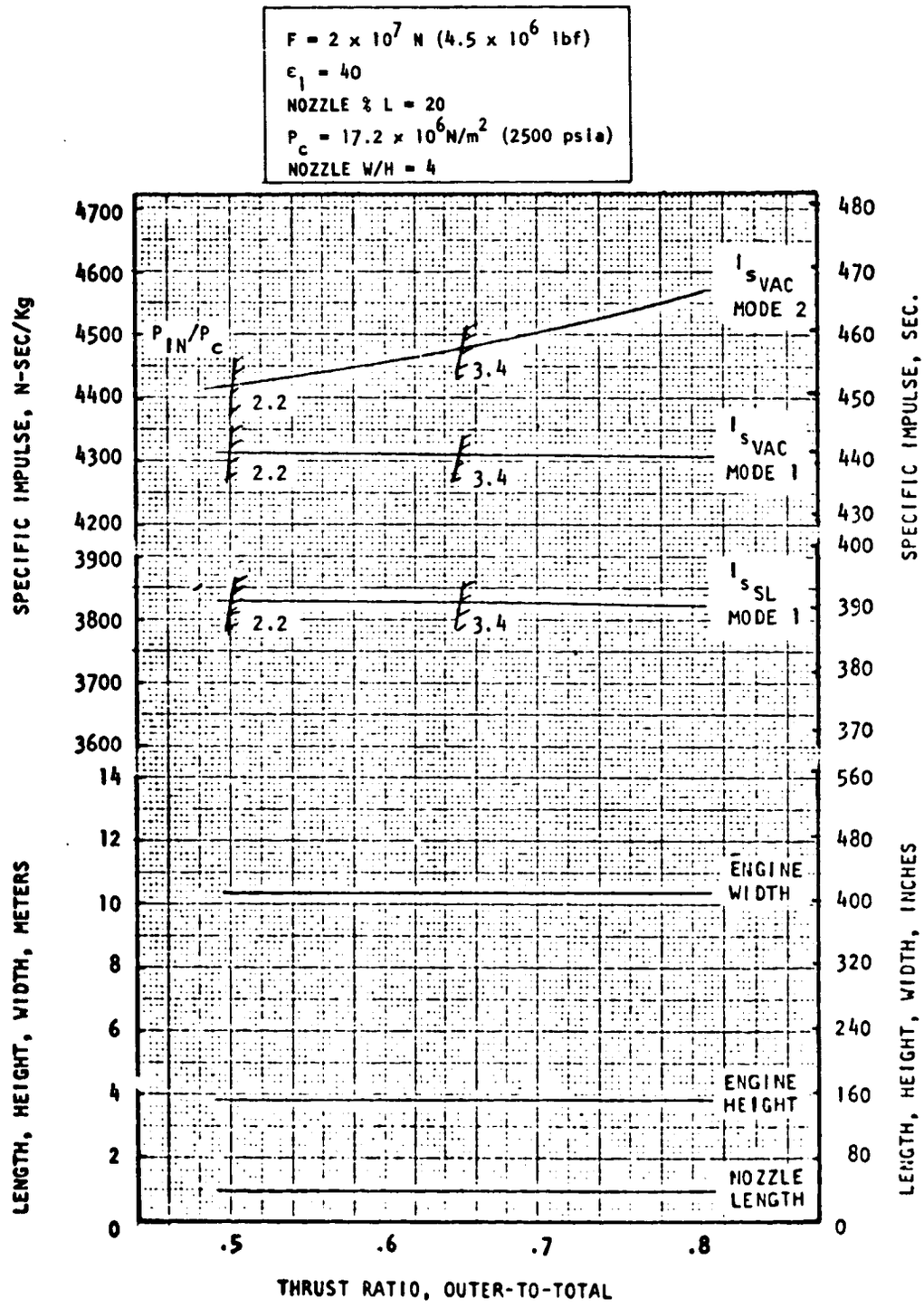

Figure 90. Split-Combustor Linear Engine Performance and Envelope vs Thrust Split LOX/H_2, Staged Combustion Cycle

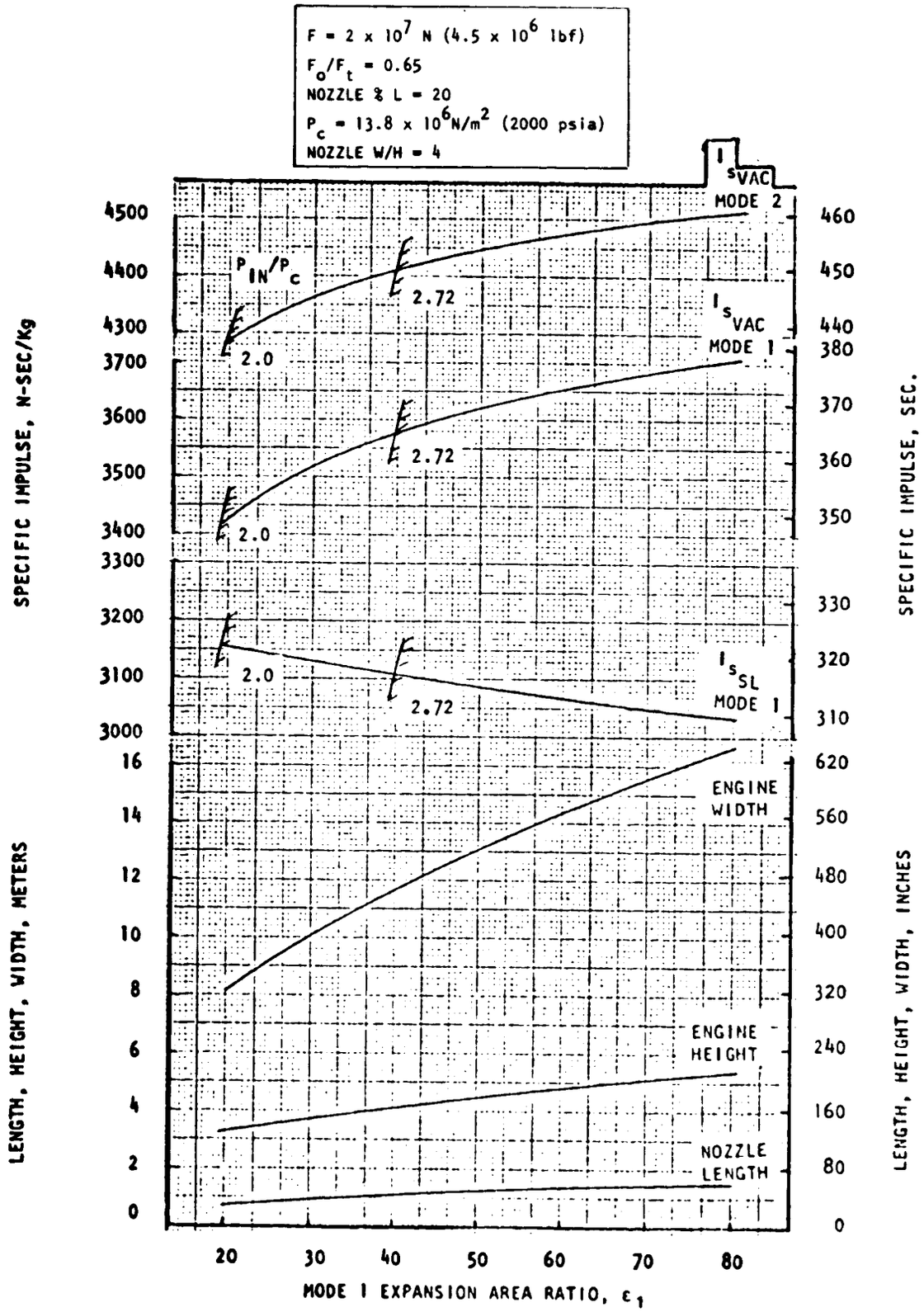

Figure 91. Split-Combustor Linear Engine Performance and Envelope vs Mode 1 Area Ratio LOX/RP-1, Gas Generator Cycle

ORIGINAL PAGE IS
OF POOR QUALITY

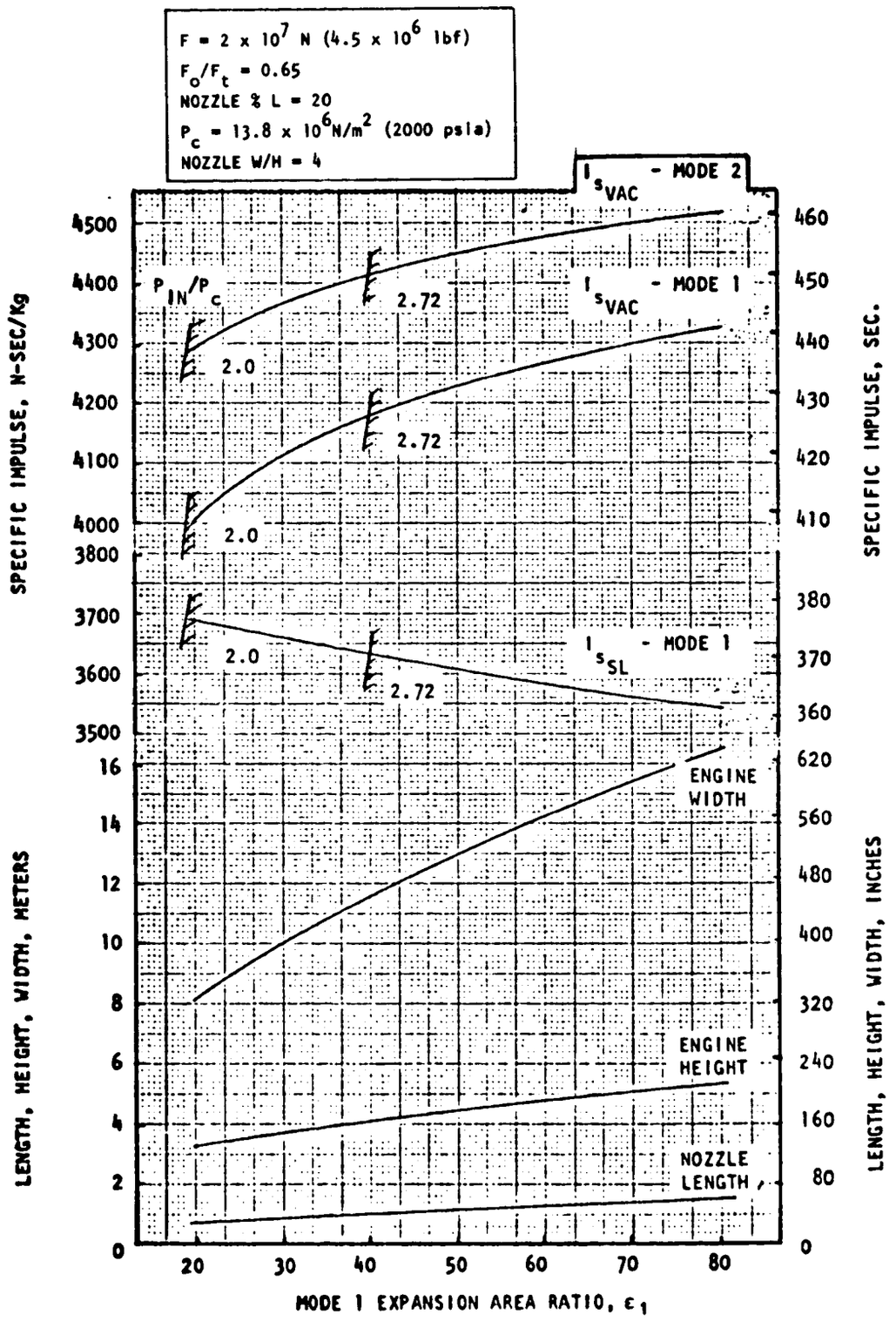

Figure 92. Split-Combustor Linear Engine Performance and Envelope vs Mode 1 Area Ratio LOX/H_2, Gas Generator Cycle

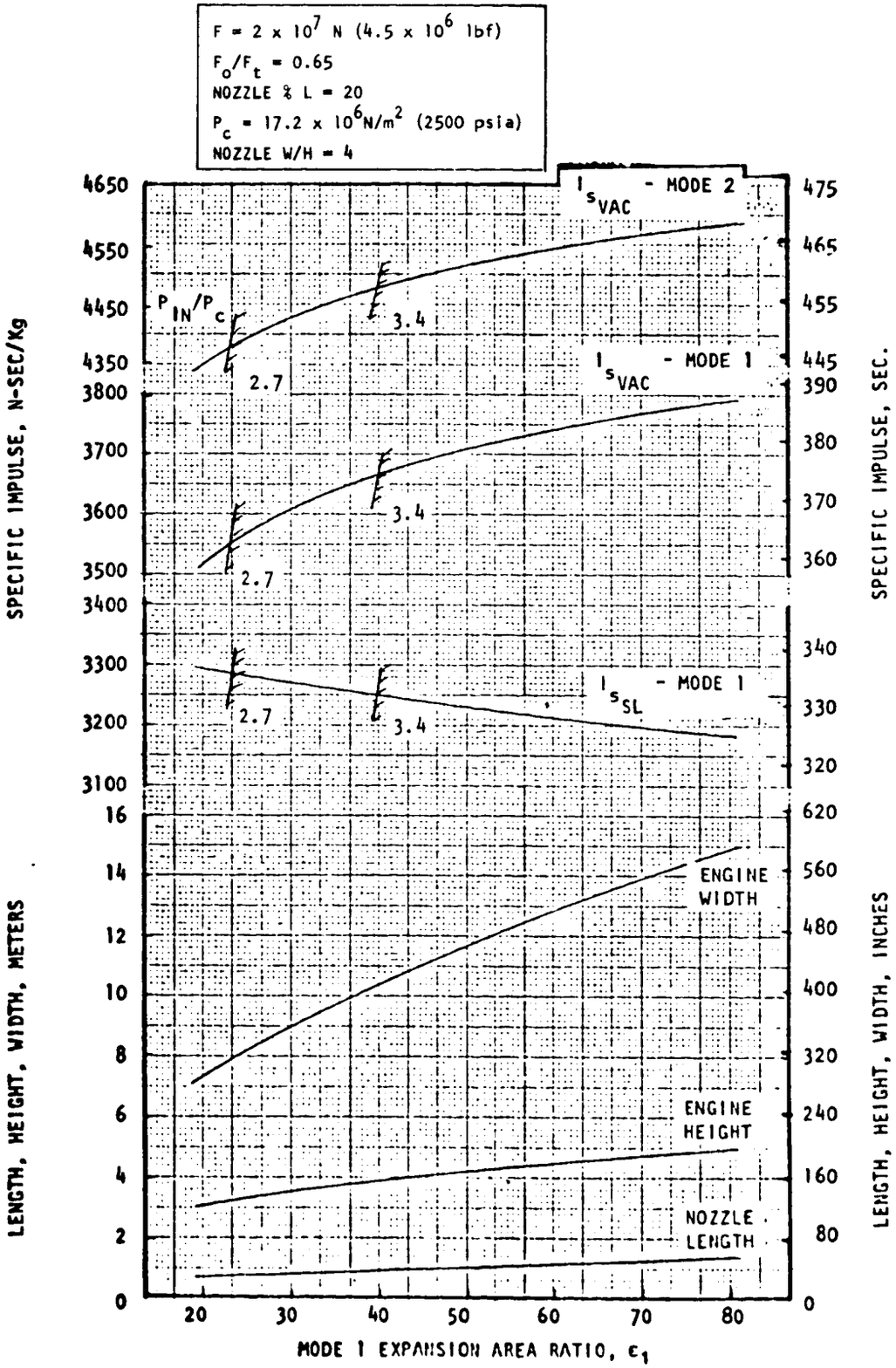

Figure 93. Split-Combustor Linear Engine Performance and Envelope vs Mode 1 Area Ratio LOX/RP-1, Staged Combustion Cycle

ORIGINAL PAGE IS
OF POOR QUALITY

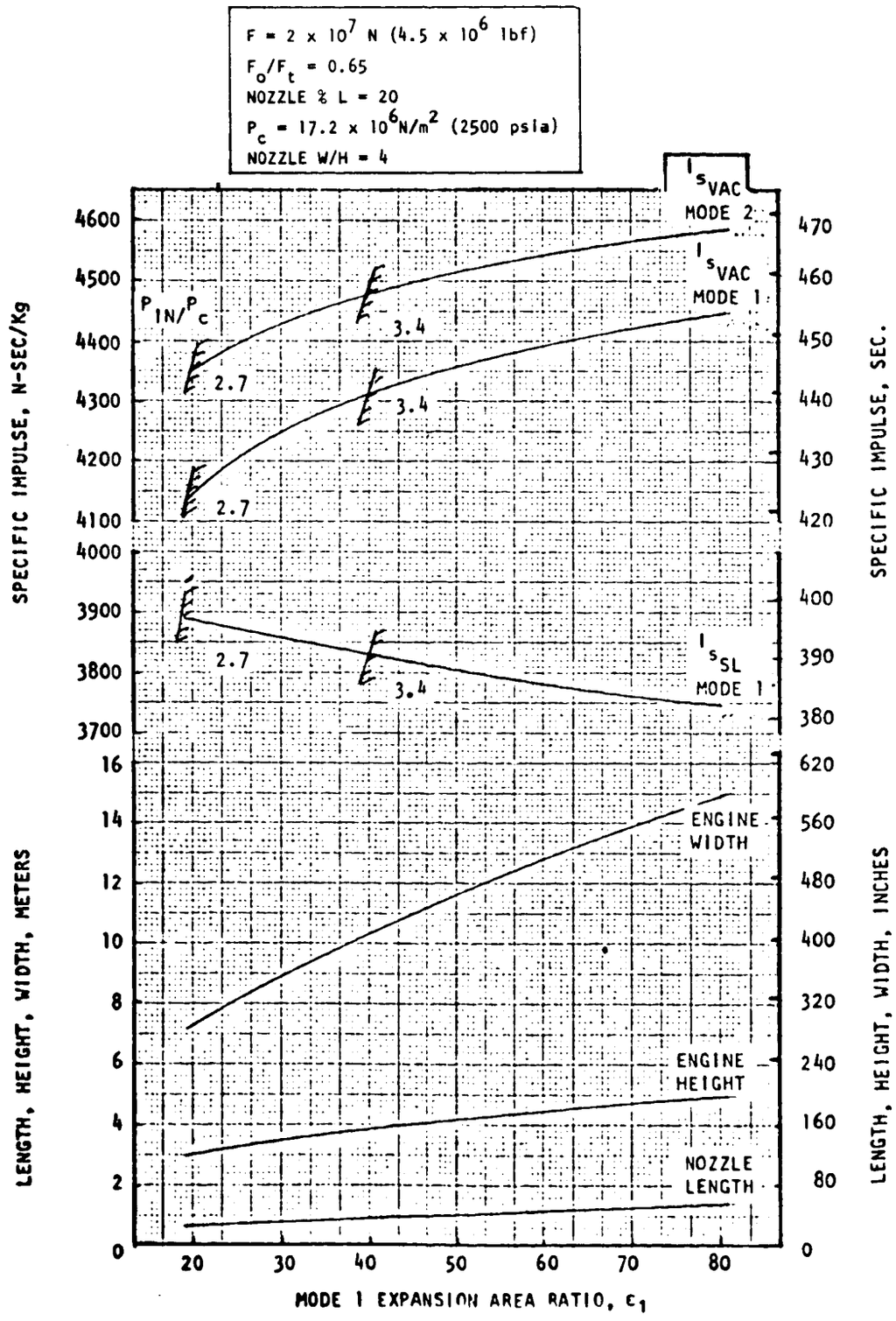

Figure 94. Split-Combustor Linear Engine Performance and Envelope vs Mode 1 Area Ratio LOX/H_2, Staged Combustion Cycle

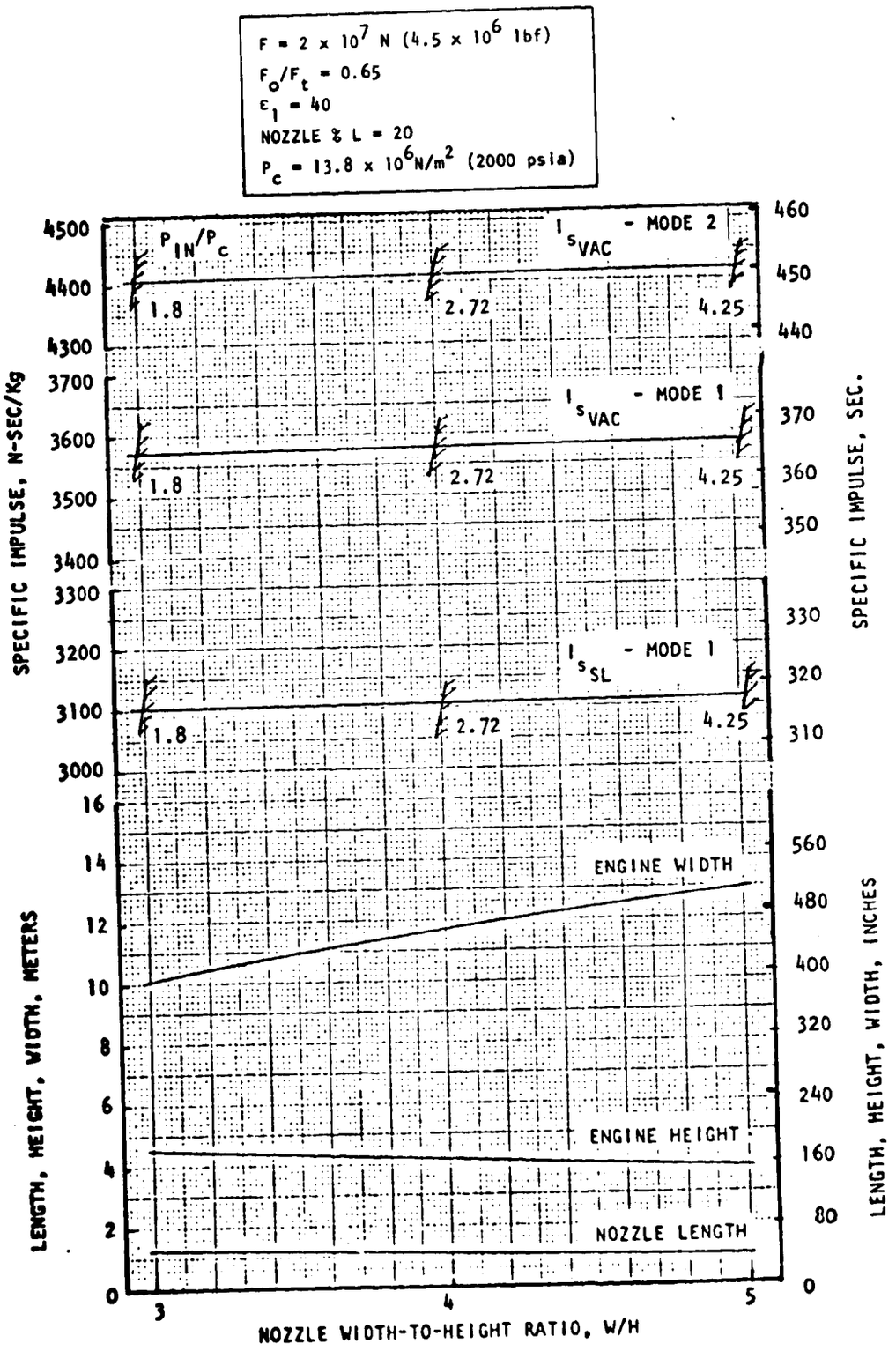

Figure 95. Split-Combustor Linear Engine Performance and Envelope vs Nozzle Width-to-Height Ratio LOX/RP-1, Gas Generator Cycle

ORIGINAL PAGE IS
OF POOR QUALITY

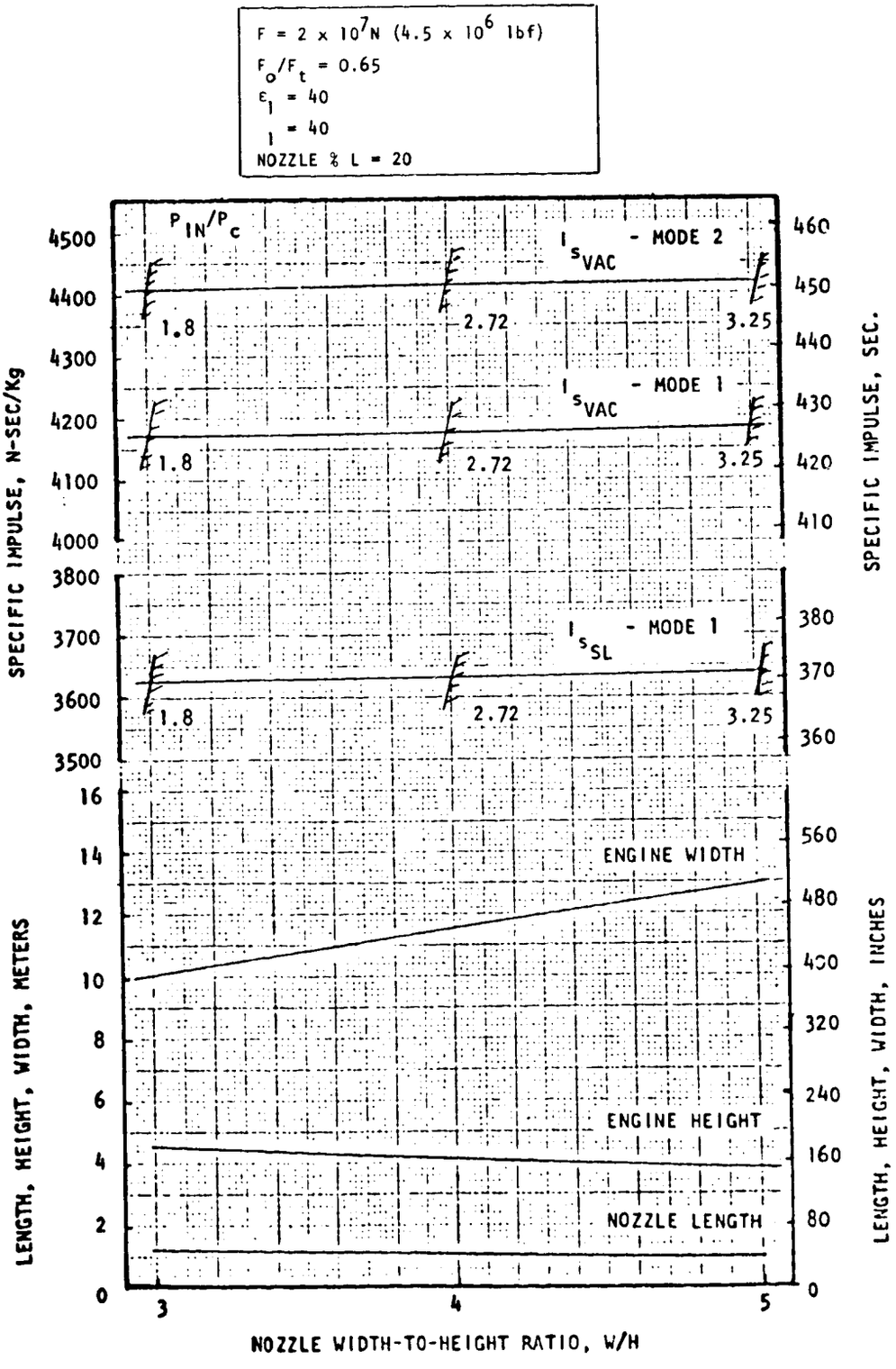

Figure 96. Split-Combustor Linear Engine Performance and Envelope vs Nozzle Width-to-Height Ratio LOX/H_2, Gas Generator Cycle

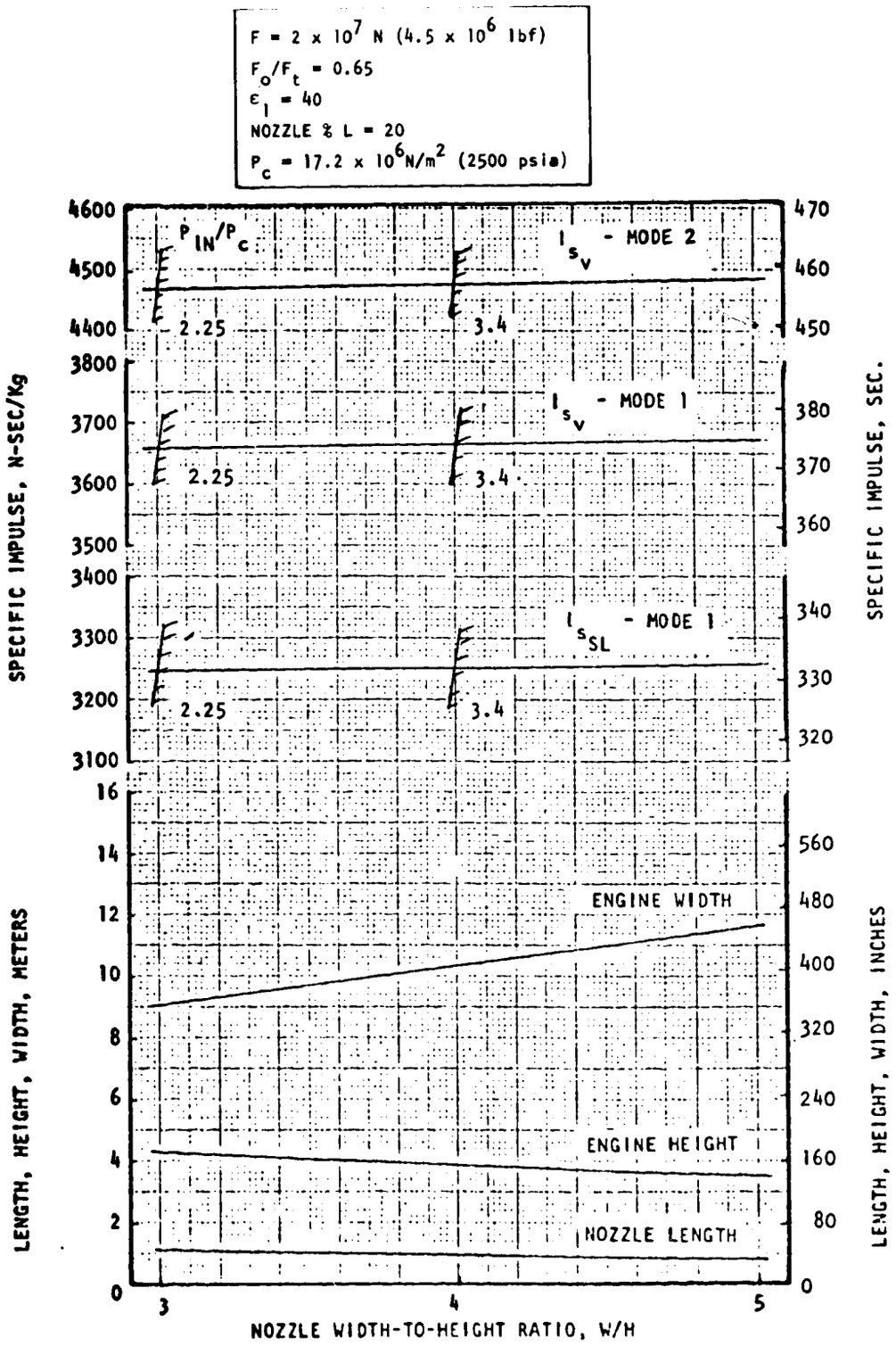

Figure 97. Split-Combustor Linear Engine Performance and Envelope vs Nozzle Width-to-Height Ratio LOX/RP-1, Staged Combustion Cycle

ORIGINAL PAGE IS
OF POOR QUALITY

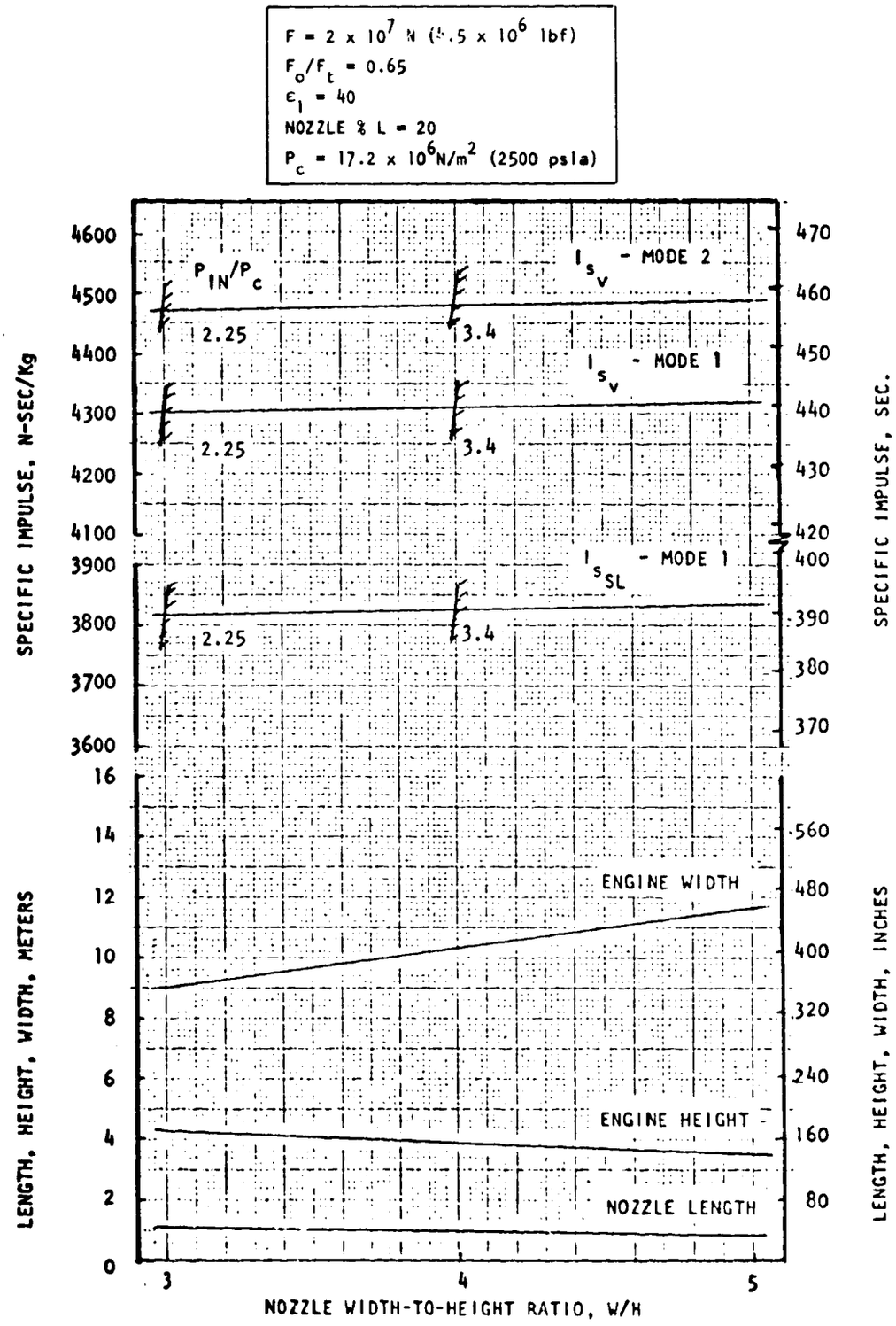

Figure 98. Split-Combustor Linear Engine Performance and Envelope vs Nozzle Width-to-Height Ratio LOX/H_2, Staged Combustion Cycle

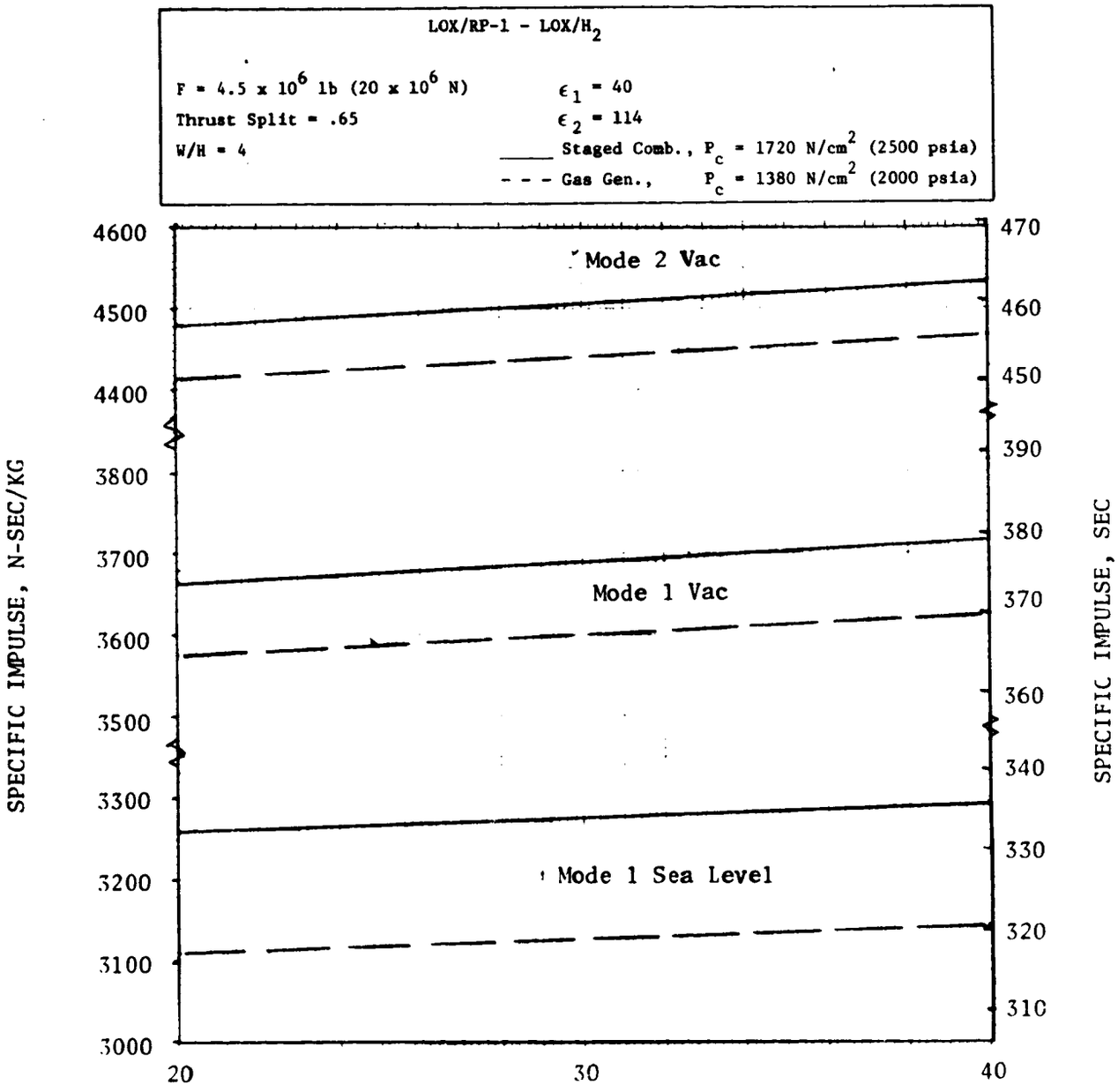

Figure 99. Linear Split-Combustor Engine Performance vs Nozzle Percent Length

ORIGINAL PAGE IS
OF POOR QUALITY

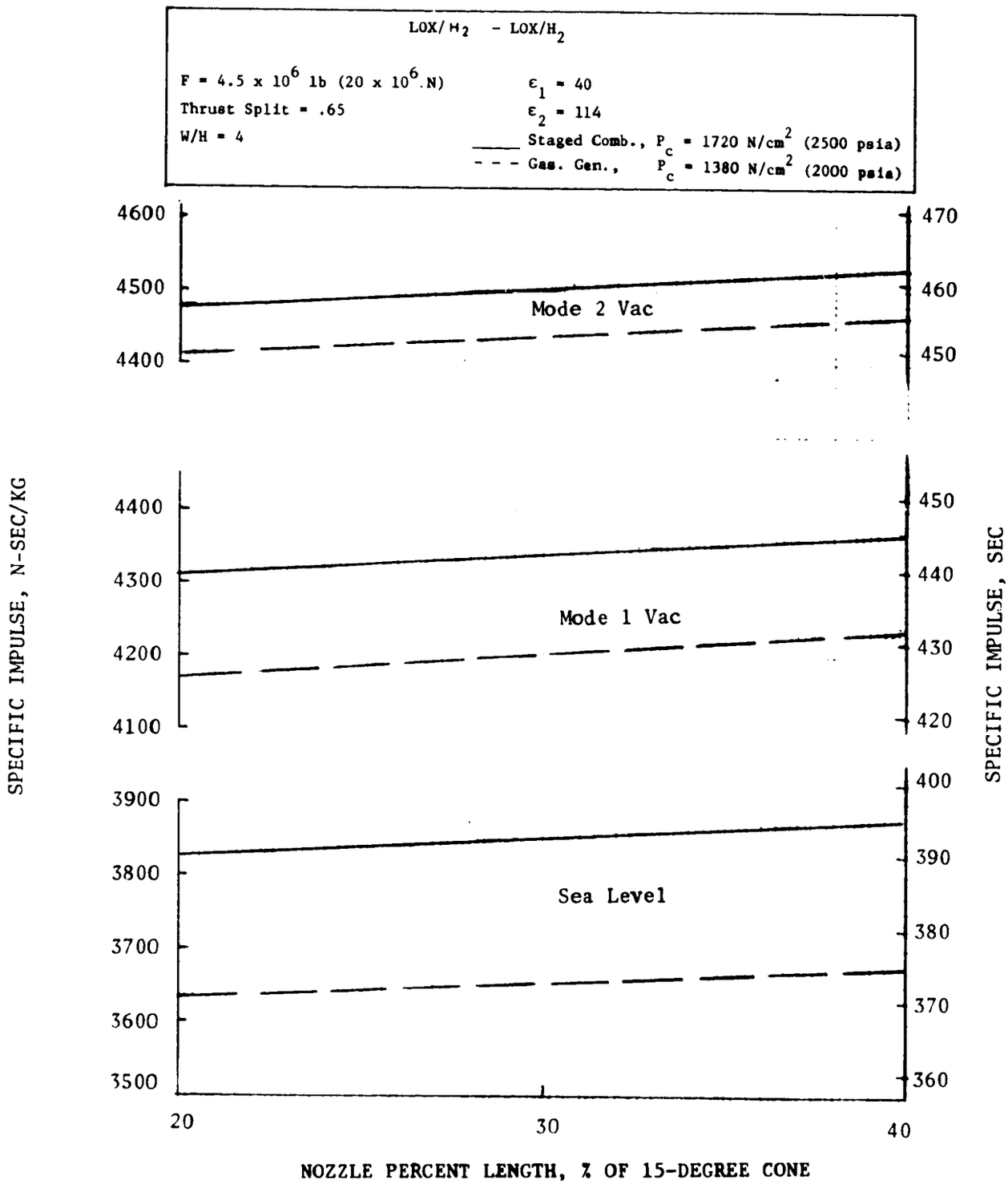

Figure 100. Linear Split-Combustor Engine Performance vs Nozzle Percent Length

were held constant during this study. It has been found that engine weight increases with nozzle percent length at a lower rate than with nozzle expansion area ratio, and that doubling the nozzle percent length does not cause any undue increases in heat loads. Therefore, increasing nozzle percent length provides a means of increasing performance without affecting cooling limits and with a relatively low weight penalty.

The following observations can be made from inspection of performance trends:

1. The staged combustion cycle provides higher performance in a more compact engine, i.e., shorter width, shorter height, and shorter nozzle.

2. For the same engine cycle type, the engine geometry and parametric engine geometry variations are identical for the LOX/RP-1/LOX/H_2 and LOX/H_2/LOX/H_2 propellants. Identical geometry and trends are expected for the other two propellant combinations (LOX/CH_4/LOX/H_2, LOX/RJ-5/LOX/H_2.

3. For the same engine cycle type, the engine Mode 2 vacuum performance and performance variations (trends) are identical for LOX/RP-1/LOX/H_2 and LOX/H_2/LOX/H_2 propellants. Identical Mode 2 vacuum performance and trends will result for the other two propellant combinations.

4. Mode 1 vacuum and sea level specific impulse performance trends for LOX/RJ-5/LOX/H_2 and LOX/CH_4/LOX/H_2 propellant combinations will be identical to those of LOX/RP-1/LOX/H_2 propellants. The performance curves of the former can be derived from their baseline engine performance (Table 21), and the performance trends with F, F_o/F_T, ε_o, and W/H of LOX/RP-1/LOX/H_2 (Fig. 83 through 98).

5. For an engine cycle and propellant type, the performance variations with thrust are due to boundary layer losses. In the thrust range 6.67×10^6 to 26.69×10^6 (1.5×10^6 to 6×10^6 lb), the boundary layer loss variation is 1.03 percent. The engine width, height, and length change with thrust level is indicated in Fig. 83 through 86 .

6. Thrust split variations do not affect engine geometry (Fig. 77 through 80). It affects LOX/H_2/LOX/H_2 Mode 1 engine sea level and vacuum performance only slightly and affects Mode 2 engine vacuum performance through increase of engine Mode 2 area ratio.

   Mode 1 vacuum and sea level performance decrease appreciably for LOX/RP-1/LOX/H_2 propellants because of the increase in engine LOX/RP-1 flows as F_o/F_t increases. For LOX/RP-1 propellants, thrust split variations affect Mode 1 and Mode 2 vacuum and sea level performance through individual Mode 1 and Mode 2 theoretical performance variations as thrust split changes.

ORIGINAL PAGE IS
OF POOR QUALITY

TABLE 21. POINT-DESIGN PERFORMANCE SUMMARY

Cycle *	Propellant	Engine Mixture Ratio	Chamber Pressure N/m^2, (psia)	Sea Level Specific Impulse N-Sec/Kgm,(Sec.) Mode 1	Vacuum Specific Impulse N-Sec/Kg, (Sec.) Mode 1	Mode 2
GG	LOX/RP-1	2.8	$1.379X10^7$(2000)	3106.9(316.8)	3577.9(364.8)	4411.7(449.9)
GG	LOX/RJ-5	2.7	$1.379X10^7$(2000)	3070.3(313.1)	3536.4(360.6)	4410.4(449.7)
GG	LOX/CH_4	3.5	$1.379X10^7$(2000)	3173.5(323.6)	3653.3(372.5)	4410.4(449.7)
GG	LOX/H_2	7.0	$1.379X10^7$(2000)	3630.6(370.2)	4179.2(426.2)	4411.4(449.8)
SC	LOX/RP-1	2.8	$1.724X10^7$(2500)	3250.7(331.5)	3664.7(373.7)	4477.4(456.6)
SC	LOX/RJ-5	2.7	$1.724X10^7$(2500)	3218.3(328.2)	3632.3(370.4)	4477.0(456.5)
SC	LOX/CH_4	3.5	$1.724X10^7$(2500)	3322.6(338.8)	3745.5(381.9)	4477.0(456.5)
SC	LOX/H_2	7.0	$1.724X10^7$(2500)	3826.9(390.2)	4210.6(439.6)	4478.5(456.7)

* GG - GAS GENERATOR
SC - STAGED COMBUSTION

7. Area ratio changes (Fig. 91 through 94) change both engine performance and geometry. Performance changes are due mostly to theoretical I_s changes with area ratio and, to a less extent, nozzle divergency efficiency changes (0.986 to 0.989) with expansion area ratio (20-80).

8. Nozzle width-to-height (W/H) variations (Fig. 85 through 88) change Mode 1 or Mode 2 engine performance only 0.38 percent. The effect on engine geometry is more pronounced. With constant thrust and area ratio, an increase in W/H requires an increase in width (W), a decrease in throat gap (and thus length), and a decrease in height.

Parametric thrust chamber cooling studies conducted provided the basis for the cooling limits indicated on the engine performance curves in Fig. 83 through 98. In general, the lower thrust levels require greater values of P_{in}/P_c than was baselined for the gas generator cycle (P_{in}/P_c = 1.8) and staged combustion cycle (P_{in}/P_c = 2.25). Larger P_{in}/P_c values are also required as thrust split, Mode 1 area ratio, and width-to-height ratio are increased. Although power cycle balance is still achievable at the higher inlet-to-chamber pressure ratios, the pump discharge pressures become excessive in many cases. Oxidizer-rich preburners could be utilized to increase turbine power by increasing turbine flow and maintaining turbine pressure ratio (and thus pump discharge pressure) at lower, more reasonable values.

PARAMETRIC WEIGHTS

In this subtask, pump weight calculation procedures developed in Task IV were used to calculate parametric weights. The standard linear engine nozzle support structure design used in Tasks II and IV weight calculations was re-evaluated and a new lighter design selected for differentially throttled linear engines. Linear engine weights were then calculated parametrically for the parameter values indicated in Table 20.

Gas generator engine weights were calculated using scaling equations in a Rocketdyne-developed computer program. To obtain staged combustion engine weights, a ratio was applied to the gas generator engine weights. The ratio was obtained by analysis of component weight differences at the baseline design point of Task IV.

Pump Weights

Pump weights are shown in Table 22 for the gas generator cycle at the nominal value of parameters of Table 19. Weights were calculated using the equations in Table 18 depending on whether the pumps are speed-limited (double entry) or stress limited types.

Inner combustor pumps are identical for all four propellant concept engines; the outer combustor pump weights account for the differences in the total pump weights. Outer combustor fuel pumps are all turbine stress-limited pumps. The RJ-5 and RP-1 pumps are lighter in weight than the H_2 and CH_4 pumps chiefly because of fuel density (Eq. 2 in Table 18), which produces the lowest volumetric

ORIGINAL PAGE IS
OF POOR QUALITY

TABLE 22. PUMP WEIGHTS*, GAS GENERATOR CYCLE

(P_c = 1379 N/cm^2, 2000 psia)

	LOX/RJ5-LOX/H_2	LOX/RP1-LOX/H_2	LOX/H_2-LOX/H_2	LOX/CH_4-LOX/H_2
LOX (outer comb.)	2541(5590)	2507(5515)	2729(6016)**	2932(6463)**
Fuel (outer comb.)	1140(2513)	1191(2626)	1645(3626)	1645(3626)
LOX (inner comb.)	1531(3376)**	1531(3376)**	1531(3376)**	1531(3376)**
H_2 (inner comb.)	1116(2461)	1116(2461)	1116(2461)	1116(2461)
Total Weight	6323(13940)	6340(13978)	7021(15479)	7224(15926)

NOTE: Units are in kilograms (pounds)

*Boost pumps included
**Double-entry pumps; all others, single entry

flowrates (Q) for the higher density fuels. Outer combustion LOX pumps are heavier for the LOX/H_2/LOX/H_2 and LOX/CH_4/LOX/H_2 engines because these latter two pumps are double-entry pumps and the LOX/RJ-5/LOX/H_2, LOX/RP-1/LOX/H_2 engine LOX pumps are turbine stress-limited pumps. The LOX/CH_4/LOX/H_2 engine LOX pump is heavier than the LOX/H_2/LOX/H_2 engine LOX pumps because the LOX flowrates in the former engine are largest. Performance and mixture ratio effects cause the LOX flowrates of the LOX/CH_4/LOX/H_2 system to be higher.

Nozzle Support Structure Weights

The nozzle support structure design is dependent on the thrust vector control concept to be used with the linear engine. In the J-2 linear engine, thrust vector control was achieved experimentally through hinging of thrust chamber side panels (Ref. 1). The engine was built so that either thrust chamber half-section could be swiveled at a point close to the combustor plane and locked in that position during testing. The nozzle loads were transmitted from the hat bands to a cantilevered beam and from this beam to the test stand structure at the point of rotation near the combustor. This concept results in a relatively heavy nozzle support structure (Fig. 101) for a linear engine using nozzle side-panel hinging for thrust vector control. The cantilevered structure weight increases rapidly with expansion area ratio and nozzle length.

In this subtask, nozzle support structure weights were determined for a linear engine which utilizes differential throttling for thrust vector control (Fig. 102). This structure picks up the nozzle loads at the hat bands and transmits them to a truss framework through two pickup points. This approach results in a considerably lighter structure whose weight grows more moderately with nozzle area ratio and length than the cantilevered structure. Relative engine weights defined in Task II were based upon the cantilever approach. Parametric engine weights calculated in Task V reflect the differential throttling nozzle support structure weights.

Parametric Engine Weights

Parametric engine weights are presented in Fig. 103 through 107 for the gas generator cycle and in Fig. 108 through 112 for the staged combustion cycle. Gas generator weights are presented at a chamber pressure of 1379 N/cm^2 (2000 psia) and staged combustion cycle weights at 1723 N/cm^2 (2500 psia). Rocketdyne-developed scaling equations were used in the calculation of engine weights.

The following comments are made from inspection of engine weight trends in Fig. 103 through 112:

1. LOX/CH_4 - LOX/H_2 engine weights are approximately 5 percent heavier than the LOX/RJ-5 - LOX/H_2 weights. LOX/H_2 - LOX/H_2 engine weights are similar to LOX/CH_4 - LOX/H_2 engine weights and LOX/RP-1 - LOX/H_2 engine weights are similar to LOX/RJ-5 - LOX/H_2 engine weights. The difference in the weights of the CH_4 and RJ-5 engine lies in the pump weights which constitute approximately 32 percent of the engine weight.

ORIGINAL PAGE IS
OF POOR QUALITY

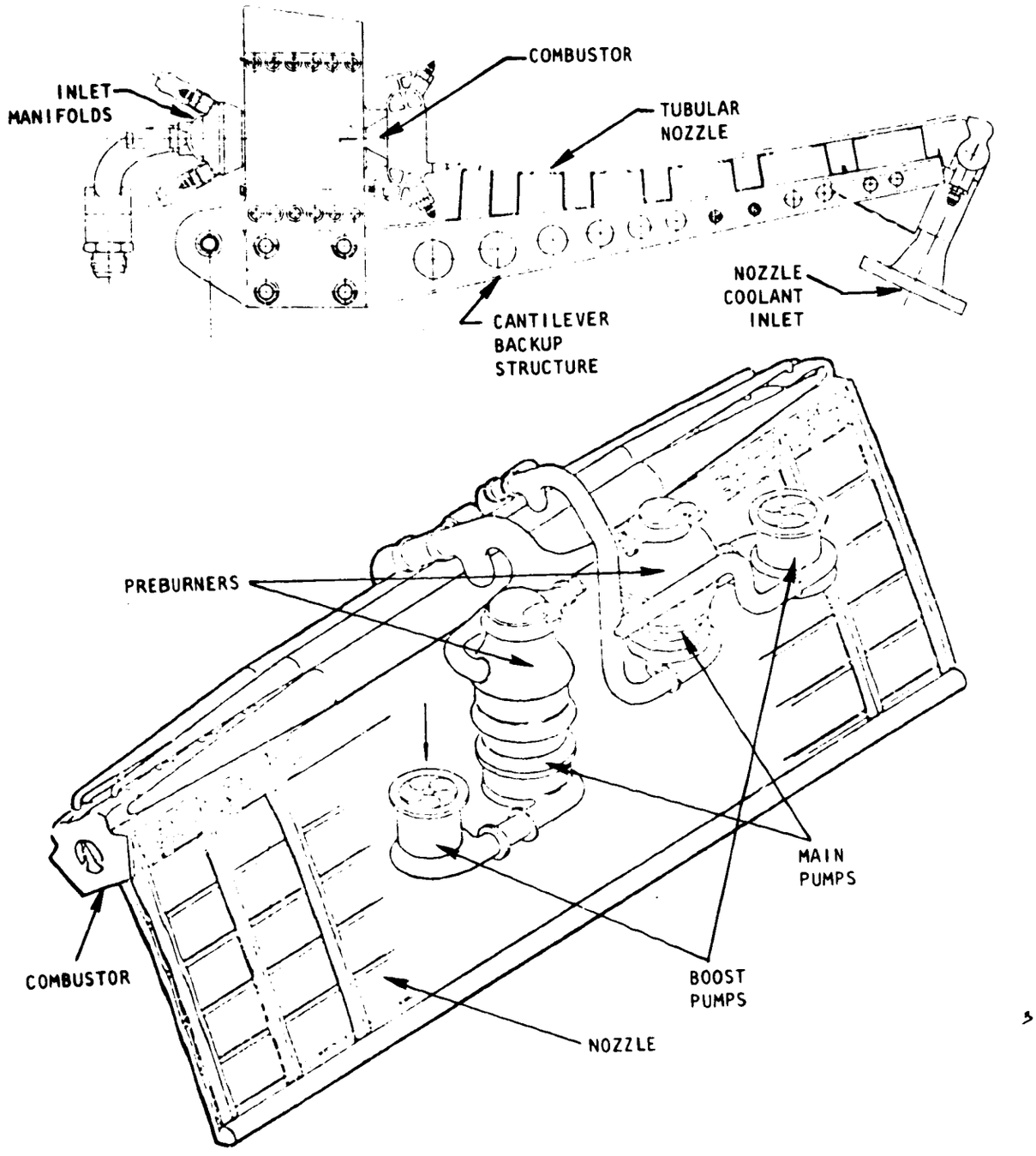

Figure 101. Typical Linear Engine Nozzle Construction With Cantilever Beams

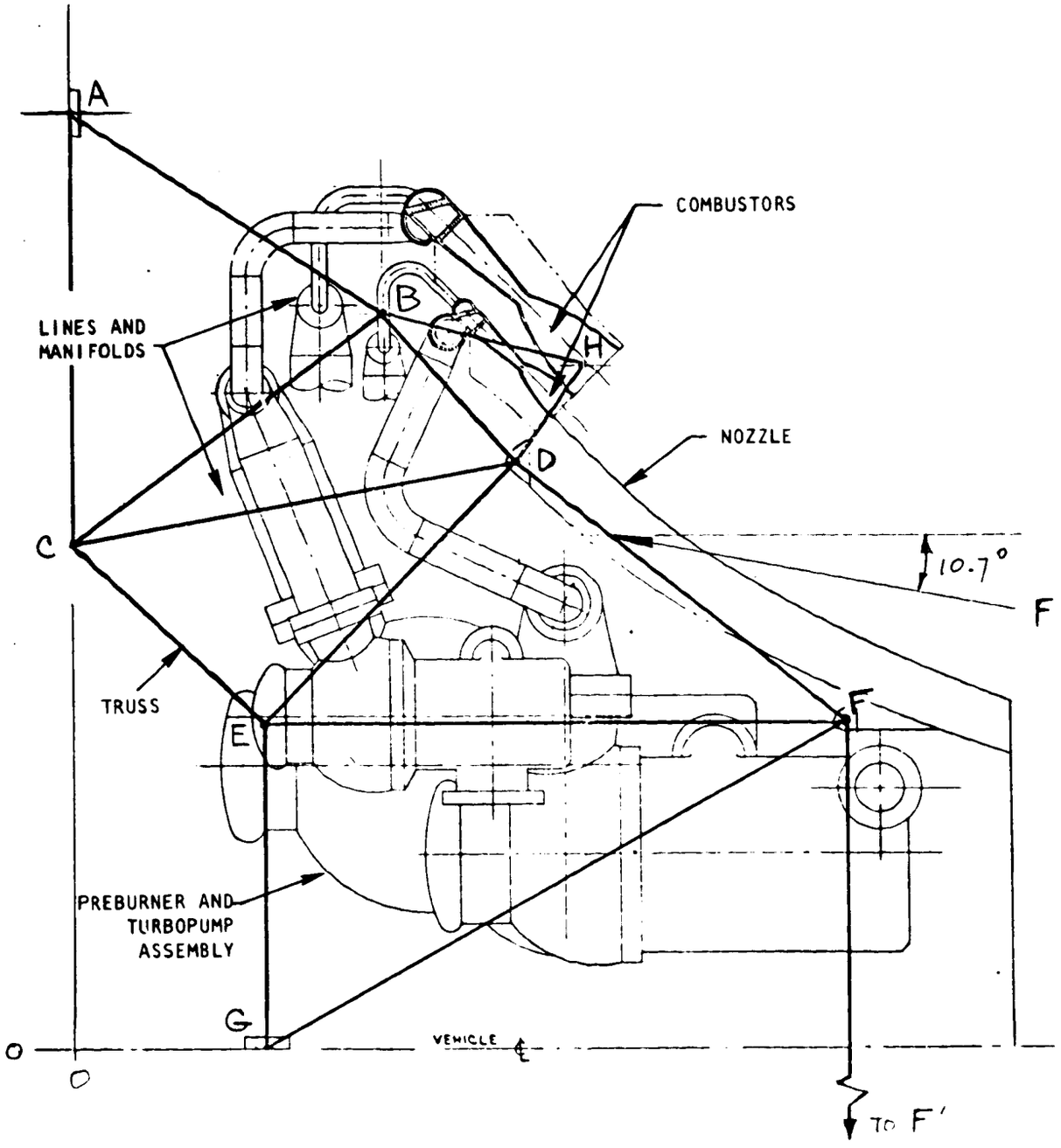

Figure 102. Truss Geometry of 4.5 M LB. Linear Engine Module

ORIGINAL PAGE IS
OF POOR QUALITY

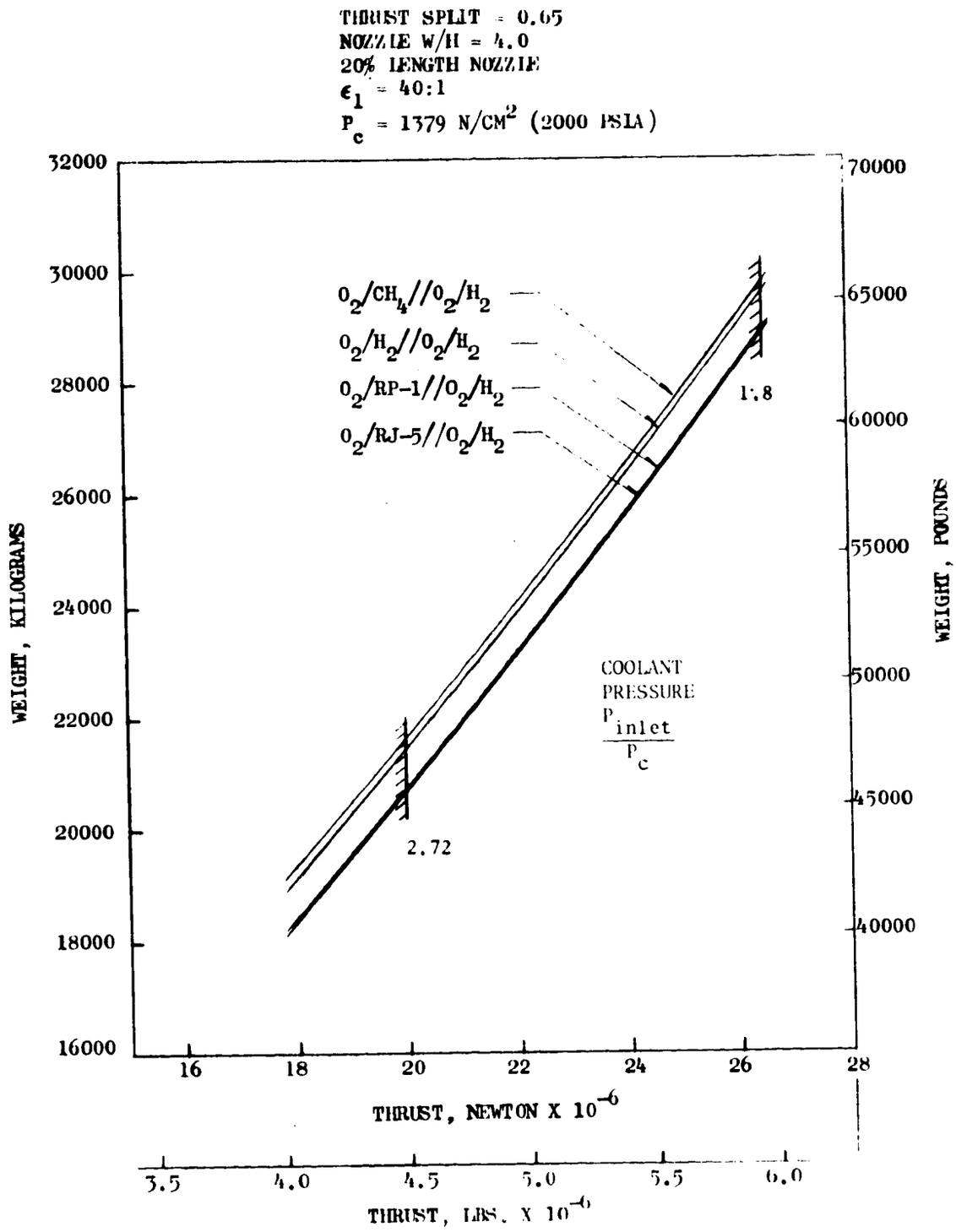

Figure 103. Linear Engine Weight vs Thrust, Gas Generator Cycle

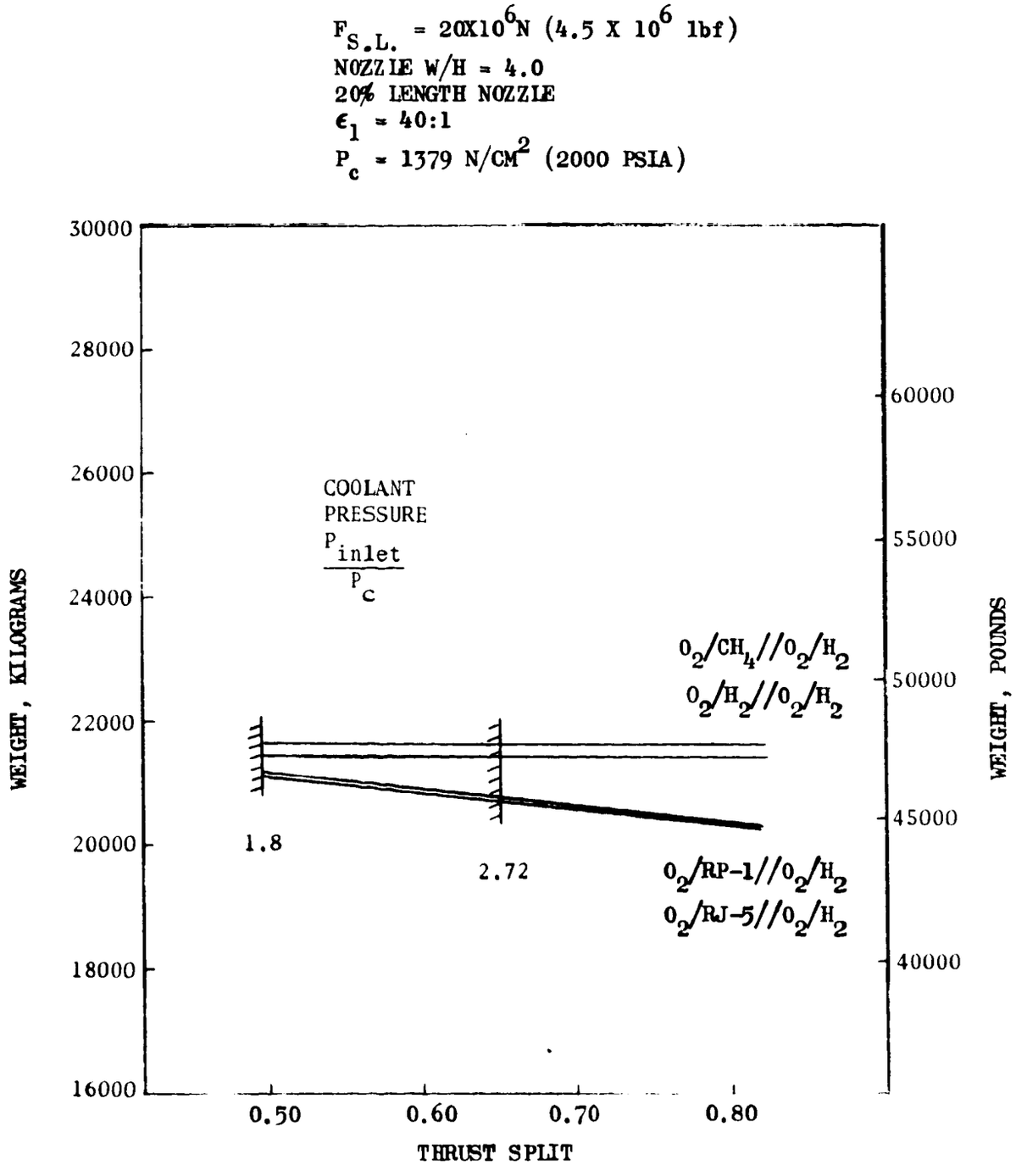

Figure 104. Linear Engine Weight vs Thrust Split, Gas Generator Cycle

ORIGINAL PAGE IS
OF POOR QUALITY

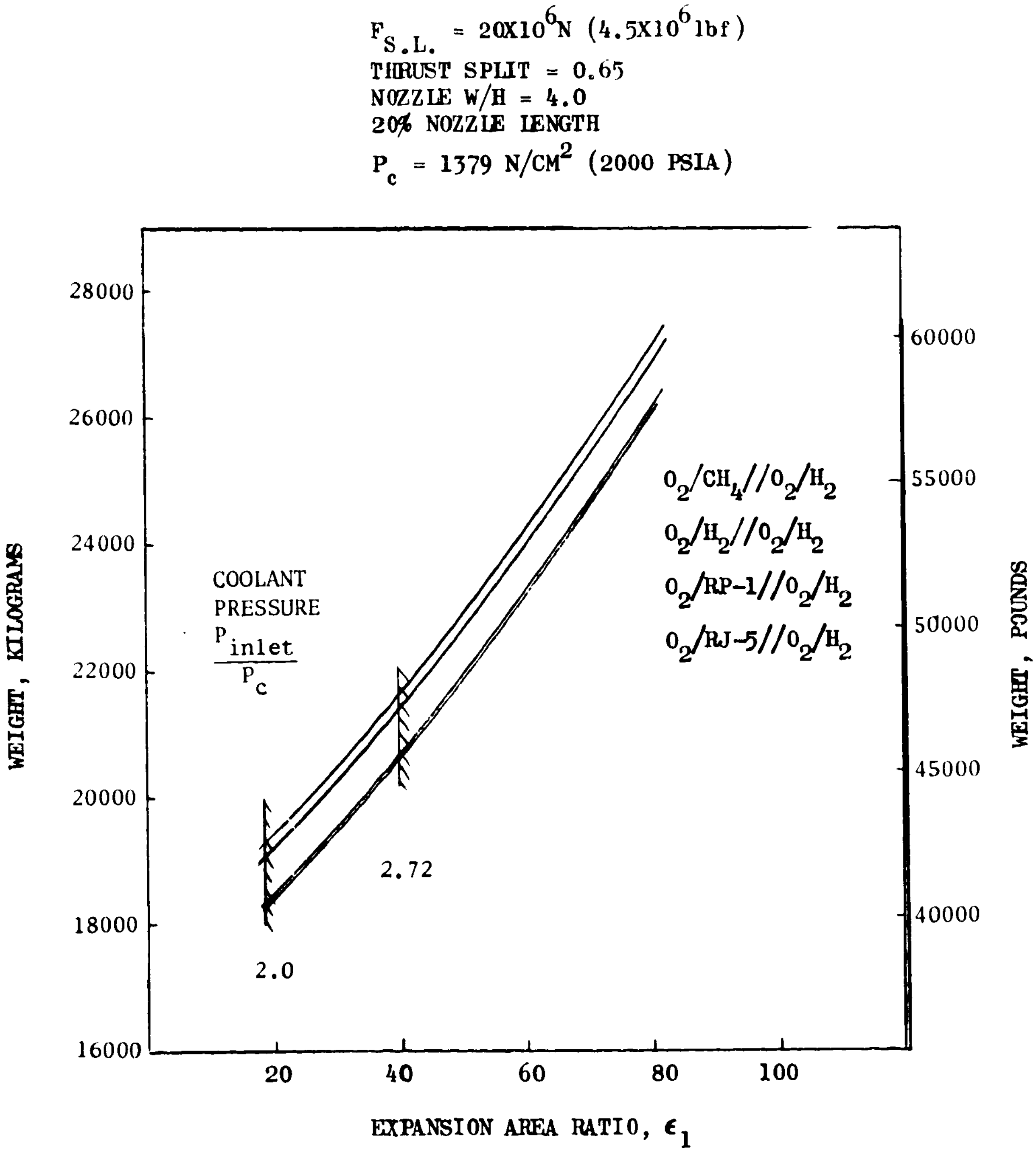

Figure 105. Linear Engine Weight vs Mode 1 Expansion Area Ratio, Gas Generator Cycle

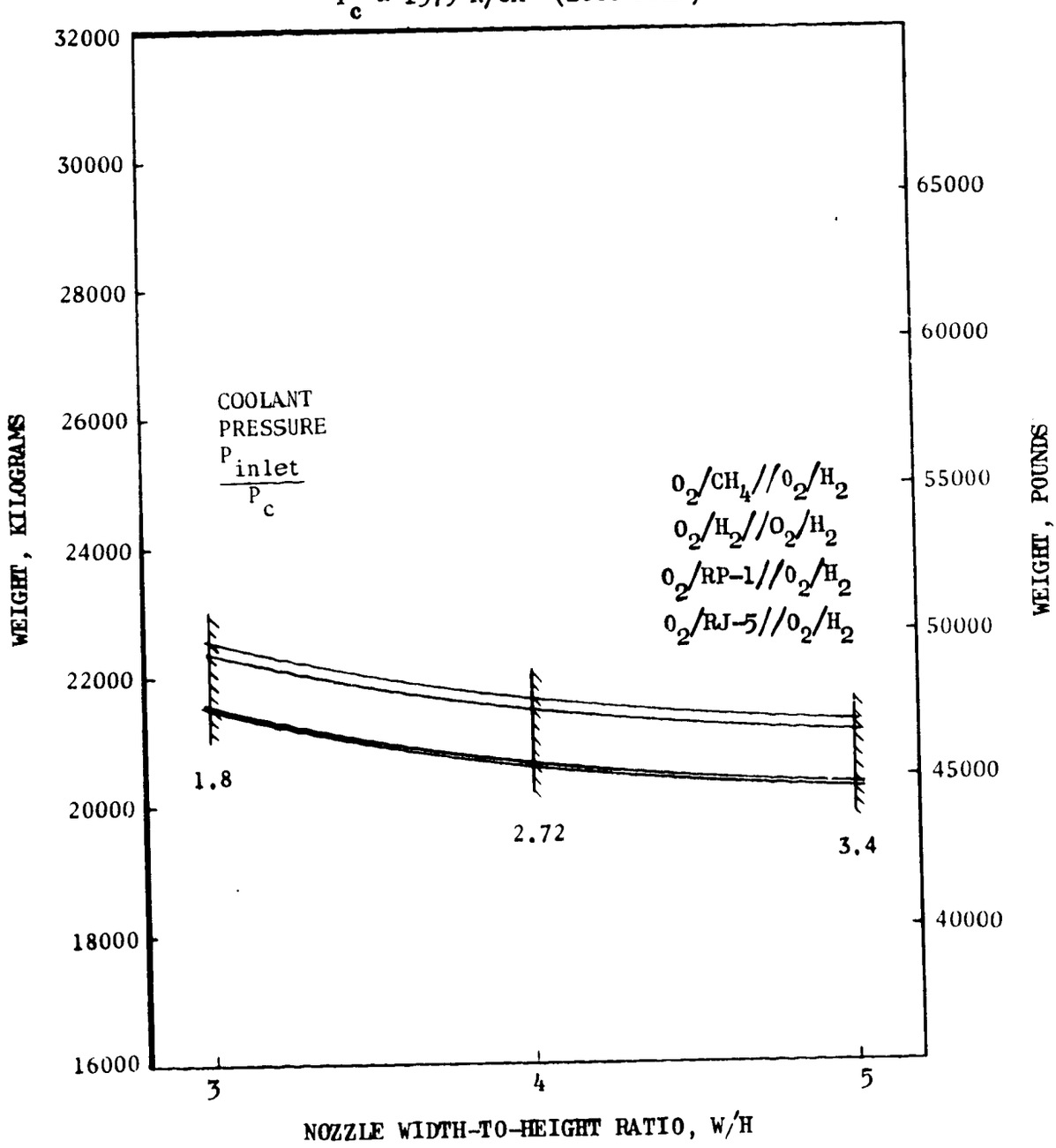

Figure 106. Linear Engine Weight vs Nozzle Width-to-Height Ratio, Gas Generator Cycle

ORIGINAL PAGE IS
OF POOR QUALITY

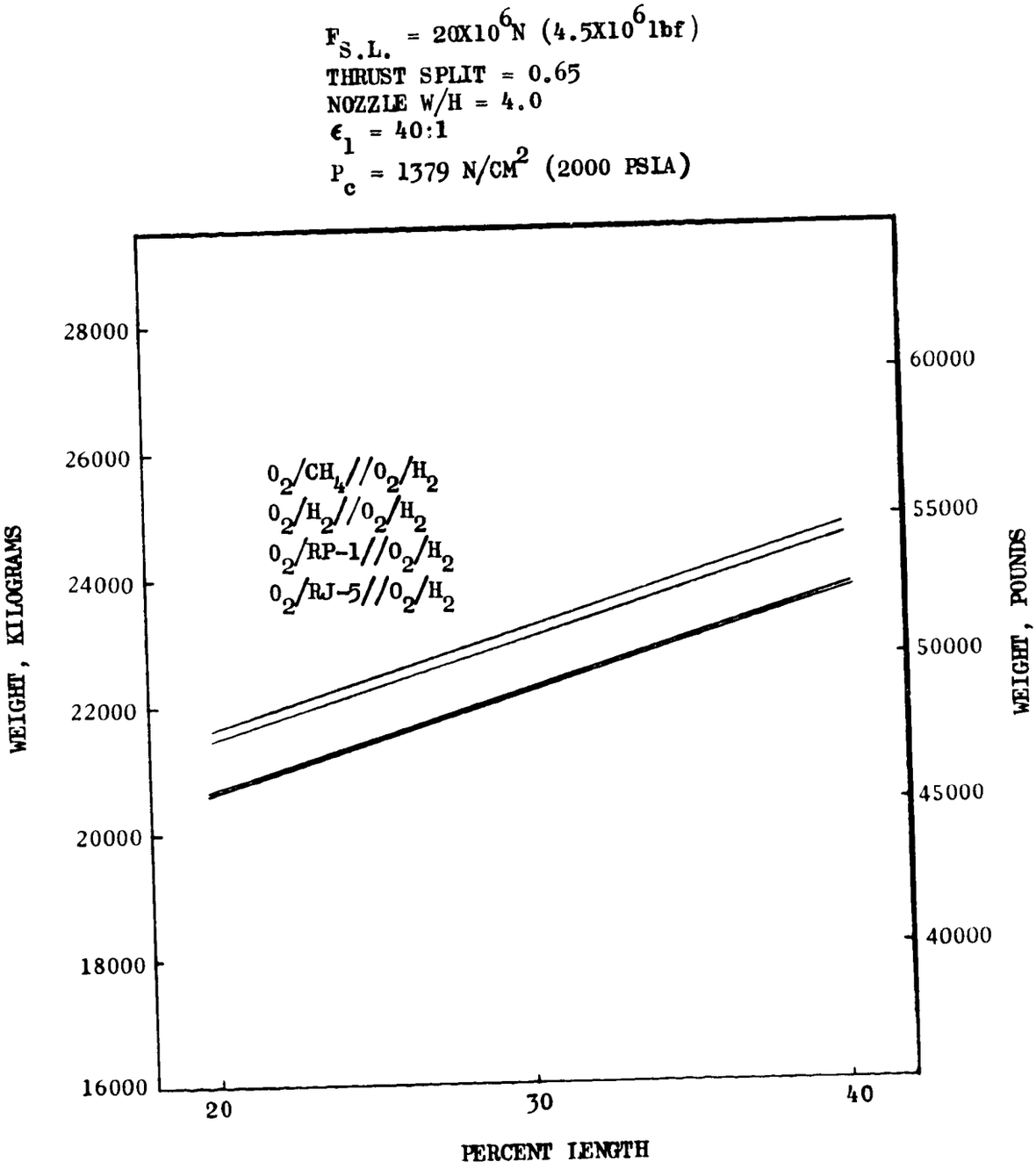

Figure 107. Linear Engine Weight vs Percent Length, Gas Generator Cycle

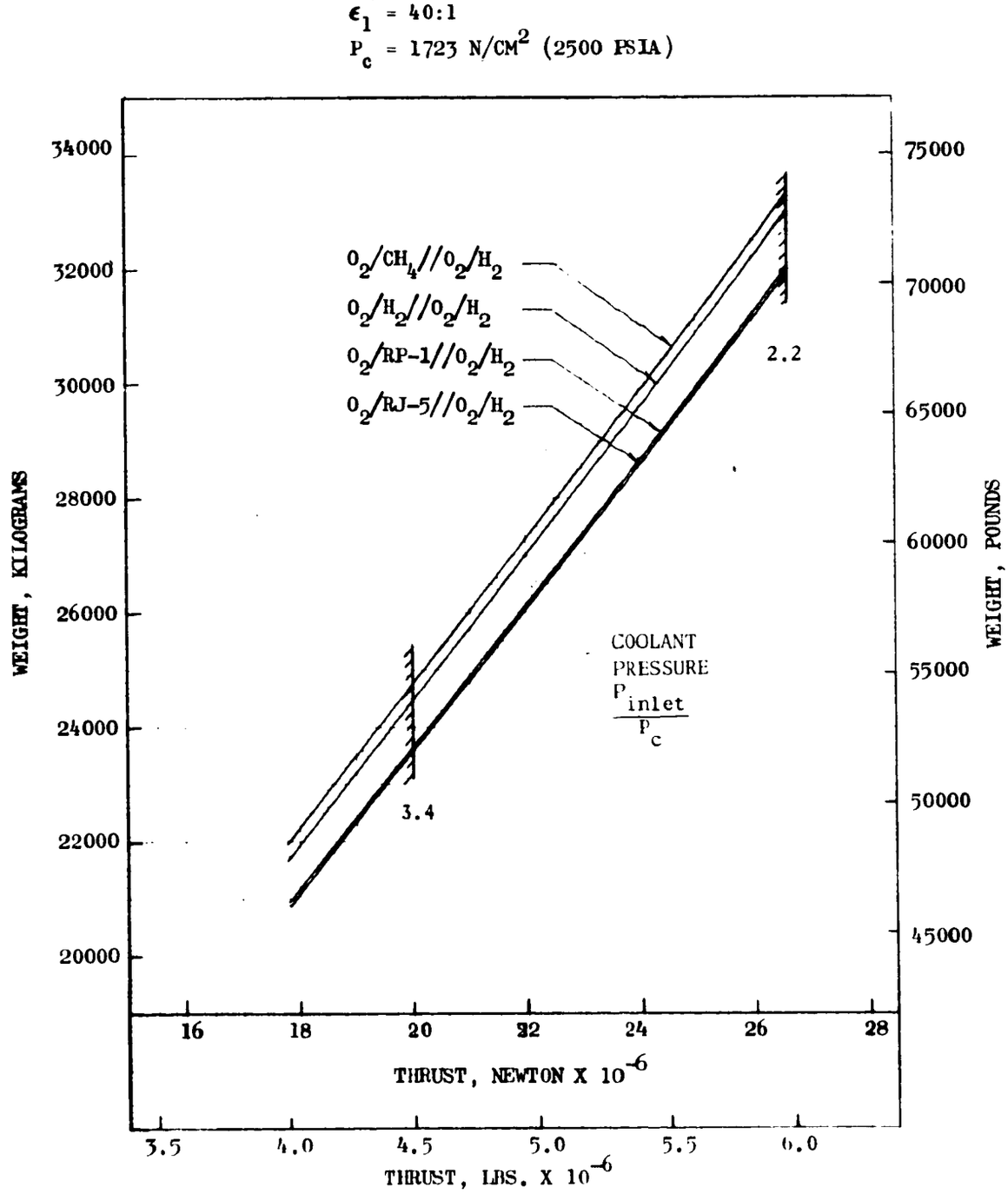

Figure 108. Linear Engine Weight vs Thrust, Staged Combustion Cycle

ORIGINAL PAGE IS
OF POOR QUALITY

ORIGINAL PAGE IS
OF POOR QUALITY

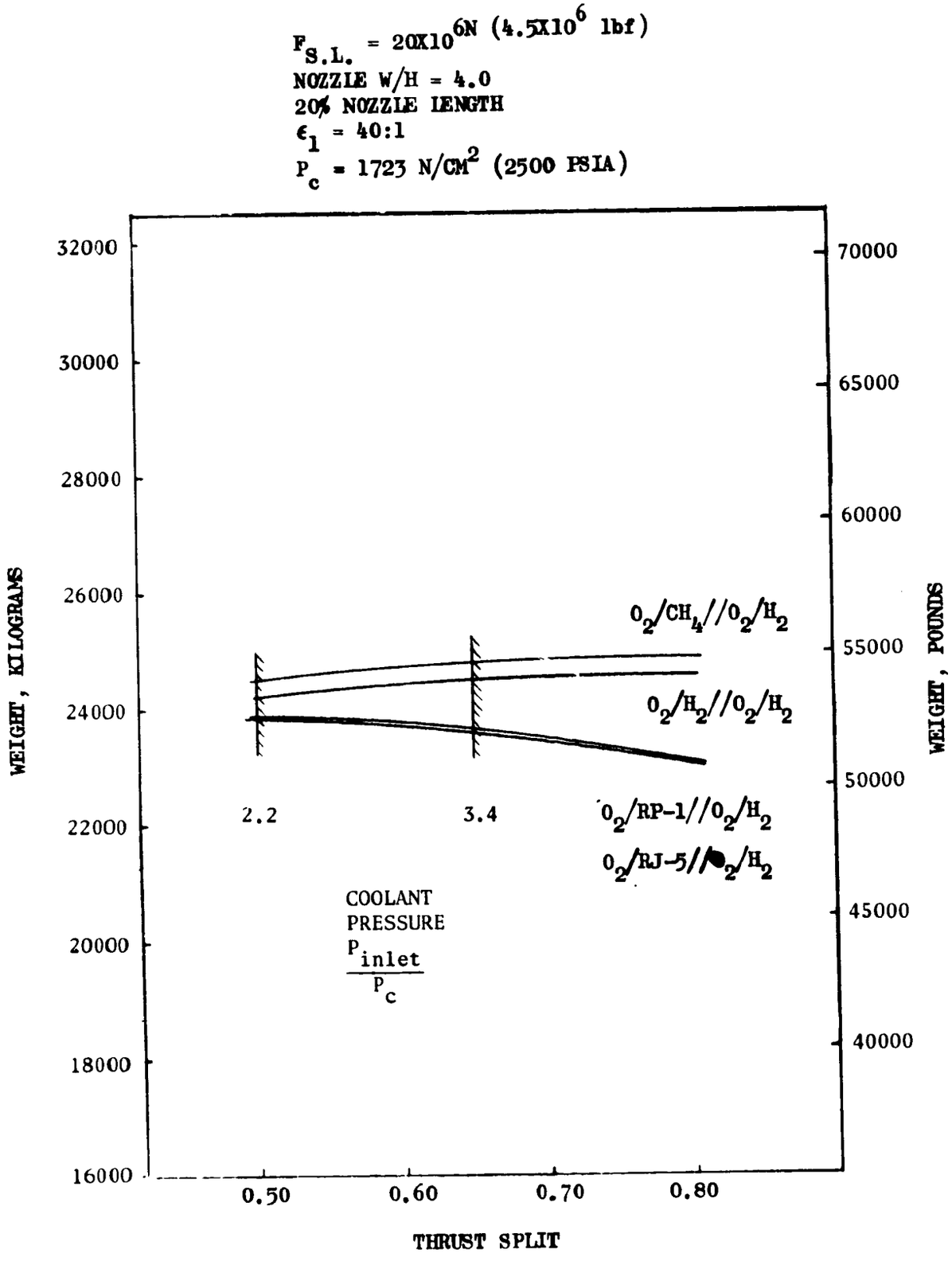

Figure 109. Linear Engine Weight vs Thrust Split Staged Combustion Cycle

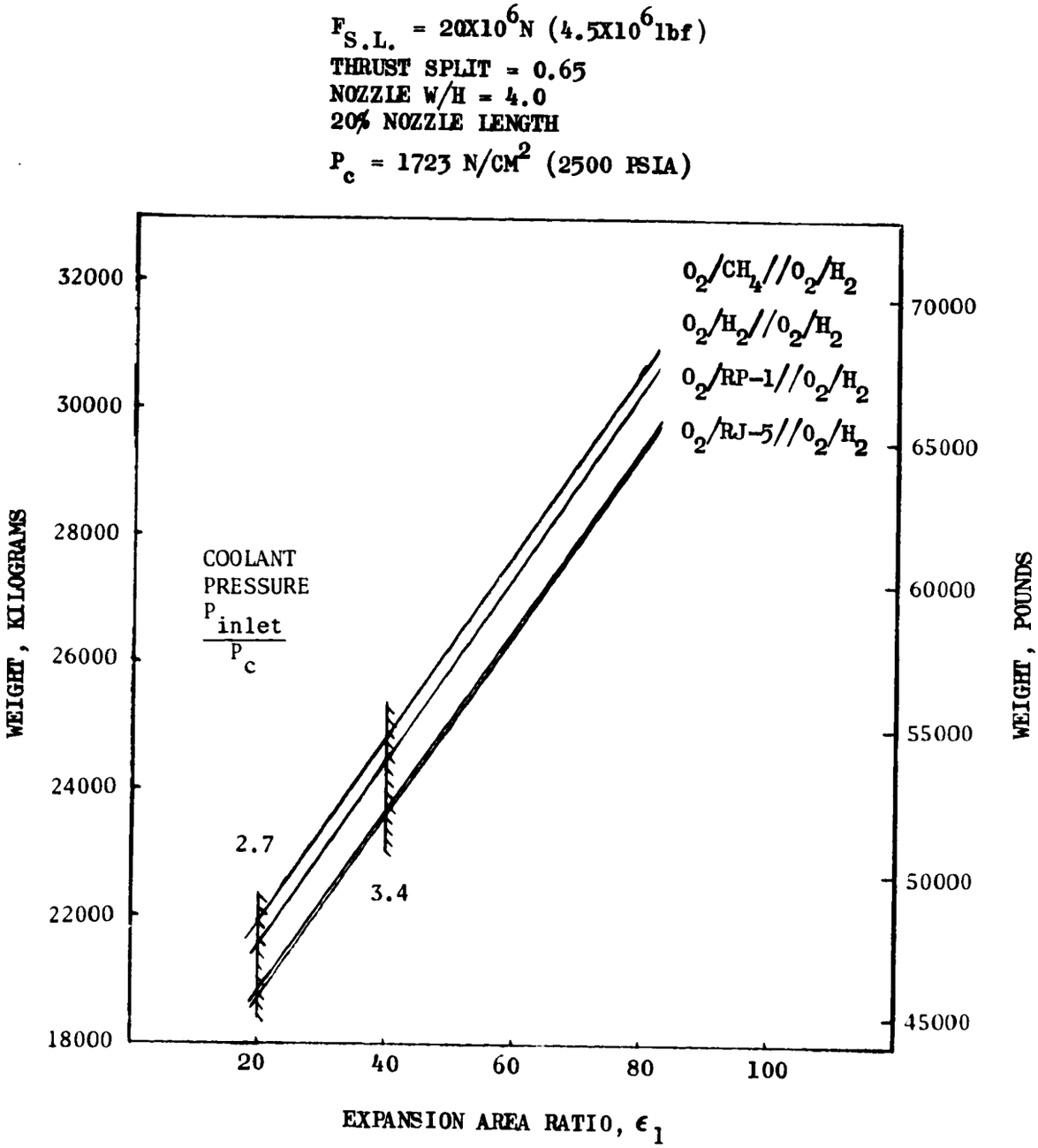

Figure 110. Linear Engine Weight vs Mode 1 Expansion Area Ratio, Staged Combustion Cycle

ORIGINAL PAGE IS
OF POOR QUALITY

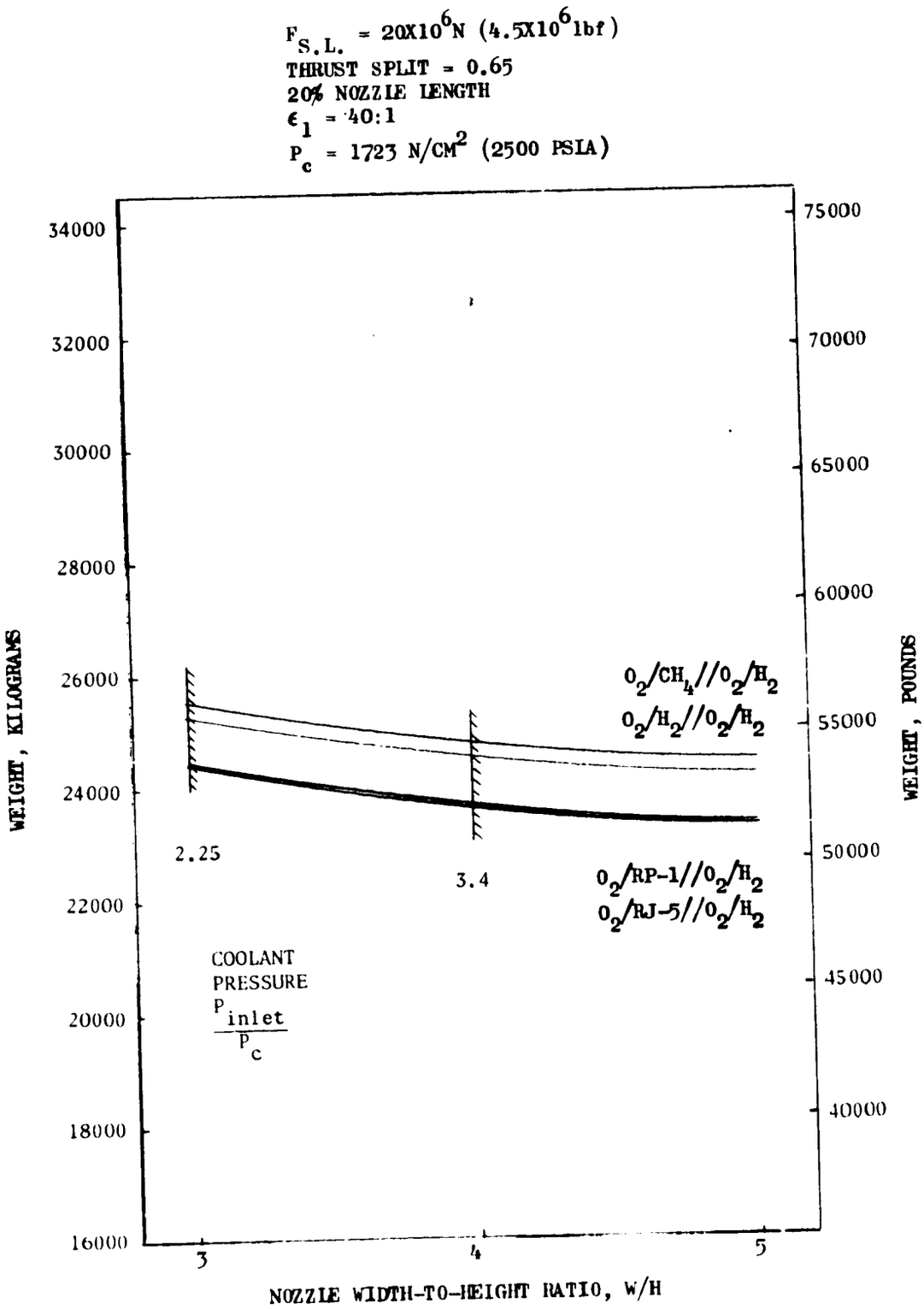

Figure 111. Linear Engine Weight vs Nozzle Width-to-Height Ratio, Staged Combustion Cycle

$F_{S.L.}$ = 20X10^{6}N (4.5X10^{6}lbf)
THRUST SPLIT = 0.65
NOZZLE W/H = 4.0
ϵ_1 = 40:1
P_c = 1723 N/CM^2 (2500 PSIA)

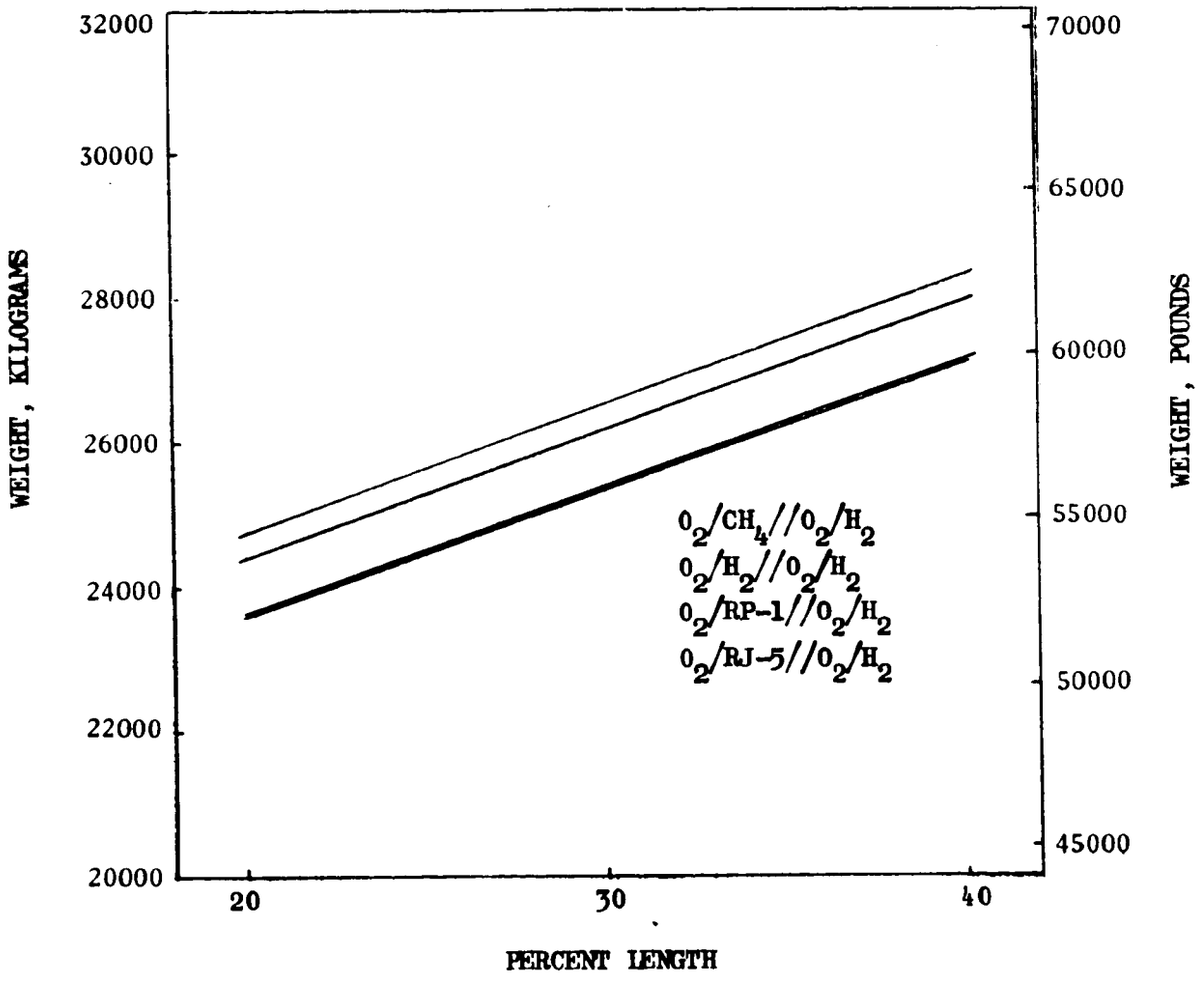

Figure 112. Linear Engine Weight vs Percent Length Staged Combustion Cycle

ORIGINAL PAGE IS
OF POOR QUALITY

2. Increasing thrust split from 0.5 to 0.8 decreases engine weight for the high-density-fuel engines (RJ-5 and RP-1)and for the low-density-fuel engines (CH_4 and H_2), the weight increases slightly. These weight changes occur in the pumps and in the thrust chamber.

3. Increasing nozzle width-to-height decreases engine weight approximately 6 percent due to a reduction in weight of the thrust chamber. Coolant pump weight increases due to higher coolant inlet pressure requirements.

4. Expansion area ratio has a large effect on engine weight. Increasing area ratio from 40 to 80 increases engine weight approximately 25 percent. The weight increase occurs to a large extent in the thrust chamber nozzle and to a lesser extent in the nozzle support structure.

5. Increasing nozzle percent length from 20 to 40 percent increases engine weight approximately 15 percent. As in the case of expansion area ratio, the weight increase is related to the nozzle support and load transmitting structure.

ENGINE SELECTION FOR TASK VI STUDIES

The four engine candidates presented in Table 23 were recommended for Task VI. Candidate engine No. 1 is a gas generator cycle LOX/H_2 - LOX/RP-1 engine with the lowest weight of all engines examined within coolant inlet-to-chamber pressure ratio (P_{inlet}/P_c) guidelines, but with the lowest sea level, Mode 1 vacuum and Mode 2 vacuum performance. Candidate engine No. 3 is a staged combustion cycle LOX/H_2 engine with the highest performance, but highest weight of all engines within coolant inlet-to-chamber pressure ratio (P_{inlet}/P_c) guidelines. Engine No. 2 is a LOX/H_2 - LOX/RP-1 engine which may offer advantages because of its high-density hydrocarbon propellant, with performance and weight intermediate between candidates 1 and 3. Engine No. 4 is a LOX/H_2 - LOX/RP-1 engine combusting LOX/H_2 in a staged combustion mode in the inner combustor, and LOX/RP-1 in a gas generator mode in the outer combustor. Performance and weight of this system are intermediate between engines 1 and 2. For LOX/RP-1 operation, this appears to be a more practical engine since it minimizes the potential carbon deposition problem with LOX/RP-1 combustion by reducing the low mixture ratio hot-gas wetted surfaces.

The nozzle percent length selection depends on the tradeoff between performance, engine weight, and resulting payload. The Mode 1 engine performance, as a function of nozzle length and altitude, is presented in Tables 24 through 27 for the LOX/H_2-LOX/H_2 staged combustion engine and the LOX/RP-1 - LOX/H_2 gas generator/staged combustion engine. Mode 2 vacuum performance and engine weight variations with nozzle percent length are provided in Table 28.

TABLE 23. TASK VI ENGINE CANDIDATES

Candidate No.	Propellants	Cycle	(1) P_c /ε/(F_o/F_t)/(W/H)/%L	Weight Kg, (Lbs.)	I_s, N-sec/Kg (sec.) Sea Level	Mode 1 Vac	Mode 2 Vac
1	$O_2/RP\text{-}1//O_2/H_2$	GG//GG	$1.38X10^7$(2000)/40/.65/4/20	20700 (45540)	3107 (316.8)	3578 (364.8)	4412 (449.9)
2	$O_2/RP\text{-}1//O_2/H_2$	SC//SC	$1.724X10^7$(2500)/40/.65/5/20	23650 (52030)	3251 (331.5)	3665 (373.7)	4477 (456.6)
3	$O_2/H_2//O_2/H_2$	SC//SC	$1.724X10^7$(2500)/40/.65/4/20	24400 (53680)	3827 (390.2)	4211 (439.6)	4479 (456.7)
4	$O_2/RP\text{-}1//O_2/H_2$	GG//SC	$1.38X10^7$(2000)/40/.65/4/20 $1.724X10^7$(2500)/40/.65/4/20	22350 (49170)	3158 (322.0)	3608 (367.9)	4479 (456.7)

(1) N/m^2 (psia)

ORIGINAL PAGE IS
OF POOR QUALITY

TABLE 24. PERFORMANCE-ALTITUDE DATA

(ENGLISH UNITS)

	Altitude, Feet	Engine Specific Impulse, sec
		20% Length
	0	390.2
	1,000	391.5
	3,000	393.9
	5,000	396.4
	7,000	398.9
	10,000	402.5
LOX/H_2-LOX/H_2	13,000	406.3
Staged Combustion Engine	16,000	409.9
	20,000	414.4
$\varepsilon_1 = 40$	25,000	419.8
$F_{SL} = 20 \times 10^6$ N (4.5×10^6 lbf)	30,000	423.7
$F_o/F_t = 0.65$	35,000	427.0
P_c:	40,000	429.7
Outer = 1724 N/cm^2 (2500 psia)	50,000	433.4
Inner = 1724 N/cm^2 (2500 psia)	60,000	435.8
w/H = 4.0	80,000	438.1
	100,000	439.0
	150,000	439.5
	200,000	439.5
	1,000,000	439.6

TABLE 25. PERFORMANCE-ALTITUDE DATA

(METRIC UNITS)

	Altitude, meters	Engine Specific Impulse, N-sec/kg
		20% Length
LOX/H_2-LOX/H_2 Staged Combustion Engine $\varepsilon_1 = 40$ $F_{SL} = 20 \times 10^6$ N(4.5×10^6 lbf) $F_o/F_t = 0.65$ P_c: Outer = 1724 N/cm^2(2500 psia) Inner = 1724 N/cm^2(2500 psia) w/H = 4.0	0	3827
	304.8	3839
	914.4	3864
	1,524.0	3888
	2,133.6	3912
	3,048.0	3947
	3,962.4	3984
	4,876.8	4029
	6,096.0	4064
	7,620.0	4116
	9,144.0	4155
	10,668.0	4187
	12,192.0	4214
	15,240.0	4251
	18,288.0	4273
	24,384.0	4296
	30,480.0	4305
	45,720.0	4310
	60,960.0	4310
	304,800.0	4311

ORIGINAL PAGE IS
OF POOR QUALITY

TABLE 26. PERFORMANCE - ALTITUDE DATA

(ENGLISH UNITS)

	Altitude, feet	Engine Specific Impulse, sec
		20% Length
LOX/RP-1 Gas Generator LOX/H_2 Staged Combustion Hybrid Engine ϵ_i = 40 F_{SL} = 20 x 10^6 N (4.5 x 10^6 lbf) P_c: Inner = 1724 N/cm^2 (2500 psia) Outer = 1380 N/cm^2 (2000 psia) w/H = 4.0	0	322
	1,000	323.1
	3,000	325.3
	5,000	327.5
	7,000	329.7
	10,000	333
	13,000	336.4
	16,000	339.7
	20,000	344
	25,000	348.9
	30,000	352.8
	35,000	355.9
	40,000	358.5
	50.000	362.1
	60,000	364.3
	80,000	366.6
	100,000	367.4
	150,000	367.9
	200,000	367.9
	1,000,000	367.9

TABLE 27. PERFORMANCE - ALTITUDE DATA
(METRIC UNITS)

	Altitude, meters	Engine Specific Impulse, N-sec/kg
		20% Length
LOX/RP-1 Gas Generator LOX/H_2 Staged Combustion Hybrid Engine ϵ_1 = 40 F_{SL} = 20 x 10^6 N (4.5 x 10^6 lbf) F_o/F_t = 0.65 P_c: Outer = 1380 N/cm^2 (2000 psia) Inner = 1724 N/cm^2 (2500 psia) w/H = 4.0	0	3158
	304.8	3169
	914.4	3190
	1,524.0	3212
	2,133.6	3233
	3,048.0	3265
	3,962.4	3299
	4,876.8	3331
	6,096.0	3373
	7,620.0	3422
	9,144.0	3460
	10,668.0	3490
	12,192.0	3516
	15,240.0	3551
	18,288.0	3573
	24,384.0	3595
	30,480.0	3603
	45,720.0	3608
	60,960.0	3608
	304,800.0	3608

ORIGINAL PAGE IS
OF POOR QUALITY

TABLE 28. LINEAR SPLIT-COMBUSTOR ENGINE MODE 2
VACUUM PERFORMANCE AND WEIGHT VS NOZZLE LENGTH

$F_{SL.} = 20 \times 10^6$ N (4.5×10^6 lbf)

P_c:

Inner combustor = 1724 N/cm^2 (2500 psia)

Outer combustor = 1724 N/cm^2 (2500 psia) staged combustion

= 1380 N/cm^2 (2000 psia) gas generator

ε_2 = 114

w/H = 4.0

Propellants	Cycle Type	Nozzle % Length	Mode 2 Vacuum I_s, N-sec/kg (seconds)	Engine Weight, kg (pounds)
Outer - Inner				
LOX/H_2-LOX/H_2	Staged Comb.	20	4479(456.7)	24400(53680)
		30	4518(460.7)	26150(57530)
		40	4533(462.3)	27950(61490)
LOX/RP-1-LOX/H_2	Gas Gen./ Staged Comb.	20	4479(456.7)	22350(49170)
		30	4518(460.7)	24150(53130)
		40	4533(462.3)	25950(57090)

TASK VI: ENGINE PRELIMINARY DESIGN

Upon completion of Tasks I through V effort, two engine configurations were recommended to NASA: the LOX/H_2 - LOX/H_2 staged combustion engine, and a LOX/H_2 - LOX/RP-1 staged combustion/gas generator hybrid engine. Review of recommended configurations by NASA led to selection of two configurations for Task VI "Engine Preliminary Design" studies. The two engine configurations (design parameters are shown in Table 29) are basically the two configurations recommended except sea level thrust is 17.8×10^6 N (4×10^6 lb) instead of 20×10^6 N (4.5×10^6 lb) and w/H is 3.0.

For the inner combustor, the values of thrust and ε selected require a coolant circuit inlet pressure to chamber pressure ratio (P_{in}/P_c) of 2.8 (Fig. 113). NASA performance-payload tradeoff studies indicated an advantage of increasing expansion area ratio to 50 for Concept 1. However, at the thrust level of interest, a P_{in}/P_c value of 5 is required to provide the necessary cooling (Fig. 113). Because of the resulting high power and pump discharge pressures with ε = 50:1, an expansion area ratio of 40:1 (P_{in}/P_c = 2.8) was selected.

The two configurations of Table 29 were carried into Task VI for engine design studies. The objectives of Task VI effort were to provide an engine design layout for the two concepts, to establish engine start/shutdown sequencing and characteristics, and to determine characteristics of engine differential throttling thrust vector control, and off-design mixture ratio operation.

Propellant flow schematics for the two concepts are presented in Fig. 14 and 114. Design parameters are presented in Appendix B. A variation of Concept 1 (presented in Appendix C) has both combustors operating at the same chamber pressure.

DESIGN LAYOUTS

Design layouts were completed of both concepts: Concept 1, the hybrid engine (Fig. 115), and Concept 2, the all-LOX/H_2 engine (Fig. 116). These drawings depict one module, four of which make up the complete engine of 17.8×10^6 N (4.0×10^6 lb) thrust. Descriptions of these two linear engine concept designs follows with the all-hydrogen engine discussed first.

Concept 2

The LOX/H_2 - LOX/H_2 staged combustion engine module (Fig. 116) weighs 6420 kg (14,150 lb) and is 2.15 meters (84.5 in.) long, 4.40 m (173.2 in.) wide, and 2.22 m (87.3 in.) high. It consists of 13 dual-chambered combustor segments firing onto a common linear nozzle surface. Propellants are supplied to the segments and preburners by two fuel and two LOX high-pressure pumps, each of which operates with an adjoining boost pump. The inlet flanges of the four boost pumps comprise the propellant interfaces with the vehicle propellant lines. The vehicle lines need not provide flexibility, as the interface flanges remain in fixed positions (no gimbaling). The combustor segments, the nozzle, and the turbopumps are mounted on a tubular frame which transmits their loads to the vehicle via 14 mounting pads, which are the structural interface between each module and the vehicle.

ORIGINAL PAGE IS
OF POOR QUALITY

TABLE 29. TASK VI - PRELIMINARY DESIGN ENGINE CONFIGURATIONS

	Concept 1	Concept 2
Engine Thrust, Newtons (pounds)		
Mode 1		
Sea Level	$17.8 \times 10^6 (4 \times 10^6)$	$17.8 \times 10^6 (4 \times 10^6)$
Vacuum	$20.0 \times 10^6 (4.5 \times 10^6)$	$20.0 \times 10^6 (4.5 \times 10^6)$
Mode 2		
Vacuum	$7.36 \times 10^6 (1.65 \times 10^6)$	$7.36 \times 10^6 (1.65 \times 10^6)$
Thrust Split at Sea Level	0.65	0.65
Chamber Pressure, N/cm^2 (psia)		
Outer Combustor	1380 (2000)	1724 (2500)
Inner Combustor	1724 (2500)	1724 (2500)
Propellant Combination		
Outer Combustor	$O_2/RP\text{-}1$	O_2/H_2
Inner Combustor	O_2/H_2	O_2/H_2
Engine Mixture Ratio		
Outer Combustor	2.8	7.0
Inner Combustor	7.0	7.0
Expansion Area Ratio		
Mode 1	40:1	40:1
Mode 2	114:1	114:1
Specific Impulse, N-s/kg (seconds)		
Mode 1		
Sea Level	3151 (321.3)	3820 (389.5)
Vacuum	3601 (367.2)	4302 (438.7)
Mode 2		
Vacumm	4466 (455.4)	4466 (455.4)
Power Cycle		
Outer Combustor	Gas Generator	Staged Combustion
Inner Combustor	Staged Combustion	Staged Combustion
Nozzle Percent Length, % of 15-Degree Cone	20	20
Engine Width-to-Nozzle Height Ratio	3.0:1	3.0:1
P_{inlet}/P_c		
Outer Combustor	2.8	2.8
Inner Combustor	2.8	2.8
Engine Envelope, meters (inches)		
Width	8.8 (346)	8.8 (346)
Height	4.4 (172)	4.4 (175)
Length	2.1 (84.5)	2.1 (84.5)
Engine Weight, kg (pounds)	20070 (44250)	22850 (50380)

ORIGINAL PAGE IS
OF POOR QUALITY

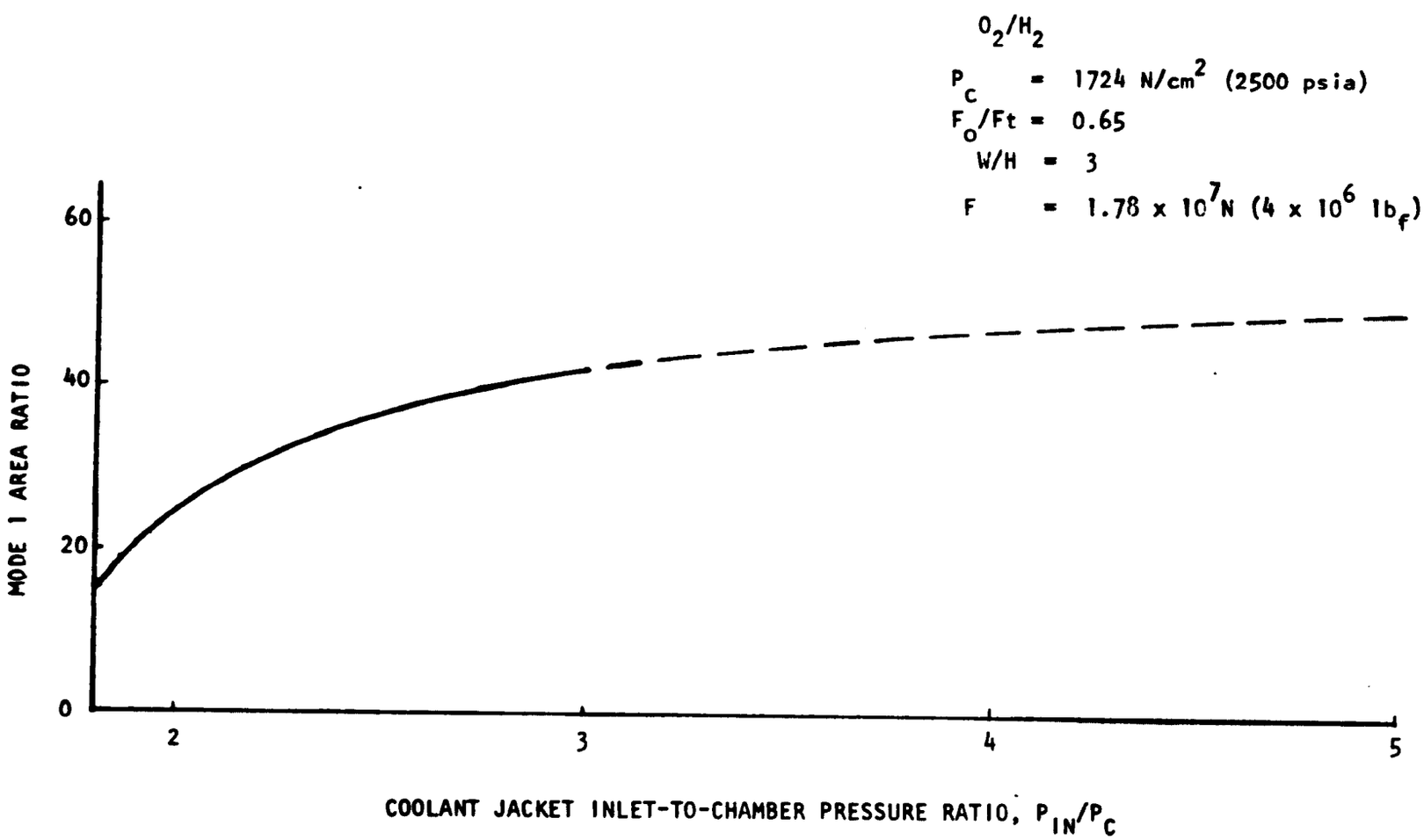

Figure 113. Inner Combustor Cooling Requirements

ORIGINAL PAGE IS
OF POOR QUALITY

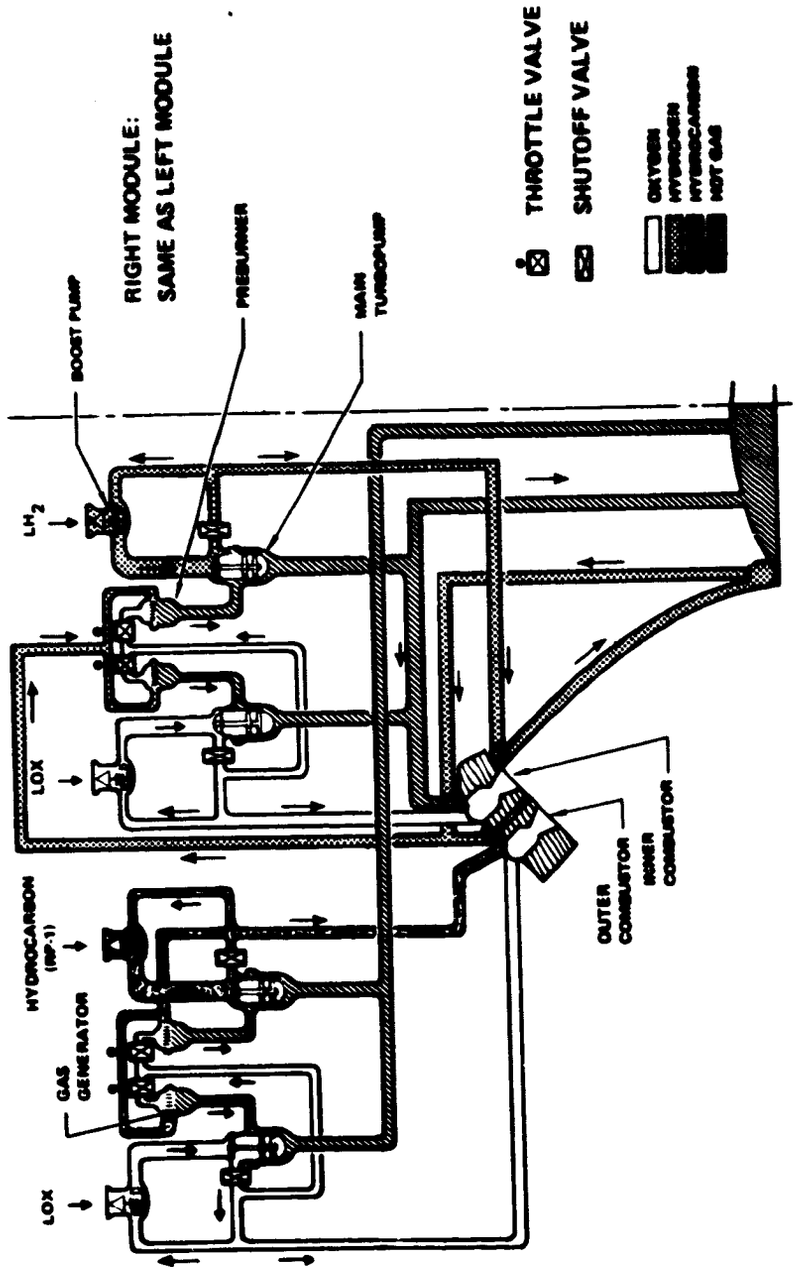

Figure 114. Staged Combustion/Gas Generator Power Cycle

ORIGINAL PAGE IS
OF POOR QUALITY

FOLDOUT FRAME

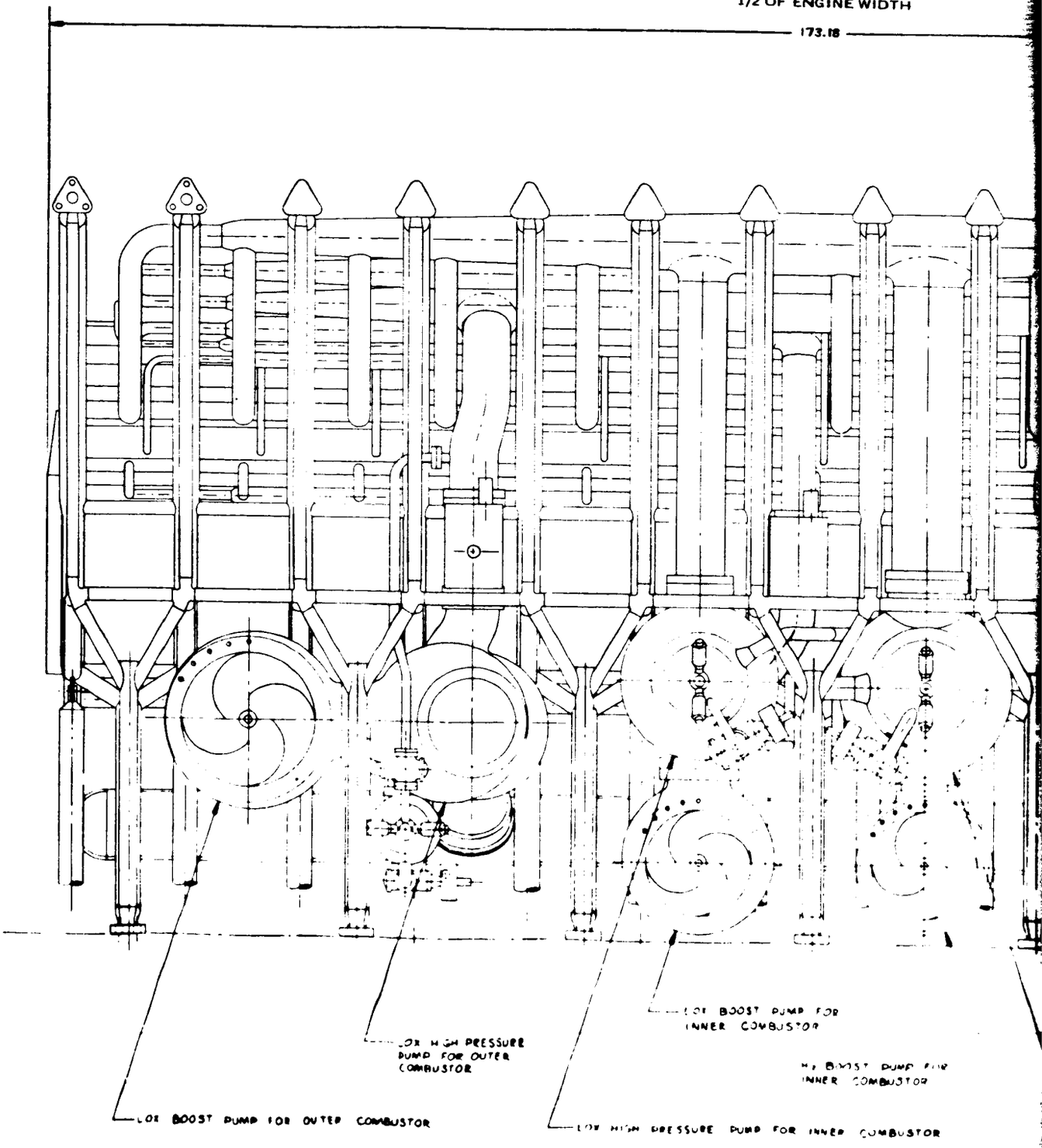

ORIGINAL PAGE IS
OF POOR QUALITY

FOLDOUT FRAME 2

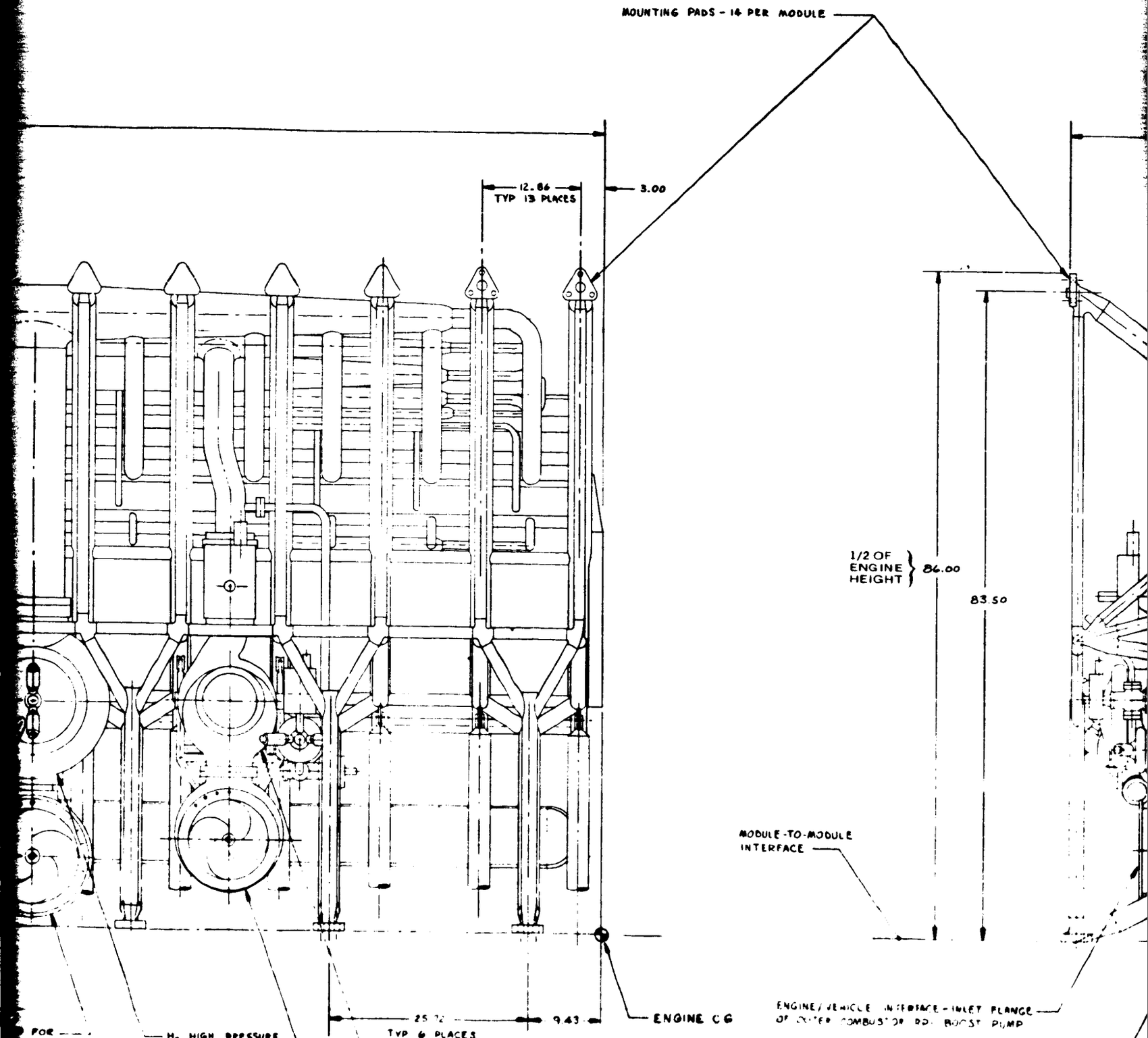

FOLDOUT FRAME 3

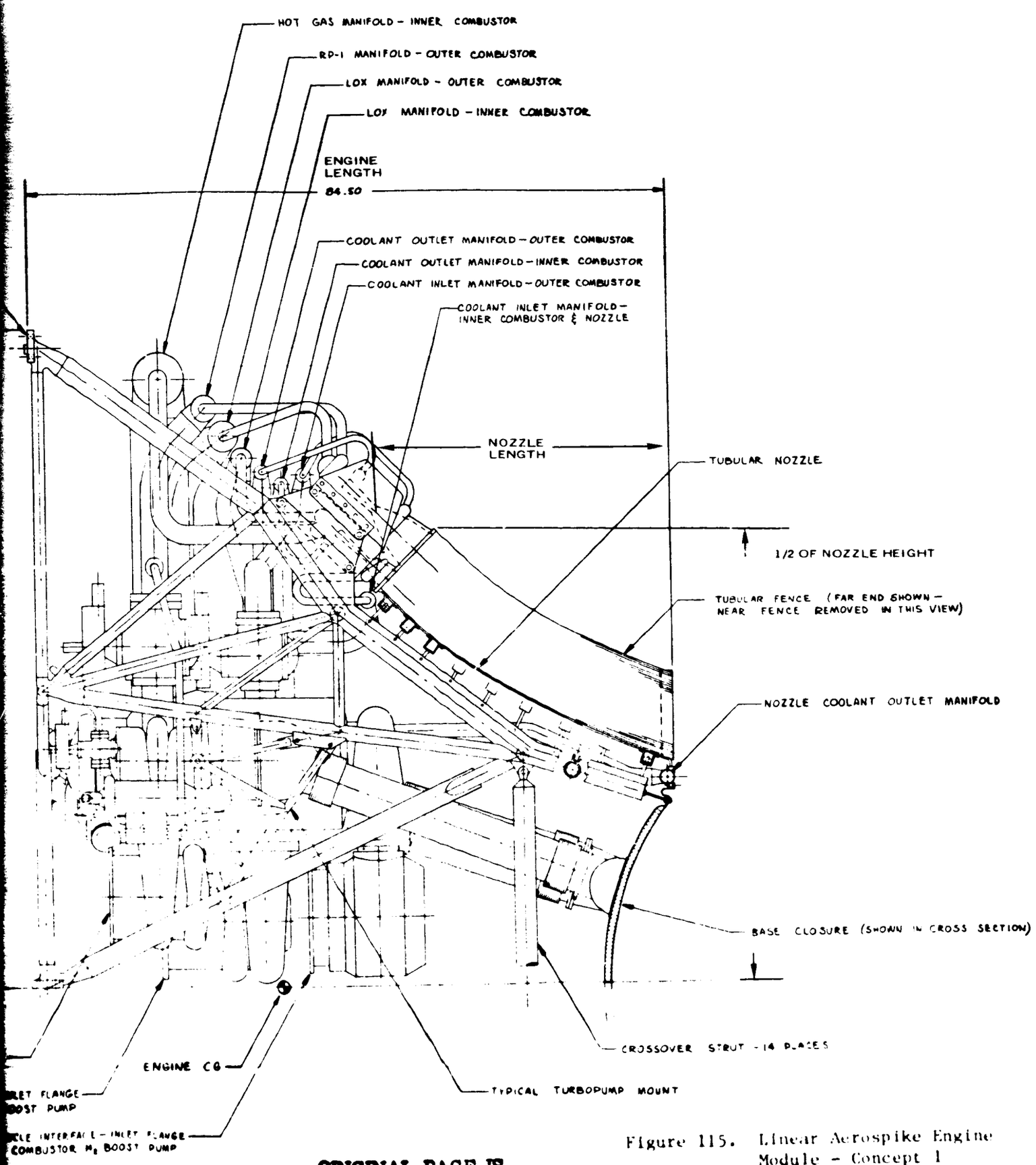

Figure 115. Linear Aerospike Engine Module – Concept 1

ORIGINAL PAGE IS
OF POOR QUALITY

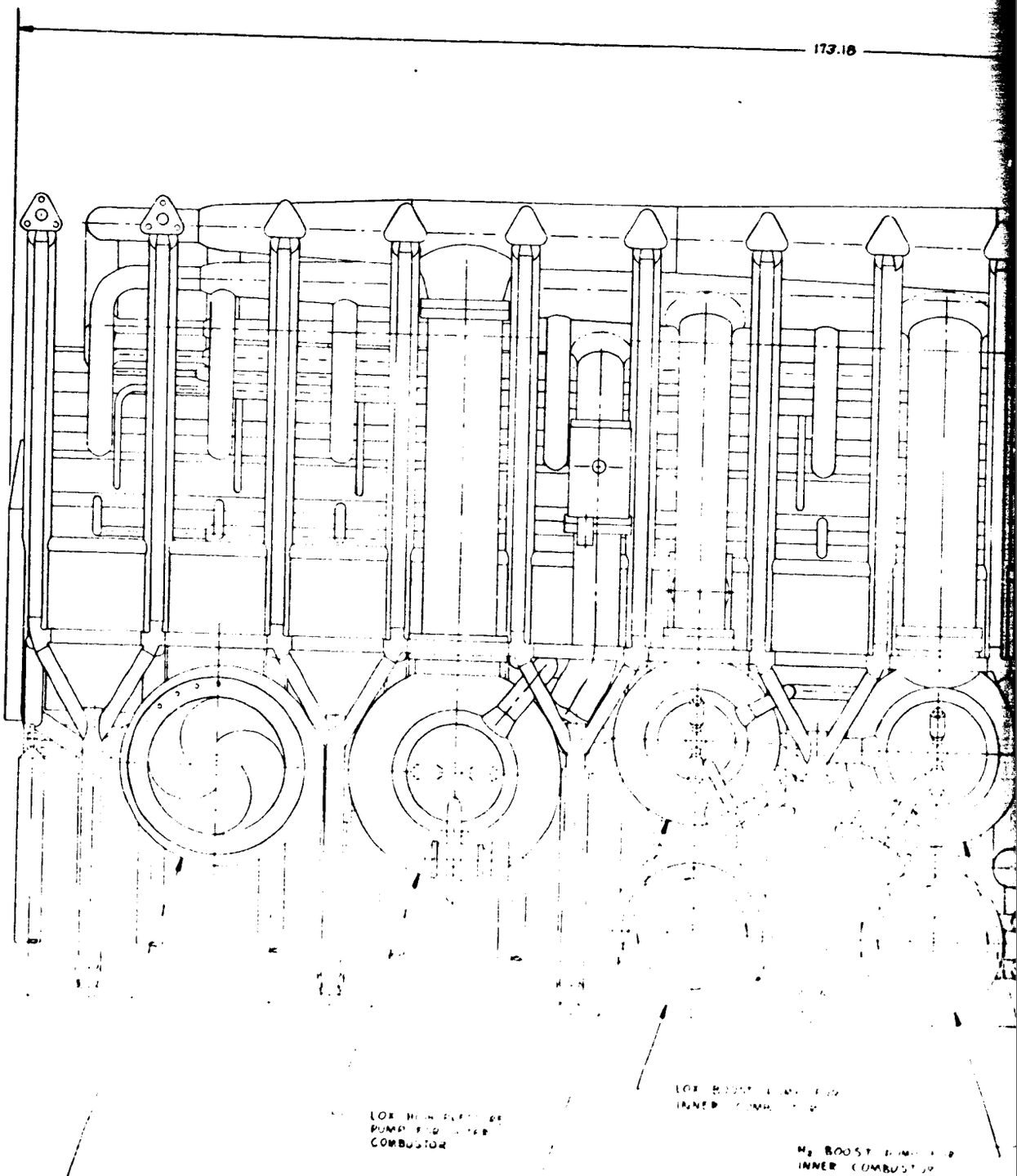

ORIGINAL PAGE IS
OF POOR QUALITY

BOOSTER FRAME 2

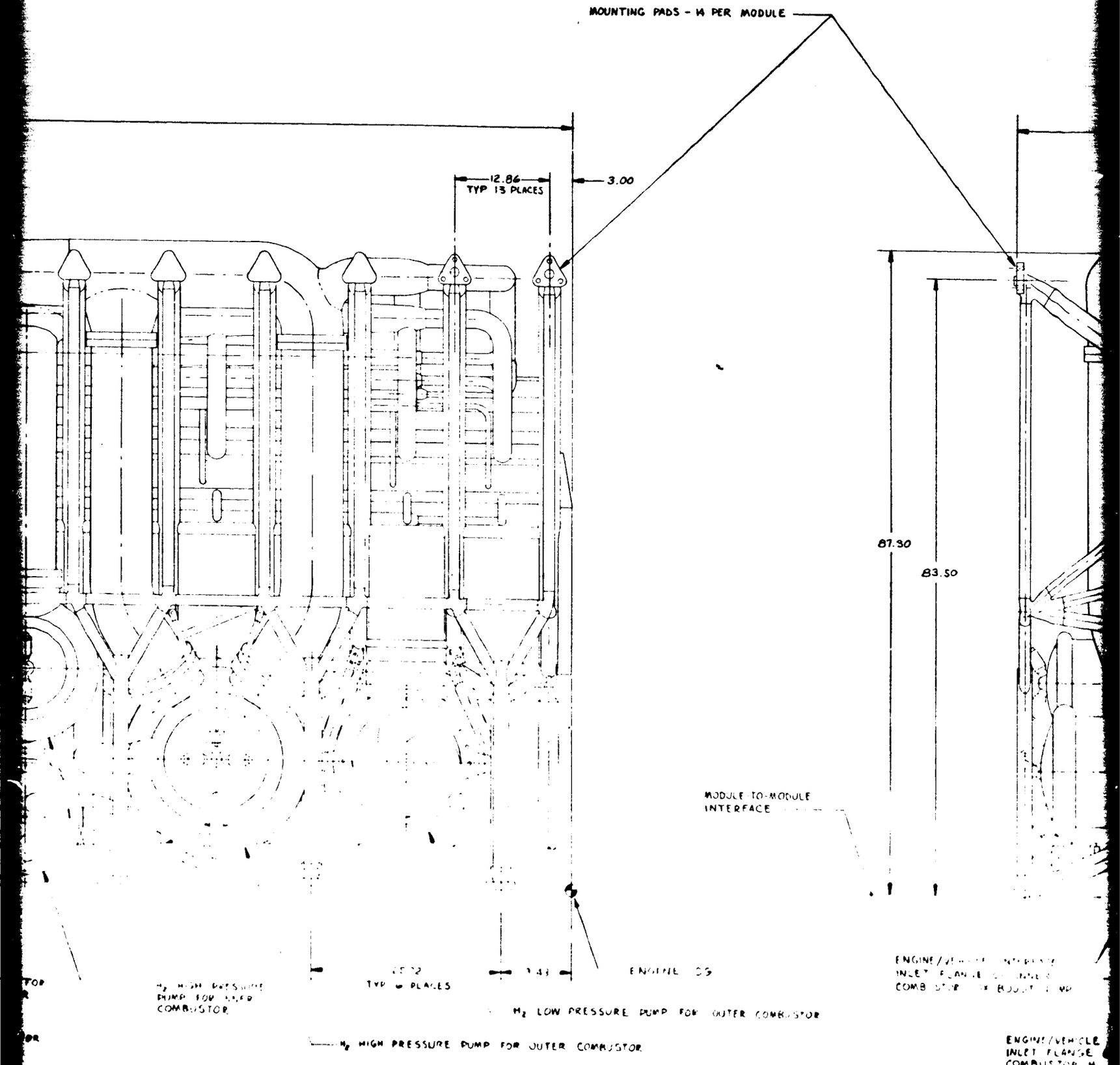

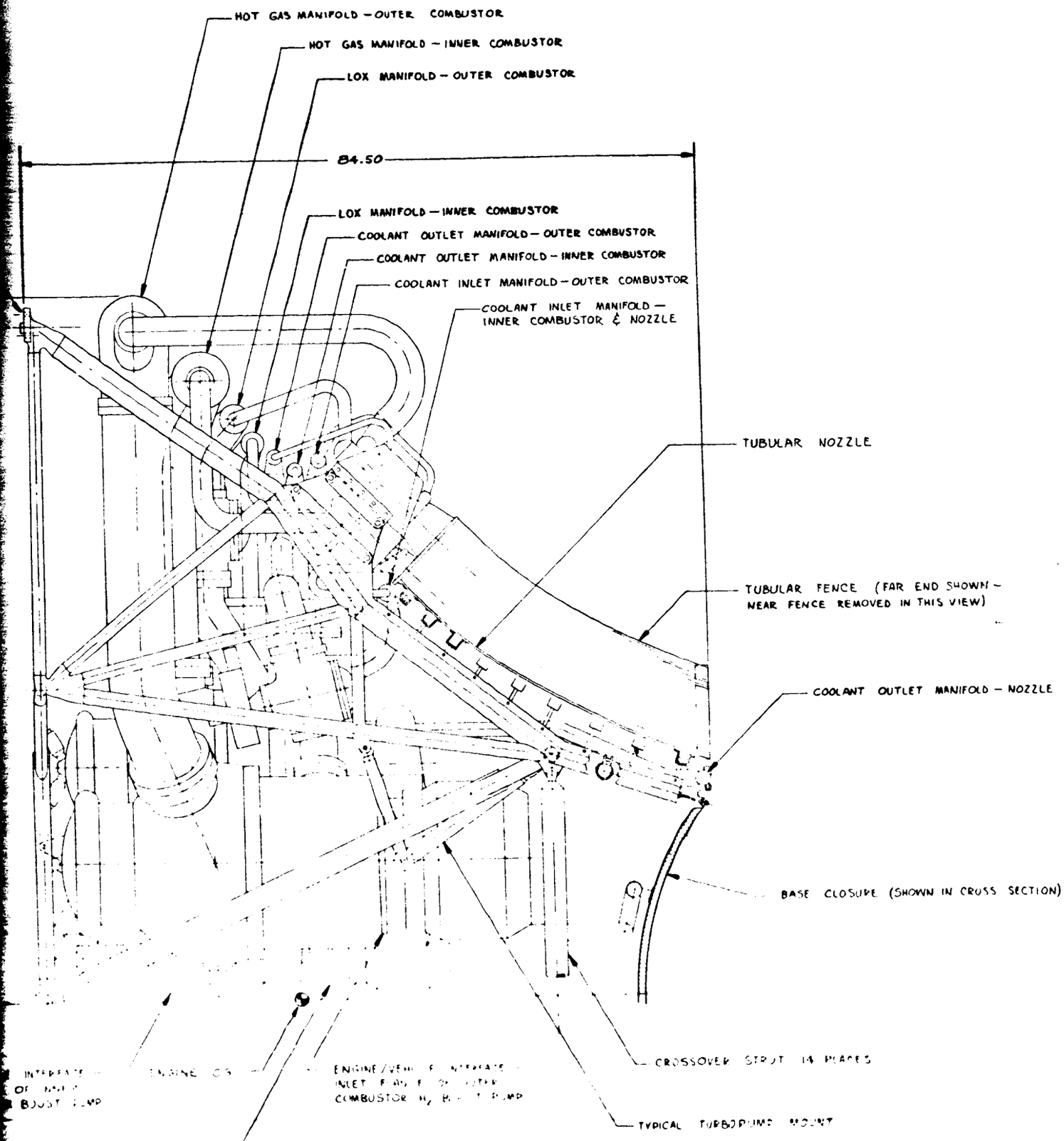

Figure 116. Linear Aerospike Engine Module - Concept 2

ORIGINAL PAGE IS
OF POOR QUALITY

Structure. The engine structure design is influenced by constraints imposed by the vehicle. In the absence of a specific vehicle with specific constraints, a potential vehicle design was used as a guideline. The aft portion of this vehicle, to which the propulsion system is mounted, includes two parallel transverse beams having a vertical separation of approximately 4.24 m (167 in.). This dimension was, therefore, assumed to be an acceptable one for mounting a linear aerospike engine. Module structure height thus became one-half, or 2.12 m (83.5 in.). Close coordination with the vehicle designers will be necessary in any final design to achieve minimum weight. Engine structural weight may be reduced if this height dimension can be made smaller, because truss members get shorter. On the other hand, vehicle structural weight may increase.

The frame design consists of 14 tubular trusses per module, which, when connected to the corresponding truss of the opposite module, form continuous trusses from one mounting pad across to the opposite mounting pad. Intermodule attachments consist of 7 bolted joints and 14 crossover struts. Using 7 bolted joints instead of 14 provides more open space in the structure which is necessary for the large turbopumps. The number of trusses (14) resulted from the selection of each combustor segment. Past analysis has shown that about 30 cm (12 in.) for segment width gives minimum weight. Fourteen mounting pads also appear to be sufficient to distribute the thrust load into the vehicle structure, normally a shell structure better suited to receiving distributed rather than concentrated loads. Baseline material for the tubular frame is heat-treated AISI 4340 low-alloy steel. Corner fittings, where many tubes intersect, may be castings or forgings.

The turbopump mounting structure consists primarily of short tubular supports to three in-line attachments on the two housings of the combined assembly of boost and high-pressure pumps. A strut attachment at the top of the high-pressure pump completes the turbopump mount. This arrangement allows free thermal expansion or contraction of the housings without generating structural loads. Proper consideration has been given to heavy propellant loads on the boost pumps resulting from pressure surges in the supply lines.

Structural support of the thin panel of tubes forming the linear nozzle is provided by hat-section beams running the full width of the nozzle. Multiple pivoting struts transmit the nozzle normal loads to the tubular frame. The pivoting feature allows the nozzle to expand thermally in two directions. The 13 combustor segments, which are structurally integral with the nozzle, are also mounted on pivoting members, two trapezoid-shaped plates for each segment. Four ball joints at the corners of the trapezoid provide 1 degree of freedom to allow for combustor thermal expansion and yet transmit combustor thrust loads to the main structure.

The tubular engine structure evolved from previous Rocketdyne experience with linear engines. An initial concept used cantilever beams to support the combustor and nozzle assembly (Fig. 101). The engine assembly was pivoted at the top to supply thrust vector control. The cantilever construction is heavy. The early parametric weights generated in Task II, which were based on this construction, were higher than weight data for the linear aerospike engine using the truss support. Figure 102 shows a tubular truss force-diagram superimposed

ORIGINAL PAGE IS
OF POOR QUALITY

on a preliminary layout of the 20 x 10^6 N (4.5 x 10^6 lb) thrust engine studied in Tasks IV and V. Structural studies derived from this and similar geometries formed the basis for revision of earlier (Task II) weights.

Combustors. Each combustion chamber liner of the dual-chambered combustor segment is shaped as illustrated by the externally grooved, cooled linear shown at left in Fig. 117. The flat sides exposed to high internal pressure require external support to prevent deflection, i.e., opening of the throat gap. External stiffening beams, shown in cross section at the right in Fig. 117, provide the support. Beam weight increases rapidly as segment width increases, and a segment width of approximately 30 cm (12 in.) is optimum.

Another view of the combustor segments is presented in Fig. 118 to illustrate how the combustion chamber width is affected by a requirement to provide space between segments for structure and coolant manifolds. Both the inlet and the outlet coolant manifolds for both combustors encircle the combustor as shown. The combustor shrouds downstream of the throat gap diverge in two dimensions instead of only one, so that the exiting jet streams fill the nozzle surface without gaps.

Nozzle and Fences. Both the nozzle and the two fences are made of parallel continuous coolant tubes welded together, forming an impervious panel. A portion of the hydrogen flow from the inner combustor high-pressure pump passes through the nozzle and fences before entering the turbine preburner. Support of the nozzle is provided by hat section beams and pivoted struts, as described in the Structures section. The fences are supported by cantilever hat-section beams which are attached to the ends of the nozzle beams.

Turbopumps. Turbopump designs were derived from the SSME turbopumps suitably scaled in accordance with propellant flowrates and pressures. Slight changes were made in the boost pump outlet ports and high-pressure inlet ports to create a compact, conveniently mounted assembly of each boost and high-pressure pump pair. Similarly, high-pressure pump outlet ports and turbine hot-gas outlet ports were modified slightly to suit the installation. Double outlet ports were incorporated in the outer combustor hydrogen turbine housing to provide outlet lines small enough to pass through the structure.

Manifolds and Valves. To provide equal flows of propellants, coolants, and hot gas to each of the 13 dual combustors (26 combustion chambers) in each module, manifolds spanning the entire width of the module are required. A total of eight such manifolds is necessary. As shown in Fig. 116, the manifolds are mounted outboard of the truss structure. Although this location means slightly longer lines from pumps to manifold, it greatly improves accessibility for making the welds on the many branch lines going to each segment. The long branch lines are provided with bends so that thermal growth or shrinkage relative to the combustors is accommodated by elastic flexing of the branch lines. Support of the manifolds to the structure will be by hangars (not shown), allowing for length change of the manifolds and their input lines from the pumps. Engine valves are assumed to be ball valves similar to the SSME ball valves. Scaling of size in accordance with flowrates has been done, with some overlap allowed

ORIGINAL PAGE IS
OF POOR QUALITY

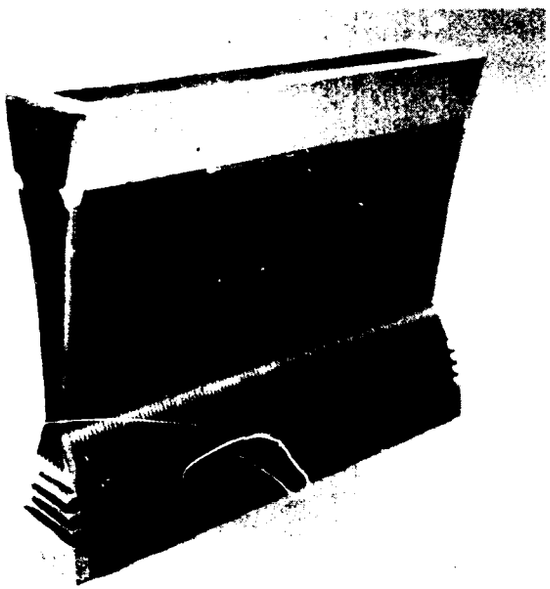

1XZ22-3/19/71-C11*

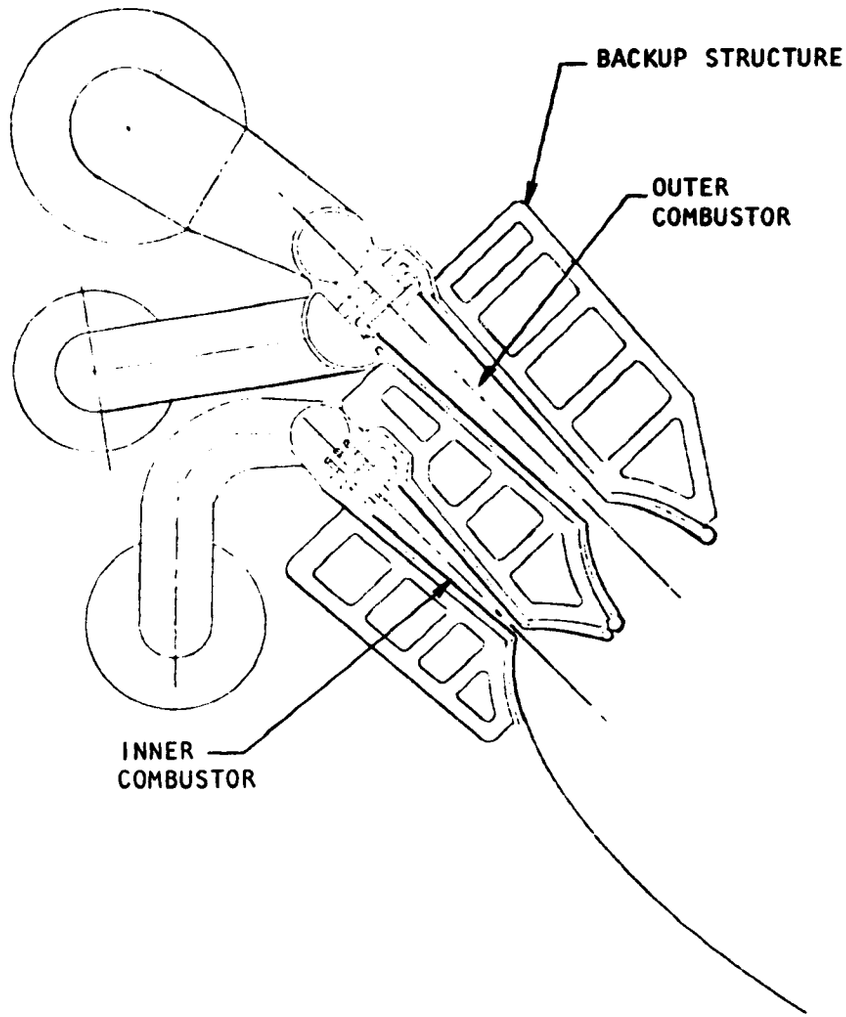

Figure 117. Typical Linear Split Combustor Arrangement

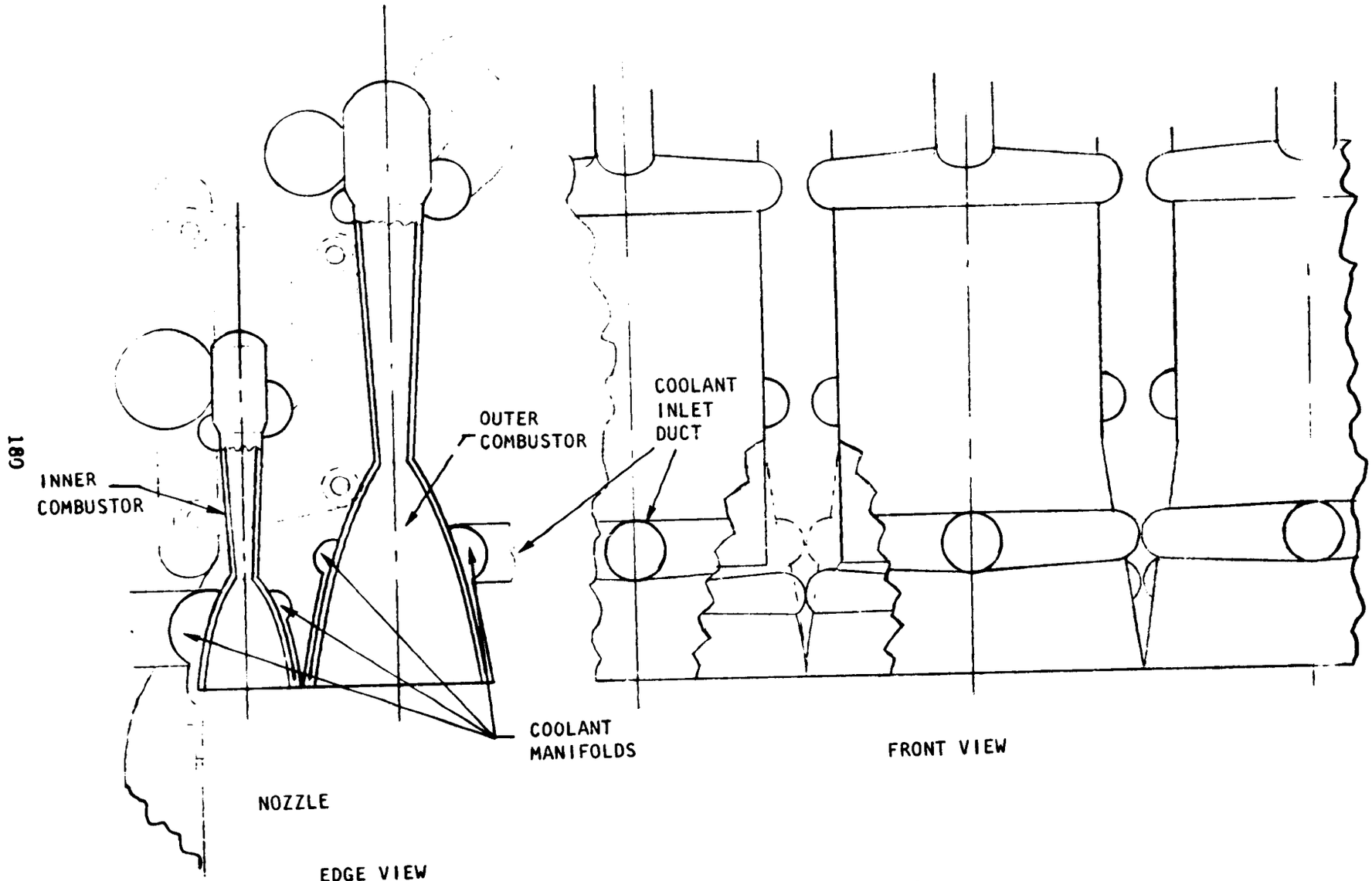

Figure 118. Combustor With Narrowed Chambers

to reduce the total number of different sized valves to three. Valve modulation is provided by hydraulic servoactuators.

Base Closure. The base closure seals off the interior of the engine from the base area and functions as a manifold for distributing hot gases bled from the inner combustor hydrogen turbopump turbine discharge line. The base closure consists of a curved sandwich panel having perforations in the outer skin and in the hex core material that joins the two skins. Gases entering the panel from multiple inlets are distributed to and exit through the multiple perforations in the outer skin. The panel is supported on short columns which flex to allow for panel thermal expansion. A U-shaped flexible closure seals the edges of the panel.

Concept 1

The above description of Concept 2, the all-LOX/H_2 engine, applies with few exceptions to Concept 1, the hybrid engine using LOX/RP-1 propellants (Fig. 115) in the outer combustors. The differences are described below.

Turbopumps. The turbopumps for the outer combustors are smaller. The H_2 turbopump of Concept 2 is replaced by an RP-1 turbopump whose size and configuration are derived from the SSME LOX pump. It is powered by an externally mounted gas generator instead of by an integral preburner, and its turbine exhausts downward toward the base closure instead of laterally toward a hot-gas manifold. Similarly, the LOX turbopump also uses a gas generator and exhausts downward. The LOX turbopump is smaller than that in Concept 2 because the LOX flowrate is smaller with the lower mixture ratio.

The gas generators for the two outer combustor turbopumps burn LOX/RP-1 and their designs are based on past designs of similar gas generators. GG valves are scaled from SSME ball valves.

Manifolds and Valves. In the outer combustor system, the hot-gas manifold of the Concept 2 engine is replaced by the smaller liquid RP-1 manifold in the Concept 1 engine. To locate the RP-1 manifold in the place of the hot-gas manifold it replaces would have meant excessively long small-diameter branch lines to the segments. To avoid this, the positions of the RP-1 manifold and the inner combustor hot-gas manifold were interchanged. In all other respects, the manifolds are like those of the Concept 2 engine. Valves are required for the two gas generators in this engine, and ball valves similar to SSME valves are shown. As in the Concept 2 engine, the number of different sizes of ball valves is held to three.

Turbine Exhaust Lines. In contrast to the Concept 2 engine, in which the high-pressure turbine exhaust gases pass into the combustors, the outer combustor turbines have low-pressure exhaust gases which are ducted to the base closure where they supply the necessary base flow. The base closure is like that of the Concept 2 engine except for having a larger inlet manifold to receive the larger volume of lower pressure gases. The base closure also receives a portion of turbine exhaust flow from the inner combustor hydrogen turbopump to supply base flow during Mode 2 operation.

ORIGINAL PAGE IS
OF POOR QUALITY

ENGINE START AND SHUTDOWN

The start sequence and control system selection for the linear split-combustor engine are patterened after the Space Shuttle Engine (SSME). During normal power level, it takes the SSME (a closed-loop controlled staged combustion engine) approximately 3.6 seconds to attain 90 percent of rated thrust (Fig. 119). The J-2 linear engine thrust start transients conformed to J-2 engine specifications. It took the J-2 linear (an open-loop controlled gas generator-cycle engine) approximately 4.4 seconds to reach 90 percent of rated thrust. With closed-loop control and proper selection of valve operating sequences, the start and cutoff transients of the split-combustor linear engine can be made to follow closely those of the SSME.

As was found in the J-2 linear engine testing, the inlet propellant manifold size had no significant effect on engine transient time delays. The J-2 linear engine oxidizer valve opening schedule, valve ramp rates, and turbine hydrogen gas spin pressure were selected to obtain acceptable J-2 fuel turbopump surge margins and gas generator bootstrap conditions. This resulted in the long rise time to 25 percent of rated thrust which accounts for most of the difference between J-2 linear and SSME engine start times. The split-combustor linear engine utilizes turbomachinery comparable to that of the SSME, similar valve opening schedules, and similar utilization of open- and closed-loop control procedures. With these features, the linear engine start times are expected to be reduced below J-2 linear values.

Concept 2 Engine

The potential energy of the propellants available in the vehicle tanks is used to provide engine start power. The start sequence for the linear staged combustion LOX/H_2 - LOX/H_2 engine (Concept 2) employs the open-loop control mode during early start phases and switches to closed-loop operation for buildup to rated thrust. Initial valve opening and sequencing provides ignition sequencing, engine priming, and initial turbine power buildup. Closed-loop control is then activated to achieve a start to the desired power level without transient overshoots or undershoots.

Open-Loop Control Mode. Start is initiated by a command from the vehicle. (Prestart procedures provide for removal of all vapor from engine passages above the main propellant valves and above the oxidizer preburner valves.)

The start sequence (Fig. 120) starts with actuation of the main fuel valves to the full-open position. This establishes module fuel flow under tank pressure to systems downstream of the valve for priming, including the main combustors, preburners, and ignition system premix chamber. Upon priming of the fuel systems, the main oxidizer valves, the oxidizer preburner oxidizer valves, and the fuel preburner oxidizer valves begin to open, retracting the valve ball seats. Before main flow begins to build up from these valves, igniter element oxidizer flows past the valve ball-seat and into the preburners, inner and outer chamber, and combustion wave ignition premix chambers. Seal retraction of the oxidizer valves establishes premixed propellant flow in the combustion wave igniter system. A combustion wave is generated by firing an integrated sparkplug/exciter

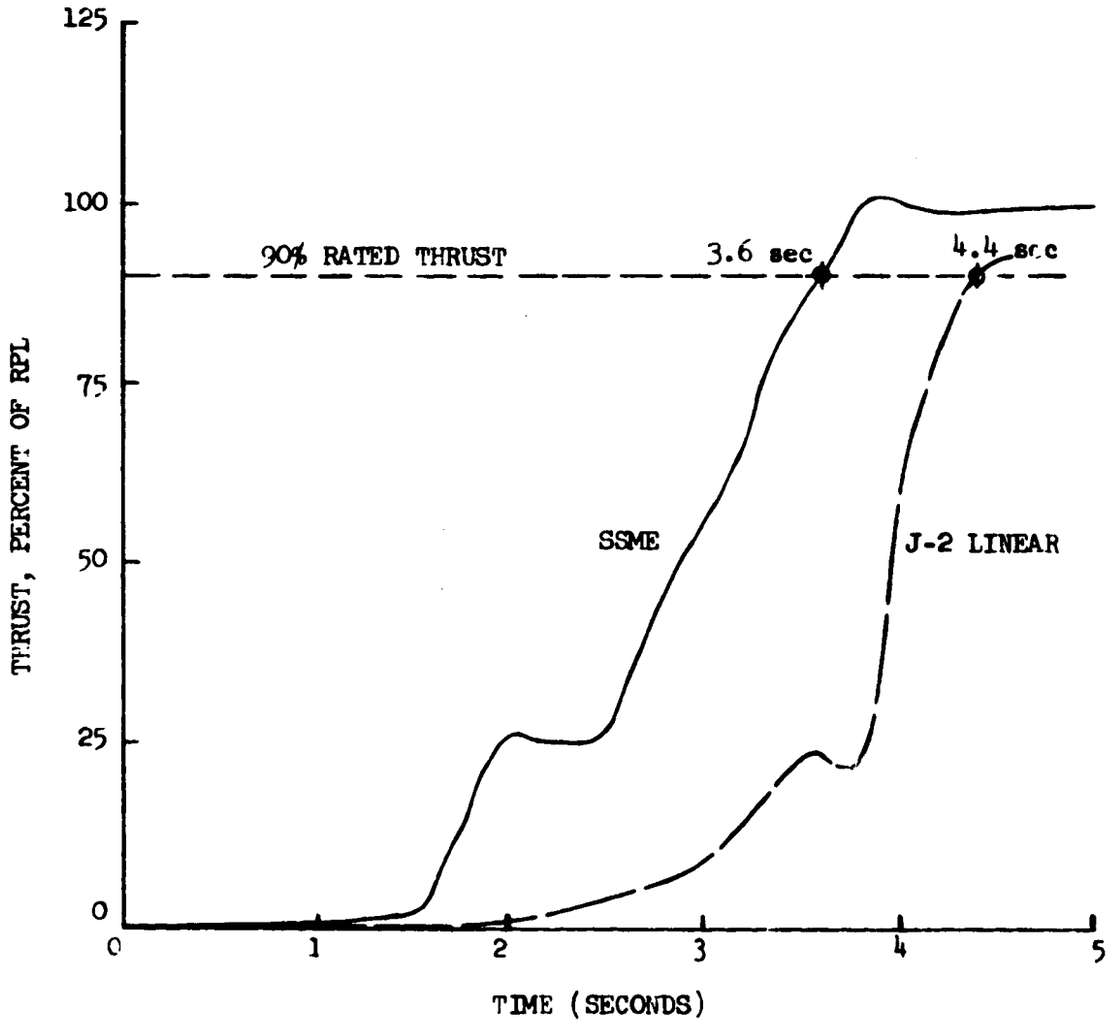

Figure 119. Engine Thrust for Nominal Start Transient, SSME and J-2 Linear Engines

ORIGINAL PAGE IS
OF POOR QUALITY

C-3

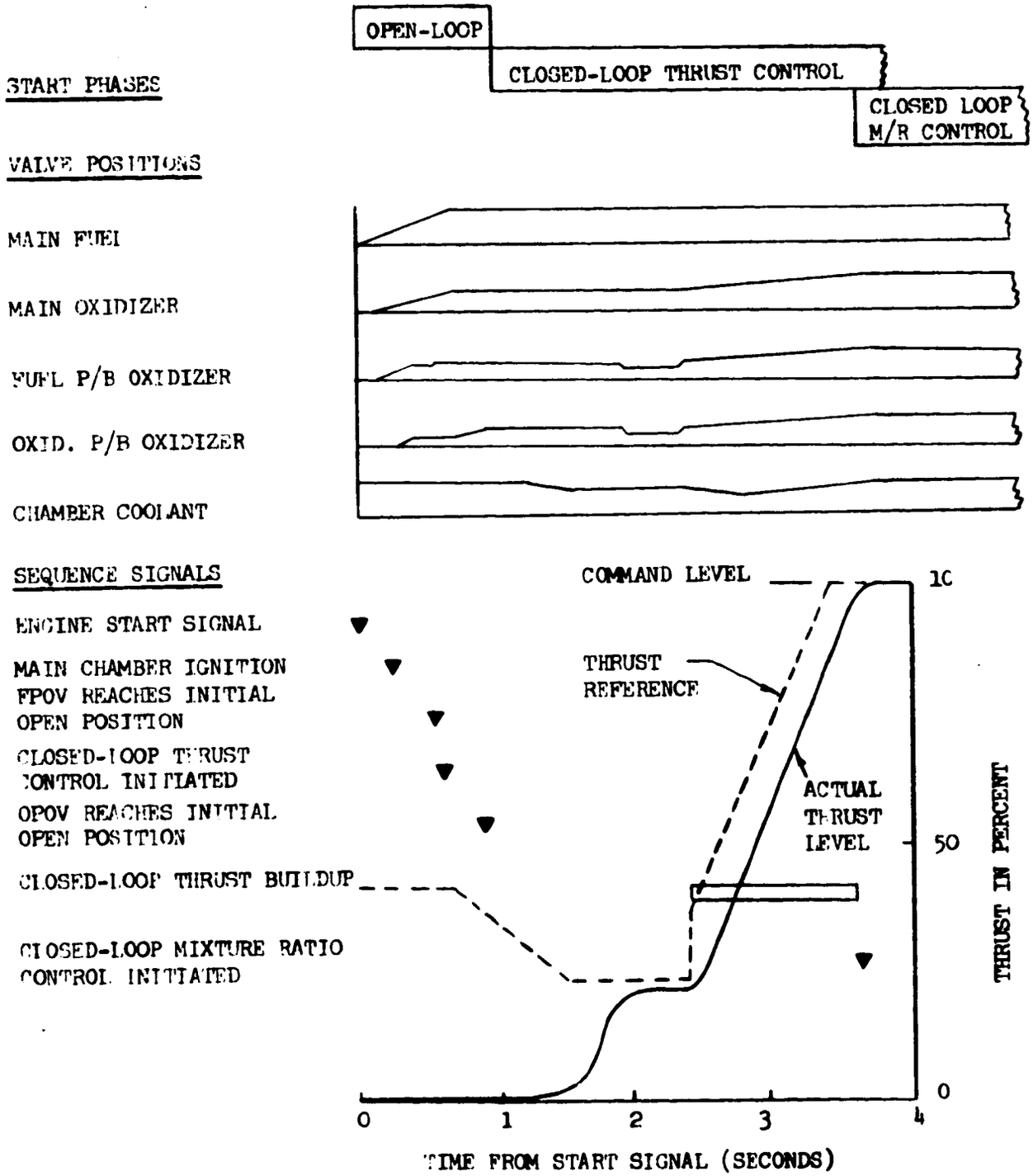

Figure 120. Typical Linear Engine Start Sequence to Full Thrust (LOX/H_2-LOX/H_2 Staged Combustion - Concept 2

unit in the premix chamber. The wave is propagated in the mixed gaseous propellants (Fig. 121) into the module preburner combustors.

Propellant flow to igniter/pilot tube elements, arranged triaxially with the combustion wave tube in each combustor segment and preburners, is ignited by the wave producing a high-temperature, hot-gas core for main propellant ignition at each injector 250 milliseconds after the engine start signal is actuated. Initiation of combustion early in the sequence provides assurance that no raw propellants are dumped into the vehicle boattail during start.

Actuated at 0.12 second, the main oxidizer valves continue to open to 62 percent of their travel. At 0.1 second, the fuel preburner oxidizer valves are ramped to the intermediate open position of 52 percent. This initiates preburner power buildup of the fuel turbomachinery. Prior to this time, the energy for fuel turbomachinery power buildup is provided by the hydrogen under tank pressure augmented by the sensible heat picked up during hardware priming.

The valve positions established by 0.9 second set the engine power level at approximately 25 percent of rated power level. The transient to this thrust level provides preburner and main combustion chamber mixture ratio variations which do not degrade component life and reliability. The engine continues in this operating mode until 2.0 seconds. By this time, all module start transients, including the slowest systems under the worst operating conditions, will have reached 25 percent of rated power level. When the thrust is increased from 25 percent to the final thrust level, all modules, regardless of environment, will respond in the same manner and with the same characteristics.

Engine start proceeds in both the inner and outer combustors of a LOX/H_2 - LOX/H_2 linear engine in identical manner. Communication between the inner and outer combustion controllers provides for synchronization of the module thrusts.

Closed-Loop Mode. Start buildup to the commanded thrust and mixture ratio levels is performed under closed-loop control (Fig. 120). At 0.64 second, the oxidizer and fuel preburner oxidizer valve positioning controls are turned over to closed-loop thrust control. This procedure is selected to maintain the engine mixture ratio between 4 and 6 in the high-impulse range during the major portion of the thrust buildup. The commanded thrust level is achieved in approximately 3.75 seconds. This method achieves repeatable start characteristics with commanded thrust and mixture ratio achieved in the same time on every start.

Start Characteristics. Start thrust, oxidizer flowrate, and fuel flowrate characteristics are depicted in Fig. 120, 122, and 123, respectively. Start characteristics from the 25 percent thrust level to commanded thrust will be identical for each module regardless of final thrust level and regardless of engine/pump inlet pressures.

Engine Shutdown. The engine modules achieve shutdown functions with the same elements used for start and mainstage control. The shutdown sequence (Fig. 124), by employing closed-loop and open-loop elements, provides repeatable shutdown transients which are insensitive to vehicle and mission operation requirements.

ORIGINAL PAGE IS
OF POOR QUALITY

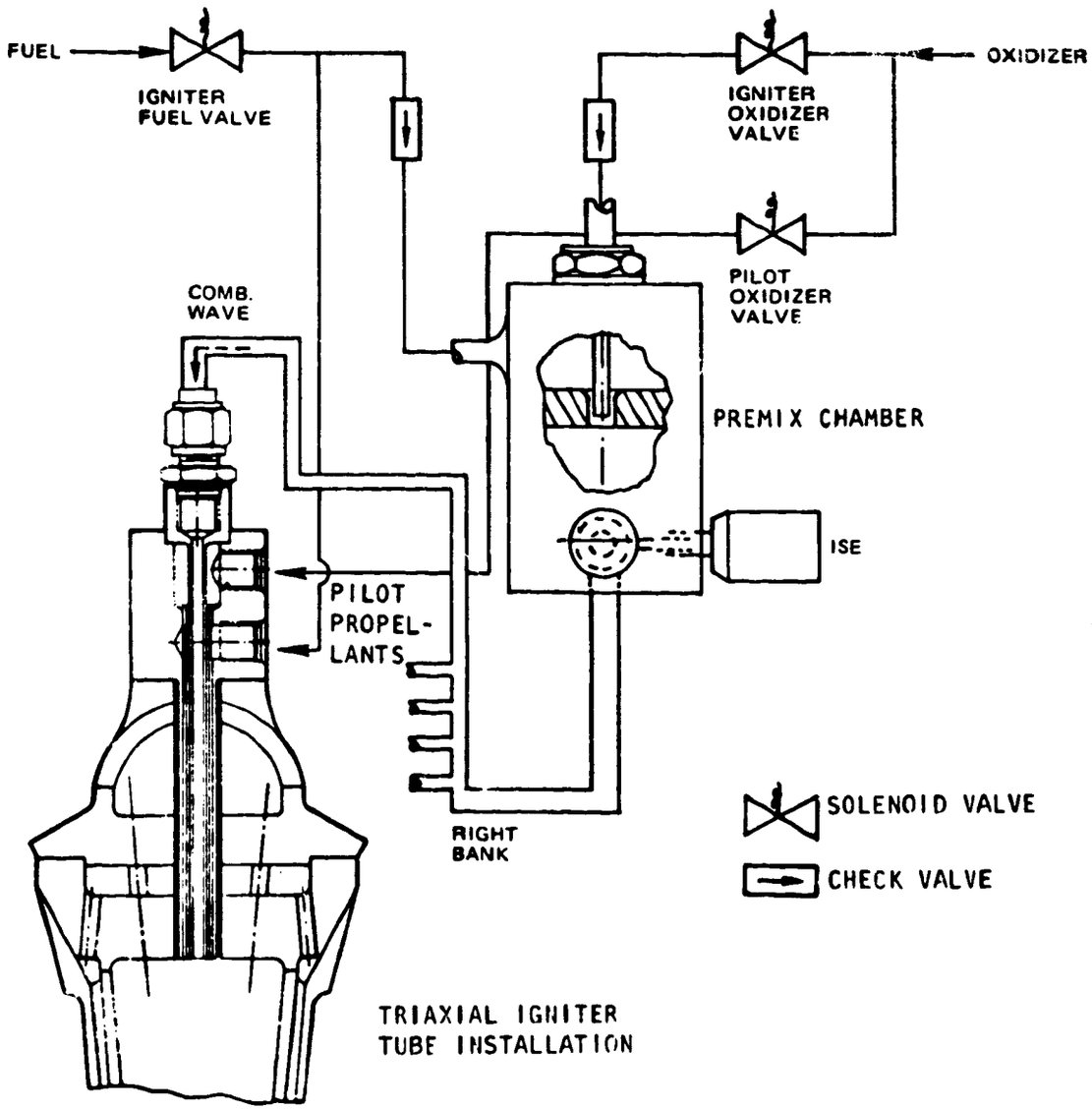

Figure 121. Linear Engine Module Combustion Wave Ignition System

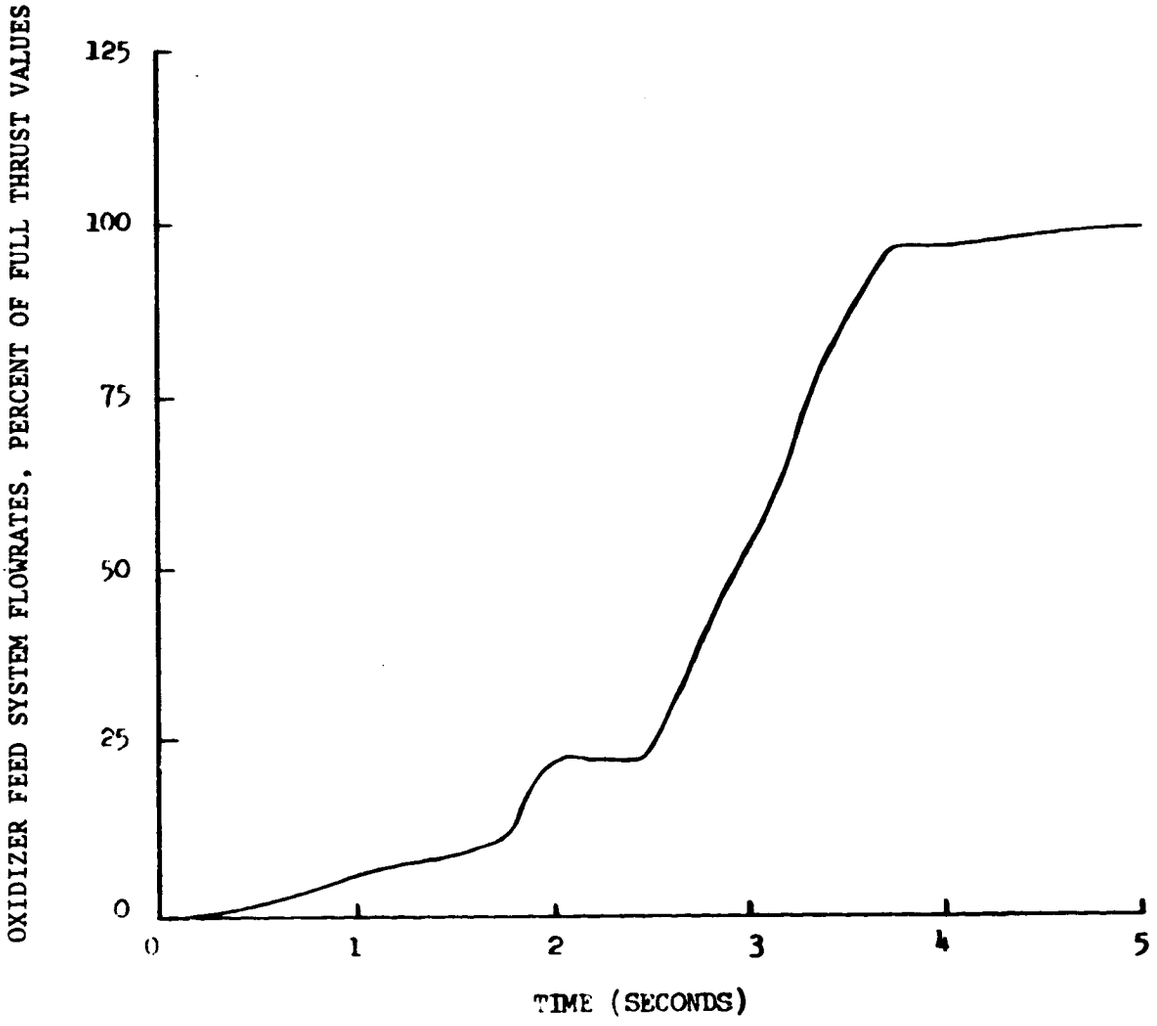

Figure 122. Oxidizer Feed System Flowrates for Nominal Linear Engine Start Transient, LOX/H_2-LOX/H_2 Staged Combustion (Concept 2)

ORIGINAL PAGE IS
OF POOR QUALITY

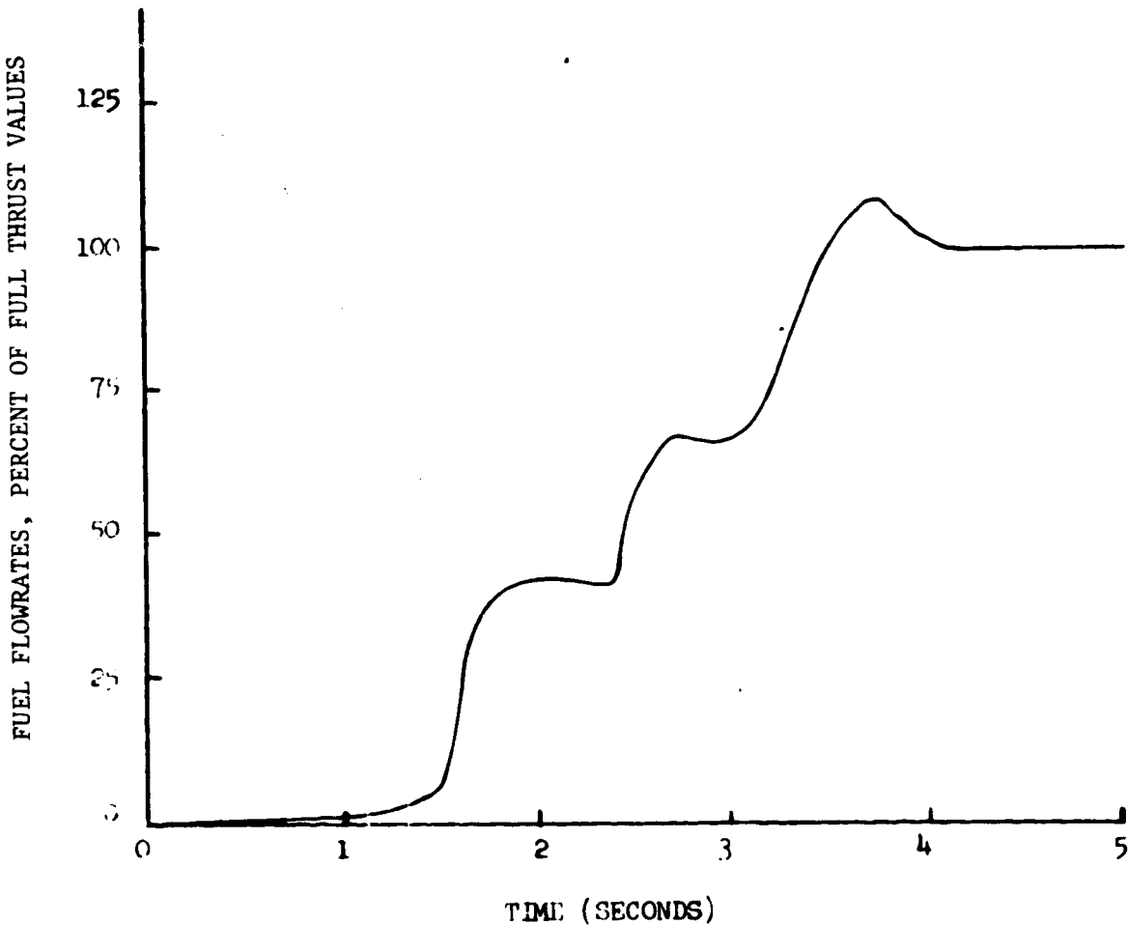

Figure 123. Fuel Flowrates for Nominal Linear Engine Start Transient, LOX/H_2-LOX/H_2 Staged Combustion (Concept 2)

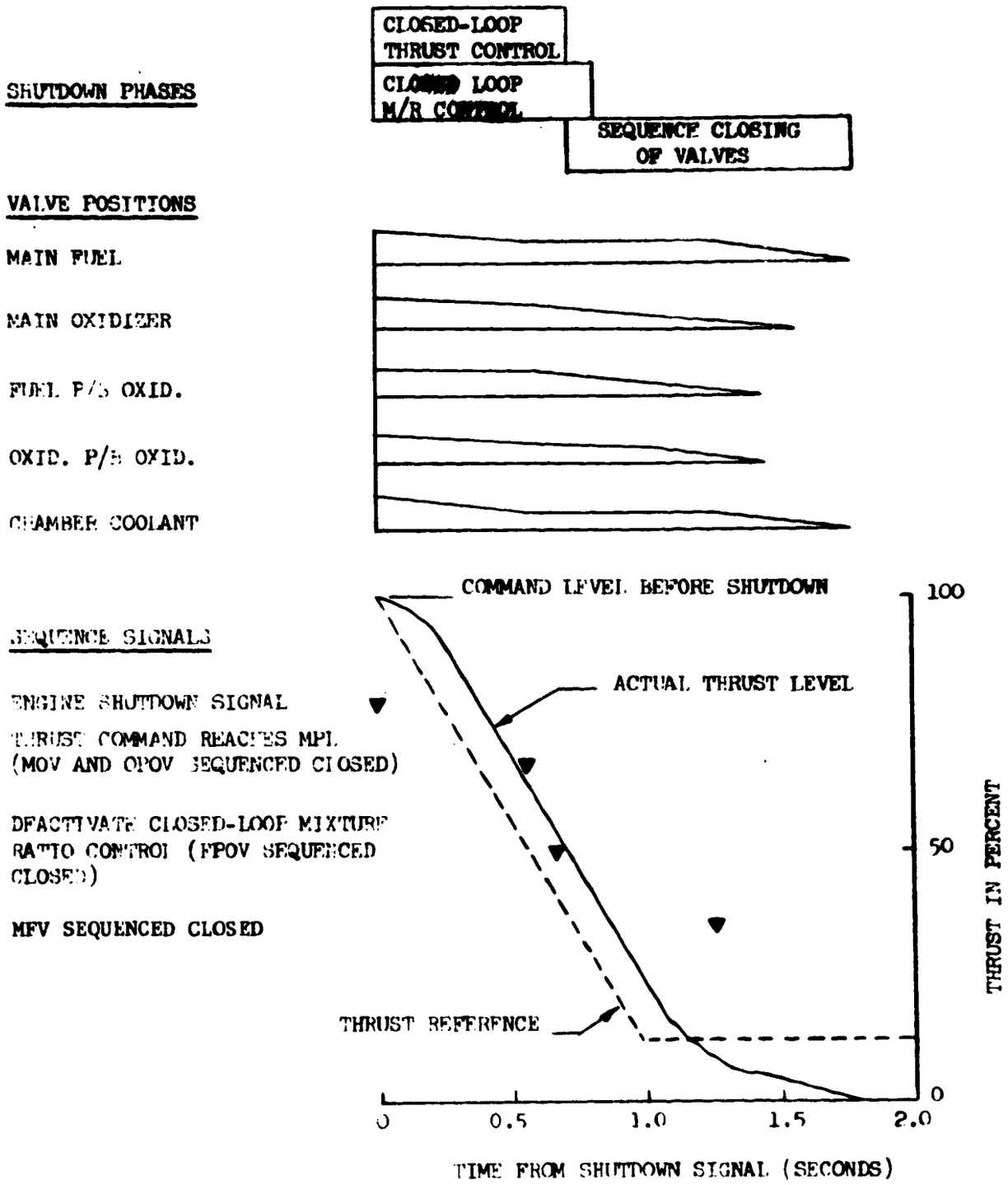

Figure 124. Typical Linear Engine Shutdown Sequence, LOX/H_2-LOX/H_2 Staged Combustion (Concept 2)

ORIGINAL PAGE IS
OF POOR QUALITY

The preburner oxidizer valves and main oxidizer valves are sequenced closed in a manner providing smooth shutdown transients without detrimental turbopump speed or preburner temperature transients. System maximum pressures including surge are limited at the engine inlets.

The main fuel valve closure is delayed to ensure that all oxidizer residuals are removed without damaging mixture ratio transients.

Upon engine shutdown command receival, a reference thrust decrease ramp is generated by the controller. The oxidizer preburner oxidizer valve adjusts to comply with the generated thrust rate and the fuel preburner oxidizer valve maintains constant mixture ratio. This shutdown rate control minimizes both the cutoff time and cutoff impulse and ensures a reasonable thrust cutoff rate. Maximum engine performance with minimum propellant consumption is assured.

Shutdown thrust, fuel, and oxidizer flow characteristics are indicated in Fig. 124, 125, and 126, respectively. Shutdown characteristics are identical for every module. With all modules operating at the same power level, a repeatable simultaneous shutdown is obtained. The main chamber pressure transient continues after valve closure due to residual propellants downstream of the valves, and contributes to the outer combustor shutdown impulse per module of 2.60×10^6 N-sec (4.86×10^5 lb-sec). The outer combustor propellant consumption per module during shutdown is 690 kg (1517 lb). The inner combustion total impulse and propellant consumption are 1.40×10^5 N-sec (3.16×10^5 lb-sec) and 371 kg (817 lb), respectively.

Concept 1 Engine

The start sequence and start characteristics of the inner combustor of the linear engine, Concept 1, are identical to that of the inner combustor of the Concept 2 engine, previously presented (Fig. 120). The start sequence of the gas generator LOX/RP-1 outer combustor is similar to the staged combustion LOX/H_2 outer combustor in that closed-loop thrust and mixture ratio control are used to maintain, within certain limits, transient mixture ratio, pump speeds, and thrust variations that could be detrimental to engine reliability and life. The start sequence and characteristics are different because of the chemical nature of LOX/RP-1 propellants, an oxidizer lead rather than a fuel lead, and ignition of the gas generator propellants which is attained with solid propellant igniters.

The start sequence for the LOX/RP-1 outer combustor is shown in Fig. 127. When the engine start signal is received, gas generator igniter ignition is initiated. Verification of GG ignition starts opening of the main oxidizer valve and priming of the engine oxidizer system under tank-head conditions. This action is followed by opening of the gas generator oxidizer and fuel valves, gas generator ignition, and subsequent initialization of the turbomachinery power phase.

Pump-pressure buildup in the oxidizer system initiates main thrust chamber igniter action and subsequent opening of the thrust chamber main fuel valve. Closed-loop thrust control is initiated approximately 0.6 second after main

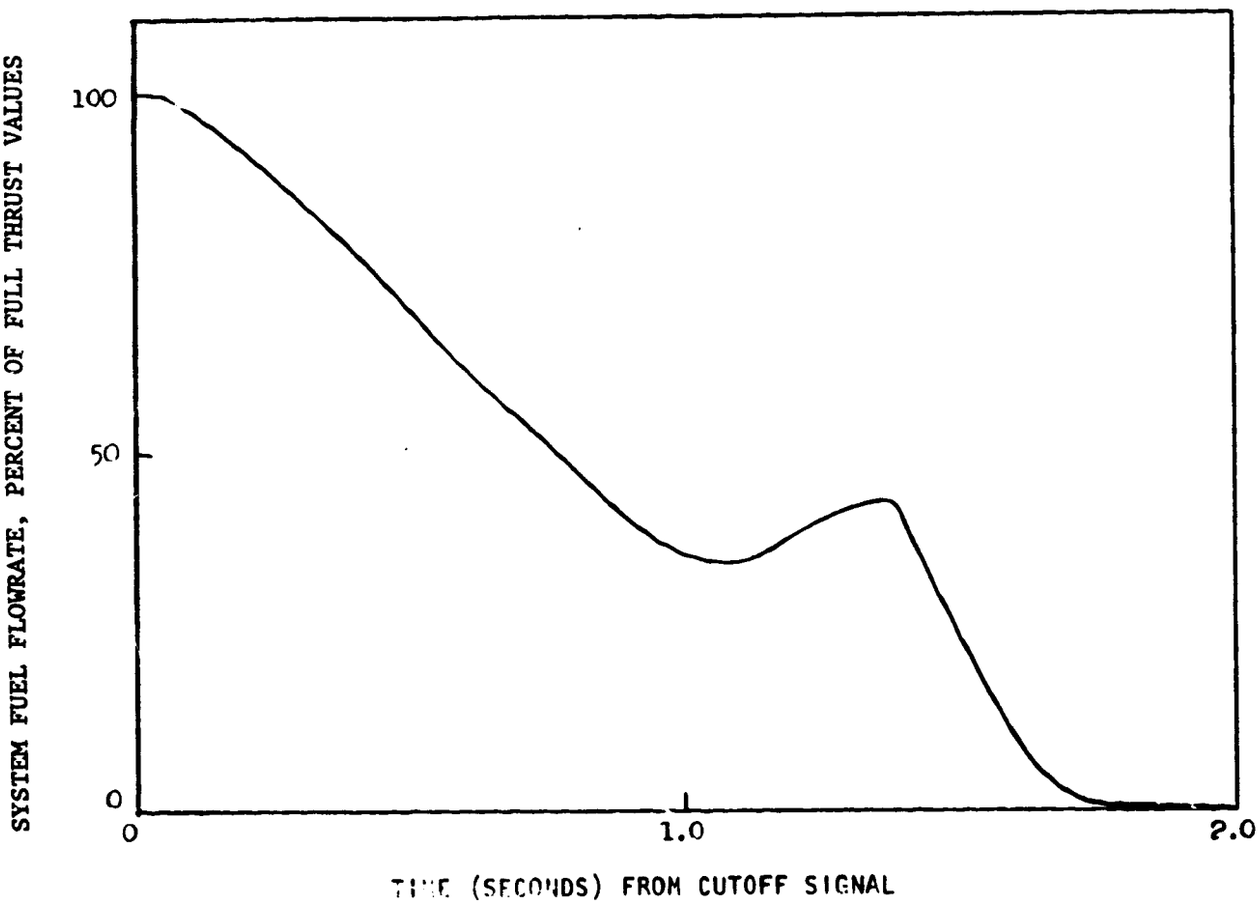

Figure 125. Fuel Flowrates for Nominal Linear Engine Shutdown Transient, LOX/H_2-LOX/H_2 Staged Combustion (Concept 2)

ORIGINAL PAGE IS
OF POOR QUALITY

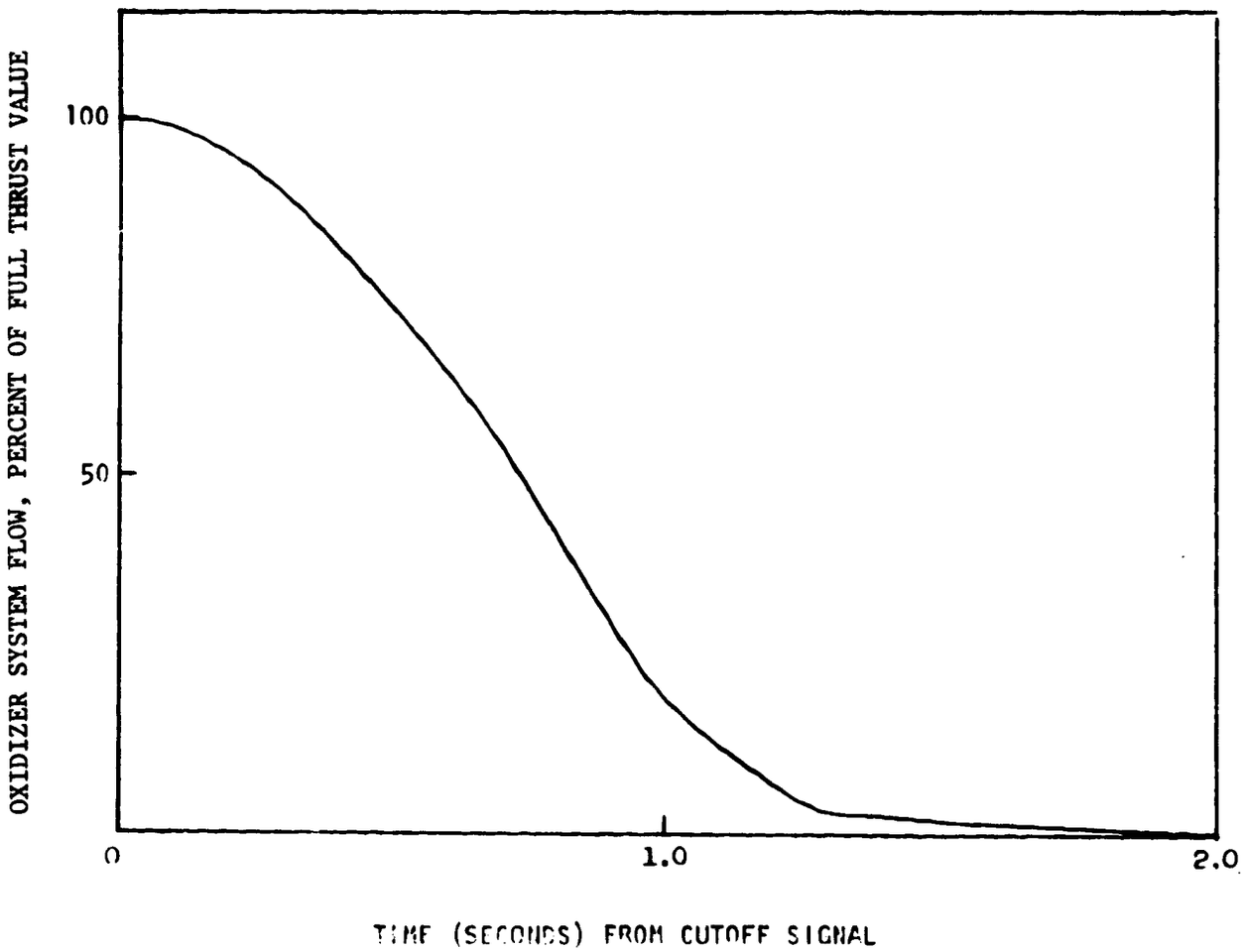

Figure 126. Oxidizer Feed System Flowrates for Nominal Linear Engine Shutdown Transient, LOX/H_2- LOX/H_2 Staged Combustion (Concept 2)

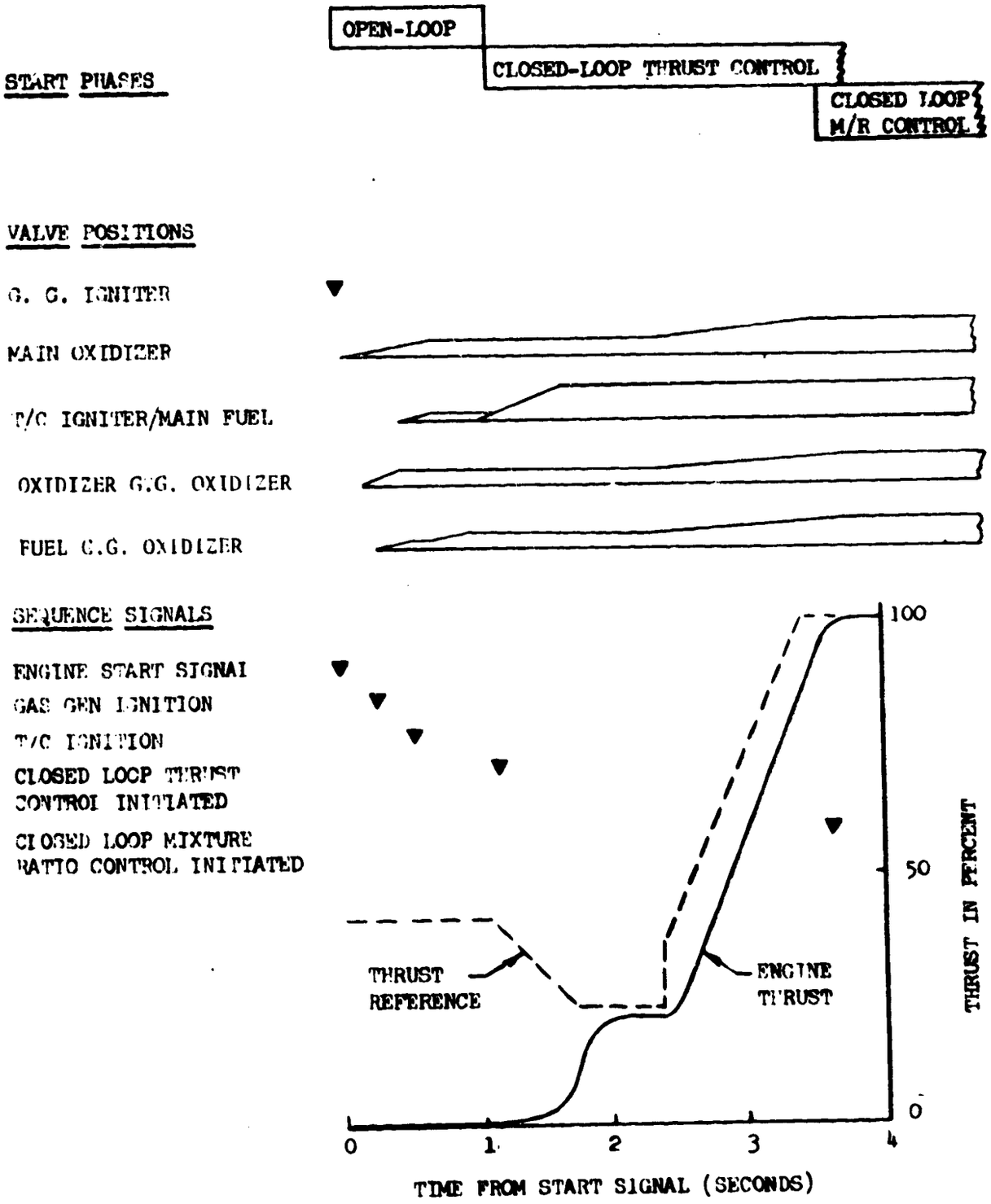

Figure 127. Typical Linear Engine Outer Combustor Start Sequence to Full Thrust, LOX/RP-1-LOX/H_2 Hybrid Engine (Concept 1)

ORIGINAL PAGE IS
OF POOR QUALITY

chamber ignition occurs. Closed-loop control raises the engine thrust to a 25 percent level with controlled mixture ratio transients. Approximately 0.5 second at this thrust level allows for stabilization of engine characteristics and repeatability of the next phase to follow, i.e., steady thrust climb to 100 RPL thrust at a controlled fixed rate of climb not to exceed prescribed values. Closed-loop mixture ratio control is activated near the end of the engine start transient period. The last phases of the control are identical for both the LOX/RP-1 outer combustor and the LOX/H_2 inner combustor, so that full thrust from both combustor banks is achieved simultaneously.

Engine Shutdown. The shutdown sequence for the LOX/RP-1 outer combustor (Fig. 128) is similar to that of the inner LOX/H_2 combustor. In both engine shutdowns, open- and closed-loop controls are used to provide smooth, repeatable engine shutdown transients avoiding detrimental pump or thrust chamber transients. In the LOX/RP-1 system, the main fuel and oxidizer valves attain full closure simultaneously. The shutdown impulse per module for the outer and inner combustors of this engine are 2.60 x 10^6 N-sec (5.86 x 10^5 lb-sec) and 1.40 x 10^6 N-sec (3.16 x 10^5 lb-sec), respectively. The propellant consumptions are respectively 895 kg (1969 lb) and 384 kg (845 lb).

THRUST VECTOR CONTROL

Differential throttling is used in fixed-linear engine applications to obtain thrust vector control. The equivalent gimbal angle achieved in such applications depends on the degree of throttling, the number of modules throttled, the location of the vehicle center of gravity, and the width of the linear engine. Typical thrust vector control engine-vehicle geometry is shown in Fig. 129. The equations showing the relationship between the various thrust-vector-angle influencing parameters are shown in Table 30 .

Figure 130 presents the magnitude of the equivalent gimbal angle in yaw orientation as a function of the above parameters. Yaw gimbal angles on the order of 7 degrees necessitates vehicle center of gravity location of less than one engine width (Lg/w = 0.5) from the engine-vehicle interface, and throttling to 25 percent of the total engine thrust. Assumed SSTO vehicle dimensions and linear engine nozzle width-to-height ratio of 3:1 results in Lg/w of approximately 1.5. This CG location allows equivalent differential throttling gimbal angles in yaw of only 0.5 to 2 degrees when throttling 10 to 25 percent.

The equations that define the pitch and yaw equivalent gimbal angles are shown in Table 30. Equation 2 is used to obtain the pitch equivalent gimbal angle. The values of the maximum pitch angles available are shown in Fig. 130. For a nozzle width-to-height ratio of 3, a vehicle length-to-width that provides a yaw gimbal angles of 7 degrees will provide only 2.4 degrees of pitch gimbal angle (i.e., Lg/H = 1.5) when throttling 25 percent. Assumed SSTO center of gravity location and linear engine nozzle width-to-height ratio of 3 provide in pitch only 1/3 of the gimbal angle provided in yaw, i.e., 0.8 degree when modules are throttled 25 percent (Lg/H = 4.5).

The loss in thrust during pitch or yaw is defined by Eq. 3 of Table 30. Loss in engine thrust is directly proportional to percent throttled.

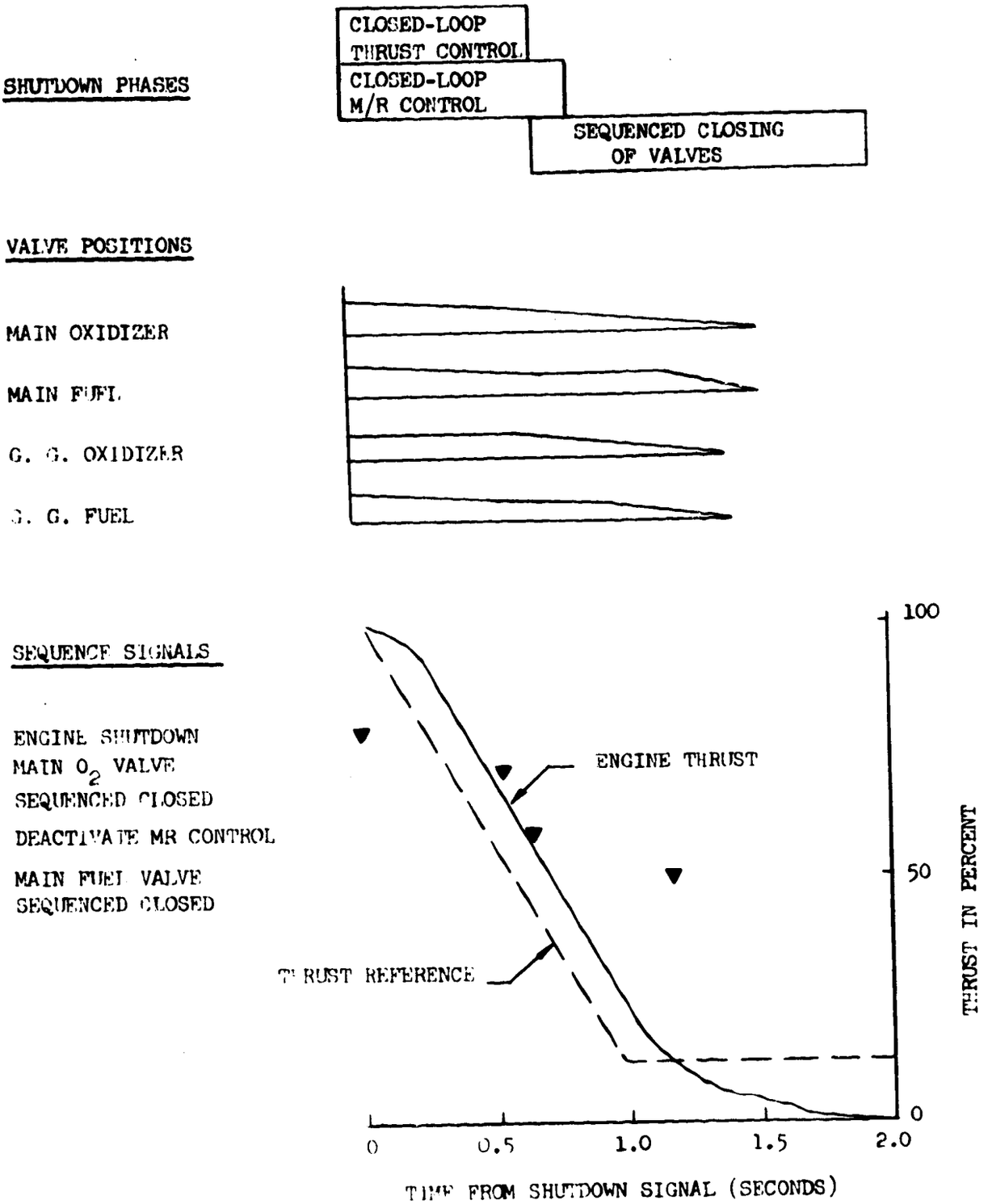

Figure 128. Typical Linear Engine Outer Combustor Shutdown Sequence, LOX/RP-1 - LOX/H_2 Hybrid Engine (Concept 1)

ORIGINAL PAGE IS OF POOR QUALITY

NOZZLE W/H = 3

$\frac{Lg}{W}$ = 1.5

$\frac{Lg}{H}$ = 6

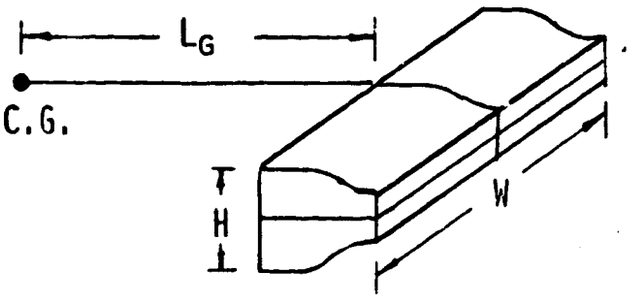

Figure 129. Linear Engine Thrust Vector Control Typical Geometry

TABLE 30. EQUIVALENT GIMBAL ANGLES DURING DIFFERENTIAL LINEAR ENGINE THROTTLING

Yaw:

$$Q_Y = \text{Sin}^{-1} \frac{WX}{2Lg} (1-X) \left(\frac{\%T}{100}\right) \quad (1)$$

Pitch:

$$Q_p = \text{Sin}^{-1} \frac{HX}{2Lg} (1-X) \left(\frac{\%T}{100}\right) \quad (2)$$

Net Thrust:

$$F_N = \frac{\%T}{100} \times F \quad (3)$$

where:

W = Engine Width

H = Nozzle Height

Lg = Length to C. G. from engine/vehicle interface

X = Fraction of Modules Throttled

%T = Percent Module Throttling

F = Nominal Thrust

F_N = Net Thrust

Q_Y = Yaw Equivalent Gimbal Angle

Q_P = Pitch Equivalent Gimbal Angle

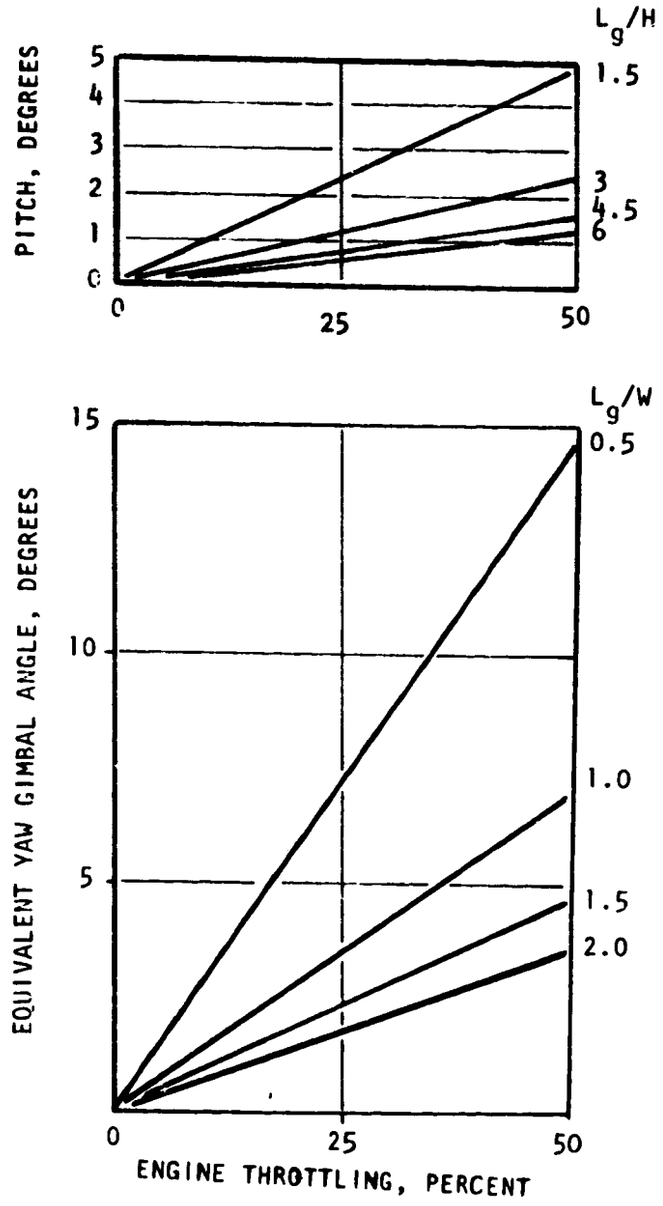

Figure 130. Linear Engine Differential Throttling

ORIGINAL PAGE IS
OF POOR QUALITY

ENGINE MIXTURE RATIO VARIATIONS

Performance variations with mixture ratio for the two selected engine concepts are shown in Fig. 131 and 132. The engine specific impulse performance is shown for sea level, vacuum Mode 1, and vacuum Mode 2 operation. Data are presented for engine mixture ratio variations 10 percent above and below the nominal values of 2.8 and 7.0 for the LOX/RP-1 and LOX/H_2 combustors, respectively.

ENGINE WEIGHTS

Engine weights for the selected Concepts 1 and 2 of Table 29 are shown in Table 31. The engine weights are provided in the form of a breakdown of the major components for the outer and inner combustors of each system.

Inner combustor component weight breakdown of either Concept 1 or 2 are identical since both are staged combustion LOX/H_2 engine systems operating at a chamber pressure of 1723.5 N/cm^2 (2500 psia). The outer combustor engine weights are 40 percent greater for Concept 2. (This is attributed to the staged combustor outer combustor operating at a chamber pressure of 1723.5 N/cm^2 (2500 psia) and the different propellant combination. Concept 1 has a gas generator outer combustor operating at 1378.8 N/cm^2 (2000 psia). Total engine system weights are 22 percent lighter for Concept 1.)

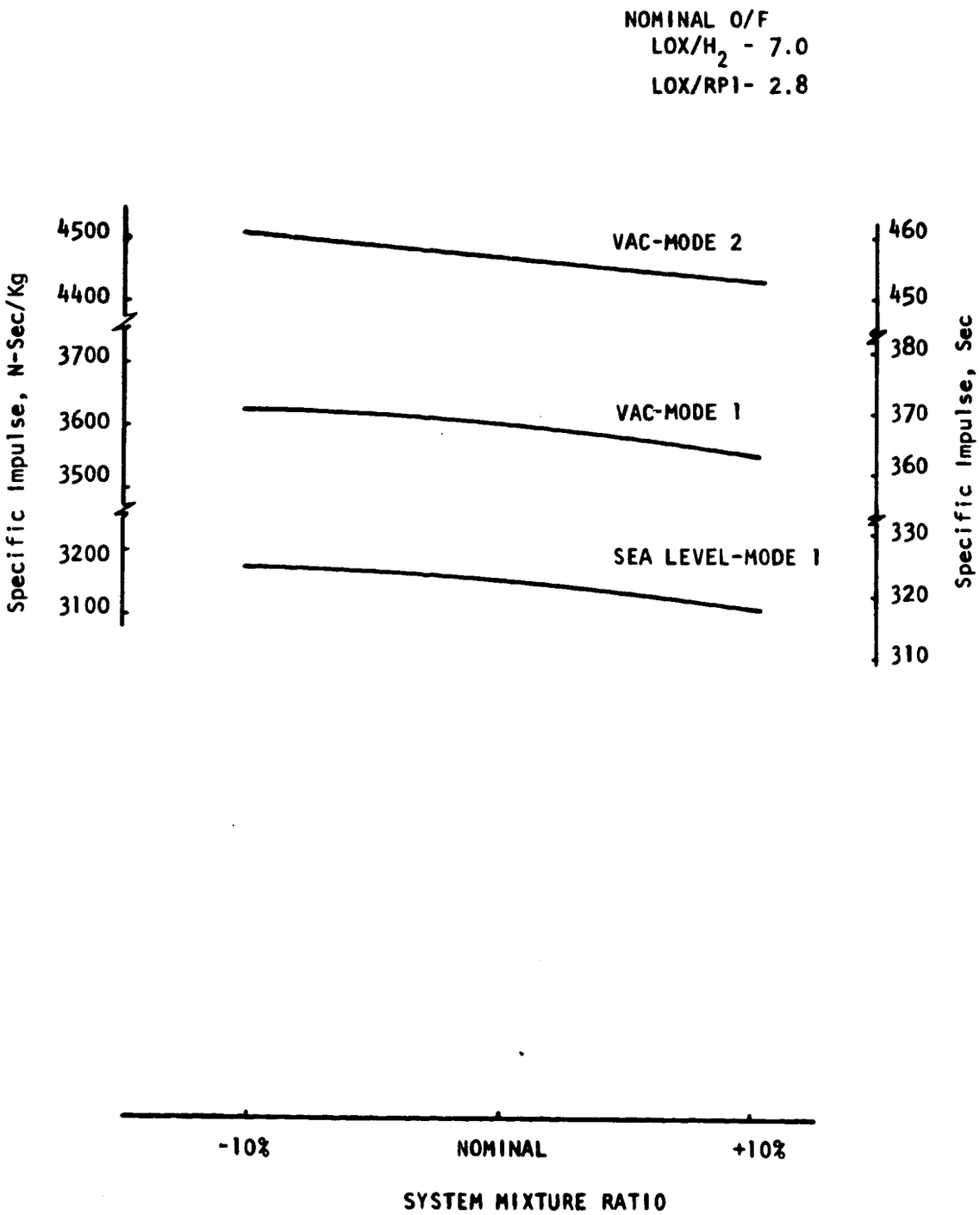

Figure 131. Split Combustor Linear Engine Performance vs Mixture Ratio, LOX/RP-1-LOX/H_2 Hybrid Engine

ORIGINAL PAGE IS
OF POOR QUALITY

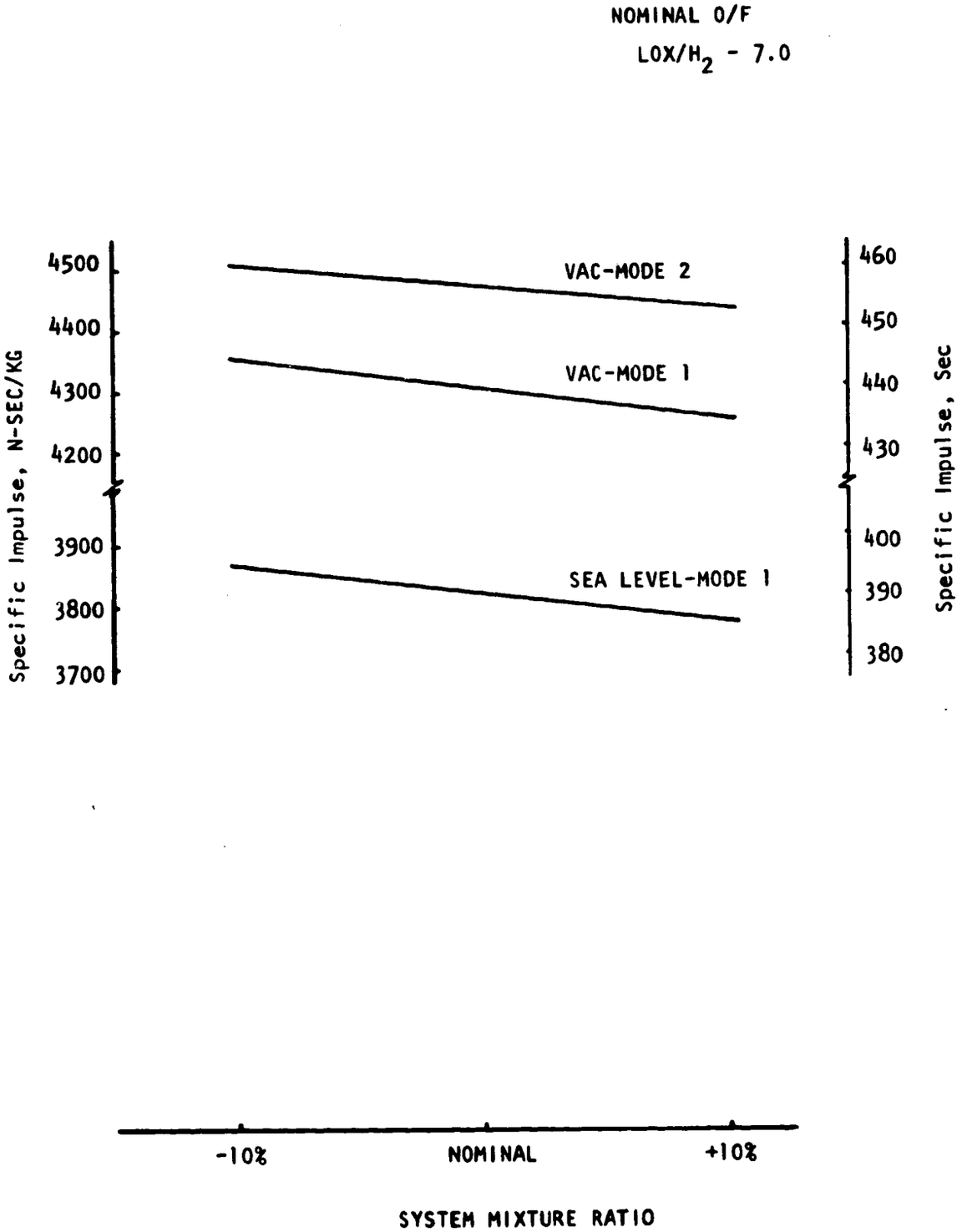

Figure 132. Split Combustor Linear Engine Performance vs Mixture Ratio, LOX/H_2-LOX/H_2, Staged Combustor Engine

TABLE 31. LINEAR SPLIT-COMBUSTOR ENGINE

WEIGHTS AND BREAKDOWN

	CONCEPT 1		CONCEPT 2	
	Kg.	Lb.	Kg.	Lb.
OUTER ENGINE	$O_2/RP-1$		O_2/H_2	
Combustion Chamber & Shroud	922	2032	891	1964
*Fuel Turbopump and Mount	1178	2598	2062	4547
Fuel Ducting	246	542	307	677
Main Fuel Valve	230	507	288	634
*LOX Turbopump and Mount	2475	5456	3422	7544
LOX Ducting	258	568	322	710
Main LOX Valve	376	829	470	1037
Hot Gas System - Fuel	624	1376	1046	2307
Hot Gas System - LOX	560	1236	842	1856
	(6869)	(15144)	(9650)	(21276)
INNER ENGINE	O_2/H_2		O_2/H_2	
Combustion Chamber and Shroud	1216	2680	1216	2680
*Fuel Turbopump and Mount	1400	3086	1400	3086
Fuel Ducting	244	537	244	537
Main Fuel Valve	155	341	155	341
*LOX Turbopump and Mount	1920	4233	1920	4233
LOX Ducting	246	542	246	542
Main LOX Valve	253	558	253	558
Hot Gas System - Fuel	702	1547	702	1547
Hot Gas System - LOX	590	1301	590	1301
Nozzle and Support	3043	6708	3043	6708
Base Closure	1396	3081	1396	3081
	(11165)	(24614)	(11165)	(24614)
Ignitor System	89	197	89	197
Controls and Misc.	1947	4293	1947	4293
TOTALS	20070	44248	22851	50380

*Sum of boost and main pumps

ORIGINAL PAGE IS
OF POOR QUALITY

CONCLUSIONS AND TECHNOLOGY RECOMMENDATIONS

This report has discussed a dual-fuel split combustor linear aerospike engine concept for a single-stage-to-orbit (SSTO) vehicle. The parametric and point design data presented herein permit the vehicle designer to select an engine design based on an optimization of the vehicle/engine system.

The concept is versatile and was found to be applicable over a wide range in thrust level. In addition, the fuel (or fuels) used in the engine does not significantly impact the engine design approach. Although hydrogen was selected as the best coolant for the engine, the analyses indicate the concept can accommodate supplemental cooling with the second fuel or with oxygen to achieve higher operating pressures if mission/vehicle trade-off studies indicate it to be advantageous.

The engine design has been based on the materials technology level of the Space Shuttle Main Engine.

Recommended supporting research and technology programs to continue work on the split combustor linear aerospike engine are presented in Table 32. Lists of the objectives for each program are presented in Tables 33 through 37.

TABLE 32. TECHNOLOGY RECOMMENDATION

Preliminary Design and Analysis-Phase II
Split Combustor Thrust Chamber Feasibility Demonstration
High-Pressure O_2/RP-1 Combustion
High-Pressure O_2/RP-1 GG Operation
Composite Materials Investigations

TABLE 33. PRELIMINARY DESIGN AND ANALYSIS, PHASE II

Study Alternate Component Arrangements
Investigate Effect of Number of Preburners (Gas Generators)
Develop Engine Computer Model and Simulate Operation
Investigate Impact of Location of Vehicle Attach Points
Design Interface Between Ends of Engine and Vehicle Structure
Analyze Engine/Vehicle Assembly Procedures
Investigate Design Alternatives to Thrust Chamber Backup Structure
Develop Analytical Techniques to Calculate Effect of Steam Mixing on Split Combustor Performance

TABLE 34. SPLIT COMBUSTOR THRUST CHAMBER FEASIBILITY DEMONSTRATION

Analyze Module to Select Optimum Segment Size
Conduct Analytical Support to Define Segment Design Requirements
Prepare Segment Fabrication Drawings
Build Split Combustor Thrust Chamber Segment
Calculate the Expected Segment Performance
Conduct Hot-Fire Testing of Segment
Compare Experimental and Analytical Results
Predict Full-Scale Engine Performance

ORIGINAL PAGE IS
OF POOR QUALITY

TABLE 35. HIGH-PRESSURE O_2/RP-1 COMBUSTION

Analytical Investigation of Main Chamber Injector Concepts to Select Design Approach
Prepare Injector Design for High-Pressure O_2/RP-1 Propellants
Conduct Stability Analysis
Experimentally Investigate Stability at High Combustion Pressures
Investigate Carbon Buildup and Coking of Injector, Cooling Passages, and Hot-Gas Wall
Investigate Combustor Length, Contraction Ratio, Throat Radius, etc., to Establish Performance and Cooling

TABLE 36. HIGH-PRESSURE O_2/RP-1 GG OPERATION

Analyze High-Pressure O_2/RP-1 Gas Generator Injector Concepts to Select Design Approach
Prepare Injector Design
Experimentally Investigate Operation
Analyze Reuse Maintenance Requirements and Procedures

TABLE 37. COMPOSITE MATERIALS INVESTIGATIONS

Identify Components/Parts That are Candidates for Composite Material Application
Conduct Supporting Analysis Providing Design Requirements
Investigate Component/Part Compatibility With Interfacing Components/Parts
Investigate Fabrication Procedures
Prepare Fabrication Drawing
Build Component/Part Using Selected Composite and Fabrication Technique
Perform Laboratory Tests
Conduct Simulated Engine Test
Compare Composite With Metallic

REFERENCES

1. NAS8-25156, Linear Test Bed Final Report, R-9049, Rocketdyne Division, Rockwell International, Canoga Park, CA, August 1972.

2. R-3999, Investigation of Cooling Problems at High Chamber Pressure - Final Report,, Contract No. NAS8-4011, Rocketdyne Division, Rockwell International, May 1963.

3. Hines, W. S., Turbulent Forced Convection Heat Transfer to Liquids at Very High Heat Fluxes and Flowrates, Contract L/C AF04(647)-318 and 672, Rocketdyne Division, Rockwell International, 30 November 1961.

4. Rousar, D., Cooling With Supercritical Oxygen, AIAA Paper No. 75-1248, presented at the AIAA/SAE 11th Propulsion Conference, Anaheim, California, 30 September 1975.

5. NASA CR-72360, Space Storable Regenerating Cooling Investigation - Interim Report, R-7338, Rocketdyne Division, Rockwell International, 25 September 1968.

6. NASA SP-8048, Liquid Rocket Engine Turbopump Bearings, NASA Space Vehicle Design Criteria Monograph, M. F. Butner, Rocketdyne Division, Rockwell International, March 1971.

7. BC 75-52, Space Shuttle Main Engine - Design Features, Rocketdyne Division, Rockwell International, March 1975.

8. NASA SP-8107, Turbopump Systems for Liquid Rocket Engines, NASA Space Vehicle Design Criteria Monograph, W. R. Bissell and A. J. Sobin, Rocketdyne Division, Rockwell International, August 1974.

9. NASA SP-8110, Liquid Rocket Engine Turbines, NASA Space Vehicle Design Criteria Monograph, S. B. Macaluso, Rocketdyne Division, Rockwell International, January 1974.

10. Moses, R. A., Physical and Thermodynamic Properties for Heat Transfer Analysis, Pub. 575-A-5, Rocketdyne Division, Rockwell International, 1966.

11. Hodgman, C. D., R. C. Weast, and S. M. Selby, Handbook of Physics and Chemistry, 39th Edition, Chemical Rubber Publishing Co., Cleveland, Ohio, 1958.

12. ADR:9734:0127, Advanced High Pressure Engine Study - Task I Propellant Properties and Performance Study, Contract NAS3-19727, J. W. Salmon, Aerojet Liquid Rocket Company, Sacramento, CA, September 1975.

ORIGINAL PAGE IS
OF POOR QUALITY

13. LAP 64-655, Turbine Drive Gas Properties at High Pressure for Fuel-Rich and Oxidizer-Rich Operation of Both LO_2/RP-1, LO_2/Para LH_2, and Pure Preheated H_2, P. D. Amdisen, Rocketdyne Division, Rockwell International, December 1964.

14. Hoshide, R. K., Review of Pump Efficiencies for Low Thrust Engine Systems, ASR 71-39, Rocketdyne Division, Rockwell International, February 1971.

APPENDIX A

NASA STUDY GUIDELINES

HIGH-PRESSURE PUMPS

Inducers and/or impellers utilized in the high-pressure pumps will be designed for operation above incipient cavitation.

Impeller burst speed will be at least 20% above the maximum operating speed.

Impeller effective stress at 5% above the maximum operating speed will not exceed the allowable 0.2% yield stress. (Does not apply to areas in which local yielding is permitted.)

LOW-PRESSURE PUMPS

Inlet Flow Coefficient: 0.06 (minimum)

Inlet Flow Maximum Velocity:

$$LH_2,\ C_m = \sqrt{\frac{2gNPSH}{1.3}}$$

$$LOX,\ C_m = \sqrt{\frac{2gNPSH}{2.3}}$$

$$\text{Mode 1 Fuels},\ C_m = \sqrt{\frac{2gNPSH}{3.0}}$$

TURBINES

Blade root steady-state stress will not exceed the allowable 1% 50-hour creep stress.

Stress state at the blade root, as defined by the steady-state stress and an assumed vibratory stress equal to the gas bending stress, will be within the allowable stress range diagram or modified Goodman diagram.

No blade natural frequencies within ±15% of known sources of excitation at steady-state operating speeds.

Disk burst speed will be at least 20% above the maximum operating speed.

Disk maximum effective stress at 5% above the maximum operating speed will not exceed the allowable 0.2% yield stress. (Does not apply to areas in which local yielding is permitted.)

BEARINGS

Turbopump designs will utilize rolling element bearings.

Maximum DN:

	LH_2	LOX	RP-1	RJ-5	CH_4
Roller	2.0×10^6	1.5×10^6	1.8×10^6	1.5×10^6	TBD
Ball	2.0×10^6	1.5×10^6	1.8×10^6	1.8×10^6	TBD

B_{10} Life $\geq$ 500 hours

SEALS

Turbopump designs will utilize conventional-type seals.

Face Contact Seal Maximum PV, FV, and P_fV Factors*:

	LH_2	LOX	RP-1	RJ-5	CH_4
PV	50,000	25,000	25,000	25,000	TBD
FV	4,000	2,000	2,500	2,500	TBD
P_fV	200,000	60,000	80,000	80,000	TBD

*PV = unit load times rubbing velocity ($lb/in.^2 \times ft/sec$)
FV = face load per unit length times rubbing velocity ($lb/in. \times ft/sec$)
P_fV= fluid pressure differential times rubbing velocity ($psig \times ft/sec$)

GENERAL

Components subject to a low-cycle fatigue mode of failure will be designed for a minimum of 250 cycles times a safety factor of 4.

Components subject to a fracture mode of failure will be designed for a minimum of 250 cycles times a safety factor of 4.

Components subject to a high-cycle fatigue mode of failure will be designed within the allowable stress range diagram (based on the material endurance limit). If stress range material property data are not available, modified Goodman diagrams, constructed as shown below, will be utilized.

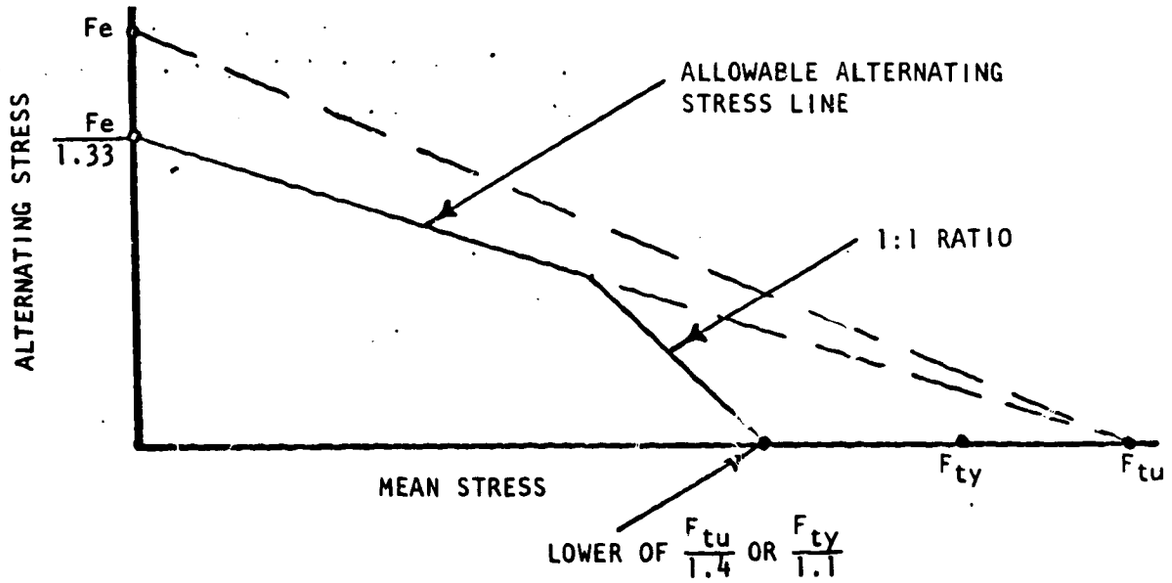

Fe = material endurance limit
F_{ty} = material yield strength (0.2% offset)
F_{tu} = material ultimate strength

Effective stress will be based on the Mises-Hencky constant energy of distortion theory.

ORIGINAL PAGE IS OF POOR QUALITY

Unless otherwise noted under component ground rules specified herein, the following minimum factors of safety will be utilized:

Factor of Safety (0.2% yield) = 1.1 x limit load

Factor of Safety (ultimate) = 1.4 x limit load

Limit Load: The maximum predicted load or pressure at the most critical operating condition

Components subject to pressure loading will be designed to the following minimum proof and burst pressures:

Proof Pressure = 1.2 x limit pressure

Burst Pressure = 1.5 x limit pressure

APPENDIX B

DESIGN PARAMETERS

Design parameters for Concepts 1 and 2 are presented in Tables 38 and 39, respectively, for both combustors operating in Mode 1, and in Table 40 for the inner combustor operating in Mode 2.

ORIGINAL PAGE IS
OF POOR QUALITY

TABLE 38. CONCEPT 1 DESIGN DATA FOR MODE 1

(Vacuum Conditions)

SYSTEM DESCRIPTION

(1) AEROSPIKE NOZZLE
(2) FIXED AREA RATIO DESIGN
(3) SEA LEVEL DESIGN
(4) GAS GENERATOR CYCLE/STAGED COMBUSTION CYCLE
(5) PARALLEL TURBINES

ENGINE PERFORMANCE DATA	COMBINED	INNER	OUTER
THRUST, LBF	0.45726570E+07		
MIXTURE RATIO, O/F	0.34989001E+01	0.70000000E+01	0.28000000E+01
SPECIFIC IMPULSE, SEC	0.36724975E+03		
TOTAL PROPELLANT FLOWRATE, LBM/SEC	0.12451083E+05		
OXIDIZER FLOWRATE, LBM/SEC	0.96834988E+04	0.32237761E+04	0.64597227E+04
FUEL FLOWRATE, LBM/SEC	0.27675837E+04	0.46053931E+03	0.23070444E+04
ENGINE EFFICIENCY			
PRIMARY(THRUST CHAMBER)PERFORMANCE DATA			
THRUST, LBF	0.44897360E+07	0.15570360E+07	0.29327000E+07
MIXTURE RATIO, O/F	0.39076204E+01	0.70914116E+01	0.31937199E+01
SPECIFIC IMPULSE, SEC	0.36947302E+03		
TOTAL PROPELLANT FLOWRATE, LBM/SEC	0.12151729E+05	0.36693699E+04	0.84823594E+04
OXIDIZER FLOWRATE, LBM/SEC	0.96756033E+04	0.32158804E+04	0.64597256E+04
FUEL FLOWRATE, LBM/SEC	0.24761228E+04	0.45348946E+03	0.20226337E+04
NOZZLE STAGNATION PRESSURE, PSIA		0.25000000E+04	0.20000000E+04
AREA RATIO	0.40000000E+02	0.12921876E+03	0.57933452E+02
CHARACTERISTIC VELOCITY, FT/SEC	0.61614134E+04		
COMBUSTION EFFICIENCY	0.99500000E+00	0.99500000E+00	0.98000000E+00
THRUST COEFFICIENT	0.19293341E+01		
DIVERGENCE EFFICIENCY		0.98750000E+00	0.98750000E+00
DRAG EFFICIENCY		0.98390000E+00	0.98390000E+00
KINETICS EFFICIENCY		0.98860000E+00	0.98860000E+00

TABLE 38. (CONTINUED)

SECONDARY PERFORMANCE DATA	COMBINED	INNER	OUTER
THRUST, LBF	0.82921000E+05		
MIXTURE RATIO, O/F	0.42906281E+00		
SPECIFIC IMPULSE, SEC	0.27699641E+03		
TOTAL PROPELLANT FLOWRATE, LBM/SEC	0.29935767E+03		
OXIDIZER FLOWRATE, LBM/SEC	0.89879353E+02	0.78958941E+01	0.81983459E+02
FUEL FLOWRATE, LBM/SEC	0.20947831E+03	0.70499058E+01	0.20242841E+03
SECONDARY FLOW RATIO	0.24634986E-01	0.40731244E-02	0.33529814E-01
BASE AREA RATIO	0.14820220E+02		
CHARACTERISTIC VELOCITY, FT/SEC	0.67313942E+04		
THRUST COEFFICIENT			
BASE PRESSURE, PSIA	0.51808222E+01		
ENGINE GEOMETRY DATA			
AERODYNAMIC THROAT AREA, SQ IN	0.10799688E+04	0.33430713E+03	0.74566162E+03
NOZZLE PERCENT LENGTH	0.20000000E+02		
NOZZLE LENGTH, IN	0.43664363E+02		
NOZZLE EXIT AREA, SQ IN	0.43198752E+05		
NOZZLE EXIT HEIGHT , IN	0.11999826E+03		
OVERALL ENGINE HEIGHT , IN	0.16819826E+03		
OVERALL ENGINE WIDTH, IN	0.35999479E+03		
BASE AREA, SQ IN	0.16005374E+05		
BASE HEIGHT , IN	0.44460170E+02		
THROAT GAP, IN	0.14999783E+01	0.46432218E+00	1.03565612E+00
THROAT HEIGHT , IN	0.12049826E+02		
THRUST/INCH, LBF/IN	0.63510044E+04		

ORIGINAL PAGE IS
OF POOR QUALITY

TABLE 38. (CONCLUDED)

TURBOMACHINERY DATA	FUEL		OXIDIZER	
	INNER	OUTER	INNER	OUTER
PUMPS				
INLET PRESSURE, PSIA	0.170000E+02	0.190000E+02	0.230000E+02	0.230000E+02
PRESSURE RISE, PSI	0.640902E+04	0.258313E+04	0.447790E+04	0.311400E+04
DISCHARGE PRESSURE, PSIA	0.642602E+04	0.260213E+04	0.450090E+04	0.313700E+04
HEAD RISE, FT	0.195945E+06	0.736577E+04	0.910759E+04	0.633356E+04
MASS FLOWRATE, LBM/SEC	0.460539E+03	0.230704E+04	0.322378E+04	0.645972E+04
EFFICIENCY	0.740000E+00	0.086000E+00	0.830000E+00	0.830000E+00
HORSEPOWER, BHP	0.221720E+06	0.383333E+05	0.643173E+05	0.896233E+05
MEAN DENSITY, LBM/CU-FT	0.471000E+01	0.505000E+02	0.708000E+02	0.708000E+02
TURBINES				
INLET TEMPERATURE, DEG R	0.196000E+04	0.196000E+04	0.196000E+04	0.196000E+04
DISCHARGE TEMPERATURE, DEG R	0.184531E+04	0.146706E+04	0.184439E+04	0.147458E+04
PRESSURE RATIO	0.132736E+01	0.200000E+02	0.133048E+01	0.200000E+02
EFFICIENCY	0.830000E+00	0.840000E+00	0.830000E+00	0.840000E+00
MASS FLOWRATE, LBM/SEC	0.758155E+03	0.852041E+02	0.218188E+03	0.199208E+03
TAU FACTOR (WT/WP)	0.206617E+00	0.100449E-01	0.594619E-01	0.234849E-01

TABLE 39. CONCEPT 2 DESIGN DATA FOR MODE 1

(Vacuum Conditions)

SYSTEM DESCRIPTION

(1) AEROSPIKE NOZZLE
(2) FIXED AREA RATIO DESIGN
(3) SEA LEVEL DESIGN
(4) TOPPING CYCLE
(5) PARALLEL TURBINES

ENGINE PERFORMANCE DATA	COMBINED	INNER	OUTER
THRUST, LBF	0.45059620E+07		
MIXTURE RATIO, O/F	0.69999981E+01	0.70000000E+01	0.70000000E+01
SPECIFIC IMPULSE, SEC	0.43872485E+03		
TOTAL PROPELLANT FLOWRATE, LBM/SEC	0.10270586E+05		
OXIDIZER FLOWRATE, LBM/SEC	0.89867578E+04	0.31413911E+04	0.58453672E+04
FUEL FLOWRATE, LBM/SEC	0.12838228E+04	0.44877002E+03	0.83505273E+03
ENGINE EFFICIENCY	0.98114222E+00		

PRIMARY(THRUST CHAMBER)PERFORMANCE DATA			
THRUST, LBF	0.44424660E+07	0.15548620E+07	0.28876040E+07
MIXTURE RATIO, O/F	0.71014547E+01	0.70648928E+01	0.71212902E+01
SPECIFIC IMPULSE, SEC	0.43449536E+03		
TOTAL PROPELLANT FLOWRATE, LBM/SEC	0.10224422E+05	0.35797764E+04	0.66446445E+04
OXIDIZER FLOWRATE, LBM/SEC	0.89623711E+04	0.31359050E+04	0.58264687E+04
FUEL FLOWRATE, LBM/SEC	0.12620471E+04	0.44187134E+03	0.81817578E+03
NOZZLE STAGNATION PRESSURE, PSIA	0.25000000E+04		
AREA RATIO	0.40000000E+02	0.11428482E+03	0.61538712E+02
CHARACTERISTIC VELOCITY, FT/SEC	0.73374258E+04		
COMBUSTION EFFICIENCY	0.99500000E+00	0.99500000E+00	0.99500000E+00
THRUST COEFFICIENT	0.19052258E+01		
DIVERGENCE EFFICIENCY		0.98750001E+00	0.98750001E+00
DRAG EFFICIENCY		0.99809998E+00	0.99809998E+00
KINETICS EFFICIENCY		0.99100001E+00	0.99100001E+00

ORIGINAL PAGE IS
OF POOR QUALITY

TABLE 39. (CONTINUED)

SECONDARY PERFORMANCE DATA	COMBINED	INNER	OUTER
THRUST, LBF	0.63496277E+05		
MIXTURE RATIO, O/F	0.11199999E+01		
SPECIFIC IMPULSE, SEC	0.13754426E+04		
TOTAL PROPELLANT FLOWRATE, LBM/SEC	0.46164246E+02		
OXIDIZER FLOWRATE, LBM/SEC	0.24388657E+02	0.54863491E+01	0.18902313E+02
FUEL FLOWRATE, LBM/SEC	0.21775574E+02	0.4898526?E+01	0.16977060E+02
SECONDARY FLOW RATIO	0.45150928E-02	0.29009846E-02	0.53846948E-02
BASE AREA RATIO	0.14820220E+02		
CHARACTERISTIC VELOCITY, FT/SEC	0.6820839?E+04		
THRUST COEFFICIENT	0.27231444E-01		
BASE PRESSURE, PSIA	0.45936289E+01		
ENGINE GEOMETRY DATA			
AERODYNAMIC THROAT AREA, SQ IN	0.93269092E+03	0.32644434E+03	0.60674658E+03
NOZZLE PERCENT LENGTH	0.20000000E+02		
NOZZLE LENGTH, IN	0.40577881E+02		
NOZZLE EXIT AREA, SQ IN	0.37307637E+05		
NOZZLE EXIT HEIGHT , IN	0.11151627E+03		
OVERALL ENGINE HEIGHT , IN	0.15971626E+03		
OVERALL ENGINE WIDTH, IN	0.33454858E+03		
BASE AREA, SQ IN	0.13822684E+05		
BASE HEIGHT , IN	0.41317413E+02		
THROAT GAP, IN	0.13939543E+01	0.48788774E+00	0.90606654E+00
THROAT HEIGHT , IN	0.11201627E+03		
THRUST/INCH, LBF/IN	0.67343906E+04		

TABLE 39. (CONCLUDED)

MISCELLANEOUS DATA	COMBINED	INNER	OUTER
PRIMARY THEOR. CHAR. VELOCITY, FT/SEC	0.73742930E+04	0.73718320E+04	0.73756289E+04
PRIMARY THEORETICAL THRUST COEFFICIENT	0.19492826E+01		
BASE PRESSURE TERM PB1	0.24366006E-01		
BASE PRESSURE TERM PB2	0.96338493E+00		
BASE PRESSURE TERM PB3	0.82856826E-02		
BASE PRESSURE TERM PB4	0.0		

TURBOMACHINERY DATA	FUEL		OXIDIZER	
	INNER	OUTER	INNER	OUTER
PUMPS				
INLET PRESSURE,PSIA	0.170000E+02	0.170000E+02	0.230000E+02	0.230000E+02
PRESSURE RISE,PSI	0.640902E+04	0.397524E+04	0.447790E+04	0.410678E+04
DISCHARGE PRESSURE,PSIA	0.642602E+04	0.399224E+04	0.450090E+04	0.412978E+04
HEAD RISE,FT	0.195945E+06	0.121536E+06	0.910759E+04	0.835277E+04
MASS FLOWRATE,LBM/SEC	0.448770E+03	0.835053E+03	0.314139E+04	0.584537E+04
EFFICIENCY	0.740000E+00	0.730000E+00	0.830000E+00	0.830000E+00
HORSEPOWER,BHP	0.216054E+06	0.252774E+06	0.626736E+05	0.106955E+06
MEAN DENSITY,LBM/CU-FT	0.471000E+01	0.471000E+01	0.708000E+02	0.709000E+02
TURBINES				
INLET TEMPERATURE,DEG R	0.196000E+04	0.196000E+04	0.196000E+04	0.196000E+04
DISCHARGE TEMPERATURE,DEG R	0.184531E+04	0.188058E+04	0.184439E+04	0.187966E+04
PRESSURE RATIO	0.132736E+01	0.121107E+01	0.133048E+01	0.121385E+01
EFFICIENCY	0.830000E+00	0.840000E+00	0.830000E+00	0.840000E+00
MASS FLOWRATE,LBM/SEC	0.738780E+03	0.124825E+04	0.212612E+03	0.522073E+03
TAU FACTOR(WT/WP)	0.206376E+00	0.187857E+00	0.593925E-01	0.785705E-01

ORIGINAL PAGE IS
OF POOR QUALITY

TABLE 40. CONCEPTS 1 AND 2 DESIGN DATA FOR MODE 2
(Vacuum Conditions)

SYSTEM DESCRIPTION

(1) AEROSPIKE NOZZLE
(2) FIXED AREA RATIO DESIGN
(3) VACUUM DESIGN
(4) TOPPING CYCLE
(5) PARALLEL TURBINES

ENGINE PERFORMANCE DATA

THRUST, LBF	0.16537090E+07
MIXTURE RATIO, O/F	0.70000000E+01
SPECIFIC IMPULSE, SEC	0.45586328E+03
TOTAL PROPELLANT FLOWRATE, LBM/SEC	0.36276401E+04
OXIDIZER FLOWRATE, LBM/SEC	0.31741853E+04
FUEL FLOWRATE, LBM/SEC	0.45345483E+03
ENGINE EFFICIENCY	0.97592914E+00

PRIMARY(THRUST CHAMBER)PERFORMANCE DATA

THRUST, LBF	0.16304050E+07
MIXTURE RATIO, O/F	0.71980219E+01
SPECIFIC IMPULSE, SEC	0.45335352E+03
TOTAL PROPELLANT FLOWRATE, LBM/SEC	0.35963203E+04
OXIDIZER FLOWRATE, LBM/SEC	0.31576389E+04
FUEL FLOWRATE, LBM/SEC	0.43868140E+03
NOZZLE STAGNATION PRESSURE, PSIA	0.25000000E+04
AREA RATIO	0.11428458E+03
CHARACTERISTIC VELOCITY, FT/SEC	0.73012227E+04
COMBUSTION EFFICIENCY	0.99500000E+00
THRUST COEFFICIENT	0.19977741E+01
DIVERGENCE EFFICIENCY	0.98750001E+00
DRAG EFFICIENCY	0.99809998E+00
KINETICS EFFICIENCY	0.99180001E+00

TABLE 40. (CONTINUED)

SECONDARY PERFORMANCE DATA

THRUST, LBF	0.23303414E+05
MIXTURE RATIO, O/F	0.11199999E+01
SPECIFIC IMPULSE, SEC	0.74404370E+03
TOTAL PROPELLANT FLOWRATE, LBM/SEC	0.31319946E+02
OXIDIZER FLOWRATE, LBM/SEC	0.16546387E+02
FUEL FLOWRATE, LBM/SEC	0.14773560E+02
SECONDARY FLOW RATIO	0.87088905E-02
BASE AREA RATIO	0.42343155E+02
CHARACTERISTIC VELOCITY, FT/SEC	0.68208359E+04
THRUST COEFFICIENT	0.28554242E-01
BASE PRESSURE, PSIA	0.16858826E+01

ENGINE GEOMETRY DATA

AERODYNAMIC THROAT AREA, SQ IN	0.32644434E+03
NOZZLE PERCENT LENGTH	0.19672119E+02
NOZZLE LENGTH, IN	0.40577774E+02
NOZZLE EXIT AREA, SQ IN	0.37307555E+05
NOZZLE EXIT HEIGHT , IN	0.11151614E+03
OVERALL ENGINE HEIGHT , IN	0.15971614E+03
OVERALL ENGINE WIDTH(OVAL AEROSPIKE), IN	0.33454834E+03
BASE AREA, SQ IN	0.13822680E+05
BASE HEIGHT , IN	0.41317429E+02
THROAT GAP, IN	0.48788810E+00
THROAT HEIGHT , IN	0.11201614E+03
THRUST/INCH, LBF/IN	0.74715530E+04

ORIGINAL PAGE IS
OF POOR QUALITY

TABLE 40. (CONCLUDED)

MISCELLANEOUS DATA

PRIMARY THEORETICAL CHARACTERISTIC VELOCITY, FT/SEC	0.73379141E+04
PRIMARY THEORETICAL THRUST COEFFICIENT	0.20439711E+01
BASE PRESSURE TERM PB1	0.25549613E-01
BASE PRESSURE TERM PB2	0.96109277E+00
BASE PRESSURE TERM PB3	0.87088905E-02
BASE PRESSURE TERM PB4	0.0

TURBOMACHINERY DATA

	FUEL		OXIDIZER	
	NO.1	NO.2	NO.1	NO.2
PUMPS				
INLET PRESSURE,PSIA	0.170000E+02	0.170000E+02	0.230000E+02	0.230000E+02
PRESSURE RISE,PSI	0.0	0.640902E+04	0.0	0.447790E+04
DISCHARGE PRESSURE,PSIA	0.170000E+02	0.642602E+04	0.230000E+02	0.450090E+04
HEAD RISE,FT	0.0	0.195944E+06	0.0	0.910759E+04
MASS FLOWRATE,LBM/SEC	0.453455E+03	0.453455E+03	0.317419E+04	0.317419E+04
EFFICIENCY	0.100000E+01	0.740000E+00	0.100000E+01	0.830000E+00
HORSEPOWER,BHP	0.0	0.218309E+06	0.0	0.633279E+05
MEAN DENSITY,LBM/CU-FT	0.471000E+01	0.471000E+01	0.708000E+02	0.708000E+02
TURBINES				
INLET TEMPERATURE,DEG R	0.196000E+04	0.196000E+04	0.196000E+04	0.196000E+04
DISCHARGE TEMPERATURE,DEG R	0.196000E+04	0.184531E+04	0.196000E+04	0.184439E+04
PRESSURE RATIO	0.0	0.132736E+01	0.0	0.133048E+01
EFFICIENCY	0.100000E+01	0.830000E+00	0.100000E+01	0.830000E+00
MASS FLOWRATE,LBM/SEC	0.746493E+03	0.746493E+03	0.214832E+03	0.214832E+03
TAU FACTOR(WT/WP)	0.207571E+00	0.207571E+00	0.597366E-01	0.597366E-01

APPENDIX C

HYBRID ENGINE DESIGN

Subsequent to the completion of the study, a design for a hybrid engine at equal inner and outer chamber pressures was completed and presented in Ref. B-1*. A summary of the design point parameters is presented in Table 41.

TABLE 41. LINEAR ENGINE PRELIMINARY DESIGN DESCRIPTION

ENGINE THRUST AT SEA LEVEL, NEWTONS (POUNDS)	
MODE 1	
SEA LEVEL	17.8×10^6 (4×10^6)
VACUUM	20.0×10^6 (4.5×10^6)
MODE 2	
VACUUM	7.36×10^6 (1.65×10^6)
CHAMBER PRESSURE, N/cm^2 (PSIA)	
OUTER COMBUSTOR	1724 (2500)
INNER COMBUSTOR	1724 (2500)
ENGINE MIXTURE RATIO	
OUTER COMBUSTOR	2.8
INNER COMBUSTOR	7.0
EXPANSION AREA RATIO	
MODE 1	40:1
MODE 2	114:1
SPECIFIC IMPULSE, N-s/kg (SECONDS)	
MODE 1	
SEA LEVEL	3201 (326.4)
VACUUM	3590 (366.1)
MODE 2	
VACUUM	4466 (455.4)
NOZZLE PERCENT LENGTH, % OF 15 DEGREE CONE	20
NOZZLE WIDTH-TO-HEIGHT RATIO	3.0:1
ENGINE ENVELOPE, METERS (INCHES)	
WIDTH	8.8 (346)
HEIGHT	4.4 (172)
LENGTH	2.1 (84.5)
ENGINE WEIGHT, kg (POUNDS)	19,900 (43,800)

*B-1. Kirby, F. M. and A. Martinez, Linear Aerospike Engine, AIAA Paper No. 77-968, presented at AIAA/SAE 13th Propulsion Conference, Orlando, Florida, July 11-13, 1977.

ORIGINAL PAGE IS OF POOR QUALITY

APPENDIX D

NOMENCLATURE

$\dot{w}$	= flowrate
$\dot{w}_I$	= weight flowrate of inner combustor
$\dot{w}_O$	= weight flowrate of outer combustor
$\dot{w}_T$	= weight flowrate of both combustors
I_{s_I}	= specific impulse of inner combustor
I_{s_O}	= specific impulse of outer combustor
$\Delta I_{s_{mix}}$	= delta specific impulse due to stream mixing
H	= height
W	= width
L	= length
F_O	= thrust of outer combustor
F_I	= thrust of inner combustor
F_T	= thrust of both combustors
F_{SL}	= sea level thrust
F_{vac}	= vacuum thrust
C^*_I	= characteristic velocity of inner combustor
C^*_O	= characteristic velocity of outer combustor
g	= gravitational acceleration
P_c	= chamber pressure
ϵ_I	= expansion area ratio of inner combustor
ϵ_O	= expansion area ratio of outer combustor
ϵ_1	= Mode 1 expansion area ratio
ϵ_2	= Mode 2 expansion area ratio
μ	= Prandtl-Meyer angle
β	= orientation of combustor shroud
X/G_2	= axial distance along aerospike nozzle centerline
Y/G_2	= radial distance from aerospike nozzle centerline
h_g	= gas-side heat transfer coefficient
h_c	= coolant-side heat transfer coefficient
k	= thermal conductivity
Re	= Reynolds number
Pr	= Prandtl number

ORIGINAL PAGE IS
OF POOR QUALITY

PRECEDING PAGE BLANK NOT FILMED

ϕ_C = coolant curvature enhancement

ϕ_E = coolant entrance enhancement

ϕ_P = propellant property correction term

D_H = hydraulic diameter

MR = propellant weight mixture ratio (oxidizer/fuel)

P_{inlet} = coolant circuit inlet pressure

T_B = coolant bulk temperature

T_{WC} = coolant side-wall temperature

C_H = Stanton number

C_p = specific heat

f = friction factor

ℓ = fluid path length

ΔP = change in pressure

T_{WG} = gas-side wall temperature

N_f = cycle life

A_a = turbine annulus area

N = turbine rotational speed

N_s = specific speed

ΔH = head rise

ρ = propellant density

Q = volumetric flowrate

U_T = tip speed

η = efficiency

P/B = preburner

MOV = main oxidizer valve

OPOV = oxygen preburner oxidizer valve

FPOV = fuel preburner oxidizer valve

MFV = main fuel valve

T/C = thrust chamber

GG = gas generator

SC = staged combustion

U_M = turbine pitch-line velocity

$P_{o_{1T}}$ = turbine inlet total pressure

γ = specific heat ratio

P_D = pump discharge pressure

P_{2t} = turbine discharge static pressure

$\dot{w}_{ft}$ = fuel flowrate to turbine

$\dot{w}_{fe}$ = fuel flowrate in engine

N_T = number of turbine stages

N_P = number of pump stages

C_o = isentropic spouting velocity for turbine

$\dot{w}_t$ = turbine flowrate

$\dot{w}_p$ = pump flowrate

ORIGINAL PAGE IS
OF POOR QUALITY